Bioprinting Human Skin Equivalents Using Reactive Jet Impingement

Thesis Submitted to the Faculty of Science, Agriculture and Engineering for the Degree of Doctor of Philosophy

by

Maria Crespo-Cuadrado

School of Engineering

Newcastle University

February 2023

ABSTRACT

Before most commercial products reach the market, their safety and efficiency must be evaluated. *In vitro* skin equivalents are extensively used to assess the toxicity and penetration of substances. However, their limited reproducibility and long manufacturing times have hindered their industrial implementation. The use of bioprinting systems has helped to automatise the production process, but the industrial scalability of these models as testing platforms is still limited.

This research aimed to optimise the manufacturing of skin equivalents by incorporating the novel Reactive Jet Impingement (ReJI) bioprinting system. The combination ReJI process with the formulation of natural-based bioinks could help to improve the complexity of the models, recreating specific skin microenvironments and accelerating the skin formation process.

The experimental results demonstrated the ability of ReJI to control cell distribution, ensuring the homogeneity of the models. In contrast to other bioprinting techniques, cell viability was not affected regardless of the printed cell density. By incrementing ten times the number of fibroblasts in the dermal models, it was possible to reduce their maturation time significantly. Meanwhile, the study of dermal bioinks allowed the identification of parameters that influence fibroblast behaviour. The selection of collagen sources and neutralisation method affected the physicochemical properties of the dermal models, along with the fibroblast proliferation and matrix remodelling. Similarly, the combination of fibrin with alginate and collagen enabled the customisation of the dermal layer. Finally, the incorporation of these biomaterials into the epidermal production also allowed an enhanced control over keratinocyte distribution and differentiation.

This research demonstrates the suitability of ReJI for the high-throughput production of models and the possibility of decreasing the manufacturing times. Additionally, the selection of natural bioinks has shown to be an important factor in the recreation of different skin microenvironments and conditions, tailoring the cellular behaviour and functionality of the final models.

"The important thing is not to stop questioning;
curiosity has its own reason for existing (…)"
- Albert Einstein

ACKNOWLEDGEMENTS

Firstly, I want to thank the Engineering and Physical Sciences Research Council, the Centre for Doctoral Training in Additive Manufacturing and 3D Printing, and Croda International Plc. for funding this project (EP/L01534X/1). This research would not have been possible without their support.

I want to express my gratitude to my academic supervisory team for their guidance over the past four years. I would like to especially thank Prof Kenny Dalgarno for following my progress and providing me with support and advice through each step of this journey. I also want to thank Dr Marina Ferreira-Duarte for her knowledge and suggestions about the biomaterial properties and characterization. One of my main motivations for pursuing a scientific career has always been the possibility of solving real problems. For that reason, I am genuinely thankful to my industrial supervisors for their inspiration and motivation. To Dr Philippe Mondon, Dr Caroline Ringenbach, and especially Dr Alba Cico, thank you for all your help and implication in this project.

I wish to thank Dr Gema Dura for all her guidance through this project, and for allowing me to delve into the biomaterial world and collaborate with her. I want to acknowledge. Dr Xin Xu for providing training and assistance on the skin model sections. To the Bioimaging Unit from Newcastle University for the training and technical support received. And to Ross Laws and Tracey Davey for the training on the SEM and their time processing my samples and attempting to characterize them by TEM.

Through these last years, I have met many people who have helped me to grow not only as a scientist, but also as a person. I want to thank all my friends and colleagues from Newcastle University and the CDT programme for all the experiences and lessons learnt together. To Dr Ana Río-Machín, thank you for being the best mentor I could wish for.

Finally, I would like to show my gratitude to my family for giving me the opportunity to pursue a scientific career and leave my home more than ten years ago. Thank you for always supporting and believing in me. To Juanjo, thanks for all your patience and understanding, being always there for me to remind me the big picture. I would like to dedicate this dissertation especially to my grandmothers. Thank you for teaching me the power of curiosity, the value of little things, and for providing me with the opportunities you never had.

TABLE OF CONTENTS

LIST OF FIGURES

LIST OF TABLES

LIST OF ABBREVIATIONS

2D	Two Dimensional
3D	Three Dimensional
ALI	Air-Liquid Interface
ATR-FTIR	Attenuated Total Reflection Fourier Transform Infrared Spectroscopy
$CaCl_2$	Calcium Chloride
CAF	Collagen-Fibrin-Alginate
Calcein AM	Calcein Acetoxymethyl
cDNA	Complementary DNA
DAPI	4',6-Diamidino-2-phenylindole
dECM	Decellularised Extracellular Matrix
DMEM	Dulbecco's Modified Eagle's Medium
dsDNA	Double-stranded Deoxyribonucleic acid
DoD	Drop-on-Demand
dsDNA	Double-stranded DNA
ECM	Extracellular Matrix
ELISA	Enzyme-Linked Immunosorbent Assay
EthD-1	Ethidium homodimer-1
F-actin	Filamentous Actin
FACs	Fluorescence-activated cell sorting
FT	Full-thickness
GAGs	Glycosaminoglycans
GelMA	Gelatin methacrylate
H&E	Haematoxylin and eosin staining
HKGS	Human keratinocyte growth supplement
hESC	Human embryonic stem cells
HUVEC	Human Umbilical Vein Endothelial Cells
IHC	Immunohistochemistry
iPSCs	Induced pluripotent stem cells
HSE	Human skin equivalent

H&E	Haematoxylin and eosin
mL	Milliliter
MMPs	Matrix Metalloproteinases
MSCs	Mesenchymal Stem Cells
neoNHDF	Neonatal normal human dermal fibroblasts
neoNHEK	Neonatal Normal Epidermal Human Keratinocyte
OECD	Organization for Economic Cooperation and Development
PBS	Dulbecco's Phosphate-Buffered Saline
Pa	Pascal
PCL	Polycaprolactone
PCR	Polymerase Chain Reaction
PEG	Polyethylene glycol
PI	Propidium iodide
PLGA	Polylactid-co-glycolid
PLL	Poly-L-Lysine
P/S	Penicillin/streptomycin
qPCR	Real-Time Quantitative Reverse Transcription Polymerase Chain Reaction
ReJI	Reactive Jet Impingement
RHE	Reconstructed human epidermis
RNA	Ribonucleic Acid
ROCK inhibitor	Rho associated kinase (Y-27632 dihydrochloride)
SEM	Scanning electron microscopy
SKALP	Skin-derived Antileukoproteinase
TE	Tissue Engineering
TEER	Transepidermal Electrical Resistance
TEM	Transmission electron microscopy
TEWL	Transepidermal Water Loss
UV	Ultraviolet
VOT	Valve opening time

CHAPTER 1. INTRODUCTION

Pharmaceutical and skin care firms spend millions of pounds on the research and development of new products. Most of this investment is dedicated to assessing the biological effects of new formulations in clinical trials (Wouters et al., 2020). Optimisation of preclinical screenings becomes essential in the selection of the best candidates for clinical trials, reducing the time and costs required for launching the products into the market. The use of animals has been a conventional procedure for evaluating the penetration and long-term effects of new formulations (Avci et al., 2013). However, animal testing has demonstrated limited reliability due to the differences in skin composition between animals and humans (Dellambra et al., 2019). Moreover, the possibility of causing discomfort to the animals has raised ethical concerns and people's awareness of animal welfare. Consequently, several countries and economic regions, including the European Union, have already banned the testing of cosmetic ingredients on animals and encouraged pharmaceutical companies to reduce their studies with animals, highlighting the urgent need for alternative methods to animal testing (Almeida et al., 2017; European Commission, 2019; Holmes et al., 2010).

Skin is the largest organ in the human body and represents one of the first protective barriers against UV radiation, pathogen entry and physical damage (Proksch et al., 2008). Its exposure to the external environment makes skin one of the main routes of entry into the body for external agents, such as chemicals, microorganisms, or medical treatments. For that reason, skin has become a key target for evaluating the safety and efficiency of commercial products (Abd et al., 2016; Niehues et al., 2018). In the last decades, different attempts to replicate the three-dimensional structure of human skin have resulted in the production of *in vitro* skin equivalents with enough complexity to be used for product assessment (Groeber et al., 2011; Klicks et al., 2017). Despite being considered a popular alternative to animal testing, the implementation of these skin equivalents at the industrial level is still restricted by their long production times and high costs. The need for manual steps during their manufacturing hinders their large-scale production and limits the quality and reproducibility of the models (Flaten et al., 2015; Planz et al., 2016; Suhail et al., 2019).

In recent years, 3D bioprinting has emerged as a potential solution to these problems. Bioprinting allows the selective deposition layer-by-layer of cells and biomaterials, reproducing the structural and biological composition of native human tissues (Murphy & Atala, 2014). The automatization of the process enables the fast production of tissue equivalents at a large scale in a cost-effective way. In addition, precise control over the location of biological components reduces the possibilities of batch-to-batch variations and opens the door to the customisation of *in vitro* models (Melchels et al., 2012; Murphy et al., 2019; Sarkiri et al., 2019). Different bioprinting techniques have already demonstrated their ability to improve the complexity and reproducibility of skin equivalents (Min et al., 2018; Derr et al., 2019; Cubo et al., 2016). As a result, the bioprinting process has significantly improved the quality of skin grafts used for medical applications. However, the bioprinting of skin models suitable for the replacement of animal experimentation has not been proven yet (Ng et al., 2016; Olejnik et al., 2022).

Some of the main restrictive factors on the quality and scalability of skin models for industrial applications are related to the operation process of each bioprinting technique (Ng et al., 2019; Sun et al., 2020). To overcome these limitations, this PhD thesis proposes the incorporation of a novel bioprinting technology named Reactive Jet Impingement system (ReJI). The following chapters will compare the advantages and limitations of ReJI system and other bioprinting techniques in terms of resolution, bioink requirements and complexity of the process, among others. From then, the suitability of ReJI system on the production of skin models will be explored, as well as the formulation of several bioinks and their capacity to mimic the physiological characteristics of each skin layer.

1.1. Thesis Structure

This thesis is organised into nine chapters, including the current Chapter 1, which introduces the research area, the relevance of this study and an overview of the thesis organisation.

Chapter 2 reviews the underlying concepts of this thesis. It starts by introducing the biology of human skin and the role of its components, and it continues by describing different strategies to produce skin *in vitro*. Additionally, an overview of current commercial skin equivalents is provided, with the description of the standard methods performed for their validation. Finally, the different types of bioprinting techniques are presented, and their implications on the production of skin models are reviewed.

Chapter 3 states a hypothesis to overcome the gaps of knowledge in the current generation of *in vitro* skin equivalents and provides a definition of the aims and main goals of this project.

Chapter 4 reports the methodology followed in this research. It includes bioink formulations and their physicochemical characterisation, ReJI setup, cell culture steps, biological assays and the studies performed on the dermal, epidermal and skin models.

The different experimental results are described and discussed in Chapters 5, 6, 7 and 8.

Chapter 5 explores the advantage of using Reactive Jet Impingement as bioprinting process. It includes the optimization of the printer setup, the control of ReJI over the cell distribution and the effect of the printing process on the formation of dermal and epidermal layers.

Chapter 6 presents the different biomaterials selected as dermal bioinks. This chapter delves into the relationship between the physicochemical and mechanical properties of the different bioinks and their influence on fibroblast behaviour.

Chapter 7 describes the implications of encapsulating keratinocytes in natural-based bioinks and their effect on the keratinocyte behaviour and generation of epidermal layers.

Meanwhile, Chapter 8 reports the attempts to produce full skin models and their evaluation, including the incorporation of the selected dermal and epidermal bioinks.

Chapter 9 provides a summary of the findings obtained in previous chapters, and an overall discussion of the novelty and implications of these results.

Finally, Chapter 10 outlines the conclusions of this research, along with recommendations for future work.

CHAPTER 2. LITERATURE REVIEW

2.1. Anatomy and Physiology of Human Skin

Skin is a complex organ with a well-defined structure (Paul & Sharma, 2015; Fenner & Clark, 2016; Kanitakis, 2002). The epidermis, dermis and hypodermis are the three main layers which define the human skin and contribute to its homeostasis (Fig. 2.1). The epidermis provides a barrier function by protecting the skin against external agents, regulating the secretion and absorption of substances and preventing water loss (Proksch et al., 2008). Meanwhile, the dermal layer supplies nutrients and structural support to the skin (Brown & Krishnamurthy, 2022). The hypodermis is the subcutaneous layer responsible for the thermoregulation and protection of underlying tissues against physical damage (McKnight et al., 2022).

Each layer comprises different cells and biomolecules with specific roles, locations and interactions between each other. Failure to reproduce this internal microenvironment often results in the emergence of specific skin conditions such as atopic dermatitis, fibrosis or melanoma, amongst others (Semlin et al., 2011; de Stefano & Christiano, 2014).

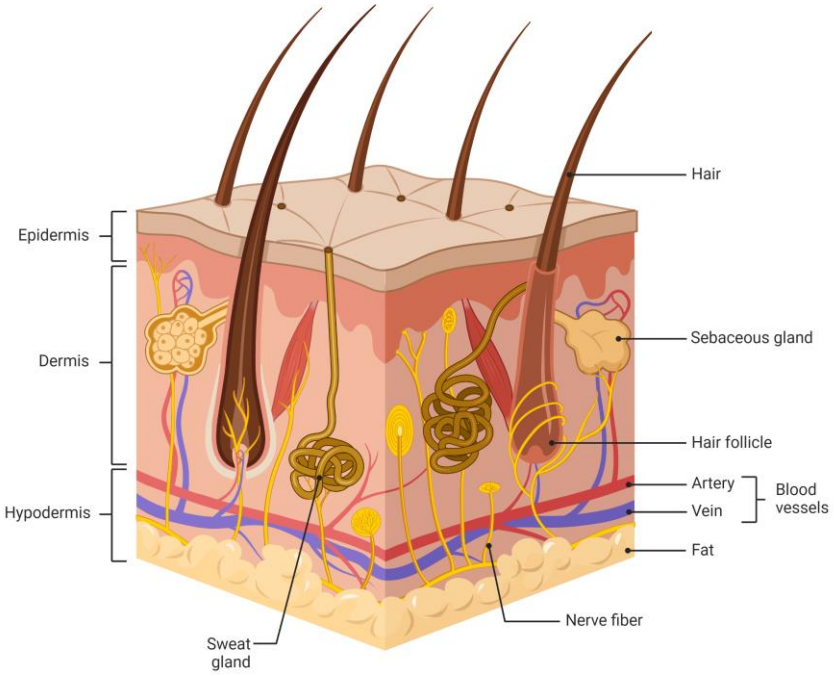

Figure 2. 1. Schematic representation of human skin architecture and its three differentiated layers: epidermis, dermis and hypodermis. Skin complexity is enhanced by the presence of vasculature and appendages, such as hair follicles, sebaceous and sweat glands. Image adapted from Biorender.com.

2.1.1. Epidermal Layer

The epidermis is the outermost skin layer with 10 to 100 µm thickness, and it is mainly composed of keratinocytes. The keratinocyte attributes vary through the epidermis defining four differentiated epidermal sub-layers: *stratum corneum, stratum granulosum, stratum spinosum and stratum basale* (Fig. 2.2) (Fenner & Clark, 2016).

Keratinocytes in the *stratum basale* present a proliferative phenotype and are defined by their cuboidal morphology. The continuous production of new keratinocytes by the basal cells allows epidermal self-renewal approximately every 28 days (Myers et al., 2014). When the basal keratinocytes start to mature, they initiate a diffusion through the upper epidermal sub-layers, undergoing a sequential differentiation (Freedberg et al., 2001). As keratinocytes migrate, they start to present a variety of structural and compositional changes. The variation in the expression of keratins through the epidermal layers exemplifies these modifications (Table 2.1) (Edqvist et al., 2015; Toivola et al., 2015). Keratin is an intermediate filament protein and plays an essential role in the epidermis, providing structural support and regulating the synthesis of proteins and keratinocyte apoptosis.

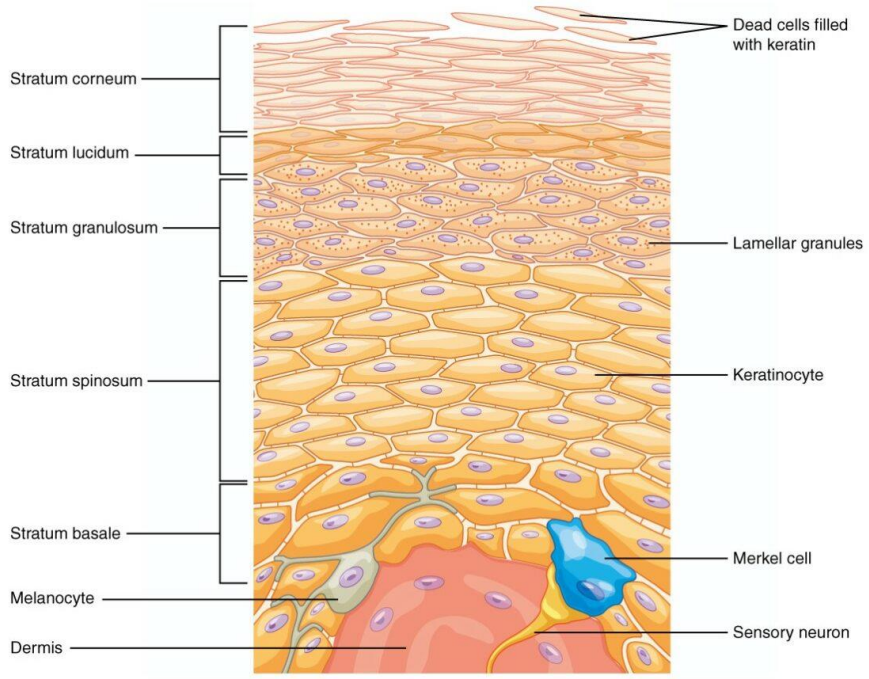

Figure 2. 2. Representation of the morphological changes experienced by keratinocytes through the different epidermal sublayers, including the stratum basale, spinosum, granulosum, lucidum and corneum. The presence of additional cell types, such as melanocytes and Merkel cells, can be observed in the stratum basale. Image adapted from OpenStax College.

Keratinocytes coexist in the basal layer with pigmented cells named melanocytes, which are responsible for skin protection against ultraviolet radiation (Brenner & Hearing, 2008). Melanocytes produce melanin granules, which are stored in melanosomes and later transferred to keratinocytes to create a melanin cap, which will protect the keratinocyte nucleus from photodamage. The number, size and distribution of melanosomes contribute to the variation in skin colour (Yamaguchi et al., 2007). Other cells resident in the basal layer are the Merkel cells, which play an essential role in skin sensation (Moll et al., 2005), and Langerhans cells, which are antigen-presenting cells act as the first line of immunological defence against microbes, being responsible for producing pro-inflammatory signals (Clayton et al., 2017).

In the following epidermal layer, the *stratum spinosum*, keratinocytes acquire a polyhedral morphology as they start to synthesise cytokeratin filaments (Deo & Deshmukh, 2018). These intermediate filaments, together with desmosomes, ensure tight bindings between adjacent keratinocytes. The presence of adheren, tight and gap junctions through the epidermis, combined with the adhesion of the basal layer to the dermo-epidermal junction through hemi-desmosomes, result in the creation of a resistant system to maintain the epidermal integrity against external forces (Simpson et al., 2011). Keratinocytes start an apoptotic process, losing their nucleus and acquiring a flat shape in the *stratum granulosum*. The presence of keratohyalin granules triggers the aggregation of keratin filaments and, consequently, the agglomeration of keratinocytes. Additionally, lamellar bodies produced previously by keratinocytes release their content creating a lipid and antimicrobial barrier, which improves cellular adhesion and avoids the loss of fluids (Bouwstra & Ponec, 2006). The *stratum corneum* is the outermost epidermal layer and contains 10 to 25 layers of dead keratinocytes, which present a flat shape. These keratinocytes are named corneocytes and are tightly held together by the remaining desmosomes and lamellar body content, forming a relatively impermeable layer (Simpson et al., 2011; Kalinin et al., 2001). The resulting lipidic matrix also contains other elements like cholesterol esters, ceramides or free fatty acids, which are essential to reduce the corneal layer permeability (Bouwstra et al., 2021; van Itallie & Anderson, 2014). Additionally, tight and adherence junctions are formed between the last living keratinocytes in the *stratum granulosum* and the corneocytes and regulate the molecule flux between layers (Chiba et al., 2008; Yoshida et al., 2013). Combining all these factors provides the *stratum corneum* of a protective barrier character. When the adhesion between corneocytes is lost, the corneal layer starts a desquamation process (Candi et al., 2005). An additional epidermal

layer named *stratum lucidum* can be found only on the palms of the hands and soles of the feet (Yousef, Alhajj, et al., 2022). This thin layer contains dead keratinocytes and oily substances, which reduce the tensional forces between the *stratum corneum and granulosum*.

Table 2. 1. Examples of the physiological roles of proteins and molecules present in the different epidermal layers.

Protein	Epidermal layer	Physiological function	Reference
Keratin 14	*Stratum basale*	Marker of the normal state of keratinocyte proliferation	Alam *et al*., 2011
Keratin 16	*Stratum basale*	Marker of keratinocyte proliferation during the wound healing process	Smiley *et al*., 2006
Keratin 19	*Stratum basale*	Marker of keratinocyte hyperproliferation	Govaere *et al*., 2014
Ki67	*Stratum basale*	Marker of early proliferation	Schonzen & Gerdes, 2000
Cadherins	*Stratum spinosum* *Stratum granulosum*	Marker of cell junction formation	Tunggal *et al*., 2005
Keratin 10	*Stratum spinosum*	Marker of keratinocyte early differentiation	Drozdoff & Pledger, 1993
Involucrin	*Stratum granulosum*	Markers of keratinocyte terminal differentiation	Watt, 1983
Claudin-4	*Stratum granulosum*	It takes part in tight junction formation	Chiba *et al*., 2008
Occludin	*Stratum granulosum*	It takes part in tight junction formation	Matter & Balda, 1999
Loricrin	*Stratum granulosum* *Stratum corneum*	Component of the cornified layer	Kalinin *et al*., 2001
Filaggrin	*Stratum corneum*	Component of the cornified layer	Sandilands *et al*., 2009

When the epidermal structure is damaged, mechanical changes occur and specific molecular factors are released to activate the keratinocyte proliferative state (Hegde et al., 2021). Basal keratinocytes closer to the wound edge start to migrate and divide to ensure the production of enough basal cells. Once keratinocytes are confluent across the lesion, their proliferation rate decreases and they start to differentiate to create the suprabasal epidermal layers (Amiri et al., 2022).

2.1.2. Dermal Layer

The dermis is situated beneath the epidermis and represents the thicker skin region with a thickness between 1 and 5mm. This layer is mainly constituted of fibroblasts and a complex matrix of proteins and elastic fibres, which provide structural strength and elasticity (Krieg & Aumailley, 2011). In addition, the dermis presents two differentiated areas with different compositions, the papillary and reticular dermis (Fig. 2.3) (Sriram et al., 2015; Sorrell & Caplan, 2009). The papillary dermis is the closest dermal layer to the epidermis. This region is mainly made up of collagen type III, collagen type I, decorin, fibronectin and elastin (Janson et al., 2012). The thin loose fibers that comprise this region affect their mechanical properties (Sorrell & Caplan, 2004). Influenced by the matrix characteristics, papillary fibroblasts present a spindle-shaped morphology and a high proliferative rate (Azzarone & Macieira-Coelho, 1982). Fibroblasts show a limited production of new extracellular matrix (ECM) components in this region (Korosec et al., 2019).

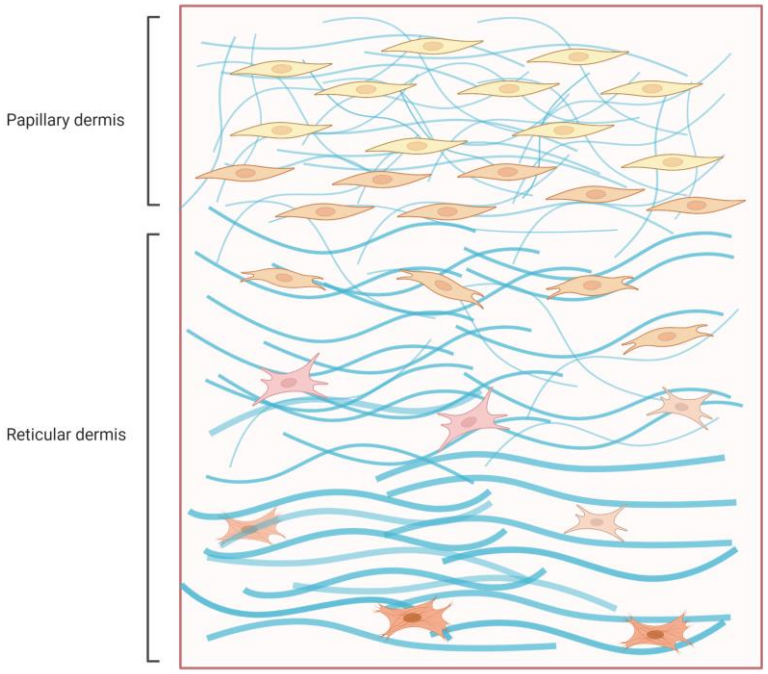

Figure 2. 3. Graphic representation of the different fibroblast morphology and distribution through the dermis. In the reticular dermis, fibroblasts present a polygonal shape and are supported by aligned fibrillar matrix. In contrast, the papillary dermis is comprised of a higher number of elongated fibroblasts surrounded by thinner and loose extracellular matrix. Image designed using Biorender.com.

The reticular dermis is the thickest dermal layer situated between the papillary dermis and the hypodermis. This region is mainly comprised of thick collagen type I fibres and large

concentrations of elastic fibres. Conversely to papillary dermis, this layer is formed by densely packed fibrillar proteins, which are distributed in parallel to the skin surface to provide resistance to the skin against tangential forces (Sherratt, 2009). Moreover, the presence of proteoglycans like versican or chondroitin provides high elasticity to this layer. Non-fibrillar proteins like proteoglycans or hyaluronic acid are situated in the dermal spaces between fibres to provide hydration to the tissue and ensure the distribution of molecules through the extracellular matrix (Uitto et al., 1989). In contrast to papillary dermis, collagen type III is present in this layer in lower concentrations than collagen type I (Ghetti et al., 2018). Another difference to the papillary dermis is the polygonal morphology adopted by reticular fibroblasts. The primary role of these cells is the production of new extracellular components and matrix reorganisation (Sorrell et al., 2004).

Mast cells are one of the additional cellular components that comprise the dermis. These cells are responsible for immunological reactions like allergic responses (Galli & Tsai, 2010). In addition, nerve endings and several appendages, such as hair follicles, sebaceous and sweat glands, can also be found in the dermal layer and provide the skin with additional functions (Yousef, Miao, et al., 2022). Besides, blood vessels are present in the dermis to provide nutrients and oxygen to the whole skin.

During the wound healing process, the previously described behaviour of fibroblasts is altered (Zou et al., 2021). Initially, the injured skin site is sealed by a blood clot made of fibrin and fibronectin, providing temporary support for the cells (Rezaie et al., 2019; Tottoli et al., 2020). When the wound site is contracted, fibroblasts in the vicinity of the lesion are activated and acquire a myofibroblastic phenotype to participate in tissue regeneration (El-Ghalbzouri et al., 2002). The tractional forces created through the injury site promote the mobility and proliferation of fibroblasts. As fibroblasts migrate, they start to remodel the matrix composition by producing new extracellular matrix components and degrading the fibrin components through the secretion of matrix metalloproteinases (MMPs) (Caley et al., 2015). The reconstruction of the dermal structural composition helps to provide stability to the skin and support the keratinocyte migration and re-epithelisation (Sivamani et al., 2007). The intervention of endothelial cells allows dermal neovascularisation and the arrival of essential elements like immune cells or pro-inflammatory molecules required for wound healing (Ono et al., 2017).

Fibroblast behaviour is also modified as the skin begins to age. During this process, fibroblast heterogeneity is compromised as papillary fibroblast starts to acquire a reticular phenotype (Mine et al., 2008; Janson et al., 2013). This modification of the skin composition results in a drop in the fibroblast renewal, the reduction of the papillary dermis and the alteration of the extracellular matrix composition. The decrease in the population of papillary fibroblasts also brings structural changes to the epidermis and the skin physiology, including the reduction of skin elasticity and the appearance of skin wrinkles (Solé-Boldo et al., 2020; Hausmann et al., 2019).

2.1.3. Dermal-Epidermal Junction

The dermoepidermal junction is responsible for connecting the epidermis and dermis (Marionnet et al., 2006). This semipermeable basement layer allows the exchange of nutrients and biomolecules between both layers. This region is mainly comprised of collagen type IV and VII, laminins, perlecan and nidogen, but also it includes other components like collagen type I and III, tenascin or fibrillin (Aleemardani et al., 2021).

The *lamina lucida* represents the area in the dermal-epidermal junction closer to the epidermis. The basal epidermal cells adhere to this region through different proteins and complexes such as collagen XVII, laminins-5 or hemidesmosomes, among others. As a result, an epithelial extension called rete ridge is formed to enhance the anchoring between the epidermis and the dermoepidermal junction (Roig-Rosello & Rousselle, 2020). On the other hand, the *lamina densa* is supported by the papillary dermis. These regions are connected by collagen type VII fibrils in combination with collagen type I and III.

Most dermoepidermal components, like laminin-5 or collagen type VII, type XVIII and XVIII, are primarily produced by keratinocytes (Marinkovich et al., 1993). Whereas other biocomponents, like laminin-10, collagen type IV or nidogen, are generated by fibroblasts (Contard et al., 1993; Fleischmajer et al., 1995). In most cases, the generation of these molecules requires the presence of both cell types (Varkey et al., 2014; Lee & Cho, 2005; Smola et al., 1998).

2.1.4. Hypodermis

The hypodermis is the innermost skin layer. It connects the skin structure to the underlying organs, protecting them against physical damage (Paul & Sharma, 2015). This region contains mostly adipocytes, which act as energy reserve and ensure thermoregulation (Dragoo et al., 2021). Fibroblast, collagen and elastin can also be found in the hypodermis forming part of the loose connective tissue (Haydont et al., 2020). Similarly to the dermis, some additional skin components like blood vessels, nerves, sweat glands and hair follicles can be found in the hypodermis (Williams et al., 2020; Wong et al., 2016).

2.2. Human Skin Equivalents

Skin homeostasis is fundamental to preserve the skin protective character against external agents. In chronic wounds and severe burns, the incapacity to heal the epidermal barrier often leads to major body infections and high mortality rates (Smolle et al., 2017). Consequently, it becomes essential to find a method capable of promoting the quick regeneration of native skin structures. Transplantation of skin tissue equivalents has become a demanded strategy in the treatment of severe burns (Kelangi et al., 2021; Concannon et al., 2022). The cellular and biomolecular components of these skin substitutes trigger specific signalling cascades and cellular functions that induce the reconstruction of damaged tissue.

On the other hand, skin equivalents are also employed in basic research, for the study of cell mechanism in skin biology, and in preclinical studies, as a tool to evaluate the safety and efficiency of chemical compounds (Abd et al., 2016; Moniz et al., 2020). In this case, skin models must mimic the physiological and morphological composition of native skin. Their resemblance with the real tissue is crucial to determine the penetration, distribution and interaction of tested products through the diverse skin layers (Flaten et al., 2015). This section explores different strategies employed for the manufacturing and validation of *in vitro* skin equivalents for product testing.

2.2.1. Tissue Engineering Skin Equivalents

Due to their active role in skin homeostasis, fibroblasts and keratinocytes are considered the most essential components for the production of skin models. Early attempts to recreate skin equivalents *in vitro* consisted of the seeding of fibroblasts and keratinocytes monolayers. Cells were expected to produce their own extracellular matrix, mimicking their behaviour in real skin. However, the lack of spatial organisation associated to their two-dimensional structure prevented their cellular mobility and vertical spreading, impeding the recapitulation of the complex architecture found in native skin (Smithmyer et al., 2019). Additionally, the alteration in the morphology and the genetic expression of these cells leads to a different response to the tested molecules than those cells found in native tissues. As a result, the utilisation of cell monolayers is often limited to the initial assessments of material cytotoxicity (Fitzgerald et al.,

2015). These studies can help to quickly discard any material which could harm or alter the biology of skin cells.

Nowadays, *in vitro* skin models aim to replicate the multi-layered structural composition found in human skin. In an attempt to generate three-dimensional structures, different matrices are introduced as scaffold for fibroblasts and as support for keratinocytes (Sheikholeslam et al., 2018). These biomaterials facilitate the cell-cell interaction and organisation, improving the skin functionality. Initially, keratinocytes were seeded on acellular dermal matrices to mimic the epithelial structure (Setijanti et al., 2019). These reconstructed human epidermal (RHE) models were used to evaluate the permeability of chemical compounds. However, in most studies, the epidermal stratification was affected by the fibroblast absence (Agonia et al., 2022). The study of this phenomenon *in vitro* confirmed the importance of the keratinocyte and fibroblast crosstalk for the expansion of keratinocytes and the complete epidermal stratification (Boehnke et al., 2007).

Full-thickness skin models are conventionally produced following a bottom-up approach (Fig. 2.4). Briefly, dermal fibroblasts are seeded into a scaffold and cultured under submerged conditions for several days. When fibroblasts adhere to the matrix, a monolayer of keratinocytes is seeded on top of the dermal structure, and the model is maintained under submerged conditions to ensure keratinocyte proliferation (Klicks et al., 2017; Nicholas et al., 2016). Subsequently, the skin model is exposed to an air-liquid interface, reproducing the conditions on real skin to induce keratinocyte differentiation. During this step, the concentration of calcium anions is risen to guarantee the correct epidermal stratification (Borowiec et al., 2013). The complete formation of the skin structure can require between 28 to 41 days (Schmidt et al., 2020; Roger et al., 2019; Sriram et al., 2015). The incorporation of additional skin cells like melanocytes, adipocytes or endothelial cells can help to improve the model complexity (Vidal et al., 2019; Sanchez et al., 2022).

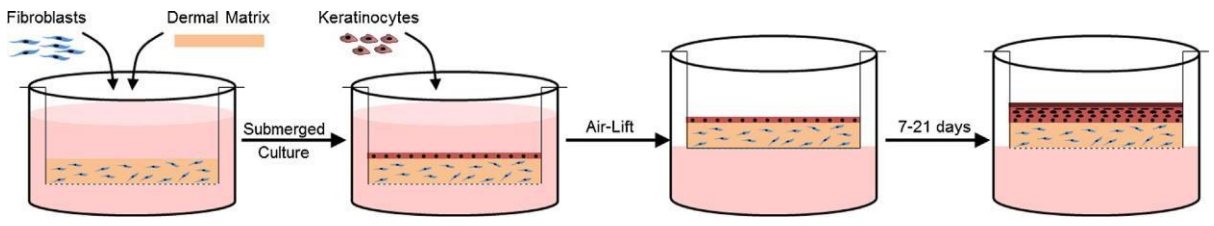

Figure 2. 4. Schematic representation of the skin model production process. Fibroblasts are cultured in a dermal matrix and maintained under submerged conditions. Subsequently, keratinocytes are seeded on top of the dermis and, after few days, the resulting model is exposed to air-liquid interface to ensure the epidermal stratification. This image was obtained from Sriram et al. 2015.

Different materials can be employed as dermal matrices for the generation of skin models. Natural materials present in the skin, like fibrillar proteins, glycosaminoglycans or polysaccharides, are the most popular choices to guarantee the replication of native structures (Caliari & Burdick, 2016; ter Horst et al., 2019). Collagen type I is the most selected biomaterial for this application due to its high abundance in native skin, and its ability to promote fibroblast proliferation and migration (Kanta, 2015; Grinnell & Petroll, 2010). The interaction between collagen and fibroblast usually leads to collagen contraction affecting the reproducibility of the models (Grinnell, 2000). For this reason, collagen is often replaced or combined with other natural polymers such as fibrin, laminin, or hyaluronic acid (Sheikholeslam et al., 2018).

In general, the utilisation of natural materials is hindered by their poor mechanical properties and the difficulties to handle them (Joyce et al., 2021; Reddy et al., 2021). Alternatively, synthetic materials are often used as cell supports due to their excellent mechanical properties and stable properties. Some of the most common synthetic biomaterials are polyethylene glycol (PEG), polylactid-co-glycolid (PLGA) or polycaprolactone (PCL) (Nikolova & Chavali, 2019). These materials are easily manufactured and some of their parameters, like elasticity, water permeability or degradation rate, can be customised (Samavedi et al., 2014). Despite their advantages, synthetic materials do not contain the biochemical domains required for cell adhesion. The combination of synthetic biomaterials and natural polymers can enhance the biocompatibility and mechanical properties of the resulting hybrid material (Yousefzade et al., 2020; Greenwood, 2016). On the other hand, the use of recombinant biomaterials has gained importance in the last years. These genetically modified proteins or hybrid polymers incorporate cell-binding motifs that resemble the ones found in extracellular-matrix proteins, such as the fibronectin-derived RGD (arginine-glycine-aspartate) sequence (Hersel et al., 2003; Werkmeister & Ramshaw, 2012). These sequences promote specific cellular functions and can be modified based on the application requirements. Other parameters like mechanical properties or the material response to external stimulus can also be adapted in each case (Dura et al., 2020; Nagapudi et al., 2005). Some of the most popular materials used as dermal matrices and their properties are detailed in Table 2.2.

As an alternative to the use of exogenous biomaterials, Roger *et al.* proved the possibility of producing skin models by seeding fibroblasts on Alvetex® scaffolds for 28 days, enabling enough time for the fibroblast to generate their own ECM components (Roger et al., 2019).

Table 2. 2. Properties and origin of biomaterials frequently used in the fabrication of human substitutes.

Material	Origin	Properties	Reference
Collagen	Natural	· Represents 75% protein content in skin · Contains cell-recognition ligands · Self-assembling under physiological conditions	Parenteau-Bareil *et al*., 2010
Gelatin	Natural	· Denatured collagen · Contains cell-recognition ligands · Gel formation at 4°C and liquid state at 37°C	Lukin *et al*., 2022
Laminin	Natural	· Main component basal membrane · Plays an important role in the cell adhesion, migration and differentiation	Talovic *et al*., 2017
Elastin	Natural	· Provides of resilience and elasticity to the skin · Insoluble and difficult to handle	Daamen *et al*., 2007
Hyaluronic Acid	Natural	· Fills gaps between collagen fibrils · Promotes cell growth, migration and differentiation · Mechanical properties can be regulated by crosslinking reactions	Dovedytis *et al*., 2020
Fibrin	Natural	· Present during wound healing process · Produced by the fast gelation of thrombin combined with fibrinogen · Support cell growth and migration	Park & Woo, 2018
Alginate	Natural	· Abundant and cheap natural polysaccharide, with fast crosslinking profile · Used as supportive matrix due to its long stability and water content	Lee & Mooney, 2012
Matrigel	Recombinant	· Resemble laminin-Collagen IV structure · Self-assembling at 37°C	Klotz *et al*., 2019
Decellularized Extracellular Matrix	Natural	· Matrix extracted from real tissue · Maintain the main components of native ECM with the exception of the cellular content	Zhang *et al*., 2022a

Selection of cell sources is also a decisive factor that affects the reliability of skin models. Cell lines are often employed due to their robustness and cost-effectiveness. These cells are immortalised, easy to grow and maintain (Wang et al., 2019a). Their low variability through their lifetime promotes the generation of reproducible results. One of the drawbacks of these cells is their inability to recreate certain characteristics or phenotypical changes from normal cells (Schoop et al., 1999; Wnorowski et al., 2019). On the other hand, cells extracted from donors present similar morphological and biological characteristics to the ones observed *in vivo*. These primary cells can proliferate and reproduce natural cellular functions (Richter et al., 2021). However, their use is restricted to a limited number of passages before they start to age and undergo senescence process. The behaviour of primary cells can be affected by the age, sex and race of the donor, or the body area of extraction, restricting the comparability and reproducibility between studies (Caddeo et al., 2017; Wang et al., 2020).

To overcome this variability and improve the complexity of the models, stem cells are often introduced into the model. Stem cells have the ability to self-renew and differentiate into multiple tissue-specific cell types when they are exposed to defined microenvironments (McKee & Chaudhry, 2017). They can be sourced from different body locations such as bone marrow, adipose tissue, umbilical cord or hair follicles (Rosenbaum et al., 2008; Pittenger et al., 1999). Mesenchymal stem cells (MSCs) could be a suitable cell source due to their capacity to differentiate into skin cells such as fibroblasts, keratinocytes, endothelial cells or sebaceous glands (Sasaki et al., 2008). However, the use of this type of cells on the development of skin models have been limited by their complex isolation and differentiation, as well as the large time and costs required to grow enough MSCs (Dos Santos et al., 2023; Pittenger et al., 2019). Alternatively, induced pluripotent stem cells (iPSCs) also have the potential to differentiate into diverse skin cell types. iPSCs are reprogrammed somatic cells, which retain genetic and phenotypic markers associated with their origin (Singh et al., 2015). Therefore, iPSCs from patients can be used to reproduce specific disorders, understand their mechanisms and predict their response to certain therapies (Avior et al., 2016; Rowe & Daley, 2019). Despite their promising properties, the implementation of iPSCs is limited by its low efficiency and the amount and time required for their maintenance and differentiation (Yamanaka, 2020).

2.2.2. Validation Methods

Skin is one of the main routes of entrance into the body and acts as the first barrier against external agents. For that reason, the development of reliable skin equivalents is essential to study skin interaction with external elements. *In vitro* skin models must undergo several validation steps before they can be considered suitable for predicting the biological effects of commercial products (de la Torre et al., 2020; Brohem et al., 2011). The penetration and diffusion of chemical compounds through the skin are affected by the specific composition of each skin layer. Consequently, verifying the presence of fundamental structural components in the skin models is considered one of the first validation phases. The use of cellular stainings like Haematoxylin and Eosin (H&E) allows the distinction between cellular and extracellular components and their distribution through the skin (Mathes & Ruffner, 2014; Ponec et al., 2002). Additionally, fluorescence labelling of specific proteins and molecules by Immunohistochemistry can provide a better understanding of the location of key anatomical elements. Other techniques, such as Western Blot, Polymerase Chain Reaction (PCR), or Flow Cytometry, are also useful for validating the presence of specific molecules expressed by the skin cells (Itoh et al., 2013; Kim et al., 2004; Bellas et al., 2012). The presence of other essential components, like water or ceramides, can be explored using chemical analysis like Raman spectroscopy. Once the presence of fundamental skin components is confirmed, the functionality of the skin barrier needs to be evaluated. Transepidermal Electrical Resistance (TEER) and Transepidermal Water Loss (TEWL) assays are the most common methods to verify the integrity of epidermal barriers (Rinaldi et al., 2019; Guth et al., 2015).

One of the most extended methods to benchmark the produced models against the properties of native human skin is the permeability test (Neupane et al., 2020). This assay is based on the comparison between the diffusion values of standard compounds through the skin equivalents against the values acquired with real skin using a Franz cell (Jacques-Jamin et al., 2017). Some of the most habitual compounds for this assessment are caffeine, salicylic acid and corticoids (Alonso et al., 2019; Jepps et al., 2013). This test represents an additional confirmation of the model reliability. The evaluation of biological effects produced by external substances can be performed following standard guidelines established by the Organization for Economic Cooperation and Development (OECD, 2022). Some of the recommended assays include penetration, corrosive and irritation studies and evaluation of skin sensitisation, among others (Almeida et al., 2017; Capallere et al., 2018; Deshmukh et al., 2012; Kleinstreuer et al., 2018).

2.2.3. State-of-the-art of Skin Models for Product Testing

One of the promoting factors for developing skin equivalents has been the search for alternatives to animal experimentation. The use of animals for the assessment of cosmetic products is currently banned in multiple countries (Silva & Tamburic, 2022). Therefore, new models are urgently required to determine the toxicity and long-term effects of commercial products. In the last decade, animal testing has been slowly replaced by *ex vivo* models and *in vitro* skin substitutes validated for the screening of chemical compounds (Ng & Yeong, 2019; Filaire et al., 2022). Some of these tissue-engineered skins *in vitro* are currently commercialised and are often incorporated into the risk assessment of industrial components.

Reconstructed epidermal (RHE) models have been extensively applied for the evaluation of different studies such as skin permeability, irritation, corrosion or genotoxicity assays (Netzlaff et al., 2005; Danilenko et al., 2016). Additionally, those models containing melanocytes are mainly used to assess phototoxicity or alternations in skin pigmentation (Nakazawa et al., 1998; Bessou et al., 1999). EpiSkin® and EpiDerm™ models were the first reconstructed epidermal models validated by TEER (Table 2.3) (Agonia et al., 2022). Both were soon accepted as predictive models for skin corrosion and irritancy (Fentem & Botham, 2019; Welss et al., 2004). Eventually, SkinEthic® was also approved for the assessment of skin irritation and corrosion (Alépée et al., 2010; Kandárová et al., 2006). The permeability of these three models was tested, comparing their permeation coefficients to caffeine and testosterone with the values obtained in native human skin. These studies reported the impairment of the barrier function in the three RHE models (Schäfer-Korting et al., 2008; Schmook et al., 2001). Further research also discovered the expression of skin-derived antileukoproteinase (SKALP) in these models (Ponec et al., 2002; Flaten et al., 2015). SKALP is a marker for skin irritation which is only present during inflammatory states like psoriasis or wound healing process (Boelsma, Susan Gibbs, Maria Ponec, 1998).

Full-thickness (FT) models have already been incorporated into the evaluation of percutaneous absorption and distribution of chemical compounds through the skin, or the evaluation of wound healing treatments, among other studies (Suhail et al., 2019; Neves et al., 2022). Commercial full-thickness skin equivalents are one of the most extended models used to assess the safety and efficiency of topical treatments and skin care ingredients at industrial level, although their percutaneous absorption is three times higher than the skin standards (Wever et al., 2013; Planz et al., 2016). These models present barrier properties closer to the

ones in native tissue than reconstructed epidermal models (Schmidt et al., 2020; Vohr & Heisler, 2005). Epiderm FT™, Stratatest® and Phenion® are the most popular commercial FT models. Their characteristics and applications can be found in Table 2.3. The comparative analysis between FT skin equivalents and native skin showed a significant difference in the lipid composition. The higher abundance of lipids in the *stratum corneum* of these skin substitutes is considered one of the main responsible for their enhanced permeability (Thakoersing et al., 2013, 2011).

Commercial full-thickness skin models are comprised mainly of fibroblasts and keratinocytes. However, some published skin equivalents also include additional cell types, vascularization and appendages such as hair follicles or sebaceous glands (Abaci et al., 2018; Nikolakis et al., 2015; Auxenfans et al., 2012; Hosseini et al., 2022). The incorporation of Langerhans cells can be helpful for the evaluation of immunological responses to applied chemicals (Ouwehand et al., 2011). Similarly, the integration of vascularisation can provide additional information about the absorption and distribution of components through the circulatory system (Abaci et al., 2016; Tremblay et al., 2005). On the other hand, the production of disease models like psoriasis or melanoma can be useful for a deeper understanding of the causes behind these conditions and the improvement of current treatments (Soboleva et al., 2014; Hill et al., 2015; Ali et al., 2015).

The industrial implementation of skin equivalents for testing purposes is currently limited by their fabrication process (Ng et al., 2016). These models are manually produced, resulting in an increment in their manufacturing time and costs. Besides, the need for manual steps directly impacts the reliability and reproducibility of the models (van Gele et al., 2011; Suhail et al., 2019). The resulting batch-to-batch variations restrict the comparability between studies.

Table 2. 3. Examples of commercial Reconstructed Human Epidermal (RHE) models and Full-thickness (FT) skin models, including a description of their composition and applications.

Commercial name	Type of model	Composition	Applications	Reference
EpiDerm™	Reconstructed Human Epidermal Model	· Neonatal human keratinocytes cultured on polycarbonate membranes	· Validated for skin irritation · Validated for skin corrosion · Used for genotoxicity testing	Kandárová *et al*., 2009; Roy *et al*., 2016; Kandarova & Liebsch, 2017
EpiSkin®	Reconstructed Human Epidermal Model	· Human keratinocytes cultured on bovine collagen	· Validated for skin corrosion · Validated for skin irritation	Flamand *et al*., 2006; Alépée *et al*., 2019
SkinEthic®	Reconstructed Human Epidermal Model	· Human keratinocytes cultured on polycarbonate membrane	· Validated for skin corrosion · Validated for skin irritation · Used for phototoxicity assays	Alépée *et al*., 2017; Pellevoisin *et al*., 2018; Bernard *et al*., 2000
EpiDerm-FT™	Full-Thickness Skin Model	· Neonatal human fibroblasts and neonatal human keratinocytes	· Validated for skin irritation · Validated for skin corrosion · Used for dermal penetration assays	Mallampati *et al*., 2010; Kubilus *et al*., 2019
Phenion®	Full-Thickness Skin Model	· Human fibroblasts and human keratinocytes	· Validated for skin irritation · Used for phototoxicity assays · Used for genotoxicity assays	Ackermann *et al*., 2010; Reisinger *et al*., 2018
StrataTest®	Full-Thickness Skin Model	· Human fibroblasts in collagen type I and immortalized keratinocytes	· Pre-validated for skin irritation	Rasmussen *et al*., 2010

2.3. Bioprinting Skin Models

In the last years, different strategies have been assessed to overcome the limitations found in traditional tissue engineering techniques. 3D bioprinting technologies have brought increased attention due to their capacity to enhance the quality and reproducibility of tissue equivalents (Fig. 2.5).

Bioprinting is based on the selective deposition layer-by-layer of cells and biomaterials to reproduce the structural composition of native tissue (Murphy & Atala, 2014). This technology allows precise control over the spatial location of each component, opening the door to the automatisation of the process. The possibility of combining various biocomponents facilitates the manufacturing of models on-demand, recreating specific biological microenvironments (Mandrycky et al., 2016; Mehrotra et al., 2019). In recent years, bioprinting has been incorporated into the production of different tissues and organs, such as the heart, liver, cartilage or bones (Ng et al., 2019; Mota et al., 2020).

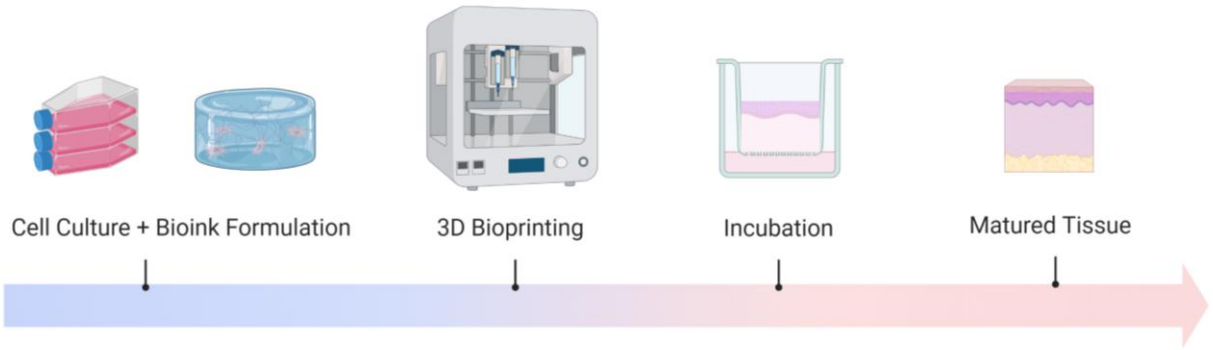

Figure 2. 5. Steps required for the 3D bioprinting of tissue equivalents, including the initial cell expansion and bioink formulation, the bioprinting process, and the subsequent tissue incubation until its complete maturation. Image created with Biorender.com.

Bioink formulation highly influences the quality and resemblance of the printed models. Bioinks are comprised of cells and biomaterials capable of mimicking the biological characteristics of native tissues (Decante et al., 2021). Biomaterials are often chosen based on their capacity to provide mechanical support to the cells, maintain cellular functions or promote specific cell behaviours (Fig. 2.6) (Correa et al., 2021; Levato et al., 2020). In some cases, part of the components is used as sacrificial biomaterials, supporting the cells only during the printing process (Liu et al., 2022a; Brunel et al., 2022). The control of the biomaterial degradation is essential to ensure the stability of the printed structure before its

replacement by new matrix components secreted by cells (Correia et al., 2020). The diffusion of oxygen, nutrients and signal molecules across the printed design is fundamental to maintaining cellular functionality. Different parameters like biomaterial porosity or swelling properties affect the distribution of oxygen and nutrients and the secretion of metabolites (Martínez et al., 2009; Zhu & Marchant, 2011). Biomaterial porosity also influences cell migration and proliferation and modifies the mechanical properties of printed structures.

Additionally, bioink formulations need to be adapted to the bioprinter requirements**.** Bioink printability varies for each bioprinting technique based on their printing principles (Hölzl et al., 2016; Gungor-Ozkerim et al., 2018). In the case of nozzle-based bioprinters, the viscoelastic properties and surface tension determine the capacity of the bioink to fluid and be dispensed through the nozzle (Seymour et al., 2017). To maintain high shape fidelity after printing and ensure uniform cell encapsulation, some formulations incorporate molecules which can be physically, chemically, photo-induced or enzymatically crosslinked. The production of toxic subproducts during the crosslinking process needs to be carefully evaluated to avoid cell damage (GhavamiNejad et al., 2020). Some bioinks present changes in their properties during the printing process, which need to be considered to guarantee the cellular survival and high shape fidelity of printed motifs. In some cases, materials respond to thermal changes or pressure. For instance, the viscosity of shear-thinning materials decreases under an applied force, and it recovers its initial values when the force is removed (Chopin-Doroteo et al., 2021).

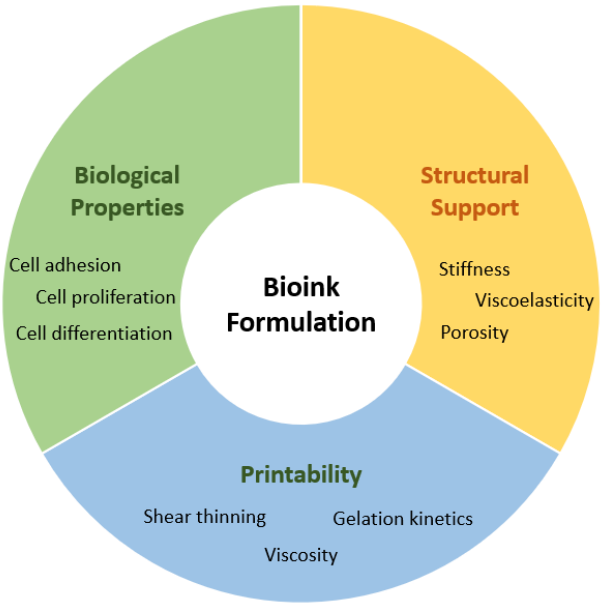

Figure 2. 6. Examples of fundamental bioink characteristics that need to be considered during their formulation. Bioinks must fulfill the bioprinter requirements and provide structural support to promote the native cellular behaviour.

2.3.1. Bioprinting Techniques

Based on their working principle, bioprinting technologies can be divided into four categories: laser, extrusion, inkjet and microvalve-based bioprinting (Moroni et al., 2018) (Fig. 2.7).

Laser-assisted Bioprinting

Laser-assisted bioprinting involves using a laser beam to transfer cells from a donor slide onto a substrate. When the laser pulse is absorbed by a conductive layer, a droplet of cell-encapsulated hydrogel is generated and propelled towards a collector slide (Dou et al., 2021). The position of the donor slide can be modified to produce pre-defined motifs. This technology allows the creation of patterns with single-cell resolution (Guillemot et al., 2010). Compared with other printing techniques, the absence of nozzle enables the printing of high cell densities of up to 10^8 cells per mL without affecting their viability (Table 2.4) (Koch et al., 2010; Guillotin et al., 2010). Printing resolution is influenced by diverse variables such as laser energy and pulse time, the distance between the donor and collector substrates, or the thickness and viscosity of the donor slide (Schiele et al., 2010). This technology is limited by the poor cell homogeneity obtained when using low cellular densities, as the presence of one cell per droplet is only ensured by incorporating high cell densities into the donor slide. Additionally, the possibility of transferring cytotoxic substances from the energy-absorbing layer constitutes the main concern (Melchels et al., 2010).

Different studies have proved the potential of this bioprinting technique to replicate skin, corneal and vascular structures (Koch et al., 2012; Sorkio et al., 2018; Gruene et al., 2011). However, the complexity, slow throughput and high costs of this technology have hindered its industrial implementation (Michael et al., 2013).

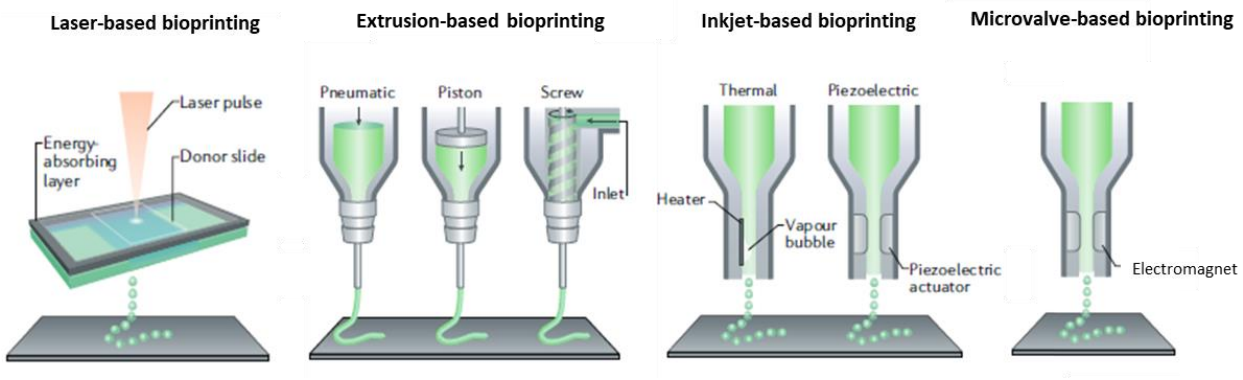

Figure 2. 7. Representation of the four main bioprinting technologies, including laser, extrusion, inkjet and microvalve-based bioprinting. Image adapted from Moroni et al 2019.

Extrusion-based Bioprinting

Microextrusion-based bioprinters employ mechanical and pneumatic forces to dispense cell-laden bioinks through a nozzle in a continuous manner (Fig. 2.7). Pneumatic mechanisms provide lower control over the bioink flow but allow the printing of broader bioink viscosities by controlling the air pressure (Ozbolat & Hospodiuk, 2016). Meanwhile, mechanical systems, like screw-based microextrusion, are capable of printing highly viscous bioinks with notable spatial control (Cohen et al., 2006). Different parameters like bioink viscosity, dispensing pressure or nozzle length and diameter influence the final printing resolution and determine the bioink printability (Cooke & Rosenzweig, 2021). The need for highly viscous inks results in the infliction of shear stresses on the cells, which can decrease their viability (Nair et al., 2009). Increasing the nozzle size and reducing the applied pressure makes it possible to reduce the shear stress values (Chang et al., 2008). However, the printing speed and resolution are also affected by these changes.

To solve these problems, bioinks can be formulated to allow their flow in the cartridge, followed by a change in their mechanical properties outside the nozzle. Shear thinning, thermal or photosensitive materials are some examples of this type of bioinks (Highley et al., 2015; Hölzl et al., 2016; Zheng et al., 2021). Alternatively, new extrusion bioprinters based on sacrificial materials have been developed in the last few years. In these new systems, the bioink is extruded into a support material that retains the material shape until the crosslinking process is completed (Shiwarski et al., 2021). Despite the reduction of cell stress, these new processes require prolonged printing times and are still under development.

Overall, extrusion-based bioprinting is a user-friendly technique, easy to implement and personalise by incorporating multiple nozzles with different bioinks (Rocca et al., 2018). Although this technology has enabled the generation of diverse biological structures, including vasculature, heart, skin and liver (Lee et al., 2014b; Maiullari et al., 2018; Pourchet et al., 2017; Nguyen et al., 2016), its application is limited by its printing resolution, slow throughput, and potential effect on cell viability (Table 2.4) (Derakhshanfar et al., 2018).

Inkjet-based Bioprinting

Inkjet bioprinting is based on the jetting of droplets containing cell suspensions onto a printing surface. The generation of droplets can be controlled by thermal or piezoelectric actuators (Fig. 2.7) (Gudapati et al., 2016; Saunders & Derby, 2014). The mechanism behind the piezoelectric system relies on voltage pulses to modify the piezoelectric crystal structure, which in turn generates enough pressure to expel the bioink through a nozzle at regular intervals. Meanwhile, thermal actuators are based on the raising of bioink temperature causing the formation of vapour bubbles, which expand until the ink droplets are ejected. The reduced exposition of the cells to high temperatures reduces the potential cellular damage.

The quality of the inkjet printing process relies on the nozzle diameter, bioink viscosity, pressure applied, and particularly on the valve opening duration (Derby, 2010). To ensure the droplet formation, the pressure must overcome the bioink surface tension at the nozzle orifice, preventing the bioink from leaking (Xu et al., 2014). The droplet deposition can be controlled by modifying the voltage waveform and its vibration frequency. These variables must be optimised for each bioink formulation to ensure droplet stability. In general, this technology provides a high printing control, with the possibility of printing volumes between the nanolitre and picolitre range and a high throughput rate (Table 2.4) (Singh et al., 2010).

Inkjet printing is limited by the need for bioinks with narrow viscosity ranges, from 3 to 30 mPa/s, which results in unstable printed structures. An additional crosslinking step is required before printing subsequent layers to ensure the support of 3D structures (Xu et al., 2013). Nebulisation of crosslinking agents or the use of photo-crosslinking polymers are usually incorporated to address this issue. Delays in the bioink gelation can cause the spreading of the printed bioink, incrementing the risk of cell drying during the printing process and compromising the cellular viability (Li et al., 2020). The use of nozzles with small diameters allows the printing of objects with better resolution than extrusion-based bioprinting (Lee et al., 2019; Miri et al., 2019). However, the reduced nozzle orifice can result in the formation of cell clogs, limiting the printing cell densities.

In summary, this technology allows a higher resolution and printing throughput than extrusion-based bioprinting (Ozbolat & Yu, 2013). Moreover, it provides the opportunity to incorporate cell gradients by altering the printing parameters (Xu et al., 2014; Miller et al., 2009). Nonetheless, the printing speed and resolution might be affected by the need for additional crosslinking steps.

Microvalve-based Bioprinting

In the same way as inkjet bioprinting, microvalve systems are based on the ejection of droplets onto a printing substrate (Ng et al., 2017). In this occasion, the droplet jetting is controlled by electromagnetic pulses, which induce a magnetic field in a solenoid coil to open the nozzle orifice by moving a piston (Fig. 2.7). In parallel, pneumatic pressure is applied through a gas regulator to generate the droplets. The droplet formation is controlled by the valve opening time (VOT) and printing pressure and depends on the nozzle diameter and bioink properties such as surface tension or viscosity (Okubo et al., 2019). Microvalve systems incorporate nozzles with a diameter ranging from 100 to 500 µm. The use of bigger nozzle orifices than inkjet bioprinting allows the printing of a broader range of bioink viscosities, from 1 to 200 mPa/s, without losing the microscale printing resolution, and ensuring a high printing throughput of approximately 1,000 droplets per second (Table 2.4) (Sun et al., 2009). However, the possibility of blocking the nozzle still restricts the printed cell densities to 10^6 cells per mL (Gudapati et al., 2016).

The cost-effectiveness and accessibility of this technology have driven their incorporation into the bioprinting of diverse tissue structures including the air-blood barrier, smooth-muscle and skin models (Horváth et al., 2015; Lee et al., 2014; Moon et al., 2010). However, the need for additional crosslinking steps after the printing process is also one of the main limitations of microvalve systems.

Table 2. 4. Differences between the main bioprinting approaches, including the required material viscosity and cell density, their resulting printing resolution and cell viability, as well as their cost, printing speed and their subsequent scalability.

	Laser-assisted	**Micro-extrusion**	**Inkjet Printing**	**Microvalve-based**
Material Viscosity	1 – 300 mPa/s	30 – 6 x10^7 mPa/s	3 – 30 mPa	1 – 200 mPa/s
Printing Resolution	High 20 – 80 µm	Medium 100 – 1000 µm	High 10 –100 µm	High 100 –500 µm
Cell Density	10^8 cells/ml	10^7 cells/ml	10^6 cells/ml	10^6 cells/ml
Cell viability	>95%	40 – 80%	>85%	>90%
Cost	Medium	Medium	Low	Low
Printing speed	Medium 200 – 1600 mm/s	Slow 10 µm/s – 700 mm/s	Fast 10,000 droplets per second	Fast 1,000 droplets per second
Scalability	Low	High	High	High

2.3.2. State-of-the-art of Skin Bioprinting

The feasibility of incorporating bioprinting systems into skin production was first evaluated by Lee *et al.* using an extrusion-based printer (Lee et al., 2009). Combining multiple cartridges, this group showed the possibility of creating stable multi-layered structures containing fibroblasts and keratinocytes. One year later, Koch *et al.* evaluated the use of laser-based bioprinters on the generation of skin models, demonstrating the functionality of printed cells and the absence of genetic alternations (Koch et al., 2009). Initially, these two techniques were the most popular for skin bioprinting. However, the complexity and limited printing speed associated with laser-based bioprinting resulted in its replacement by other drop-on-demand technologies like inkjet or microvalve-based systems (Kim et al., 2017; Min et al., 2018; Ng et al., 2018a).

Most studies concerning skin bioprinting have focused on developing skin structures suitable for wound treatments. The printing of tissue grafts containing autologous cells has demonstrated to accelerate the healing of large and deep wounds (Albanna et al., 2019; Desanlis et al., 2021). Moreover, the incorporation of additional cell types, such as pericytes or endothelial cells, has also helped to induce graft vascularisation, promoting its integration into the body (Baltazar et al., 2020). In other studies, further complexity has been accomplished with the generation of skin pigmentation in the injured site or the regeneration of hair follicles (Nanmo et al., 2022; Chen et al., 2022). Furthermore, the possibility of printing directly on the wound site has recently become a reality (Pazhouhnia et al., 2022; Hakimi et al., 2018). *In situ* bioprinting allows the uniform deposition of cells and biomaterials in non-flat surfaces, reducing the time and complications associated with graft transplantation.

The manufacturing of full-thickness skin models has gained interest in the last few years (Table 2.5). After initial optimisation studies, the first skin models presenting a complete epidermal stratification were published in 2016 (Pourchet et al., 2017; Cubo et al., 2016). The possibility of producing uniform skin pigmentation is one of the first milestones achieved by the bioprinting processes compared to manually seeded models (Min et al., 2018; Ng et al., 2018a). Later works have used these advances to recreate the hyperpigmentation present in natural skin age spots (Ignatov et al., 2022). The incorporation of additional cell types, such as umbilical vein endothelial cells (HUVEC) or human adipocytes, have helped to introduce vascularisation and the hypodermal recapitulation in the models (Kim et al., 2019; Jin et al., 2021). Reproduction of skin conditions such as atopic dermatitis has also been possible with

the incorporation of additional elements like monocytes, inflammatory molecules or induced pluripotent stem cells (Lègues et al., 2020; Liu et al., 2020). Despite the differences in the cellular content between models, most bioprinted skin equivalents are produced using collagen as support biomaterial (Lee et al., 2014; Min et al., 2018; Koch et al., 2012). In the last years, collagen have started to be replaced by fibrin-based gels combined with other natural materials or by biomaterials adapted to the bioprinting requirements like gelatin methacrylate (GelMA) (Barros et al., 2021; Jin et al., 2021; Pourchet et al., 2017). However, the impact of these choices on the reliability of bioprinted skin models has not been studied in depth.

Bioprinting processes have made possible the production of skin models closely resembling native skin structures. However, the formation of cornified epidermal layers has been reported in a limited number of studies (Min et al., 2018; Kim et al., 2019; Liu et al., 2022b). As mentioned previously, the correct epidermal stratification is essential for assessing skin interaction with external components. And further validation steps are required before incorporating these models into the product testing process. Only a few articles have demonstrated the presence of a complete functional epidermal barrier. In 2019, Derr *et al.* conducted the Trans Epidermal Electrical Resistance (TEER) technique for the first time to confirm the barrier function of their bioprinted skin models (Derr et al., 2019). Another recent study by Liu *et al*. also used this technique to confirm the presence of a protective barrier in their bioprinted atopic dermatitis model (Liu et al., 2020). In this work, the bioprinted models were applied to screen the effects of diverse treatments already tested in clinical trials, such as anti-inflammatory corticosteroids and kinase inhibitors. In parallel, Wei *et al.* reported the assessment of the irritation effects of topical compounds on bioprinted skin equivalents (Wei et al., 2020).

These previous studies reveal the potential of bioprinting to produce complex models suitable for product testing. Nonetheless, the automatisation of the skin production process and the requirements for their incorporation into the industry have not been properly considered. The implementation of bioprinting processes has not been reported yet to considerably reduce the time required for the production of the skin models of their maturation. In many studies, microvalves and extrusion techniques have required the incorporation of additional nebulisation steps to ensure the stability of the printed skin structures, increasing the overall manufacturing time (Min et al., 2018; Lee et al., 2010). Only the work performed by Cubo *et al*. has claimed the possibility of generating skin equivalents in 35 minutes using a

microextrusion-based system (Cubo et al., 2016). On the other hand, a new strategy was proposed by Kim *et al* to reduce the time and cost on the production of skin models. This group suggested the printing of transwell and skin models in one step to reduce by 50 times the manufacturing times (Kim et al., 2017). In the future, it will be necessary to ensure the full automatisation of the bioprinting process to allow its industrial scalability, reducing the time and cost associated with this practice.

Table 2. 5. Examples of the most relevant bioprinted skin models published to date, including the biomaterial and cells used for their production and the characteristics of the resulting models.

Technique	Cellular components	Biomaterials	Outcome	Reference
Extrusion-based bioprinting	Primary human fibroblasts, primary human keratinocytes	Gelatin, alginate, fibrin	Structural similarity to human skin Absence of corneal layer	Pourchet *et al*. 2017
Extrusion + Inkjet based bioprinting	Primary human fibroblasts, primary human keratinocytes	Collagen type I - PCL containing gelatin mesh	Skin model with stratified epidermis Reduction of costs by printing transwells	Kim *et al.* 2017
Microvalve-based bioprinting	Fibroblasts, keratinocytes and neonatal melanocytes	Collagen type I neutralised with sodium bicarbonate	Pigmented skin model with epidermal cornification	Min *et al.* 2018
Microvalve-based bioprinting	Fibroblasts, keratinocytes, and melanocytes	Collagen type I – PVP membrane	Pigmented skin model with epidermal cornification	Ng *et al.* 2018a
Extrusion-based bioprinting	Neonatal human fibroblasts, neonatal human keratinocytes	Gelatin, fibrin, collagen I, elastin Laminin/entactin	Skin model with functional epidermal barrier	Derr *et al.* 2019
Extrusion + Inkjet based bioprinting	Fibroblasts, keratinocytes, HUVEC, preadipocytes	Gelatin, dECM-fibrinogen bioink Transwell made of PCL	Gelatin, dECM-fibrinogen bioink Transwell printed with PCL	Kim *et al.* 2019
Extrusion-based bioprinting	Fibroblasts, keratinocytes, pericytes, endothelial iPSCs	Fibrin	Vascularised atopic dermatitis model with functional epidermal barrier used for drug testing	Liu *et al.* 2020
Extrusion-based bioprinting	Neonatal human fibroblasts, neonatal human keratinocytes	Fibrin, collagen, fibronectin	Skin model with functional epidermal barrier used for irritation tests	Wei *et al.* 2020

2.3.3. Reactive Jet Impingement System

Bioprinting techniques are one of the main restrictive factors on the properties and scalability of skin model production. Therefore, selection of a suitable bioprinting technology can become in a key factor on the manufacturing of skin models for product testing. In this project, a novel bioprinting system named Reactive Jet Impingement (ReJI) is introduced. This technology was developed by Newcastle University researchers with the aim of overcoming some of the limitations found in conventional bioprinting techniques (da Conceicao Ribeiro, 2019).

ReJI system is based on the jetting of two liquid precursors from two opposite microvalves (Fig. 2.8). The ejected droplets meet and react in mid-air, generating a gel before reaching the printing surface. The fast gelation of the liquid droplets allows the encapsulation of the cells and their protection before their arrival to the plate.

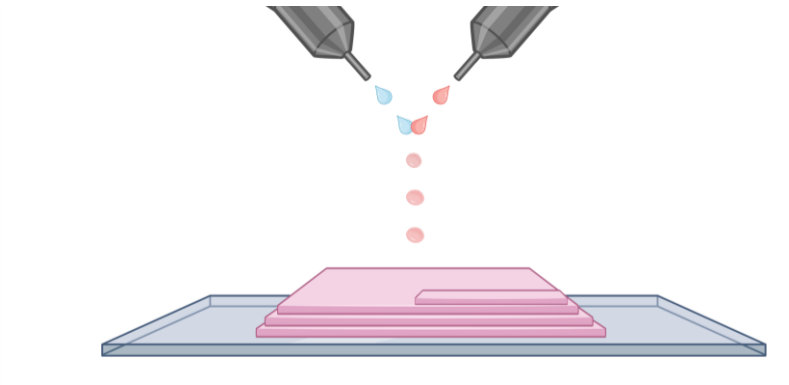

Figure 2. 8. Schematic representation of Reactive Jet Impingement system (ReJI). This bioprinting technology is based on the jetting of two liquid precursors which meet and crosslink in the mid-air producing a solid gel before reaching the printer bed. Image designed using Biorender.com.

ReJI system combines the advantage of microvalve and extrusion-based techniques. On the one hand, the use of low viscous precursors allows the formulation of complex bioinks and the reduction on shear stress over the cells during the printing process. On the other hand, the fast crosslinking between the ink precursors provides stability to the printed structure without losing resolution and facilitates the production of multi-layer structures without conventional waiting times. Furthermore, the development of this printing system in-house facilitates the customisation and optimisation of the printer components based on the requirements for the

generation of tissue models. This customisable character could be an advantage for future scalability and incorporation into the industry of this printing technology.

ReJI system has already been implemented in the production of other biological models, such as bone or cartilage micro-tissues (Kotlarz et al., 2022; da Conceicao Ribeiro et al., 2018). In these previous studies, ReJI process has demonstrated its ability to produce robust structures with high fidelity and reproducibility. Moreover, this system has proved to print high cell densities of up to 90 million cells per mL without affecting their viability. By incrementing the number of cells to their physiological level, it was possible to observe an early expression of genes associated with mature tissue and the enhanced production of new extracellular matrix after a few days. These results suggest the acceleration of the tissue maturation compared to models obtained with conventional bioprinting techniques.

CHAPTER 3. PROJECT AIM AND OBJECTIVES

Despite the potential of conventional bioprinting process to automatise and improve the control in the production of *in vitro* skin equivalents, the long production times and the limited reliability of the resulting skin models restrict their industrial application as alternative to animal experimentation. As a solution to this problem, this PhD thesis proposes for the first time the implementation of Reactive Jet Impingement system (ReJI) in the manufacturing of human skin equivalents. The ability of this technology to generate stable construct containing high cell densities could help to improve the model quality and reduce the time required to develop skin equivalents, facilitating their large-scale production and the industrial scalability of the process.

On the other hand, the choice of bioink components also plays an essential role in the resemblance of the generated skin layers to the native tissue. Due to the lack of consensus on the best biomaterials for the recreation of skin *in vitro* and the objective of improving the complexity of skin models, this research project explores the impact of diverse bioinks based on natural skin materials. The effect of the bioink formulations on the cellular behaviour and their capacity to mimic the physiological characteristics of each skin layer are explored.

Considering all these elements, this PhD thesis aims to optimise the production of skin equivalents to obtain more reliable models adapted to the industrial requirements. To accomplish this project aim, the following goals were defined:

1. To explore the advantages and limitations of a novel bioprinting technology named Reactive Jet Impingement (ReJI) on the generation of skin structures and to assess its potential scalability.
2. To formulate dermal bioinks adapted to the printer requirements and capable of mimicking the diverse dermal micro-environments found in human skin.
3. To develop epidermal bioinks adapted to the printer requirements and capable of improving the homogeneity and the quality of skin epidermal layers.
4. To implement the formulated bioinks, along with the ReJI bioprinting process, in the manufacturing of *in vitro* skin equivalents to determine their benefits in enhancing the quality and scalability of the final models.

CHAPTER 4. MATERIALS AND METHODS

4.1. Introduction

The methodology followed in this project is divided into nine defined categories:

The first two sections describe the formulation of dermal and epidermal bioinks, and the diverse characterisation methods employed to assess the physicochemical and mechanical differences between these bioinks.

Section 4.4 introduces the protocols followed for the culture of fibroblasts and keratinocytes, and the steps required to produce dermal, epidermal and skin models.

Subsequently, the different biological studies performed to evaluate the impact of the dermal and epidermal bioinks on the fibroblast and keratinocyte behaviour are described in sections 4.5, 4.6 and 4.7. These studies include quantitative assays, three-dimensional imaging of the different models and immunostaining of tissue sections.

The setting up and optimisation of the ReJI process are detailed in section 4.8, along with the parameters utilised for printing dermal, epidermal and skin models using this technology.

Finally, the statistical analysis performed on the obtained results is detailed in the last section.

4.2. Biomaterial Development

4.2.1. Formulation of Dermal Bioinks

To evaluate the impact of biomaterials on the recreation of the dermal layer and assess their printability, two types of dermal bioinks based on collagen type I and fibrin were formulated.

Collagen type I from different animal sources were selected to study their differences and impact on the final properties of dermal models. They included collagen type I solutions from rat tail (Institut of Biotechnologies Jacques Boy), bovine tendons (Collagen Solutions Plc.), calf skin (Sigma-Aldrich) and jellyfish (Jellagen Pty Ltd.). Collagen type I from human placenta (Corning Inc.) was selected as control sample. All these commercial collagen solutions were extracted employing acid treatments. An additional sample of bovine collagen obtained by pepsin treatments, named atelo-bovine collagen, was included in these studies to determine the impact of the extraction method (Collagen Solutions Plc.). Collagen gels were prepared by neutralising the collagen solutions to a physiological pH of 7.4 followed by their incubation at 37°C. The neutralisation process was optimised for each of collagen solutions to ensure a higher control over the gelation process and the generation of homogeneous gels. The effect of the neutralisation method on the collagen matrix was evaluated by comparing collagens neutralised with 0.1M NaOH in phosphate buffered saline (PBS) and 7.5% NaHCO3 in distilled water. The final concentration of all collagen gels was adjusted to 2.5mg/mL using PBS.

Additionally, the effect of incorporating a new commercial method called RAFT^{TM} absorption system (Lonza) on the production of collagen gels was assessed (Fig. 4.1). This system was tested in rat collagen gels to determine its impact on the matrix organization. Rat collagen solutions were neutralised with 0.1M NaOH and 7.5% $NaHCO_3$ and incubated for 1 hour at 37°C before applying the RAFT^{TM} system. Subsequently, RAFT^{TM} membranes were placed on top of the gels for 30 minutes, ensuring the removal of the excess of water from the collagen hydrogels by the absorbers without affecting the collagen gel integrity.

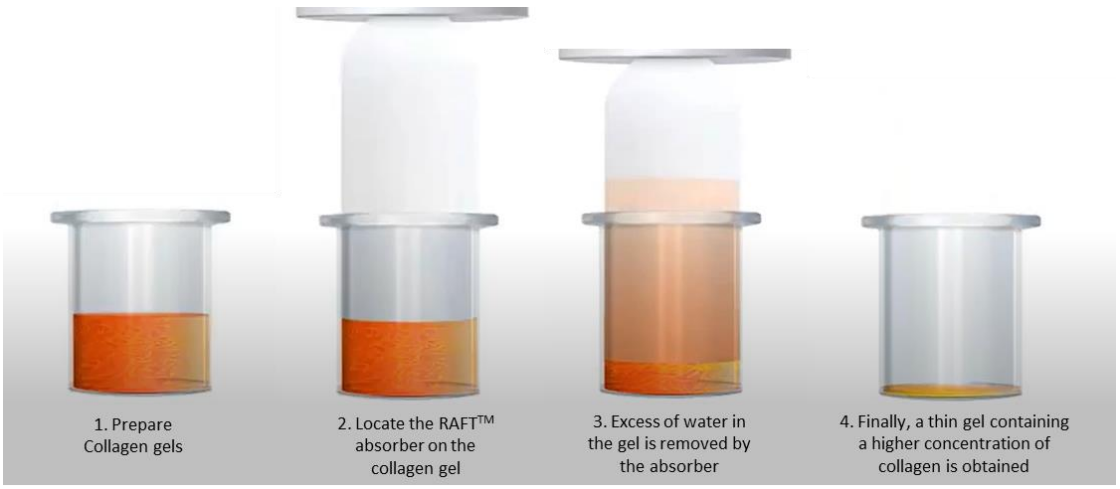

Figure 4. 1. Representation of the RAFT™ system on the production of dermal models. The contact of RAFT™ absorbers with collagen gels allows the removal of the water excess, resulting in the enhancement of the final collagen concentration and the reduction of the gel thickness without affecting its integrity. Image obtained from Lonza Bioscience Ltd. (D'Souza et al. 2017).

In previous studies, the formulation of a gel that combined fibrin with collagen and alginate (CAF) was optimised for its printability using ReJI system (da Conceicao Ribeiro, 2019). Due to its printability and the presence of two important skin biocomponents in its formulation, such as fibrin and collagen, CAF gel was considered a biomaterial of interest for this study. The production of CAF gels requires the formulation of two differentiated bioinks, a gel precursor and a gel crosslinker, capable of quickly reacting and generating a stable gel. CAF gel precursor was prepared by mixing 6mg/mL atelo-bovine collagen (Collagen Solutions Ltd.), 2.5% sodium alginate (Sigma-Aldrich) and 37mg/mL bovine fibrinogen (Sigma-Aldrich) in a 1:2:8 volume ratio. The gel crosslinker was formulated with 50U bovine thrombin in Advanced Dulbecco's Modified Eagle Medium (DMEM) with 0.1% $CaCl_2$ (Sigma-Aldrich). Based on the initial experimental results, thrombin concentration was modified from the original formulation from 500U/mL to 50U/mL to avoid the quick degradation of CAF gels by fibroblasts and improve the model stability and reproducibility. To generate the fibrin gels, an equal volume of gel precursor and crosslinker were mixed and incubated at 37°C.

To explore the role of each CAF component on the dermal models, the formulation of bioinks containing only fibrin, only alginate and only collagen, as well as those formulated with fibrin mixed with collagen, fibrin mixed with alginate and alginate mixed with collagen were evaluated. These gels were produced maintaining the same final concentration of their individual components and the ratio between them. The incapacity to produce gels with only alginate, collagen or alginate mixed with collagen at the selected concentrations made

impossible their use for the generation of dermal models. The formulation of the finally selected fibrin-based gels is described in Table 4.1.

Table 4. 1. Concentrations and volumes of collagen type I, sodium alginate, fibrinogen and PBS used during the formulation of fibrin-based gel precursors.

Gel Precursor	6 mg/mL Collagen type I	2.5% Sodium Alginate	37 mg/mL Fibrinogen	PBS
CAF (1:2:8)	0.091 mL	0.181 mL	0.727 mL	-
CF (1:8)	0.091 mL	-	0.727 mL	0.181 mL
AF (2:8)	-	0.181 mL	0.727 mL	0.091 mL
F (:8)	-	-	0.727 mL	0.272 mL

4.2.2. Formulation of Epidermal Bioinks

The effect of keratinocyte encapsulation on their behaviour and epidermal formation was assessed by formulating five different bioinks based on alginate, fibrin and collagen.

Gels containing only fibrin were prepared by mixing 27mg/mL and 13 mg/mL bovine fibrinogen (Sigma-Aldrich) with 50U of bovine thrombin in DMEM, respectively. The effect of combining fibrin with collagen and alginate was explored by preparing CAF gels following the instructions described in the section 4.1.1. Meanwhile, collagen gels were prepared by neutralizing 6 mg/mL of bovine collagen with 0.1M NaOH to a pH value of 7.4. Finally, alginate gels were produced by mixing 2.5% sodium alginate precursor with different concentrations of calcium chloride. The effect of calcium ions on the final alginate gels was studied by comparing the crosslinking of alginate with 0.1% and 1% $CaCl_2$ solutions.

4.3. Biomaterial Characterisation

4.3.1. Chemical Analysis by Fourier Transferred Infrared Spectroscopy

Attenuated Total Reflection Fourier Transform Infrared Spectroscopy (ATR-FTIR) spectrometer was used to analyse the differences on the chemical composition of collagen solutions based on their animal source and extraction method. Collagen solutions were freeze-dried for 24 hours to remove their water content before their analysis. Their chemical spectra in the range of 750 to 2000 cm^{-1} was obtained using a PerkinElmer UATR-Two spectrometer.

4.3.2. Measurement of Triple Helix Content by Circular Dichroism

The triple helix content of collagen solutions and its thermal degradation in collagen solutions and gels were measured using a Jasco J-810 spectropolarimeter. Collagen solutions were diluted to a final concentration of 0.1 mg/mL with 0.02M acetic acid solution to maintain an acidic pH and avoid collagen precipitation. Collagen gels were diluted to a final concentration of 0.1 mg/mL using 1xPBS to maintain their structural conformation. Samples were loaded into a 0.1 mm path-length quartz cuvette (Hellma), and all measurements were corrected for buffer baseline to reduce background noise.

Circular dichroism spectra was measured in the range of 200 to 250nm maintaining a temperature of 4°C. Triple helix content was calculated by studying the values obtained at its characteristic wavelength of 222nm. Meanwhile, degradation of the triple helix structure was assessed by increasing the temperature from 4°C to 60°C, performing the measurements at a constant wavelength of 222nm.

4.3.3. Characterization of Dermal Matrix by Scanning Electron Microscopy

The micro-scale fibrillar organisation of dermal gels and their porosity were characterised by Scanning Electron Microscopy (SEM). Acellular collagen and fibrin-based gels were prepared and incubated at 37°C for 24 hours and subsequently fixed in 2% glutaraldehyde overnight at 4°C. Afterwards, gels were dehydrated by their incubation in serial dilutions of ethanol. Finally, gels were critically point dried using a Baltec Critical Point Dryer and coated with 15 nm gold layer using a Polaron SEM coating unit before their imaging with a Tescan Vega 3LMU Scanning Electron Microscope. Images were taken in at least five different areas to ensure the reliability of the analysis.

4.3.4. Rheological Studies

Fibrillogenesis and mechanical properties of collagen and fibrin-based gels were studied using a Discovery Hybrid Rheometer (TA Instruments) with a 20mm parallel plate, maintaining a 900µm gap.

To evaluate the gelation process, gel precursors and crosslinkers were added to the rheometer plate to a final volume of 0.4mL just before the start of the measurement. The gelation profile was measured by increasing the temperature from 4°C to 37°C in the case of collagen gels, and from 20°C to 37°C in the case of fibrinogen. The changes in the storage modulus (G') over time were recorded, maintaining a strain value of 1% and a frequency of 1Hz.

To evaluate the final mechanical strength of the samples, gels were prepared and incubated at 37°C for 24 hours before proceeding to their analysis. The stiffness values were assessed by measuring their storage modulus (G') at a strain value of 1% and a frequency of 1Hz, maintaining a temperature of 37°C.

Additional measurements were also performed to understand the response of dermal gels against external stimulus. The variations on the storage modulus (G') and loss modulus (G'') after the increase on the angular frequencies were measured to determine the capacity of the matrix to be remodelled. These studies were performed at 37°C, using an angular frequency range from 0.1 to 100 rad/s and maintaining a strain value of 1%.

4.4. Cell Culture

4.4.1. General Cell Culture

All cell culture procedures and biological assays were performed in aseptic conditions using sterile materials and a Class 2 Safety Cabinet, previously decontaminated with 70% ethanol.

4.4.2. Passaging of Neonatal Human Fibroblasts

Neonatal Primary Normal Dermal Human Fibroblasts (NHDF) from ATCC were grown in Advanced Dulbecco's Modified Eagle Medium (DMEM) (Gibco, Thermal Fisher Scientific) supplemented with 10% fetal bovine serum, 1% GlutaMaxTM (Fisher Scientific) and 1% penicillin/streptomycin (Sigma-Aldrich) in an incubator at 37°C and 5% CO_2. Fibroblasts were split when they reached 70-80% of confluency. Briefly, fibroblasts were passaged by first washing them with Dulbecco's phosphate-buffered saline (PBS) without calcium or magnesium and, subsequently, incubating them with 0.25% Trypsin-EDTA solution (Sigma-Aldrich) for at least 3 minutes at 37°C and 5% CO_2. After confirming cells were completely detached from the flask, trypsin was neutralised with DMEM, and the cell suspension was centrifuged at 1200 rpm for 5 minutes. The supernatant medium was removed, and the cell pellet was resuspended in DMEM. Cells were counted using a 0.1mm depth Neubauer chamber haemocytometer (Hawksley), and DMEM volumes were adjusted to transfer fibroblasts to tissue-culture flasks at a density of 10,000 cells/cm^2. Neonatal dermal human fibroblasts were used within passages 8-10 for all the biological assays and corresponded to the same lot number.

4.4.3. Passaging of Neonatal Human Keratinocytes

Neonatal Primary Normal Epidermal Human Keratinocytes (NHEK) (Caltag Medsystems Ltd.) were grown in EpiLife™ medium with 60µM calcium, supplemented with human keratinocyte growth supplement (Thermo Fisher Scientific) and 1% penicillin/streptomycin at 37°C and 5% CO_2.

During the thawing of keratinocytes from liquid nitrogen, 10µM of Y-27632 dihydrochloride (ROCK Inhibitor) (Tocris) was incorporated into the EpiLife medium, to support the

proliferation and avoid the early differentiation of keratinocytes. After one day of incubation, the cell medium containing ROCK inhibitor was removed, and the cells were washed with PBS before incubating them with a standard supplemented EpiLife medium.

Keratinocytes were passaged when they reached a cell confluency lower than 70% to avoid their differentiation. Briefly, keratinocytes were passaged by washing them with Dulbecco's phosphate-buffered saline (PBS), before proceeding to their incubation with Accutase® solution (Sigma-Aldrich) for 10 minutes at 37°C and 5% CO_2. After confirming keratinocytes were detached from the flask, accutase was neutralised with EpiLife medium, and the cell suspension was centrifuged at 2800 rpm for 5 minutes. Then, the supernatant medium was removed, and the cell pellet was resuspended in EpiLife medium. Cells were counted using a 0.1 mm depth Neubauer chamber haemocytometer (Hawksley), and EpiLife medium volumes were adjusted to transfer keratinocytes to tissue-culture flask at a density of 5,000 cells/cm^2. Neonatal epidermal human keratinocytes were utilised within passages 9-11 for all the biological assays and corresponded to the same lot number.

4.4.4. Seeding of Dermal Models

The effect of the bioink formulation on the dermal model reliability was assessed by incorporating fibroblast into the dermal bioinks. Dermal gels were prepared following the steps described in section 4.1.1.

In the case of dermal models based on collagen type I, 50,000 fibroblasts were encapsulated inside each collagen gels a few seconds after their neutralisation and before the complete collagen gelation to ensure its homogeneous distribution. Similarly, RAFT™ systems were used for the production of dermal models. Following the manufacturer's instructions, collagen gels containing 50,000 fibroblasts were incubated for 1 hour at 37°C for their complete crosslinking before applying the RAFT™ absorbers on them for 30 minutes to reduce the water excess and rise the collagen concentration. In the case of fibrin-based gels, 50,000 fibroblasts were introduced to the gel crosslinker solution containing thrombin, ensuring the number of fibroblasts encapsulated per gel was the same as in the collagen gels. In all cases, gels were seeded in tissue cultured-treated 48 well plates (Corning Inc.), maintaining a final gel volume of 400µL. Additionally, 50,000 fibroblasts were seeded as two-dimensional control.

All dermal models were incubated at 37°C and 5% CO_2, and DMEM medium was changed every 48 hours. Samples were fixed after 1, 3 and 7 days. The specific fixation method for each biological assay is described in the following sections.

4.4.5. Seeding of Epidermal Models

The impact of the epidermal bioink components on the keratinocyte behaviour was assessed by encapsulating the keratinocytes on the epidermal gels. All epidermal bioinks were formulated following the steps described in section 4.1.2. Fibrin-based gels were produced incorporating keratinocytes into the crosslinking solution. Whereas, keratinocytes resuspended in EpiLife medium were encapsulated in bovine collagen gels after their neutralisation with 0.1M NaOH. In the case of alginate-based inks, keratinocytes were resuspended in a crosslinking solution containing EpiLife medium with 0.1% and 1% $CaCl_2$, respectively. In all cases, 50,000 keratinocytes were encapsulated per gel in 48 well plates (Corning Inc.), maintaining a final gel volume of 200 µL. Additionally, 50,000 keratinocytes were seeded as two-dimensional controls. An additional control was introduced to assess the effect of calcium ions on the keratinocyte functionality. This control was based on keratinocytes cultured in EpiLife medium containing 1% $CaCl_2$.

All Epidermal models were incubated at 37°C and 5% CO_2, and EpiLife medium was changed every 48 hours. Samples were fixed after 1, 3, 7 and 14 days. The specific fixation method for each biological assay is described in the following sections.

4.4.6. Development of Skin Models

Thincert inserts for 12 well plates with 0.4µm pore diameter (Greiner Bio-One) were selected as support for the skin models. The dermal layer was prepared using bovine collagen gels neutralised with 0.1M NaOH and 50,000 fibroblasts encapsulated. The resulting dermis was cultured under immersed conditions for three days in DMEM to ensure fibroblast adaptation to the dermal matrix. Subsequently, DMEM was removed, and keratinocytes resuspended in 200µL of EpiLife medium were uniformly seeded on top of the dermal structure. Initially, the effect of incorporating different keratinocytes densities including 100,000; 250,000 and 500,000 keratinocytes per model on the correct formation of a stratified epidermis was

studied. To ensure the adhesion and boost the keratinocyte proliferation, 10µM of Y-27632 were incorporated into the EpiLife medium during the first 24 hours of incubation. Then, models were washed with PBS, and new EpiLife medium was added to the models and was constantly replaced every 48 hours. After seven days of seeding the keratinocytes, skin models were exposed to the air-liquid interface by removing the media from the top of the models. Additionally, the calcium chloride concentration in the EpiLife medium was increased from 60µM to 1.64mM to ensure complete keratinocyte differentiation. The models were incubated at 37°C and 5% CO_2 during the process. The progression of the epidermal layer formation was assessed by fixing the models after 14 and 21 days of seeding the keratinocytes.

The effect of the dermal bioinks on the properties of the skin models was assessed by producing skin models using different collagen and fibrin-based gels. Rat, telo-bovine and atelo-bovine collagen neutralised with 0.1M NaOH and 7.5% $NaHCO_3$ were selected as collagen-based dermal layers, incorporating 50,000 fibroblasts per gel. After their incubation for three days, 250,000 keratinocytes were seeded on top of these dermal constructs. The subsequent steps in the production of skin models were as described previously. In the case of fibrin-based dermal layers, the protocol for skin model production had to be modified due to the quick degradation of fibrin by keratinocytes. On this occasion, skin models were incubated using EpiLife medium containing 200U/mL of aprotinin (Sigma-Aldrich) to ensure their stability. Keratinocytes seeded in a tissue culture-treated plate were used as control to evaluate the effect of aprotinin on the keratinocyte proliferation and differentiation. Models were fixed after 14 and 21 days of seeding the keratinocytes.

The effect of keratinocyte encapsulation on the epidermal formation during the skin model maturation was assessed by incorporating fibrin-based epidermal gels. Skin models were prepared using the standard protocol described initially. Briefly, the dermal layer was comprised of bovine collagen gels containing 50,000 fibroblasts. After three days of incubation, the epidermal bio-inks were prepared encapsulating 250,000 keratinocytes per model, and were homogeneously dispensed on top of the dermis to generate the epidermal layer. After seven days, skin models were exposed to the air-liquid interface by removing the media from the top of the models and incorporating the differentiating cell media. Models were fixed after 14 and 21 days of seeding the keratinocytes.

4.5. Biological Assays

4.5.1. Cell Counting

Trypan blue solution (Sigma-Aldrich) was used to quantify the number of viable cells before their seeding. This method is based on the interaction of trypan blue dye with the cytoplasm of cells, allowing the selective staining in blue of dead cells with disrupted cell membranes. Before proceeding to the cell counting, the cell suspension was mixed with an equal volume of 0.4% trypan blue solution. Then, the percentage of viable cells was quantified using a 0.1mm depth Neubauer chamber haemocytometer (Hawksley) after considering the dilution factor.

This method was also used during the quantification of printed cells. However, on this occasion, cells were quantified using a Countess Automated Cell Counter (Thermofisher). Manual counting using the chamber haemocytometer was utilised only to validate the data obtained from the cell counter.

4.5.2. Quantification of dsDNA Content by Picogreen Assay

Initial quantitative experiments performed in 3D gels, including the measurement of metabolic activity by Alamar Blue (Sigma-Aldrich) or CellTiter-Glo® (Promega) assays, resulted in inaccurate values due to the inconsistent diffusion of reagents through the gels. As a solution to this problem, the degradation of the gels before performing quantitative assays was explored. The incubation of gels using proteinase k was selected as the best degradation method.

Proliferation of fibroblasts in the dermal gels was assessed by assessing the variations on the double-stranded DNA (dsDNA) content in the dermal layers over time. Dermal models were first fixed on days 1, 3 and 7 by storing the gels at -80°C. On the day of the assay, gels were incubated with 0.3mg/mL proteinase k in RLT buffer (Qiagen) at 37°C for 30 minutes to complete their digestion and stabilise the released DNA content. dsDNA quantification was performed using the commercial Quant-iT™ PicoGreen™ dsDNA Assay kit (Thermo Fisher Scientific). Following the manufacturer's instructions, 200 µL of cell lysate was incubated with 200 µL of PicoGreen working solution for 10 minutes at room temperature. Three replicates containing 100µL of each sample were transferred to 96 black well plates. A standard curve of known fibroblast concentrations was performed to correlate the fluorescence signal with the

amount of fibroblasts present in the samples. Fluorescence intensity was measured at 485nm excitation and 520m emission wavelengths using a FLUOstar Omega microplate reader (BMG Labtech).

4.5.3. Gene Expression Analysis by Quantitative Polymerase Chain Reaction

The expression of genes associated with fibroblast reticular and papillary phenotypes and proteins present in the dermis were evaluated through Real-Time Quantitative Reverse Transcription Polymerase Chain Reaction (RT-PCR). Primer sequences complementary to the human genes DCN, VCAN, MMP1, COL1A1, COL3A1, FN1 and ELN, were purchased from Bio-Rad to perform this study. RT-PCR was also utilised for confirming the presence in the produced skin models of specific molecules of each epidermal layer and the dermal-epidermal junction. The selected human genes on this occasion were KRT14, KRT10, IVL, FLG, CLDN1 and COL4A1. In addition, primers associated with the human genes GADPH and PSMC4 were selected as housekeeping genes. All primers were purchased as PrimePCR SYBR Green Assays from Biorad Inc.

Dermal models were incubated for 1, 3 and 7 days, before storing the samples at -80°C to preserve the RNA content for the RT-PCR studies. In the case of skin equivalents, models were fixed after 14 and 21 days after seeding the keratinocytes. The different models were degraded following the steps described in section 4.5.2, incubating the gels with proteinase k in RLT buffer. Subsequently, RNA was precipitated using ethanol and isolated in a RNeasy column following the steps described in the RNeasy® Fibrous Tissue Mini kit (Qiagen) instructions. Briefly, RW1 washing buffer was used to remove any biomolecules such as carbohydrates, proteins or fatty acids remaining in the RNeasy column. DNA present in the sample was degraded by incubating the samples in an RDD solution containing DNase. Finally, RPE buffer containing ethanol was used to wash the membranes before precipitating the RNA from the column using DNA-free water. The concentration of the extracted RNA was measured using a NanoDrop Spectro-photometer (Thermo Fisher Scientific).

Complementary DNA (cDNA) was synthesised using iScript cDNA synthesis kit (Bio-Rad Inc.). Following the manufacturer's instructions, the reaction mix was prepared by mixing 2 µL of 5x iScript reaction mix with 1 µL of iScript reverse transcriptase and 500ng of mRNA extracted. The reaction mix was annealed for 5 minutes at 25°C and extended at 46°C for 20 minutes in

a thermal cycle. Finally, the reverse transcriptase was inactivated, incubating the samples at 95°C for 1 minute. Samples were held at -4°C before performing the reverse-transcription process; alternatively, they were stored at -80°C to avoid cDNA degradation. A DNA-free water sample was used as a negative control to ensure the absence of contamination on the iScript cDNA synthesis kit.

SsoAdvanced™ Universal SYBR® Green Supermix (Bio-Rad Inc.) was selected for the RT-PCR. Following the manufacturer protocol, a reaction mix was prepared in ice with 0.5 µL of the primer of study, 5 µL of SsoAdvance universal supermix and 25 ng of cDNA sample. In this case, two types of negative controls were incorporated into this process. On the one hand, primers were substituted with DNA-free water to test the presence of contamination on the supermix. On the other hand, the SsoAdvance universal supermix was replaced by DNA-free water to detect any potential signal from the primers. Samples were submitted to the following thermal cycle (Table 4.2), and the resulting signals were quantified using a ViiA™ 7 Real-Time PCR System (ThermoFisher) with a 384-well block.

Table 4. 2. RT-PCR thermal cycling protocol including the activation, denaturation, annealing and melting steps.

Step	**Temperature**	**Time**
Activation	50°C	2min 1 cycle
	95°C	2min 1 cycle
Denaturation	95°C	5sec 40 cycles
Annealing	60°C	30sec 40 cycles
Melt Curve	95°C	15sec 1cycles
	60°C	15sec 1cycles
	60°C – 95°C (0.5°C increment)	5sec/step 1 cycle

4.6. 3D Imaging of Biological Samples

4.6.1. Cell Viability Assay

LIVE/DEAD® viability kit (Invitrogen TM, Thermo Scientific) was used to determine the viability of fibroblasts and keratinocytes after being printed with different densities, including 5 million, 1 million and 0.5 million cells/mL. Similarly, the distribution of live and dead fibroblast within printed CAF gels containing 0.5 million and 5 million cells/mL was studied. After cultivating the models for 1, 3 and 7 days, samples were incubated in 10 µM Calcein-AM and 4µM ethidium homodimer-1 in PBS for 1 hour, following the manufacturer's instructions. Immediately after the staining, three-dimensional maps of each sample were obtained using the confocal microscope Nikon A1R at 4x and 10x magnification.

This assay was also performed on the epidermal bioinks to determine the viability and distribution of keratinocytes after 1, 3 and 7 days of their encapsulation. Samples were incubated with 10 µM Calcein-AM and 4µM ethidium homodimer-1 in PBS for 1 hour. On this occasion, stained keratinocytes were visualised using an EVOS M5000 imaging system (ThermoFisher).

4.6.2. Study of Fibroblast Morphology and Distribution by Immunostaining

Fibroblast distribution and their morphology in the printed and manually seeded dermal models were characterised by staining the cytoskeletal filamentous actin (F-actin) using rhodamine-phalloidin.

Samples were fixed after 1, 3 and 7 days in 4% paraformaldehyde (Thermo Fisher Scientific) for 24 hours and maintained at 4°C. Then, the models were permeabilised with 0.1% Tween-20 in PBS and 2% bovine serum albumin (BSA) (Sigma-Aldrich) for 1 hour. Subsequently, samples were incubated with 1:100 rhodamine-phalloidin (Thermo Fisher Scientific) for 1 hour. Finally, samples were incubated with 1:1000 4,6-diamidino-2-phenylindole (DAPI) for 30 minutes to stain the cell nucleus (Sigma-Aldrich). Nikon A1 confocal microscope was used to visualise the gel volume at 10x magnification, and images were taken in at least five different regions to obtain representative results.

4.6.3. Characterisation of Cellular Matrix by Scanning Electron Microscopy

The distribution of fibroblasts within the printed and manually-seeded CAF gels and the variations on the extracellular matrix components over time were imaged using a Tescan Vega 3LMU SEM. CAF models were printed with ReJI system using 500,000 and 5,000,000 fibroblasts per mL. After 1, 3 and 7 days, samples were fixed in 4% paraformaldehyde for 24 hours at 4°C before proceeding to its fixation with 2% glutaraldehyde solution at 4°C overnight, and subsequent dehydration in serial dilutions of ethanol. Before their imaging, samples were critically point dried using a Baltec Critical Point Dryer and coated with 15nm gold-layer using a Polaron SEM coating unit. Images were taken in at least five different areas to ensure the reliability of the samples.

4.6.4. Evaluation of Epidermal Biomarkers by Immunostaining

Epidermal models were fixed after 1, 3, 7 and 14 days to study the phenotypic changes experienced by encapsulated keratinocytes. Samples were initially fixed with 4% paraformaldehyde (Sigma-Aldrich) for 24 hours at 4°C.

Proceeding with the immunostaining, models were washed with PBS and permeabilised with 0.1% Tween-20 in PBS and 2% bovine serum albumin (BSA) (Sigma-Aldrich) for 1 hour. Afterwards, sections were washed with PBS and incubated overnight at 4°C with 1:250 final dilution of anti-cytokeratin 14 antibody (ab181595), anti-involucrin antibody (ab53112) (Abcam) or filaggrin antibody (sc-80609) (Santa Cruz Biotechnology), respectively. After the incubation, the models were washed with 0.1% Tween-20 in PBS and 2% bovine serum albumin (BSA) (Sigma-Aldrich) and incubated with a 1:1000 final dilution of Goat Anti-Rabbit IgG Alexa Fluor® 488 (ab150077) and Donkey Anti-Mouse IgG Alexa Fluor® 568 (ab175472), where corresponding, for a minimum of 4 hours at 4°C. Finally, samples were incubated with 1:1000 4,6-diamidino-2-phenylindole (DAPI) for 30 minutes to stain the cell nucleus (Sigma-Aldrich). EVOS M5000 imaging system was used to image the sections at 10x and 20x magnification.

4.7. Immunostaining of Tissue Sections

4.7.1. Cryosection of Dermal and Skin Models

Dermal and skin models were fixed in 10% formalin (Sigma-Aldrich) for 24 hours at 4°C. Subsequently, the models were transferred to cryomolds and embedded in an optimal cutting temperature (OCT) compound (Agar Scientific). The embedded models were frozen in dry ice and stored at -80°C. Cryo-preserved models were sliced into 10 µm sections using a Leica CM1950 cryostat and transferred to SuperFrost® Plus slides. Sections were kept at -80°C until their use.

4.7.2. Paraffin Embedding of Skin Models

Skin models were fixed in 10% formalin for 24 hours at 4°C. The models were dehydrated through their incubation in serial dilutions of ethanol. Afterwards, the models were permeabilised using different dilutions of xylene with ethanol before proceeding to the paraffin-embedding process. This last step and the sectioning of tissue blocks were performed by specialised personnel from the Newcastle University Biobank.

4.7.3. Haematoxylin and Eosin Staining of Skin Sections

Haematoxylin and eosin (H&E) staining of skin models was performed to determine the structural organisation of the produced models. Initially, slides containing cryo-sectioned skin models were thawed at room temperature for 30 minutes before the staining. Sections from paraffin-embedded samples were deparaffinised using Histoclear solution (Thermo Fisher Scientific) and were gradually dehydrated in ethanol before their staining.

For the H&E staining of the produced model, sections were incubated in filtered Mayer's haematoxylin solution (Sigma-Aldrich) for 5 minutes and rinsed in water for 30 seconds before their incubation in 30% ethanol. Afterwards, samples were incubated in filtered eosin solution (Sigma-Aldrich) for 30 seconds. Sections were imaged using an EVOS M5000 imaging system at 10x magnification.

4.7.4. Immunohistochemistry of Skin Sections

The complexity and reliability of skin models were evaluated by immunohistochemistry (IHC). Similar to the haematoxylin and eosin staining, slides containing cryo-sectioned models were thawed at room temperature for 30 minutes before the staining. Paraffin-embedded samples were deparaffinised in Histoclear (Thermo Fisher Scientific) and gradually dehydrated in ethanol. Antigen retrieval of deparaffinised samples was achieved by incubating samples with citrate buffer (Sigma-Aldrich) at 95°C overnight.

The areas in the slides containing the models were delimitated with a liquid blocker marker (Agar Scientific). Then, sections were permeabilised with 0.1% Triton-X (Sigma-Aldrich) for 10 minutes and incubated in 2% BSA solution for 1 hour. Afterwards, samples were washed with PBS and incubated overnight at 4°C with 1:250 final dilution of Anti-Cytokeratin 14 antibody (ab181595), Anti-Involucrin antibody (ab53112) (Abcam) or Anti-Filaggrin Antibody (sc-80609) (Santa Cruz Biotechnology). Subsequently, sections were washed with 0.1% Triton-X and incubated with a 1:1000 final dilution of Goat Anti-Rabbit IgG Alexa Fluor® 488 (ab150077) and Donkey Anti-Mouse IgG Alexa Fluor® 568 (ab175472), where corresponding, for a minimum of 4 hours at 4°C. Finally, sections were mounted with an antifade mounting medium with DAPI (Vectashield). EVOS M5000 imaging system was used to image the samples using 10x and 20x magnification.

4.7.5. Immunostaining of Dermal Models

Printed and manually-seeded dermal models were fixed after 3 and 7 days to assess the presence of different proteins associated to specific dermal regions. In the case of printed dermal models, the presence of collagen type I, collagen type III, fibronectin and elastin were assessed. Meanwhile, the production by fibroblasts of collagen type I and collagen type III was evaluated in the manually seeded dermal models. The immunostaining of acellular gels was performed to ensure the absence of background signal related to the gel composition. Meanwhile, 500,000 fibroblasts were seeded in a tissue culture plate, and stained after 7 days as positive control.

Cryo-sectioned dermal models were thawed for 30 minutes at room temperature before proceeding to their staining. Initially, the area containing the models was delimited with a liquid blocker marker (Agar Scientific). Next, sections were permeabilised with 0.1% Triton-X (Sigma-Aldrich) for 10 minutes and incubated in 2% BSA solution for 1 hour. Afterwards, sections were washed with PBS and incubated overnight at 4°C with 1:100 final dilution of anti-Collagen III antibody (ab7778) and anti-Collagen I antibody (ab90395). Alternatively, samples were incubated with 1:100 final dilution of anti-Fibronectin antibody (ab23750) and anti-Elastin antibody (ab9519) (Abcam). Subsequently, sections were washed with 0.1% Triton-X and incubated with a 1:1000 final dilution of Goat Anti-Rabbit IgG Alexa Fluor® 488 (ab150077) and Donkey Anti-Mouse IgG Alexa Fluor® 568 (ab175472) (Abcam) for a minimum of 4 hours at 4°C in the dark. Finally, sections were mounted using an antifade mounting medium with DAPI (Vectashield). All antibody concentrations were optimised to obtain a correct fluorescence signal. EVOS M5000 imaging system (ThermoFisher) was used to image the sections at 10x and 20x magnification.

4.8. Reactive Jet Impingement as Bioprinting Process

4.8.1. Setting Up the ReJI System

The printing process was performed using a Reactive Jet Impingement (ReJI) system setup incorporated into a Jetlab® 4 printing platform (Microfab Technologies, Inc). ReJI configuration is based on a printhead that incorporates two solenoid microvalves INKX0514950A (Lee Company) in opposite locations with 55º inclination (Fig. 4.3) (Benning & Dalgarno, 2019). Each valve is connected to one ink reservoir, and a spike and hold drivers (Lee Company) to control the opening and closing of the valves. Based on the microvalve specifications, the spike voltage was set to 24V and reduced to a hold voltage of 3.2V. The jetting process is dictated by a rectangular waveform that controls the opening and closure of the microvalve actuators. In this project, a waveform with a frequency of 400Hz, a dwell time of 800µs and an amplitude of 5V was set to ensure the correct droplet ejection (Fig. 4.2).

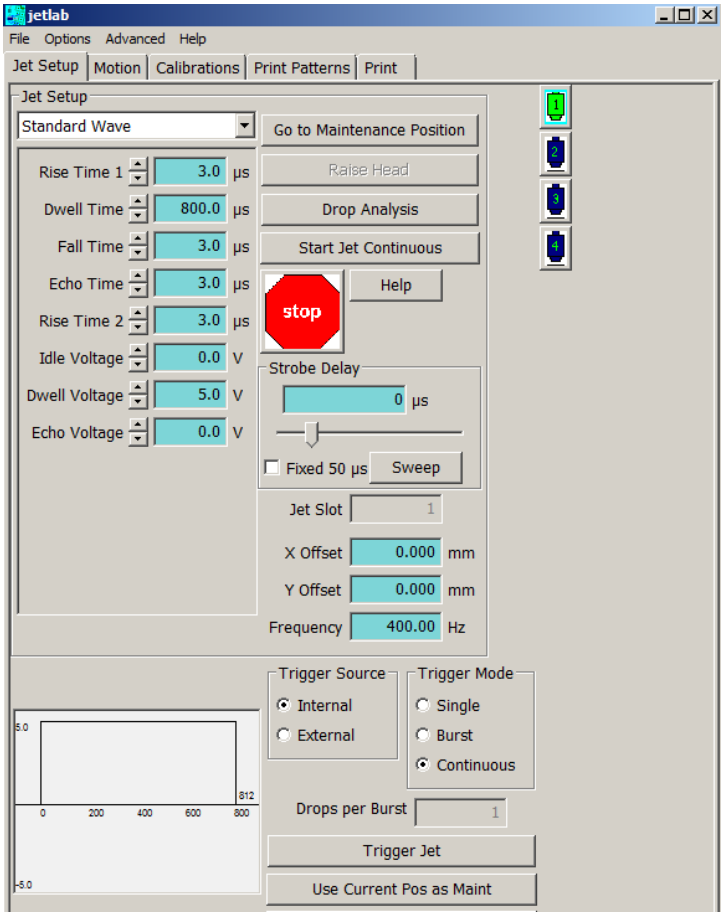

Figure 4. 2. Jetlab® 4 software window with some printing parameters selected for this study, including the waveform set for the microvalve actuation.

Additionally, a pneumatic CT-PT4 pressure controller (Microfab Technologies, Inc) was used to adjust the pressure on each microvalve. Gel precursor and crosslinker were incorporated into two different ink reservoirs. Each bioink holder was connected by tubes to the pressure controller and one microvalve. When the microvalves are opened, and the correct pressure is applied, droplets from each microvalve are jetted. The microvalve position allows the meeting of the droplets in mid-air and their reaction generating a stable gel that is deposited on the printer bed (Fig. 4.3). This impingement process was optimised and visualised with a stroboscopic camera incorporated into the Jetlab® 4 system. The motion of the ReJI head and most printing parameters were controlled using the Jetlab® 4 software.

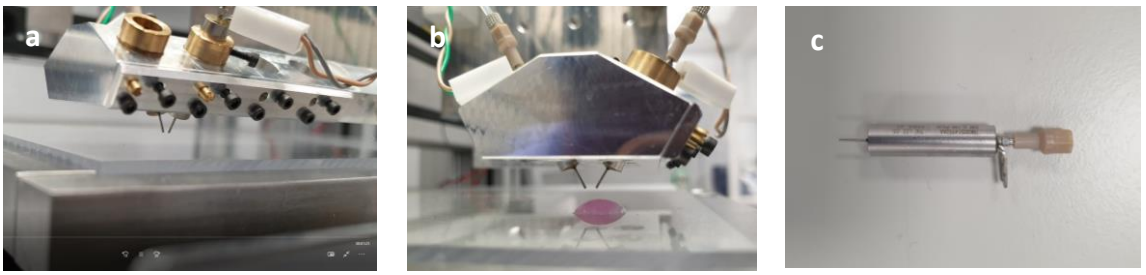

Figure 4. 3. Images of the (a) ReJI head and (b) the microvalves in their opposite position and (c) the solenoid microvalves INKX0514950A selected for the printing with ReJI.

Before and after using the printer, most of their components, including reservoirs, tubes and valves, were cleaned to eliminate any potential contamination. Valves were flushed with PBS to ensure the removal of any denaturalised cell or protein from previous printing. Subsequently, valves were jetted with trypsin-EDTA solution to remove any biological residues. Finally, cells were jet with sterile PBS to ensure the system was cleaned and ready for printing. At the end of the printing sessions, the same steps were followed, and valves were kept overnight in trypsin-EDTA solution to clean the valve nozzle and avoid any blockage.

4.8.2. Optimisation of Bioprinting Process

The optimisation of the reactive jet impingement process was performed using acellular CAF gel precursor and crosslinker as bioinks. The printing pattern was designed to have a 10 mm x 10 mm square surface with a 15 mm height. The instructions were provided to the printer in the form of a black and white bitmap image and a script loaded to the Jetlab® 4 software. The microvalve positions were optimised to ensure the correct impingement and formation of the desired gel structure with high resolution. The printing pressure was set to 380 mmHg to print the gel crosslinker containing thrombin and was increased to 420 mmHg for the CAF precursor to ensure the correct droplet and gel formation.

The homogeneity of the printing process and its effect on cell viability were evaluated by printing different suspensions of fibroblasts and keratinocytes. Three cell densities were selected for these studies, 500,000 cells/mL, 1,000,000 cells/mL and 5,000,000 cells/mL. To evaluate the reliability of the printing process, a square pattern of 10 mm x 10 mm was designed and printed in tissue-culture treated 24 well plates (Corning). The number of printed layers was progressively increased to assess the consistency of the number of cells printed per layer and the homogeneity between samples. The printing patterns were created by depositing cell media and cell suspensions from each microvalve, respectively, and maintaining a pressure of 380 mmHg on both microvalves.

4.8.3. Bioprinting of Dermal, Epidermal and Skin Models

CAF-based bioinks were selected as dermal matrices to evaluate the effect of the ReJI printing process on the quality of dermal models. The printing and manual seeding of two fibroblast densities, 500,000 and 5,000,000 cells/mL, were compared to determine their impact on dermal development. CAF gel precursor was prepared following the steps described in section 4.1.1, combining collagen, alginate and fibrinogen in a 1:2:8 ratio. Before its printing, the gel precursor was filtered using a 0.22 µm filter to avoid the presence of fibres which could clog the microvalve nozzle. Fibroblasts were incorporated into the CAF crosslinker bioink containing thrombin. The dermal construct was designed with a volume of 10 mm x 10mm square surface with 15mm height and printed in tissue-culture treated 24 well plates (Corning). The printing pressure was set to 380 mmHg to print the gel crosslinker, which contained thrombin and cells, and it was increased up to 420 mmHg to ensure the correct droplet

formation and jetting of CAF precursors. The printed models were maintained in DMEM and incubated at 37°C and 5% CO_2.

The impact of the printing process on the keratinocyte survival and their behaviour after their printing were assessed by printing 500,000 keratinocytes/mL suspended in EpiLife medium supplemented with 10µM of Y-27632 dihydrochloride (ROCK inhibitor). The distribution of printed keratinocytes was compared to keratinocytes manually seeded. The printing pattern was set to a single layer of 10 mm x 10 mm area, the printing pressure was maintained at 380 mmHg and the samples were printed in tissue-culture treated 24 well plates (Corning). EpiLife medium was changed after 24 hours in all samples to remove the presence of ROCK inhibitor, and it was renewed every 48 hours afterwards. Samples were incubated at 37°C and 5% CO_2 and fix after 1, 3 and 7 days.

Skin models were printed using CAF formulation as dermal matrix. On this occasion, the printed dimensions were increased to 15 mm x 15 mm and 20 mm in height to fit the insert dimensions. The printing pressure was maintained at 380 mmHg to print the gel crosslinker containing thrombin and was increased to 420 mmHg for the CAF precursor. As proof of concept, 500,000 fibroblasts/mL were incorporated into the bioinks. After three days of incubating the printed dermis, 250,000 keratinocytes/model in EpiLife medium supplemented with ROCK inhibitor were printed on top of the CAF-based dermal structure. The EpiLife medium was supplemented with 200U/mL aprotinin after 24 hours to avoid the degradation of CAF gels by keratinocytes. The resulting model was maintained under submerged conditions for 7 days, before exposing it to the air-liquid interface and raising the calcium chloride concentration in the EpiLife medium from 60µM to 1.64mM. During the process, the models were incubated at 37°C and 5% CO2 and fixed after 14 and 21 days of seeding the keratinocytes.

4.9. Statistical Analysis

All measurements were repeated at least three times to ensure their reproducibility. Quantitative data were represented by their mean and standard deviation. Results were analysed using Prism® 9 statistical analysis software (GraphPad Software, USA) using one-way ANOVA followed by Tukey Post hoc test to determine the statistical differences between the control group and samples under the same conditions and samples at different time points. P-values lower than 0.05 (*), 0.01 (**) and 0.001 (***) were considered statistically significant.

CHAPTER 5. REACTIVE JET IMPINGEMENT AS A BIOPRINTING SYSTEM

5.1. Introduction

The implementation of bioprinting systems into the manufacturing of skin equivalents have demonstrated to enhance the control over the structural composition and reproducibility of skin models compared to traditional tissue engineering techniques. Nevertheless, the limited reliability and the long time required to produce skin equivalents still hinder their application at the industrial level. As a solution to these problems, Reactive Jet Impingement (ReJI) process is proposed in this project as alternative to conventional bioprinting techniques. The following chapter explores the advantage and limitations of the ReJI system and the implications of incorporating this technology into the generation of skin components. Parameters such as printing resolution, shape fidelity and homogeneity between printings were assessed to determine the quality and scalability of the ReJI process compared to other bioprinting technologies. Additionally, the impact of the printing process on the viability and distribution of fibroblasts and keratinocytes was also investigated to determine the suitability of ReJI system as bioprinting technique. Finally, the consequences of implementing this technology on the production of dermal and epidermal layers were determined by evaluating the proliferation, differentiation, and production of new extracellular matrix components in the bioprinted models in comparison to manually seeded samples.

5.2. Evaluation of the Printing Process

5.2.1. Optimisation of the Impingement Process

Reactive Jet Impingement (ReJI) process is based on the jetting of two opposite liquid droplets, one containing a gel precursor and another a gel crosslinker. Both droplets collide and react in mid-air generating a stable gel before reaching the substrate (Fig. 5.1). Impingement of both bioinks is indispensable for the creation of a three-dimensional structure with high resolution. Misalignment of the printer microvalves can result in the bioink scattering and the formation of gels with two differentiated phases (Fig. 5.2a). In this study, the correct alignment of the valves and the encounter between the jetted droplets in mid-air were optimised and confirmed by the images obtained from the stroboscopic camera (Fig. 5.1 a-b).

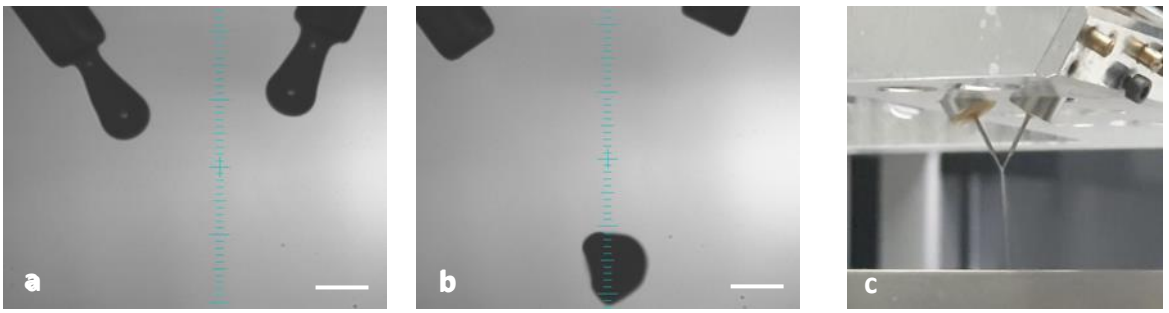

Figure 5. 1. Images obtained from the stroboscopic camera showing (a) the droplets being formed in the microvalves before being released, and (b) the impingement of the jetted droplets in mid-air before reaching the printer bed. Photograph (c) shows the continuous jetting of the liquid bioinks from the microvalves, and the gel column resulting from the impingement of the opposite jetted droplets. Scale bars correspond to 500 µm.

The height between the valves and the printer bed was also optimized, as it plays an essential role in the quality of the final printed structure. In the case of low height values, gel droplets were scattered (Fig.5.2a). Meanwhile, overestimated height values resulted in the deformation of printed structures (Fig. 5.2b). Only the selection of 5mm distance between the nozzle and the printing surface enabled the optimal printing of the gel constructs (Fig. 5.2c).

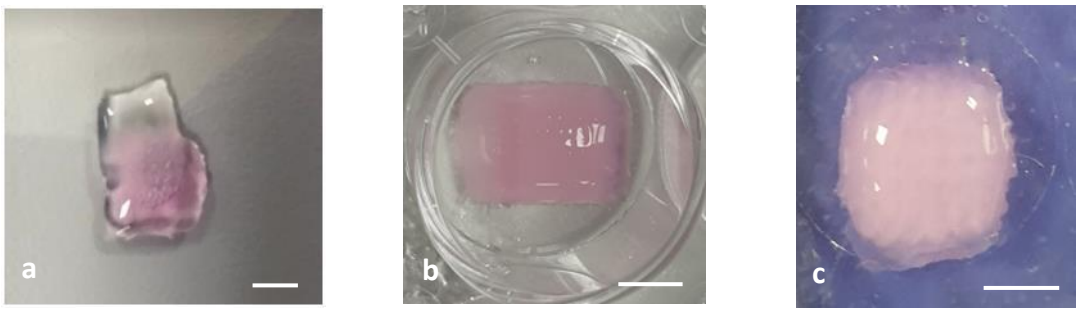

Figure 5. 2. Printed gel resulting from (a) the microvalve misalignment, (b) incorrect distance between the microvalve and (c) correct printing parameters. Scale bars correspond to 5 mm.

ReJI allowed the printing of intricated patterns with a resolution of at least 500 µm in this study. The printing patterns were designed using black and white bitmaps, which were decoded by the printer software to determine the jetting of droplets (Fig. 5.3). The characteristics of the printed dot arrays, such as their distance or droplet volume, could be customised using specific scripts in the Jetlab® 4 software.

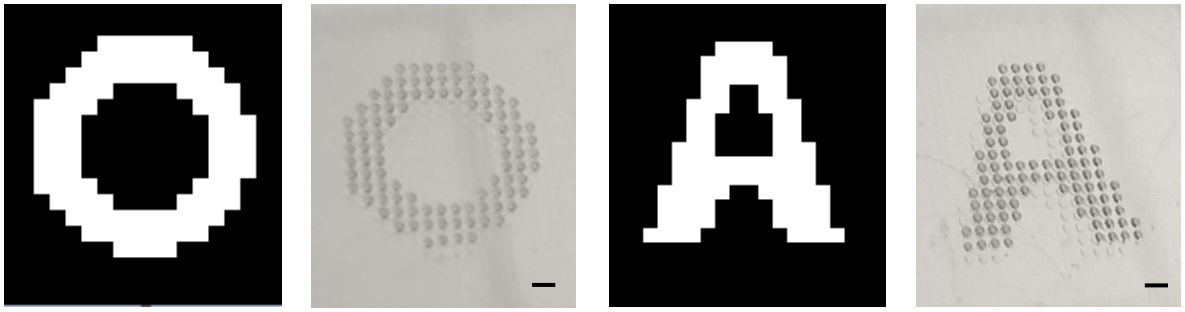

Figure 5. 3. Comparison between black and white bitmaps and the corresponding printed pattern. Scale bars represent 1000 µm.

The printing of subsequent layers using ReJI resulted in the formation of visible lattices inside the gels (Fig. 5.2c, 5.4c). These structures were generated by the union of crosslinking points created by the reaction between the droplets. In contrast to manually seeded CAF gels (Fig. 5.4a), printed samples presented a more defined structure with a homogeneous distribution of cell media through the gel, represented by the pink colour inside the samples (Fig. 5.4c). The hydrophobicity of the printing surface also needs to be considered before printing (Fig. 5.4 b-c). The use of a hydrophilic surface resulted in the spread of the water content outside the printed gel, resulting in the loss of shape over time.

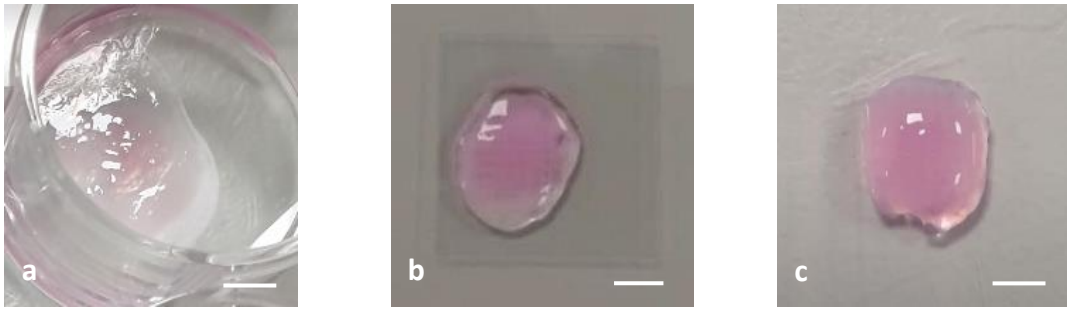

Figure 5. 4. Comparison between the cell media content represented in pink in (a) manual-seeded CAF gels and (c) printed CAF gel. The printing of CAF gels in (b) hydrophilic surfaces affect their shape fidelity in comparison to the printing on (c) hydrophobic surfaces. Scale bars correspond to 5 mm.

Optimisation of ReJI printing process facilitated the printing in parallel of more than 12 models with a volume of 10 mm x 10 mm x 15 mm in approximately 20 minutes (Fig. 5.5).

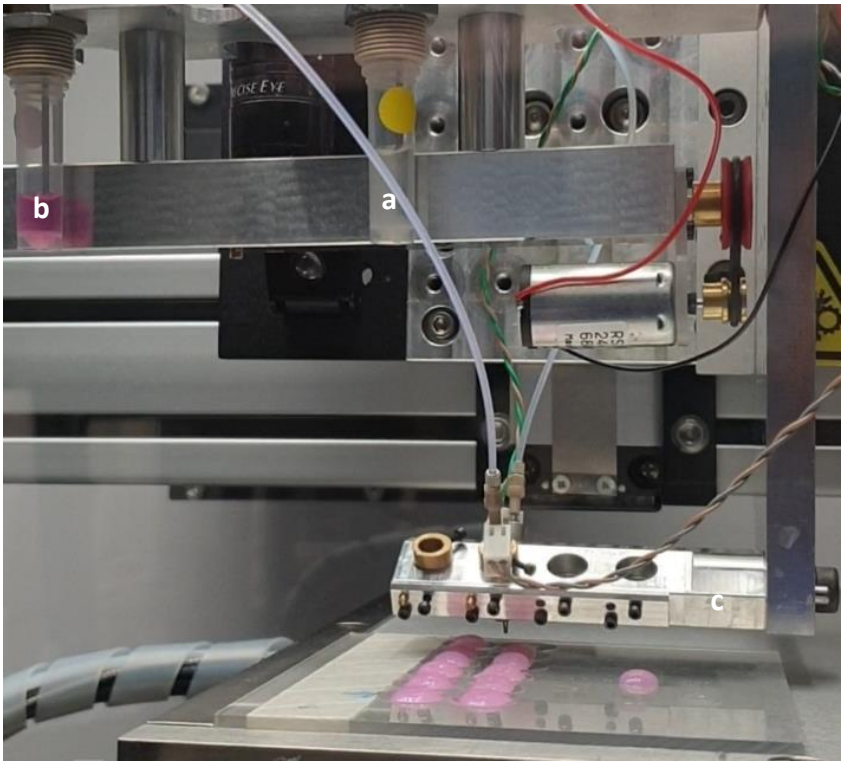

Figure 5. 5. Picture of the sequential bioprinting of CAF-based dermal models using the Reactive Jet Impingement process. (a) CAF precursor – containing collagen, alginate and fibrinogen – and (b) CAF crosslinker – containing thrombin, calcium chloride and fibroblasts – are jetted from the opposite microvalves located in (c) the printer head. The formation of gel droplets during the impingement of the jetted droplets enables the printing of subsequent layers, facilitating the large-scale production of models in a short period of time.

5.2.2. Assessment of the Printing Reproducibility

The reproducibility of the ReJI printing process was assessed by examining the number of cells deposited while increasing the number of printed layers (Fig. 5.6-5.7).

The printing of fibroblasts showed a linear increment in the cell values as the number of printed layers increased (Fig. 5.6). The printing of different fibroblast densities, including 500,000; 1,000,000 and 5,000,000 cells/mL, did not show an effect on the homogeneity of the printing process. Only the printing of the highest fibroblast densities exhibited a slight increase in their standard deviation values when printing more than 10 layers.

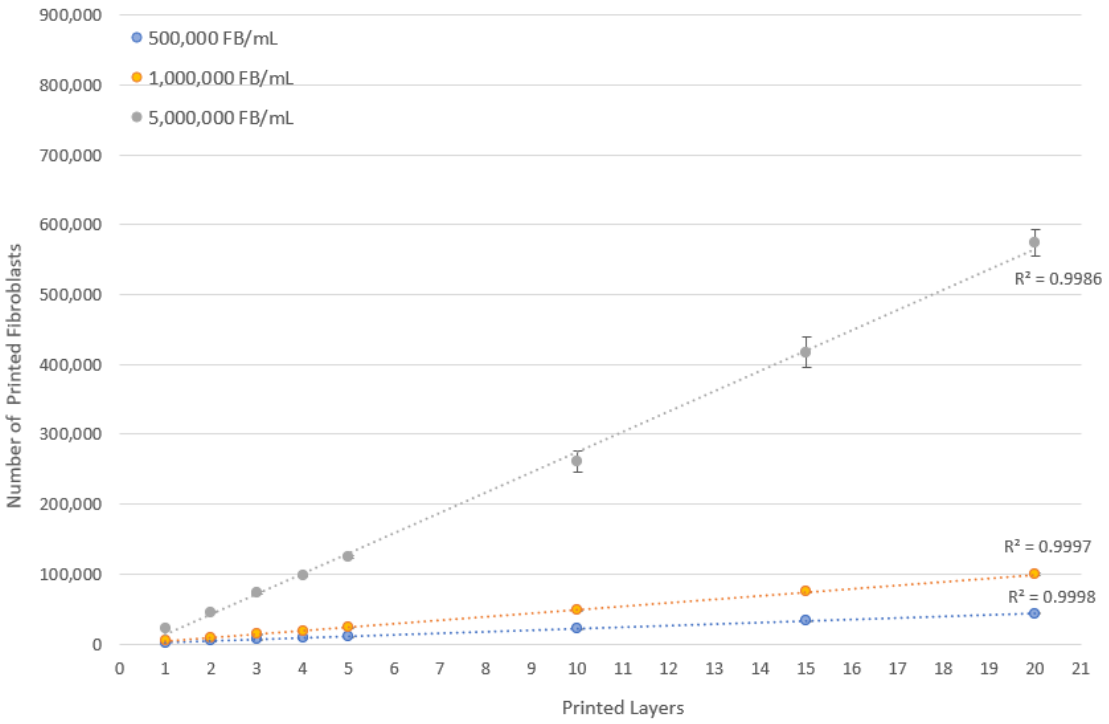

Figure 5. 6. Evaluation of the ReJI printing homogeneity by quantifying the number of fibroblasts contained in the printed layers. The effect of cell densities was assessed by comparing the printing of 500,000; 1,000,000 and 5,000,000 fibroblasts/mL. Data represents mean ± SD, n = 3.

The printing of subsequent layers of keratinocytes also presented a linear progression in the total number of printed cells (Fig. 5.7). Similar to the results observed when printing fibroblasts, the number of deposited cells increased as the number of layers rose. However, in this occasion the printing of 5,000,000 keratinocytes/mL presented a notable higher standard deviation after printing more than 10 layers.

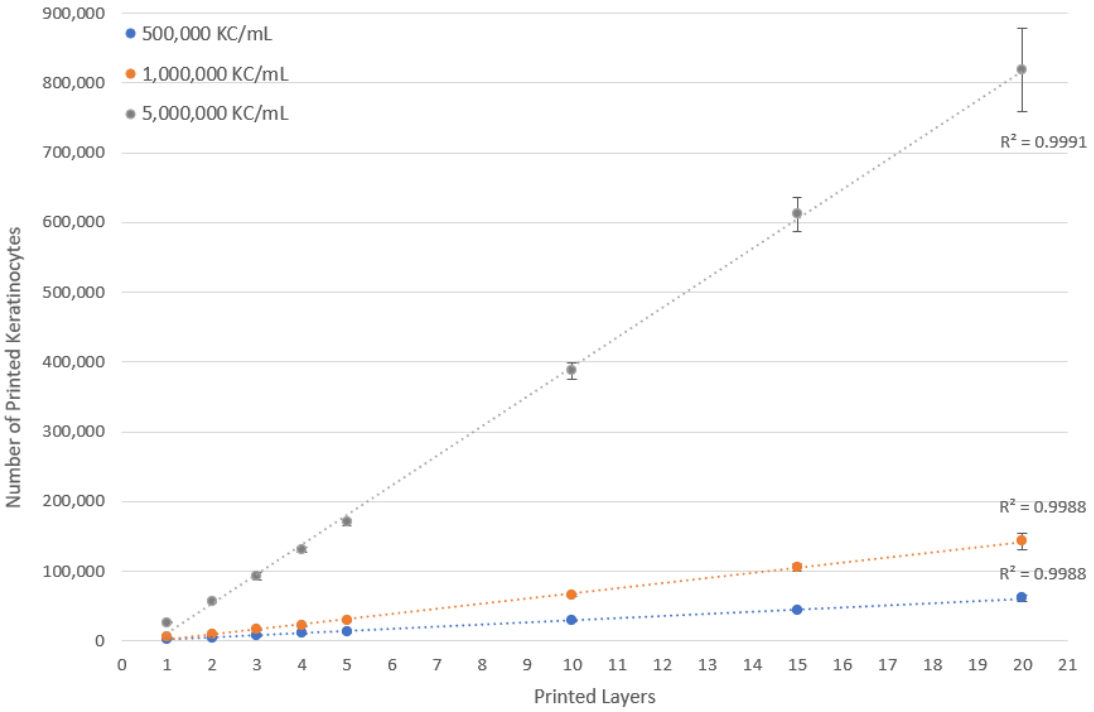

Figure 5. 7. Evaluation of the ReJI printing homogeneity by quantifying the number of keratinocytes contained in the printed layers. The effect of cell densities was assessed by comparing the printing of 500,000; 1,000,000 and 5,000,000 keratinocytes/mL. Data represents mean ± SD, n = 3.

The comparison between the values of fibroblasts and keratinocytes printed per layer underlined the influence of the cell type on the number of deposited cells. When printing the lowest cell densities, the number of cells printed per layer did not show significant variations regardless of the cell type. Only after printing more than 5 layers, a symbolic variation on the cell values could be distinguished between both cell types, with keratinocytes showing higher number of deposited cells.

5.2.3. Cell Survival of Printed Cells

The effect of the printing process on cell survival was evaluated by printing different cell densities. Regardless of the printed cell density, fibroblast and keratinocytes presented high viability (Fig. 5.8). Only a slight increase in the number of dead cells could be observed when printing high cell densities. Cells showed a homogeneous distribution independently of their density and cell type. Furthermore, the increment in the cell density was reflected in the images with the increase of observable cells. Only the printing of 5,000,000 keratinocytes/mL resulted in a significantly broader rise in the number of deposited cells than expected.

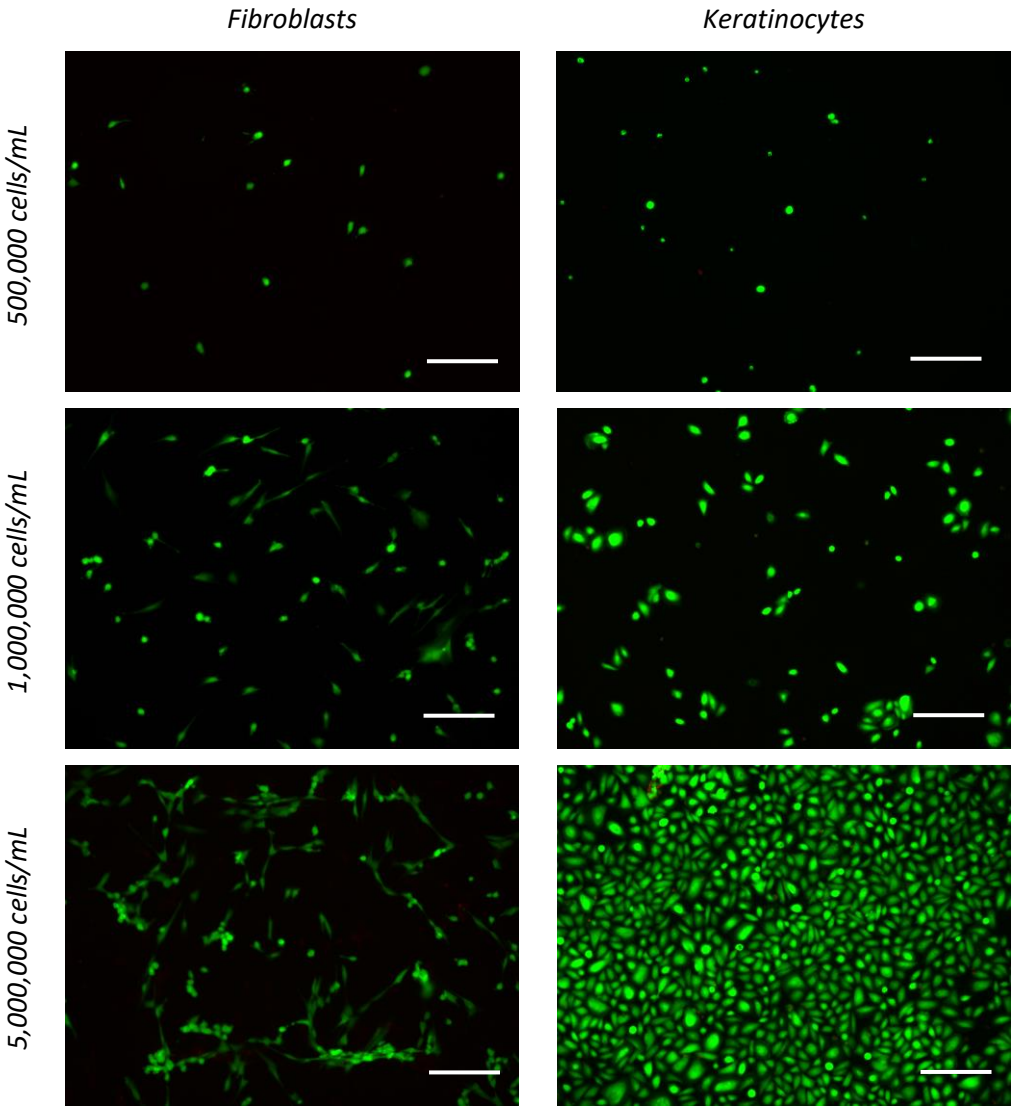

Figure 5. 8. Evaluation of the viability after 1 day of printed fibroblast and keratinocyte monolayers using the ReJI system. The effect of the printed cell density on the cell survival and distribution was assessed by printing different cell densities including 500,000; 1,000,000 and 5,000,000 cells/mL. Living cells are represented in green and dead cells in red. Scale bars correspond to 200 µm.

5.3. Bioprinting Dermal Models

5.3.1. Fibroblasts Viability

The staining of live and dead cells in the printed dermal models evidenced the high viability of fibroblasts after 1 day, regardless of the printed cell density (Fig. 5.9). Models containing 500,000 fibroblasts/mL presented fibroblasts distributed uniformly in distant positions between each other on the first day. As fibroblasts proliferated, their viability was maintained.

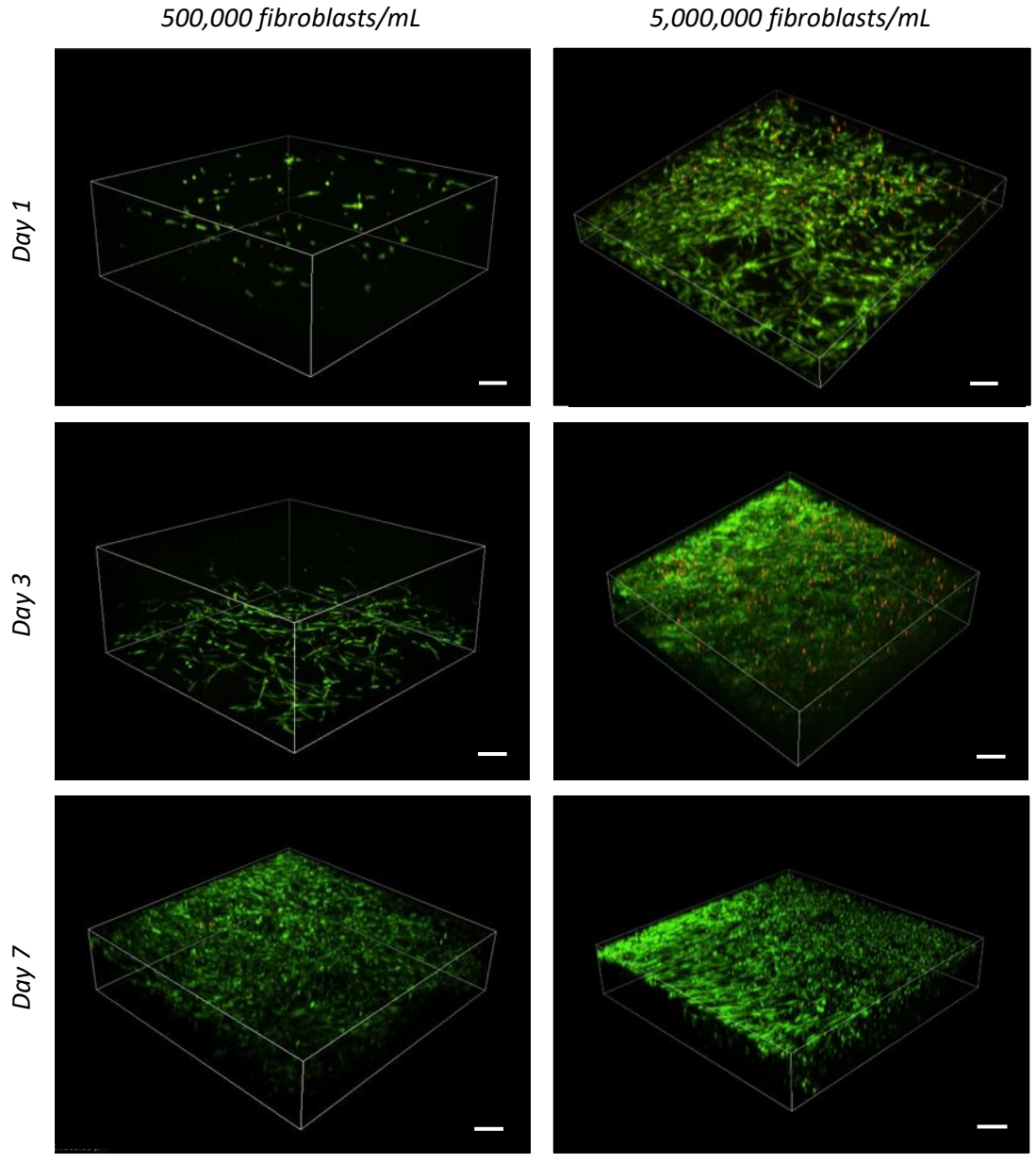

Figure 5. 9. Three-dimensional representation of fibroblast viability and their distribution within the printed CAF models after 1, 3 and 7 days. The impact of the ReJI process on the survival and distribution of fibroblasts in the dermal models was assessed by comparing the printing of 500,000 cells/mL and 5,000,000 cells/mL. Living cells are represented in green and dead cells are represented in red. Scale bars correspond to 200 µm.

After 3 days, fibroblasts showed a higher interaction, resulting in a homogeneous distribution through the printed model after 7 days, with a proportion of living cells above 94%. The printing of dermal models containing 5,000,000 fibroblasts/mL resulted in a homogenous cell distribution. This uniformity in the cell organisation was maintained over time, with the creation of a compacted cellular matrix after 3 days. An increment in the number of dead cells could be observed on day 3 on the upper layers of the dermal models. However, cell viability was maintained over time, with a significant decrease on the number of dead cells after 7 days as the proportion of living cells increased to 88%.

5.3.2. Fibroblast Morphology and Distribution

The organisation of printed fibroblasts and the changes in their morphology were assessed by staining their cell nuclei and F-actin filaments, which promote cell mobility and define the cellular shape. On day 1, fibroblasts printed with the lowest cell density presented a round morphology (Fig. 5.10). However, after 3 days, they started to show a spindle-like shape as they adapted to the new environment. The proliferation of fibroblasts resulted in their higher confluency after 7 days and the formation of aligned groups of cells.

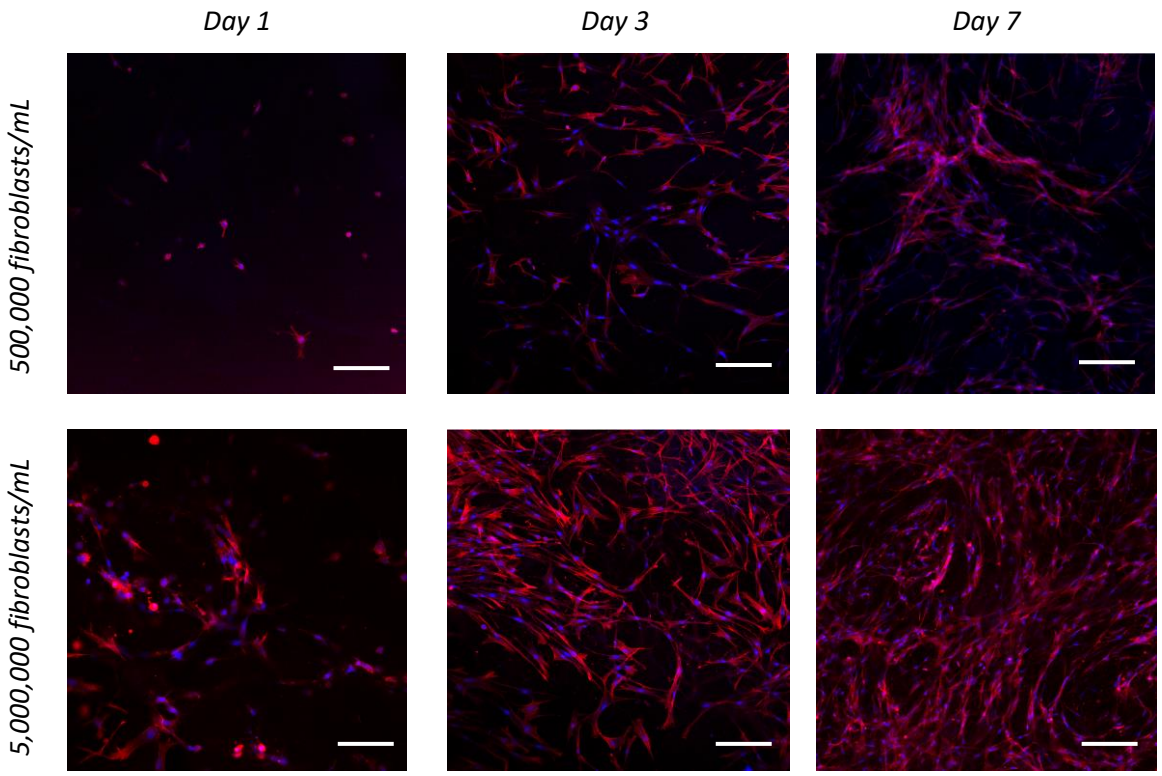

Figure 5. 10. Evaluation of the morphology and distribution of fibroblasts printed in CAF gels after 1, 3, 7 days. The effect of the printed fibroblast density was assessed by comparing the printing of 500,000 cells/mL and 5,000,000 cells/mL. Blue signal corresponds to cell nuclei and red signal to F-actin filaments, associated with cell morphology. Scale bars represent 200 µm.

The increase of fibroblasts from 500,000 to 5,000,000 cells per mL resulted in a faster adaptation of the cells to the CAF gel microenvironment. In the samples printed with higher fibroblast densities, cells were distributed homogeneously, covering a wider area and creating interactions with each other, in contrast to other samples on day 1. As a result, fibroblasts already presented a defined spindle-like morphology after only 1 day. Over time, the number of fibroblasts increased, resulting in dermal models with higher cell confluency after 3 days than the one observed when printing 500,000 cells/mL after 7 days. The fibroblast network slightly expanded from day 3 to day 7, reaching a stable confluency.

5.3.3. Fibroblast Proliferation

The fibroblast proliferation rate was evaluated by comparing the changes in the dsDNA content in the samples over time. The correlation between the number of fibroblasts present in the dermal models and the measured cDNA content was calculated using the following standard curve (Fig. 5.11).

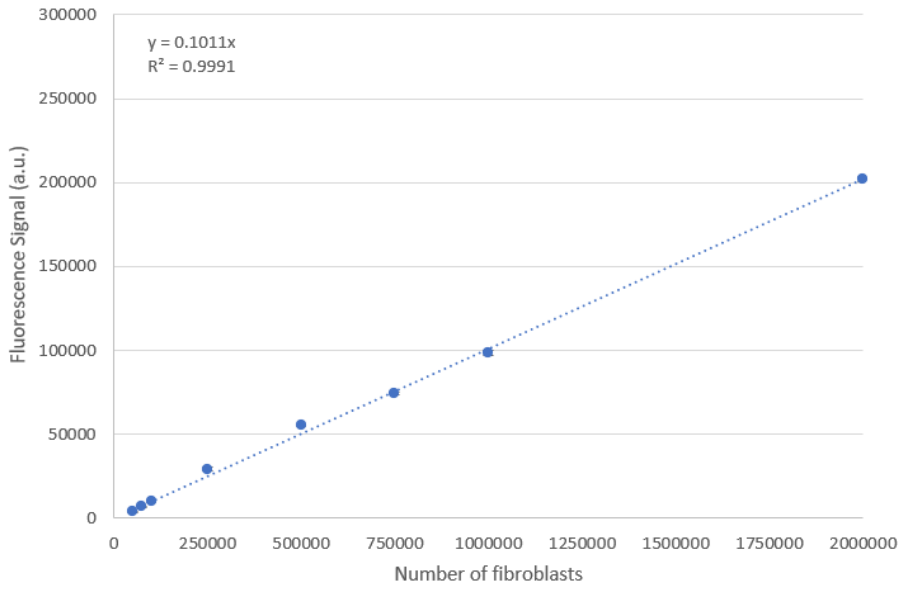

Figure 5. 11. Standard curve for the Quant-iT PicoGreen dsDNA Assay, representing the correlation between the measured fluorescence signal and the number of fibroblasts present in the sample. Data represents mean ± SD, n = 3.

Fibroblasts exhibited a distinct proliferative behaviour depending on the printed or manually seeded cell densities (Fig. 5.12). Manually seeded models produced with 500,000 fibroblasts/mL triplicated their cell number from day 1 to day 3 and increased the number of cells by five from day 3 to day 7. In the case of printed models with the same initial cell density, the fibroblast proliferation rate was higher from day 1 to day 3, with an increment by five on the number of cells. The fibroblast growth rate was maintained, with an increase by four from day 3 to day 7. As a result, cell values were significantly higher at day 7 in printed models than in manually seeded samples.

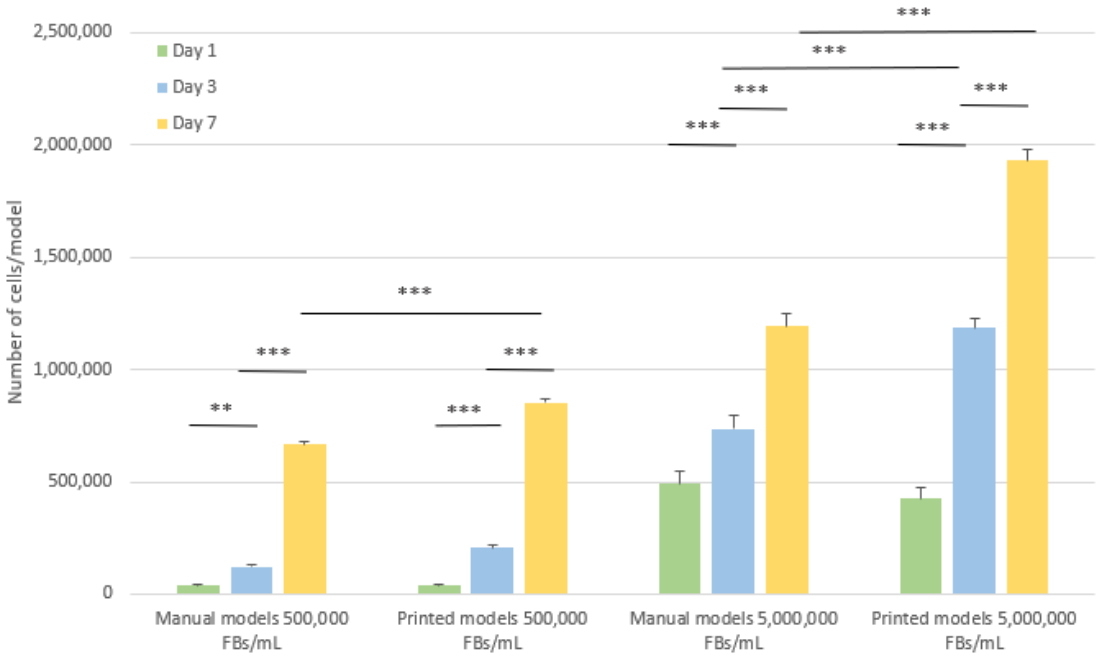

*Figure 5. 12. Comparison between the fibroblast proliferation in printed and manually seeded CAF gels prepared with 500,000 cells/mL and 5,000,000 cells/mL. Evaluation of cell proliferation was performed by comparing the cDNA content on each model after 1, 3 and 7 days. Error bars represent the standard deviation (SD), n = 3. The symbols *, ** and *** indicate the significant difference between groups at the level p<0.05, p<0.01 and p<0.001, respectively.*

In the case of dermal models prepared with 5,000,000 fibroblasts/mL, the differences between printed and manually seeded models were more representative. In manually seeded models, the number of cells stabilised with an increase of 1.5 between day 1 and 3 and day 3 and 7. Contrarily, the number of fibroblasts was triplicated in the printed samples from day 1 to day 3. The comparison between the cell values at day 3 and day 7 in printed samples showed a stabilisation with an increase of 1.5 between these time points. Consequently, the number of cells in the dermal models was significantly different between manually and printed samples on day 3 and day 7.

5.3.4. Fibroblast Production of Extracellular Matrix Components

Fibroblasts are responsible for the secretion of new extracellular matrix components to maintain the integrity of the dermal structure. Characterisation of printed and manually seeded dermal models using Scanning Electron Microscope (SEM) was performed to visualise the changes in the matrix organisation and the fibroblast distribution and their interaction with the dermal matrix. The comparison between printed and manually prepared acellular CAF gels showed an important difference in the fibrillar arrangement and porosity of the dermal matrices (Fig. 5.13). The manual production of CAF gels resulted in the generation of a disorganised fibrillar arrangement, with slight variations in the fibre thickness through the matrix and the presence of porous with approximately 5 µm diameter. Contrarily, printed acellular CAF gels presented a more compacted fibrillar organisation, with lower porosity and thinner and more uniform fibres. These differences in the matrix characteristics were also present in the printed and manually seeded dermal models on day 1 (Fig. 5.14-5.15).

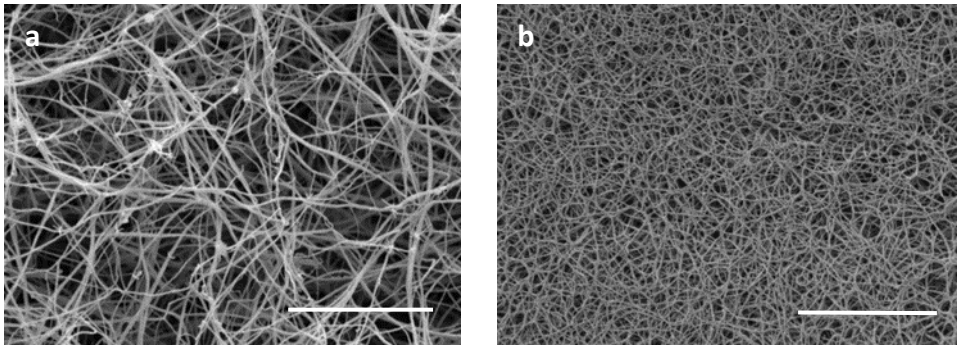

Figure 5. 13. Comparison between the fibrillar organisation of (a) manually seeded acellular CAF gels and (b) printed acellular CAF gels observed by SEM. Scale bar represents 10 µm.

The use of the lowest fibroblast densities to manually produce the dermal models resulted in the individual distribution of fibroblasts at day 1 (Fig. 5.14). The seeded cells presented a rounded morphology as they started to adhere and tug on the CAF fibres. The tension applied to the matrix showed an enhancement as the fibroblasts acquired an elongated shape after 3 days. As a result, the fibrillar components of CAF gels presented a more organised arrangement. After 7 days, the number of fibroblasts increased, and most of them were found in the inner layers of the model. In some areas, the matrix exhibited several changes in their reorganisation and the appearance of thicker fibres near the cell location. The increase in the seeded cell density to 5,000,000 fibroblasts/mL also entailed a rise in the number of cells observed in the dermal models. At day 1, the interaction between fibroblasts could already be

distinguished. These cells already displayed a spindle-like morphology at day 1 and their surrounding matrix presented a more stretched and organised appearance. After 3 days, a network of interconnected fibroblasts was found surrounded by new fibrillar content. As fibroblasts proliferated, they started to form a more confluent cellular network and modify the matrix organisation and composition.

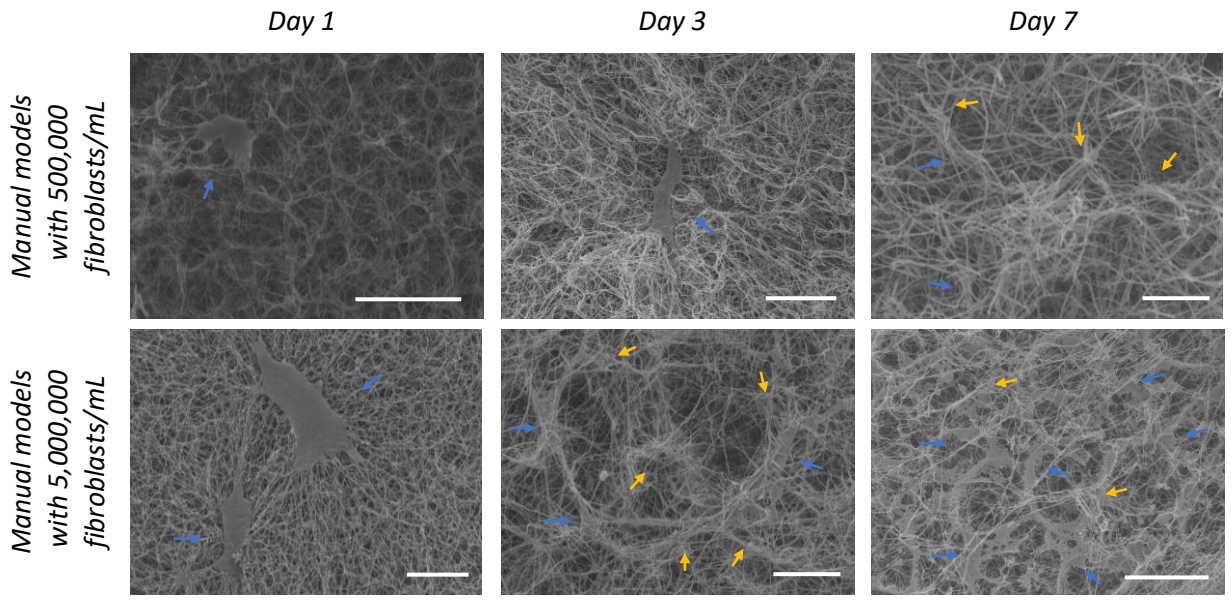

Figure 5. 14. Characterisation by SEM of CAF gels manually seeded with 500,000 fibroblasts/mL and 5,000,000 fibroblasts/mL. These images show the changes on the fibroblast morphology and distribution (blue arrows) after 1, 3 and 7 days, and the interaction of the cells with CAF fibres and new extracellular matrix components (orange arrows). Scale bar represents 20 µm.

In contrast to manually seeded samples, printed models showed a more homogeneous distribution of fibroblasts (Fig. 5.15). Printed samples with 500,000 fibroblasts/mL exhibited cells with rounded morphology and the presence of cell groups with a more elongated morphology interacting with the compacted matrix arrangement after 1 day. The fibroblast proliferation promoted the confluency of cells and their parallel organisation. At this point, some areas exhibited some small fluctuations in the matrix properties. However, the major changes on the CAF matrix could be observed after 7 days with the degradation of matrix components in some areas and their replacement by thicker fibres. In some regions, fibroblast reached a high confluency.

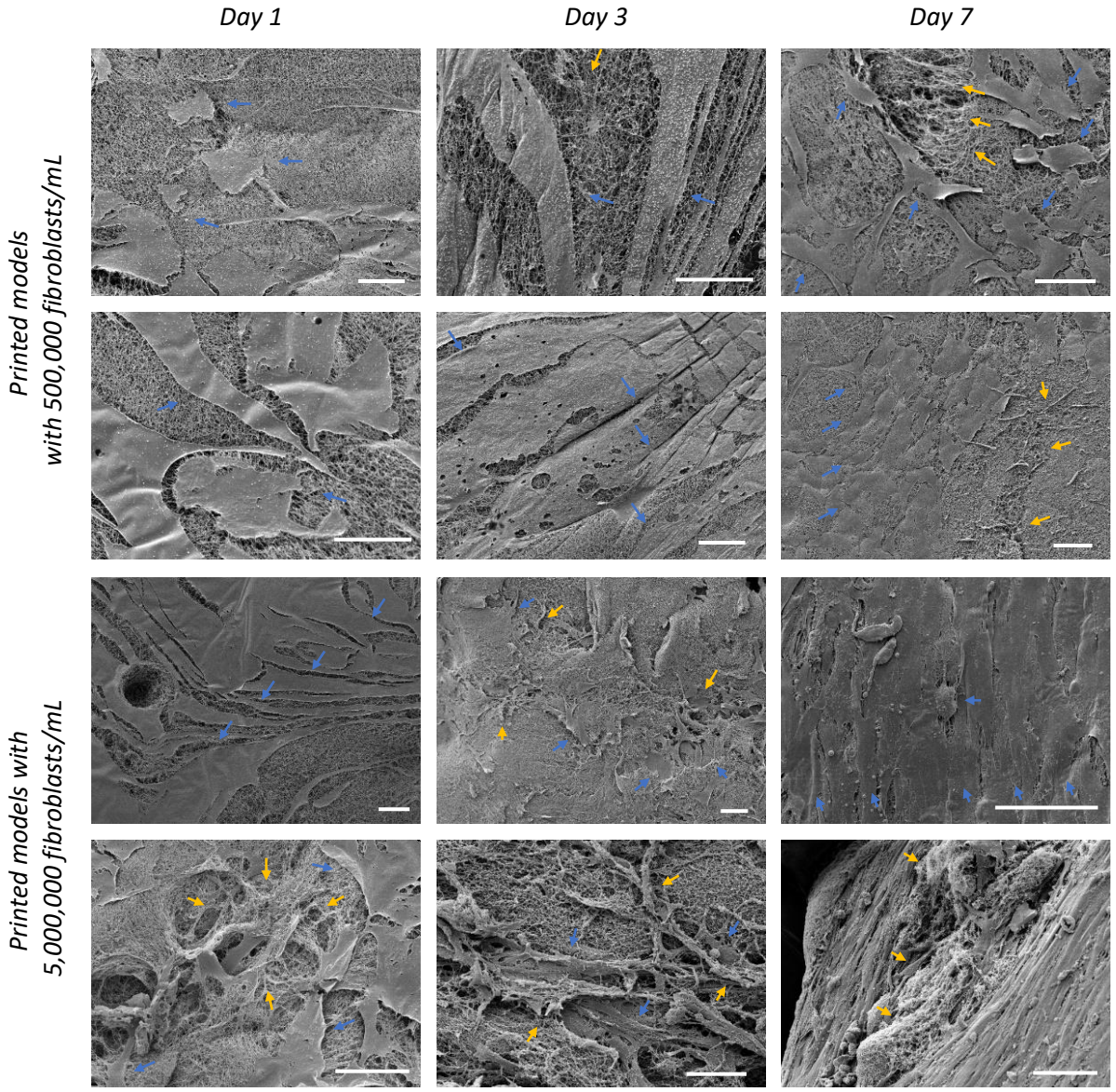

Figure 5. 15. Characterisation by SEM of printed CAF gels containing 500,000 fibroblasts/mL and 5,000,000 fibroblasts/mL. The images show the changes on the fibroblast morphology and distribution (blue arrows) and their interaction with the initial CAF matrix and the new extracellular matrix components (orange arrows) after 1, 3 and 7 days. Scale bar represents 50 µm.

The printing of the highest cell density resulted in the generation of dermal models with an elevated cell confluency (Fig. 5.15). As a result, fibroblasts already presented an elongated shape on day 1, and initial changes on the matrix composition could be observed. In these samples, the tensional forces applied by the fibroblasts to the CAF components and the appearance of new matrix components could already be observed from the first day. These modifications on the matrix could be especially discerned on day 3 with the presence of thicker fibres in contact with the fibroblasts. After 7 days, cellular confluency was almost completed, with fibroblasts covering most of the characterised surface. Moreover, the high complex

matrix containing different fibrillar proteins could be discerned in some regions, contrasting with the results obtained in other samples.

Immunostaining studies assessed the presence of some extracellular matrix components specific from the dermal matrix. The immunostaining of fibroblasts seeded for 7 days in tissue-culture treated plastic verified the capacity of the studied fibroblasts to produce collagen type I, collagen type III, elastin and fibronectin (Fig. 5.16).

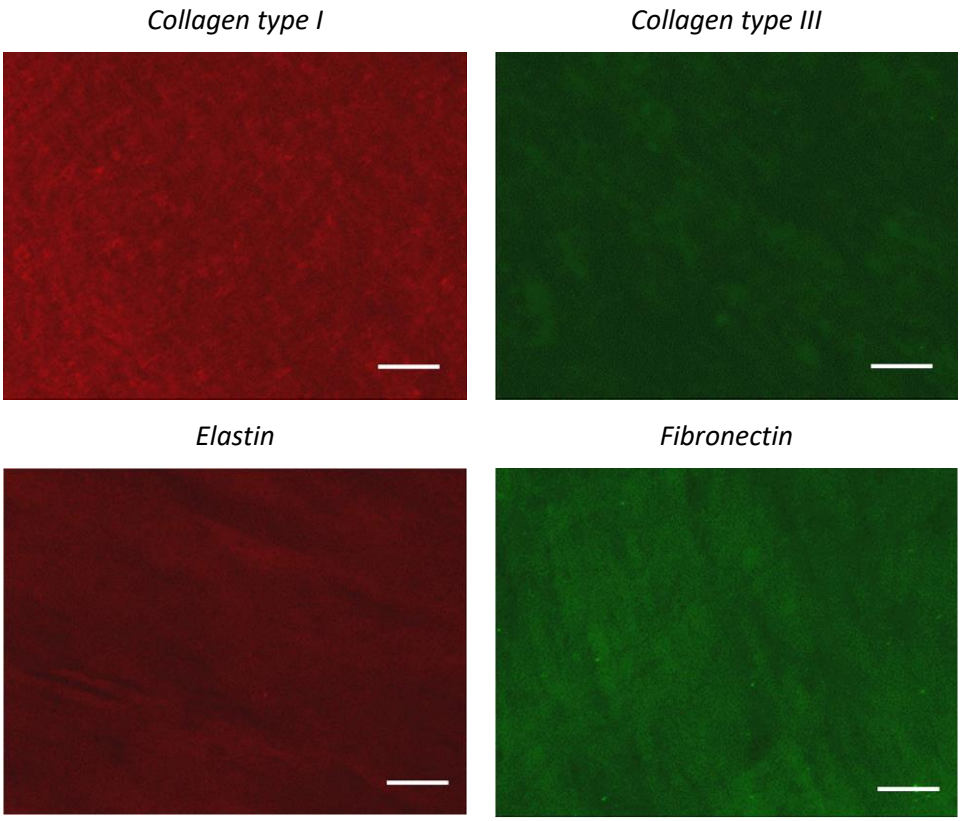

Figure 5. 16. Immunohistochemistry of 500,000 fibroblasts seeded in a tissue culture treated plastic and fixed after 7 days, selected as positive control to prove the ability of the studied fibroblasts to produce dermal ECM components. Red staining corresponds to collagen type I and elastin, and green staining corresponds to collagen type III and elastin, respectively. Scale bars represent 200 µm.

Meanwhile, the staining acellular CAF gels confirmed a low presence of collagen type I and almost a negligible existence of elastin and fibronectin (Fig. 5.17). Collagen type III could not be found in acellular CAF gels. The obtained fluorescence signals were used as negative controls to benchmark the presence of these proteins in the produced dermal models over time.

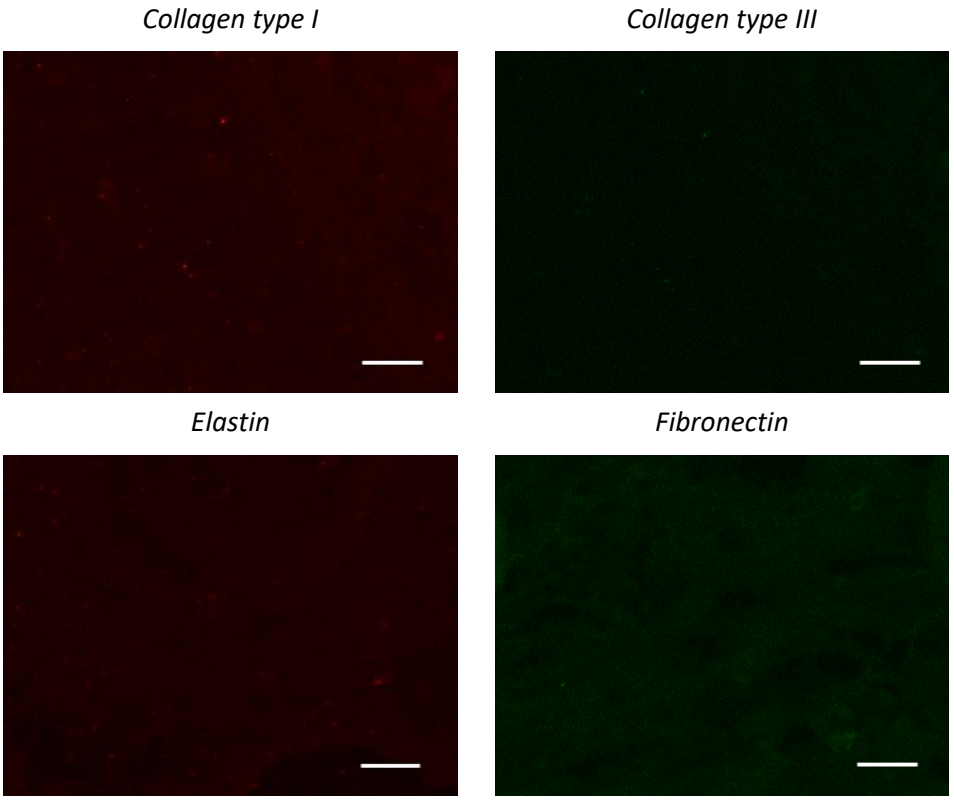

Figure 5. 17. Immunohistochemistry of acellular CAF gels was selected as negative control to confirm the absence of collagen type I, type III, elastin and fibronectin in the CAF gels without the presence of fibroblasts. Red staining corresponds to collagen type I and elastin, and green staining corresponds to collagen type III and fibronectin. Scale bar represents 200 µm.

The presence of collagen type I could be observed in all models at day 3, especially in the printed models (Fig. 5.18). After 7 days, the signal of collagen type I increased in all samples.

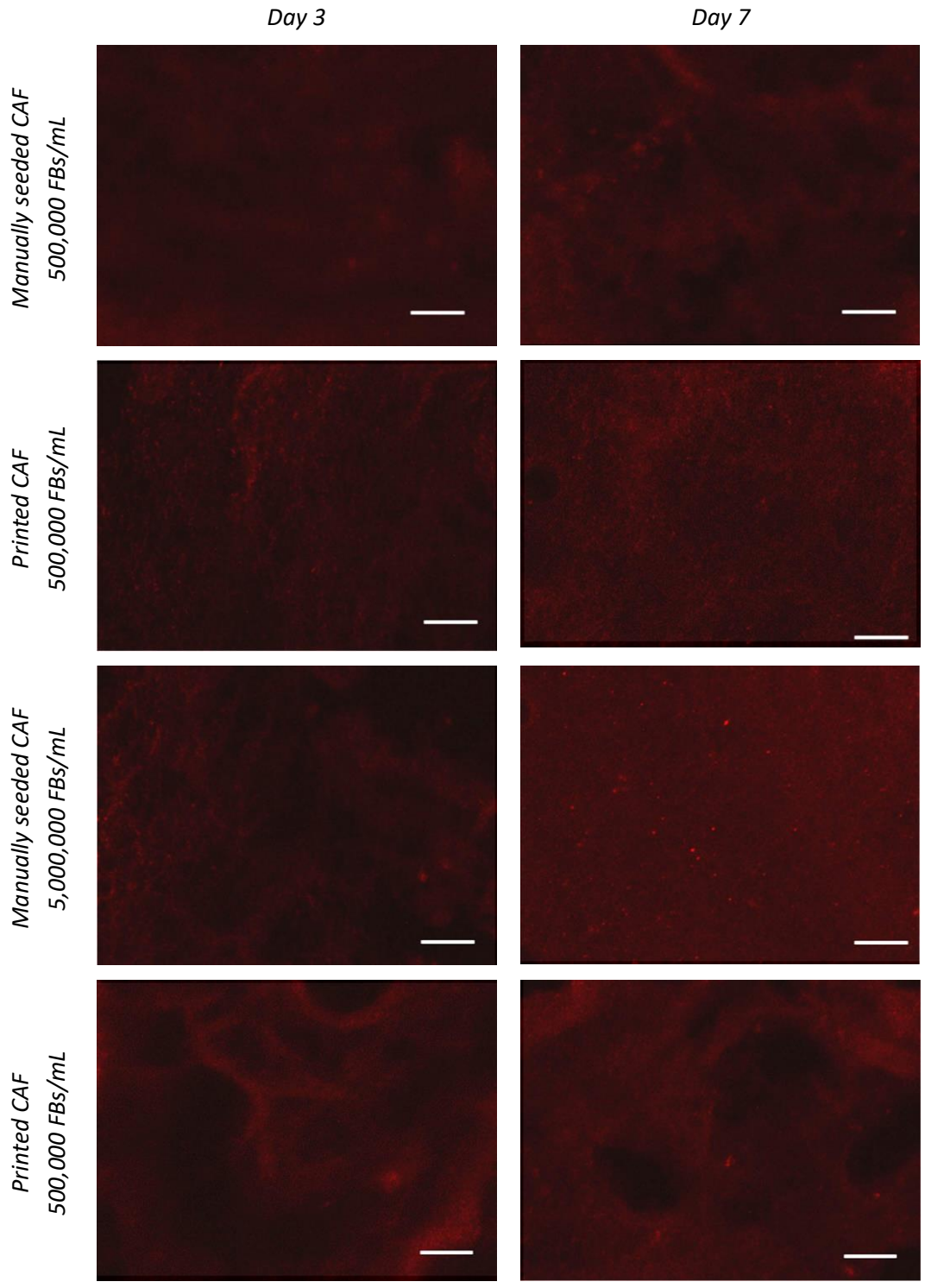

Figure 5. 18. Comparison between the production of new collagen type I (red) after 3 and 7 days by printed and manually seeded fibroblasts at 500,000 cells/mL and 5,000,000 cells/mL after 3 and 7 days. Scale bar represents 200 µm.

Collagen type III could only be found after 3 days in the samples produced with the highest fibroblast density, with a significantly higher presence in the printed models (Fig. 5.19). After 7 days, collagen type III signal appeared in all models, maintaining a higher expression in the printed models with 5,000,000 fibroblasts/mL.

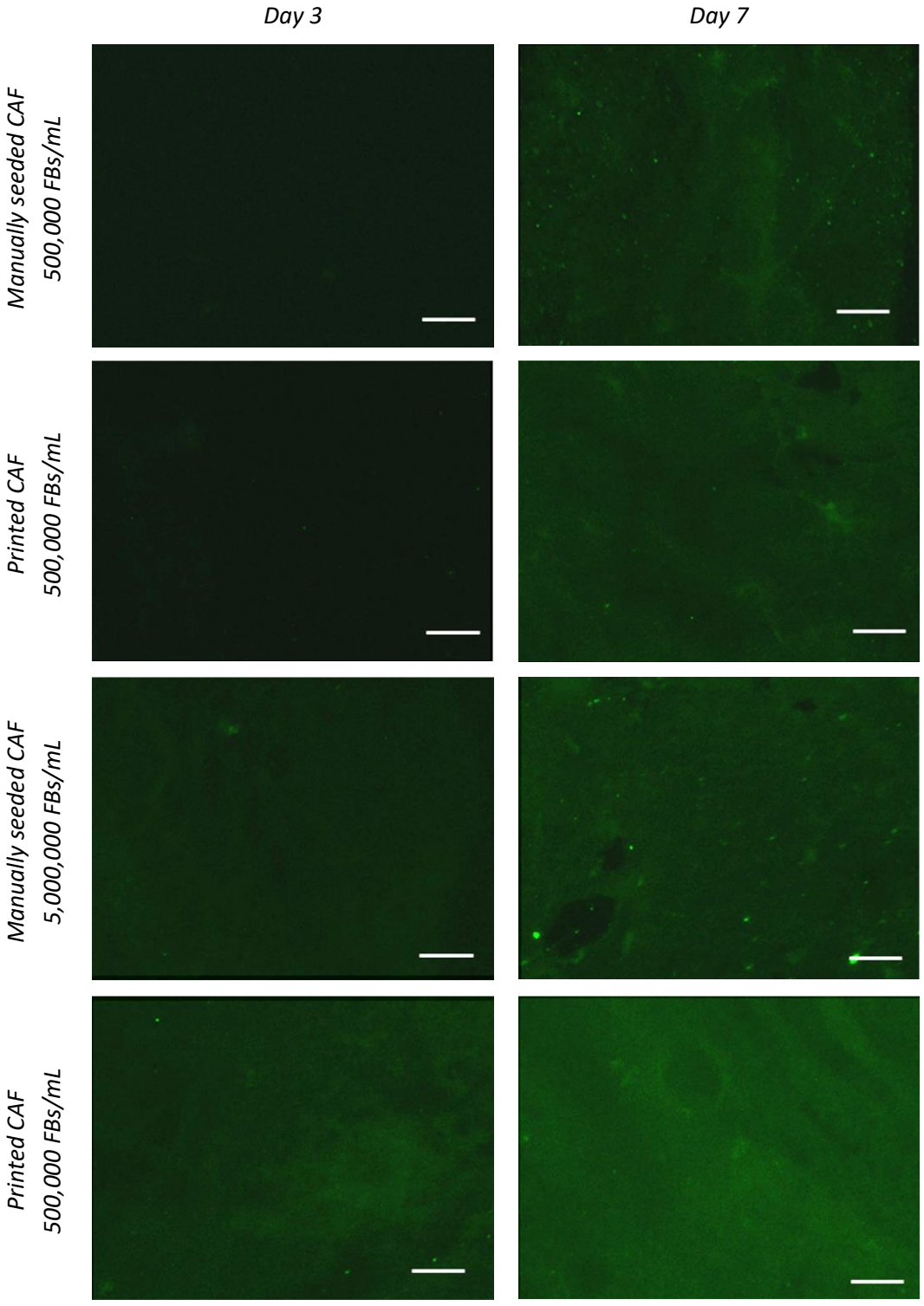

Figure 5. 19. Comparison between the present of new collagen type III (green) after 3 and 7 days in printed and manually seeded models with 500,000 fibroblasts/mL and 5,000,000 fibroblasts/mL. Scale bar represents 200 µm.

The presence of elastin could only be detected in some areas of the samples at day 3 (Fig. 5.20). Only after 7 days, a slight increase on the elastin signal could be identified in the models, with no specific difference between the samples.

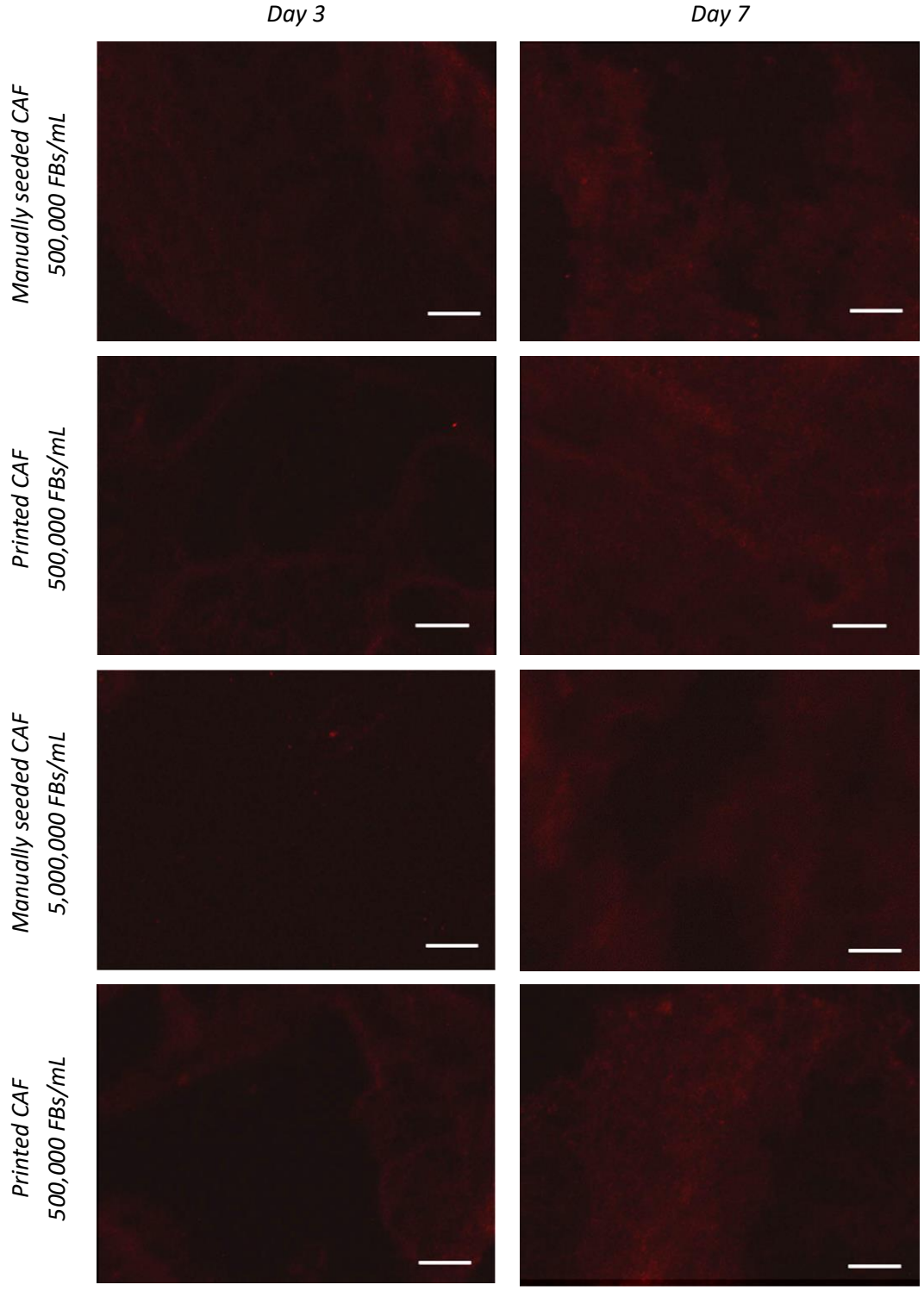

Figure 5. 20. Comparison between the production of elastin (red) after 3 and 7 days by printed and manually seeded fibroblasts at 500,000 cells/mL and 5,000,000 cells/mL after 3 and 7 days. Scale bar represents 200 µm.

Fibronectin was found in all samples after 3 days, especially in the printed models (Fig. 5.21). A significantly higher signal was detected in the samples printed with the highest fibroblast cell densities. After 7 days, the fibronectin signal showed a drop in all samples.

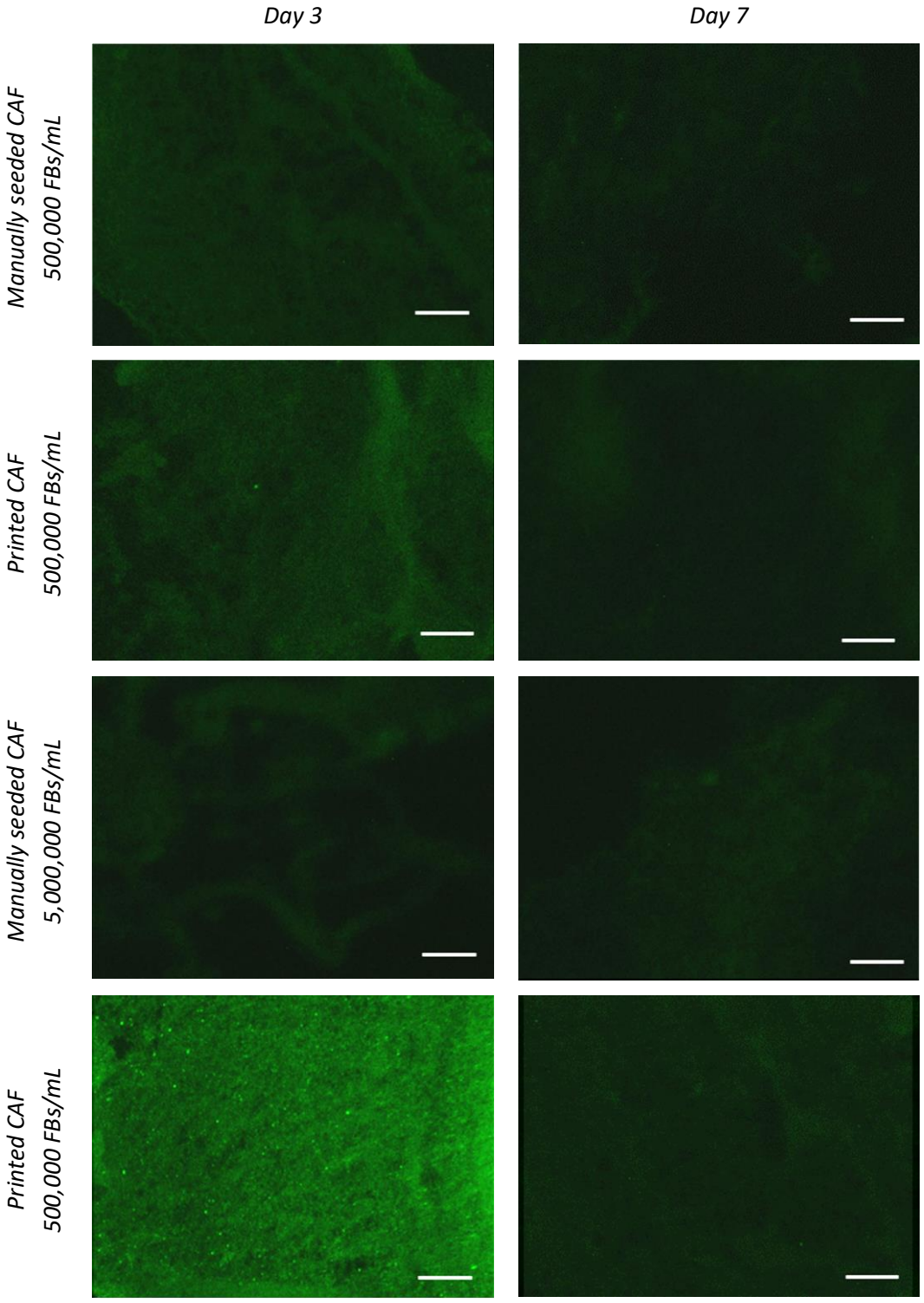

Figure 5. 21. Comparison between the present of fibronectin (green) after 3 and 7 days in printed and manually seeded models with 500,000 fibroblasts/mL and 5,000,000 fibroblasts/mL. Scale bar represents 200 µm.

5.4. Bioprinting Epidermal Layers

5.4.1. Keratinocyte Proliferation

The printing of keratinocytes using ReJI system did not show any impact on the adhesion of keratinocytes to the print bed (Fig. 5.22). Moreover, the printing process did not alter keratinocyte growth and the changes on their morphology over time. By comparing the arrangement of printed and manually seeded keratinocytes after 1 day, it was possible to prove the ability of ReJI to selectively control the keratinocyte location. The uniform distribution of printed keratinocytes promoted their proliferation after 3 days, and their spread along a broader area than manually seeded cells. Consequently, a homogeneous layer of confluent printed keratinocytes was produced after 7 days. In contrast, manually seeded keratinocytes showed an irregular proliferation and distribution, resulting in the early differentiation of some keratinocytes, represented by the change on their morphology.

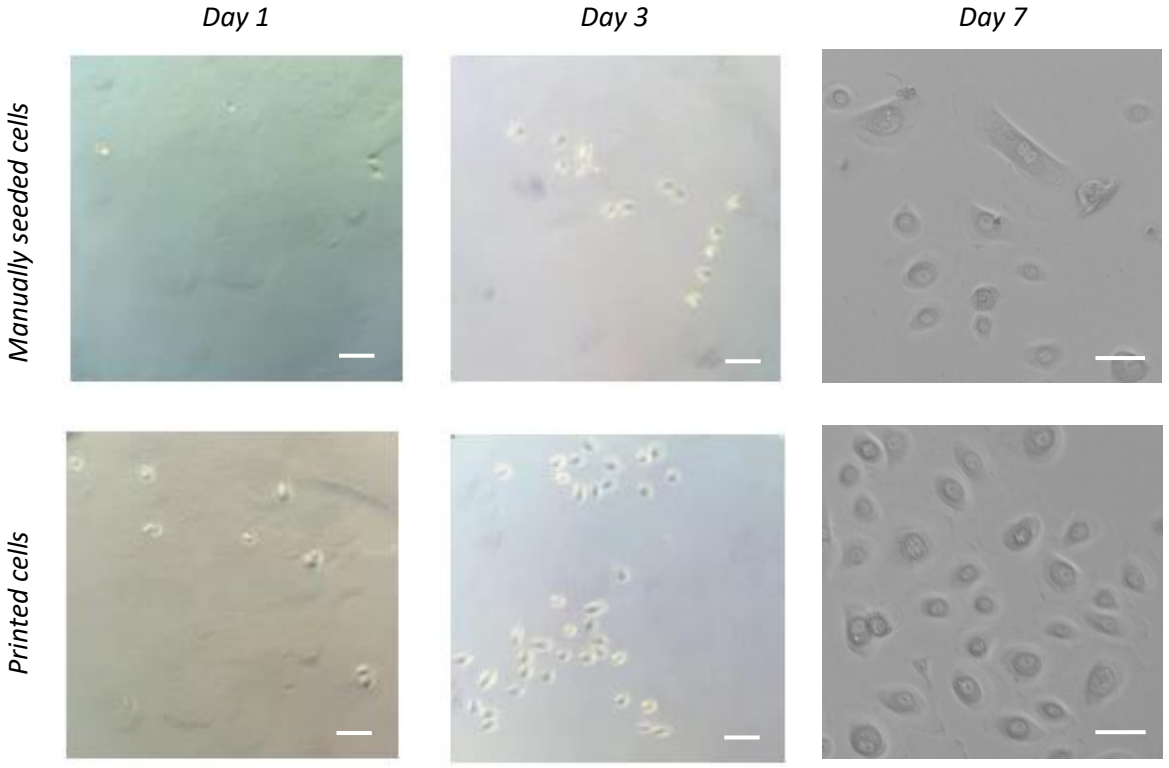

Figure 5. 22. Proliferation and distribution of printed and manually seeded keratinocytes monolayers after 1, 3 and 7 days. Scale bar represents 100 µm.

5.4.2. Keratinocyte Differentiation

The immunostaining of keratinocytes at day 7 confirmed the capacity of printed keratinocytes to present phenotypical changes (Fig. 5.23). The expression of cytokeratin-14 verified the proliferative character of seeded and printed keratinocytes. Meanwhile, the high intensity of involucrin staining in manually seeded cells contrasted with a lower signal in the printed samples, suggesting an earlier differentiation in the manually seeded samples. Finally, the presence of filaggrin stained cells confirmed the capacity of printed keratinocytes to complete their differentiation. Although, the expression of filaggrin by printed keratinocytes was rarely observed after 7 days, with the existence of few stained cells in areas with high cell confluency. By contrast, the presence of keratinocytes in their late differentiation stage was more common in manually seeded cells due to the high distance between them.

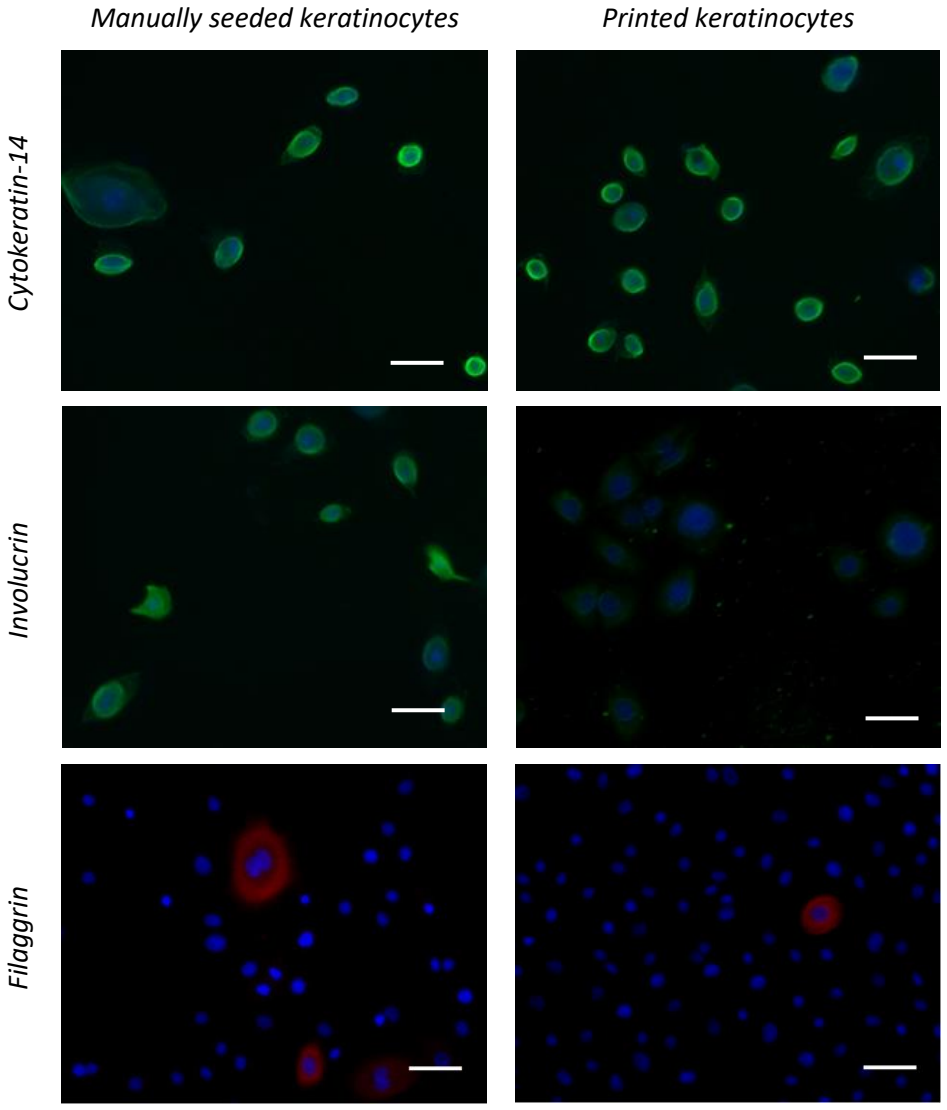

Figure 5. 23. Comparison between the expression of cytokeratin 14 (green), involucrin (green) and filaggrin (red) by manually seeded and printed keratinocytes monolayers after 7 days. The cell nucleus of keratinocytes was stained with DAPI (blue) in all samples. Scale bar represents 100 µm.

5.5. Chapter Discussion

5.5.1. Optimisation of ReJI Printing Process

This chapter has explored some fundamental parameters that must be considered before implementing the Reactive Jet Impingement system. Different elements like the microvalve alignment or the distance between the nozzle and the printer bed can be optimised and applied to all printing works. However, other variables like the applied pressure or the surface hydrophobicity depend on the selected bioinks (Gudapati et al., 2016; Adhikari et al., 2021). By optimising these parameters, it was possible to print a hydrogel construct with high resolution using ReJI system. The precise reaction of the jetted droplets and the controlled deposition of the resulting gel helped to create a network of connected crosslinked dots. The outcoming gridded structure supported the adhesion of the following printed layers, ensuring the stability of the entire printed construct. The quality of the printed assemblage produced with ReJI is highlighted when it is compared to the structures produced by other bioprinting techniques. In a recent work from Schmidt *et al.*, extrusion bioprinting process was optimised to generate cellular scaffolds using different bioinks (Schmidt et al., 2019). In comparison to the constructs produced with ReJI, the shape fidelity of these printed samples was undermined by the low resolution of the extrusion technique (Fig. 5.24). In this study, Matrigel was the printed material with a higher resemblance to the CAF components. The printing of this gel resulted in an undefined architecture, suggesting the limited stability and reproducibility of the final Matrigel construct. Similarly, the resolution of the motifs produced by inkjet bioprinters is limited by the requirement of additional crosslinking steps after the printing of each layer (Fig. 5.24) (Lee et al., 2014). Consequently, the structures made by inkjet bioprinters sometimes resemble the quality of the gels created by conventional casting methods (Duarte Campos et al., 2019).

Extrusion bioprinting					***Inkjet bioprinting***
Cellink Bioink	*Cellink RGD*	*GelXA*	*GelXA Laminink+*	*Matrigel*	*Collagen type I*
					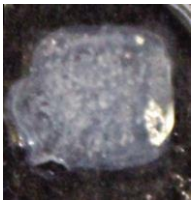

Figure 5. 24. Comparison between the printing quality of gels printed by extrusion and inkjet-based bioprinting using different bioinks. Images obtained from Schmidt et al. 2019 and Lee et al. 2014.

The possibility to define the printing structure using bitmaps and a simple script facilitates the accessibility of ReJI to non-experienced users. This intuitive approach contrasts with the complexity of G codes and STL files required in most commercial bioprinters (Fay, 2020). Additionally, the capacity of printing biomaterials with similar viscosities to the ones conventionally used in the laboratories, like collagen or fibrin, makes it easier to adapt ReJI process to current research projects.

In this study, ReJI has demonstrated its capacity to produce in parallel a significant number of models in a short period. The time required to generate tissue models using other bioprinting techniques is not often stated, and it is difficult to benchmark (Ke et al., 2022). The process speed is usually defined only as the number of droplets printed per second without considering the overall printing time. Only in a recent work, Cubo *et al*. claim the production of full skin models in 35 minutes using extrusion bioprinting (Cubo et al., 2016). This duration is still far from the 180 seconds required to produce a model using ReJI. However, Cubo *et al*. state that most of this time is necessary for the complete crosslinking of the printed fibrin structure. This declaration highlights the advantage of the impingement process in eliminating waiting times, and, consequently on the high-throughput production of skin models.

Moreover, ReJI has shown a highly homogeneous printing, maintaining a linear progression on the number of printed cells through the different layers regardless of the cell type and density. The increment in the standard deviation after printing more than ten layers using high cell densities could be explained by the effect of the interaction between cells. When cells communicate with near cells and begin to associate, their morphology starts to change and they create groups of interacting cells, as seen in figure 5.10. The formation of cell aggregates occurs mainly in solutions containing high cell densities and could justify these variations in the number of cells printed per droplet. The incorporation of bioink agitators during the printing of high cell densities could help to minimise these standard deviations in future studies. Additionally, the significant variations between the printing of fibroblast and keratinocytes could be explained by their different behaviour. The confluence of keratinocytes can have a direct effect on their phenotype, promoting their differentiation and their adhesion to the exposed surfaces (Poumay & Pittelkow, 1995a). The aggregation of keratinocytes could clarify the growth on the number of cells observed during the live/dead staining of printed keratinocytes with a density of 5,000,000 cells/mL (Fig. 5.8). The presence of differentiated keratinocytes can also be distinguished in these samples, supporting this hypothesis. To solve

this issue, Rho-kinase (ROCK) inhibitor was introduced to the EpiLife medium during the printing of keratinocytes in the experiments performed in section 5.4. The incorporation of this component helped to reduce the instability of keratinocytes, without affecting their adhesion or proliferation based on the results obtained in this section (Anderson et al., 2018; Chapman et al., 2014; Strudwick et al., 2015).

In contrast to the homogeneous results obtained with ReJI, extrusion bioprinting has shown limited reproducibility on the number of cells deposited per layer (Emmermacher et al., 2020). Due to the high viscosity of bioinks, the control over the cell distribution is restricted. The use of homogenisation methods is also limited by their effect on cell viability (Müller et al., 2022). In the case of inkjet or microvalve bioprinting, printing consistency could be perturbed by cell sedimentation in the nozzle, especially during the waiting times required to perform the crosslinking process between layers (Saunders et al., 2008; Lee et al., 2009). Incorporating agitators into the bioink reservoir is one of the most extended approaches to solve this problem (Dudman et al., 2020). In contrast to other microvalve-based technologies, ReJI presented a higher control over the cell deposition and a reduced nozzle blockage, which could be explained by its capacity to perform continuous printing. The constant pneumatic pressure on the bioink could promote the bioink flow, avoiding cell precipitation. Additionally, optimisation of the microvalve cleaning process helped to prevent the nozzle blockage during ReJI process. The presence of remaining cells and protein bodies in the microvalve was initially observed to affect the reproducibility of the printing process in the initial studies. Therefore, different cleaning processes were tested and optimised to determine the best method to remove any biological product from the nozzle without affecting the microvalve internal mechanism.

Finally, the printing pressure is one of the most fundamental parameters that need to be adapted for the correct impingement process. The pressure required for each bioink is defined as the minimum value necessary to overcome the surface tension in the nozzle and produce a continuous jet of defined droplets (Fromm, 1984; Elkaseer et al., 2022). In this study, the values for each bioink were established experimentally using the stroboscopic camera to assess the droplet formation. However, if ReJI process needs to be standardised for industrial application in the near future, it will be necessary to define a theoretical method to determine the best printing pressure. For microvalve-based technologies, the bioink printability is defined by the inverse of the Ohnesorge number denominated Z value (McKinley & Renardy,

2011). This dimensionless number can be calculated by dividing the Reynolds number (N_{Re}), which represents the ratio of inertial to viscous forces, by the square root of the Weber number (new), which exemplifies the balance between inertial and capillary forces (Fig. 5.25) (Liu & Derby, 2019).

$$N_{Re} = \frac{v\mathrm{r}\rho}{\eta} \quad (1)$$

$$N_{We} = \frac{v^2\mathrm{r}\rho}{\gamma} \quad (2)$$

$$Z = \frac{N_{Re}}{(N_{We})^{1/2}} = \frac{(\mathrm{r}\rho\gamma)^{1/2}}{\eta} \quad (3)$$

Figure 5. 25. Theoretical calculation of (1) Reynolds number (N_{Re}) and (2) Weber number (N_{We}), necessary to determine the Ohnesorge number (Z value) associated with material printability using microvalve-based systems. The values v, r, ρ, η and γ represent the flow velocity, nozzle radius, density, viscosity, and surface tension of bio-inks, respectively.

Z value depends on factors like the nozzle radius, the mean droplet velocity, the density and viscosity of bioinks or the surface tension between the nozzle and the bioink. Bioinks with a Z value comprehended between 4 and 12 are considered printable (Ng et al., 2017). Those bioinks with Z values lower than 4 experiment the formation of elongated droplets, denominated satellite droplets. Apart from the studies of droplet formation, it will be essential to assess the crosslinking speed of the jetted droplets during the impingement process to determine the bioink printability using ReJI. Therefore, rheological characterisation of bioinks will become essential to determine some of the parameters that determine the biomaterial printability.

5.5.2. Effect of Printing Process on Dermal Models

As proof-of-concept, dermal models were printed using collagen-alginate-fibrin (CAF) gels as dermal matrices. These bioinks consist of a gel precursor and crosslinker with a formulation already adapted and tested for its use in the ReJI system (da Conceicao Ribeiro, 2019). CAF is comprised of collagen type I and fibrin, which are components already present in human skin, facilitating its integration into the production of skin equivalents (Sheikholeslam et al., 2018). Sodium alginate is also present in the CAF formulation, and despite not being present in native skin, its natural origin, biocompatibility and biodegradability make it suitable for its incorporation to the skin model (Lee & Mooney, 2012).

In this chapter, ReJI system has demonstrated its ability to maintain fibroblast viability and functionality regardless of the printed cell density. Controlling the three-dimensional location of cells made it possible to generate dermal models with a homogeneous fibroblast distribution in contrast to manually seeded dermal models. The creation of crosslinked points during the impingement process favoured the encapsulation of cells and the precise definition of the initial cell position, and the production of a more consistent and reproducible dermis. As a result, cells could move and populate the printed architecture in an organised manner, occupying the dermal matrix uniformly.

Skin models need to own a stable structure during long periods, maintaining an equilibrium between dermal matrix degradation and producing new extracellular matrix components by fibroblasts. One of the main reported disadvantages of fibrin-based biomaterials for manufacturing skin models is their quick natural degradation by fibroblasts (Mirshahi et al., 1991). However, the creation of crosslinking nucleus and the control over the spatial distance between cells by the ReJI process has demonstrated to slow down the degradation of fibrin-based gels like CAF and provide stability to the dermal models. This precise control on the crosslinking reaction at the microscale level could justify the high condensation and enhanced fibrillar organization in acellular printed CAF gels compared to manually seeded samples observed in the figure 5.13. In this work, manually seeded CAF gels showed a complete degradation at day 7 when a solution of 500,000 fibroblasts/mL was used to produce the dermal models, and after only 1 day when the number of encapsulated fibroblasts was 5,000,000 fibroblasts/mL. In contrast, printed CAF-based models maintained their structure for at least 28 days, as will be demonstrated in future chapters.

Furthermore, the design of the printed structure also acquires a high relevance in the diffusion of nutrients, gases and signal molecules across the dermal model (Zhang et al., 2022b). The distance between the generated gel droplets allowed the creation of a matrix capable of ensuring the transportation of essential molecules and survival of fibroblasts, regardless the printed cell densities. These results contrast with the appearance of necrotic bodies observed when high cell concentrations were used in previous publications. For instance, the lack of cell organisation in organoids often leads to cellular apoptosis in their nucleus due to the restricted diffusion of oxygen and nutrients (Grebenyuk & Ranga, 2019).

The selection of fibroblast densities on the generation of skin equivalents has demonstrated to be a key influencing factor on the final properties of the dermal layer. The incorporation of high cell densities into the dermal models has proved to boost the adaptation of the fibroblasts to the gels after only 1 day. Cells usually require time to adapt to new three-dimensional environments and to adhere to new surfaces. However, the interaction between fibroblasts generated during the printing of 5 million cells/mL results in their faster adaptation to the new conditions, presenting a spindle-like morphology after only 1 day. The proximity and communication with other cells are the main triggers for cell adhesion in these samples (Katsumi et al., 2004; Tanaka et al., 2009). As a result, cells start to proliferate and expand through the dermal constructs enhancing the model complexity after only three days. These findings contrast with the maturation of dermal models prepared with ten times lower cell densities. Printed fibroblasts are found homogeneously dispersed and isolated in these samples on day 1. They need at least three days to adapt to their new microenvironment and adhere to the CAF matrix. Therefore, fibroblasts in these samples require at least 7 days to reach the same confluency as the models seeded with higher cell densities at day 3. Despite the apparently delayed adaptation to the new matrix, the number of fibroblasts linearly increased from day 1 to day 7 in printed samples, in contrast to the reduced proliferation from day 1 to day 3 in manually seeded models. These differences in the initial proliferation ramp between printed and manually seeded samples can also be observed in models containing higher cell densities. This finding underlines the advantages of ReJI printing process in reducing the time required to produce dermal models.

The printing models also diverge from the manual models on the production of new extracellular matrix. As it can be observed in the SEM images, more pronounced changes in the matrix content and arrangement can be seen in the printed samples at earlier time points.

These differences could also be monitored by assessing the presence of characteristic dermal components in the models. In the case of printed models containing 500,000 cells/mL, a slight rise in collagen type I and fibronectin could be observed in the printed models compared to the manually seeded samples at this concentration. However, these results provide a general overview, and a more exhaustive analysis of extracellular matrix composition will be required to conclude their impact on the complexity of the dermal models. An initial attempt to quantify the presence of dermal proteins was performed using Real-Time Quantitative Polymerase Chain Reaction (qPCR). Unfortunately, due to some problems experienced during the cDNA synthesis, it was not possible to produce enough representative data, and further attempts will need to be performed in the future.

In the case of printed dermal models prepared with 5,000,000 cells/mL, the fast adaptation of their fibroblasts to the new environment accelerates their maturation. At the initial time points, a number of dead cells were observed on the surface of the gel. The presence of these cells could be caused by the initial high confluency of fibroblasts. As the fibroblasts acquire their final distribution through the gel and their numbers are stabilised, the viability of the models is increased. Additionally, the quick conformation of these models promotes early changes in the extracellular content. After only one day, fibroblast applied tensional forces over the CAF matrix producing a contraction on the fibrillar matrix and encouraging the secretion of new matrix components observed in figure 5.15. The higher presence of collagen type III and fibronectin on day 3 highlights the advanced complexity of these models in comparison to the other samples. The acceleration of the dermal maturation could help to reduce the time required to produce the skin models and improve the complexity of the models.

The comparison between the two studied fibroblast densities and those selected in previous studies is hindered by how the selected cell densities are reported. Most publications associated with skin bioprinting describe the use of $1x10^6$ fibroblasts/mL solutions, but they do not detail the volume of the printed model or the number of cells printed per droplet. As a result, the total amount of the fibroblasts deposited per model and their final confluency significantly varies between samples (Fig. 5.26) (Lee et al., 2009; Pourchet et al., 2017).

Additionally, the effect of the printing process on cell viability or the resulting fibroblast distribution has been reported in a few studies (Lee et al., 2009; Koch et al., 2012; Lee et al., 2014). Only *Lee et al.* details the printing of approximately 23,250 fibroblasts per model in

2009, and the increase to 140,000 fibroblasts/cm^2 in their publication in 2014. This last value is comprehended between the cell density quantified in this work. However, the impact of the fibroblast density on dermal maturation and in the skin model properties has not been reported yet in these studies.

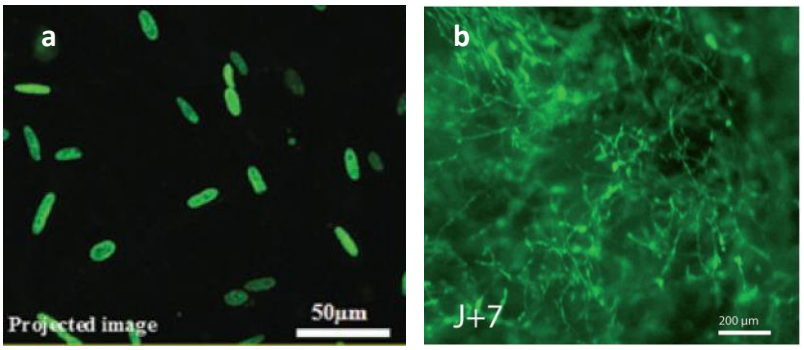

Figure 5. 26. Comparison between the confluency of fibroblasts at day 7, in two publications reporting the use of 1x10^6 fibroblasts/mL. Images obtained from (a) Lee et al. 2009 and (b) Pourchet et al. 2016.

The increment in the cell density has already been reported to promote the maturation of other *in vitro* tissue models (Shamsul et al., 2019; Daly et al., 2021; da Conceicao Ribeiro et al., 2018). These studies have demonstrated that the confinement effect in some cell types can enhance their contact guidance and encourage their motility and the population of the matrix. Furthermore, the rise in the fibroblast densities in skin models has already been reported to impact the epidermal architecture, with just an increase on the fibroblast concentration from 2x10^4 to 8x10^4 cells/mL (El-Ghalbzouri et al., 2002). Selection of fibroblast concentration for the creation of skin should be carefully selected, as high fibroblast densities could lead to the recreation of specific skin conditions such as fibrosis (Doolin et al., 2021). Therefore, a balance between tissue maturation and the homology to healthy skin must be found. The comparison between the number of fibroblasts in the human dermis and the values obtained in the printed models after seven days confirms the suitability of the selected initial densities. Based on previous studies on human skin, the number of cells in the native dermis corresponds to a range from 2.1 to 1 million fibroblasts/cm^2 (Randolph & Simon, 1998; Helary et al., 2005). These fibroblast densities are comprehended between the 1.3 million fibroblasts/cm^2 quantified in the models printed with the highest cell densities after their stabilisation at day 7, and it is lower than the 0.6 million fibroblasts/cm^2 found in the models printed with the lowest cell density at the same time point.

5.5.3. Effect of Printing Process on Keratinocytes

Printing keratinocytes with ReJI system did not affect their viability, regardless of printed cell density. Moreover, essential keratinocyte functions, such as their proliferation or differentiation were also preserved after the printing process. The possibility of controlling the cell location using ReJI printing process allowed the creation of more uniform keratinocyte deposition compared to manually seeded samples. Due to the homogenous distribution of printed cells, keratinocytes showed more consistent growth, covering a wider area and reducing the number of empty spaces found in manually seeded samples. Additionally, the formation of a confluent keratinocyte layer at day 7 could have also been promoted by an increment in the cellular growth rate. Keratinocyte requires the presence of other cells in the immediacy to maintain their proliferative state (Deyrieux & Wilson, 2007). In the case of printed samples, the proximity between keratinocytes observed at day 3 was higher than in the manually seeded cells, and it could have been responsible for their different growth rate. On this occasion, the occurrence of keratinocytes helped to unify and promote cellular proliferation. However, an excessive accumulation of keratinocytes can also trigger their differentiation, as observed in figure 5.23 (Poumay & Pittelkow, 1995b; Pavel et al., 2018). This factor must be considered during the selection of keratinocyte densities, and a balance between keratinocyte proliferation and differentiation must be found to produce epidermal layers in the skin models. Oppositely, the distance between keratinocytes observed in manually seeded samples resulted in the generation of separated cellular patches. Besides, the isolation of some keratinocytes in these samples implied a reduction in their growth rate and their early differentiation, evidenced by their morphological changes and expression of involucrin and filaggrin. The lack of control over the keratinocyte location is one of the most critical issues associated with the skin equivalents produced by conventional methods. Furthermore, the lack of consistency in the epidermal properties between samples implies a high variation in the results obtained during the assessment of commercial products (Suhail et al., 2019). Therefore, the control over the deposition of keratinocytes acquires a high relevance during the manufacturing of skin models. ReJI process has demonstrated its capacity to produce homogeneous epidermal layers, which could help to improve the reproducibility and quality of skin models. However, to confirm this hypothesis, it will be necessary to assess the epidermal stratification in the printed skin models and optimise the keratinocyte density to ensure the correct epidermal formation.

5.5.4. Overview of ReJI as Bioprinting Process

ReJI system has demonstrated to produce structures with remarkable shape fidelity aided by the high precision of the impingement process. In contrast to other bioprinting technologies, ReJI is a user-friendly system which allows the printing of high cell densities without affecting their viability. Additionally, ReJI process guarantees the production of multi-layered structures without the conventional waiting times required with other bioprinting techniques.

This novel bioprinting system has also proved a high regulation over the number of cells deposited, guaranteeing the production of reproducible samples. By controlling the cell location in the gels with the ReJI system, some of the limitations experienced by traditional tissue engineering methods have been overcome. Printed fibroblasts in dermal models have proved to boost their proliferation and the generation of their own extracellular matrix components in a shorter time than manually seeded models. Additionally, the organised fibroblast arrangement supports the maturation of printed dermal models containing high cell densities, avoiding the premature gel degradation observed in manually seeded models. Moreover, the printing of homogeneously distributed keratinocytes promotes the generation of uniform epidermal basal layer, contrasting with the results obtained by manually seeded keratinocytes. The acceleration of the dermal and basal epidermal layer formation in the printed samples could help to reduce the conventional times required to manufacture the skin models. On the other hand, the capacity of ReJI system to print in parallel models in a reduced time without losing resolution highlights their suitability for the large-scale manufacturing of skin equivalents. The automation of this process could help to reduce the time and costs required to produce skin models, stimulating their use as testing platforms in the industry.

All these aspects highlight the advantages of ReJI process on the production of skin models. However, further experimental work will be required before concluding the feasibility of the ReJI process to improve the quality of current skin equivalents. The optimisation of the dermal and epidermal bioink formulation will be essential to replicate the complexity of native skin microenvironments and guarantee their printability. Additionally, printing keratinocyte density will need to be adjusted to ensure the formation of a homogeneous epidermal layer. In the case of fibroblast densities, their impact on skin maturation and on the properties of the final model will also need to be assessed. Finally, the combination of all these parameters will help to determine the impact of ReJI system on the quality of *in vitro* skin models and on their industrial scalability.

CHAPTER 6. SELECTION OF DERMAL BIOINKS

6.1. Introduction

The dermal layer plays an essential role providing structural support and stability to the skin. Some variables like the mechanical properties or the extracellular components that populate the dermis are responsible for supporting the fibroblast mobility and promoting cell proliferation and ECM renewal. Despite the relevance of the dermal characteristics, they are often disregarded during the manufacturing of skin models. As a result, the biomaterials used to mimic the dermal matrix are often selected without following any specific criteria. Focusing on this research gap, this chapter aims to investigate the correlation between the formulation of dermal bioinks and its ability to influence the fibroblast behaviour to recreate biological microenvironments like the ones found in the native dermis.

This chapter is focused on exploring the differences between the dermal models produced with two natural skin components, such as collagen type I and fibrin. On one hand, the importance of collagen type I origin and extraction method was assessed by comparing the physicochemical properties and the influence on the fibroblast behaviour of collagen solutions obtained from different animal sources. Additionally, the effect of the collagen neutralisation method and the incorporation of commercial RAFT^{TM} absorbers on the production of collagen matrices was also studied. On the other hand, the possibility of customising the properties of fibrin gels was also explored by introducing alginate and collagen into the fibrin bioinks. Analysis of the chemical structure, matrix arrangement and mechanical properties of the selected bioink formulations was performed to understand the differences between them.

The impact of the different dermal formulations on the fibroblast behaviour was determined by exploring the morphology and distribution of the encapsulated fibroblasts, along with their proliferation and production of new extracellular matrix. By comparing the physicochemical and biological characteristics of each dermal model, it was possible to understand the role of the bioink components and determine the resemblance of each sample to specific dermal regions. Finally, the assessment of the bioink printability was performed to determine the best formulation for mimicking the dermal structure using the ReJI bioprinting system.

6.2. Characterisation of Dermal Bioinks

6.2.1. Chemical Differences between Collagen Solutions

The evaluation of the chemical bonds by Fourier Transform Infrared spectroscopy (FTIR) allowed the study of the chemical similarities and differences between the commercial collagen solutions (Fig. 6.1). The appearance of specific chemical groups associated with collagen type I in all FTIR spectra, confirmed the presence of type I collagen monomers in the selected collagen solutions regardless their animal source or extraction method. Some of these characteristic absorption peaks were found at 1659 cm^{-1},1555 cm^{-1},1340 cm^{-1},1240 cm^{-1}, and corresponded to the C=O stretching in the primary amide, the N-H bending in the secondary amide, and the N-H bending and C-N stretching associated with the tertiary amide, respectively (Table 6.1). Despite the high similarities between most absorption bands in the samples, some variations in the chemical composition could be observed, especially at wavelengths below 1000 cm^{-1}. The presence of extra signals and the differences in the relative intensities between the amides underlined some chemical differences between the collagens.

Table 6. 1. Examples of the most characteristic FTIR bands obtained after the analysis of human, rat, telo-bovine, atelo-bovine, calf and jellyfish collagen solutions.

Characteristic Bands (cm^{-1})	***Human Collagen***	***Rat Collagen***	***Bovine Collagen***	***Atelo-Bovine***	***Calf Collagen***	***Jellyfish Collagen***
Amide I *(C=O stretching)*	1658	1653	1652	1651	1633	1647
Amide II *(N-H bending)*	1549	1548	1551	1549	1548	1542
CH_3 bending *CH_2 bending*	1452	1453	1455	1454	1456	1453
COO- *(C=O stretching)*	1405	1405	1407	1407	1409	1406
Amide III *(N-H bending)*	1338	1339	1338	1337	1338	1338
Amide III *(C-N stretching)*	1235	1243	1241	1243	1235	1244
C-O stretching	1081	1078	1082	1079	1080	1079
C–O–C stretching	1040	1028	1032	1032	1027	1027

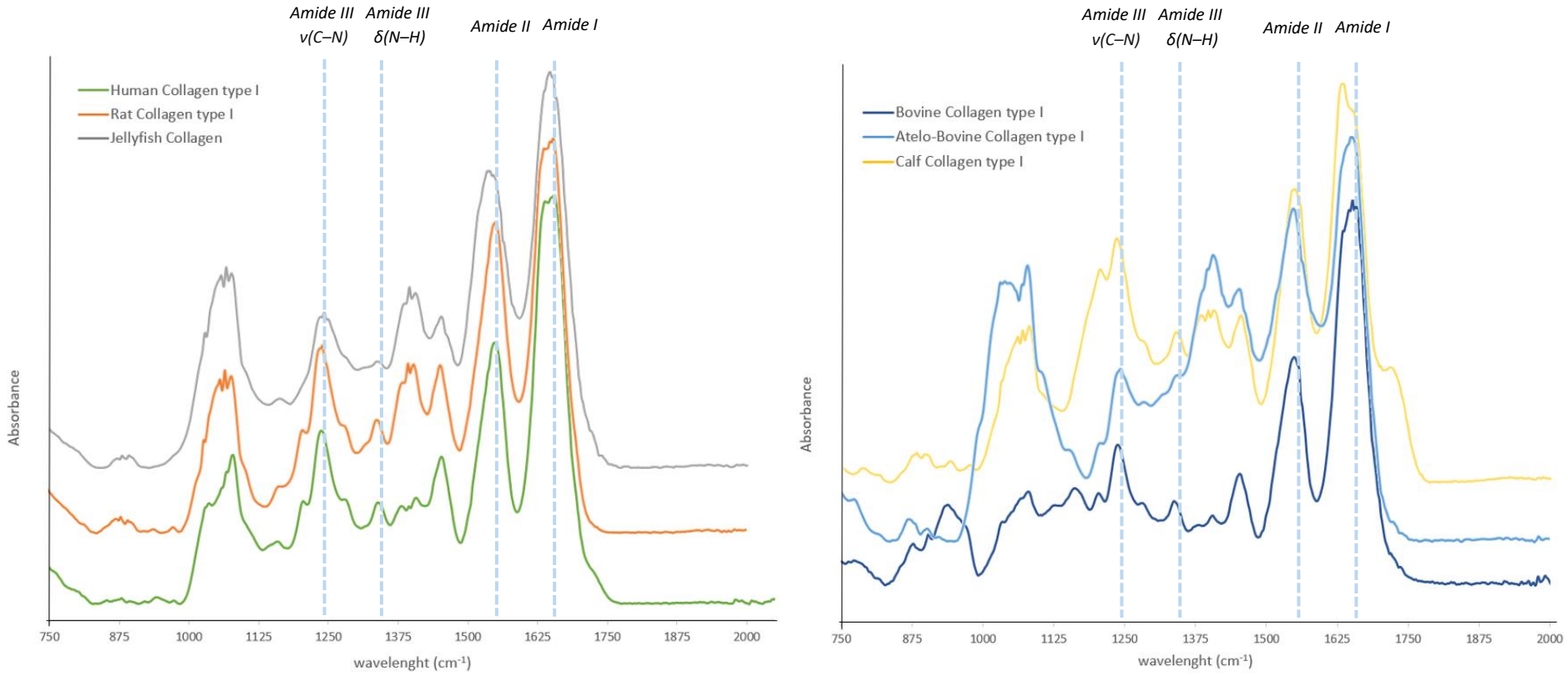

Figure 6. 1. Chemical analysis by FTIR of collagen solutions extracted from different animal sources, including human, rat, bovine, calf and jellyfish. The effect of the collagen extraction method was assessed by comparing telo-bovine and atelo-bovine collagen. Blue discontinuous lines indicate the wavelengths corresponding to amide I, II and III groups characteristic of native collagen type I.

6.2.2. Triple Helix Content in Collagen Solutions

Collagen type I is distinguished by their triple helical conformation as its main secondary structure. The measurement of triple helix content in the collagen solution was performed by circular dichroism spectroscopy, analysing its specific absorption band at 222 nm, to compare the quality of the collagen solutions. Despite studying the same collagen concentration, the quantification of triple helices revealed significant variations depending on the animal origin of the collagen solutions (Fig. 6.2). Collagen obtained from rat tail and bovine tendons showed a similar amount of triple helix compared with the lower quantity measured in human collagen. The effect of the extraction method on the triple helix content was visible when comparing telo- and atelo-bovine collagen. A slight reduction in the triple helix values could be observed in atelo-bovine collagen. In the case of collagen derived from jellyfish and calf skin, the triple helix content presented values three and five times lower than rat collagen.

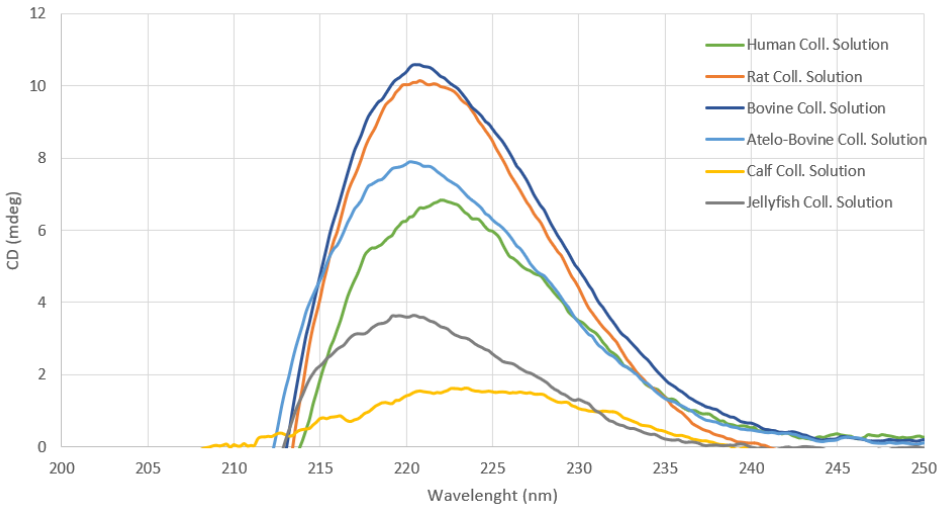

Figure 6. 2. Evaluation of triple helix content at its characteristic peak wavelength of 222nm by Circular Dichroism Spectroscopy. The triple helix content was compared between collagen solutions obtained from different sources, including human, rat, calf, jellyfish and bovine collagen. The effect of the collagen extraction method on the triple helix content was studied by comparing telo-bovine and atelo-bovine collagen solutions.

The evaluation of the triple helix content at different temperatures also uncovered remarkable variations in the thermal stability of the collagen solutions depending on their origin (Fig. 6.3). Rat collagen showed a higher thermal resistance than other collagen solutions, presenting a fast decrease in the triple helix content only at temperatures higher than 40°C. In the case of human and bovine collagen solutions, their triple helix values started to decrease after 30°C, but their degradation rate was different. On the one hand, bovine collagen presented a complete degradation of the triple helix content at 40°C, whereas human collagen required a

temperature above 47°C. The similarities between telo and atelo-bovine collagen profiles suggested the lack of influence of the extraction method on the thermal degradation of the triple helix.

In contrast to previous samples, jellyfish collagen presented a reduced thermal stability with the drop in the triple helix values at 24°C, whereas calf collagen presented a negligible triple helix content, without showing any variations regardless the temperature.

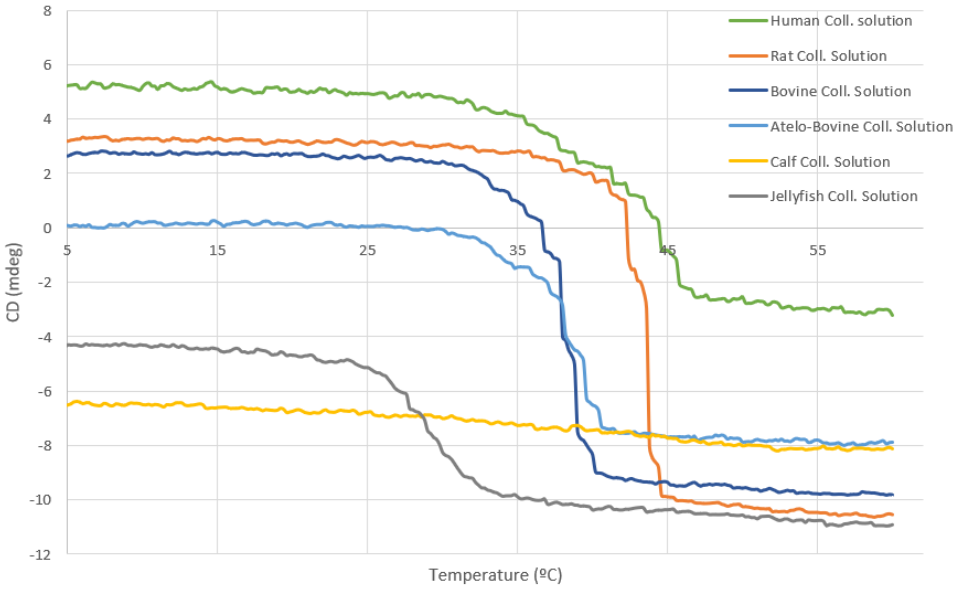

Figure 6. 3. Characterisation of the thermal degradation of the triple helix content in collagen solutions by analysing their Circular Dichroism spectra at 222nm. The impact of the collagen source and its extraction method on the triple helix stability was assessed by comparing human, rat, telo-bovine, atelo-bovine, calf and jellyfish collagen.

The incorporation of NaOH and $NaHCO_3$ into the collagen solutions to produce collagen gels demonstrated to enhance the thermal stability of human, rat and bovine collagens (Fig. 6.4). In the case of human, telo- and atelo-bovine collagen, the stability of the triple helix was maintained until reaching 38°C. At this temperature, the triple helix values presented a slight variation, showing only a significant reduction at temperatures higher than 41°C. Meanwhile, rat collagen gels presented a similar thermal degradation profile than rat collagen solution. In general, the neutralisation method employed for the generation of collagen gels did not influence the thermal stability of the samples.

The inability to produce gels using the selected calf and jellyfish collagen solutions impeded their utilisation on the production of dermal models, and consequently the continuation of the studies with them.

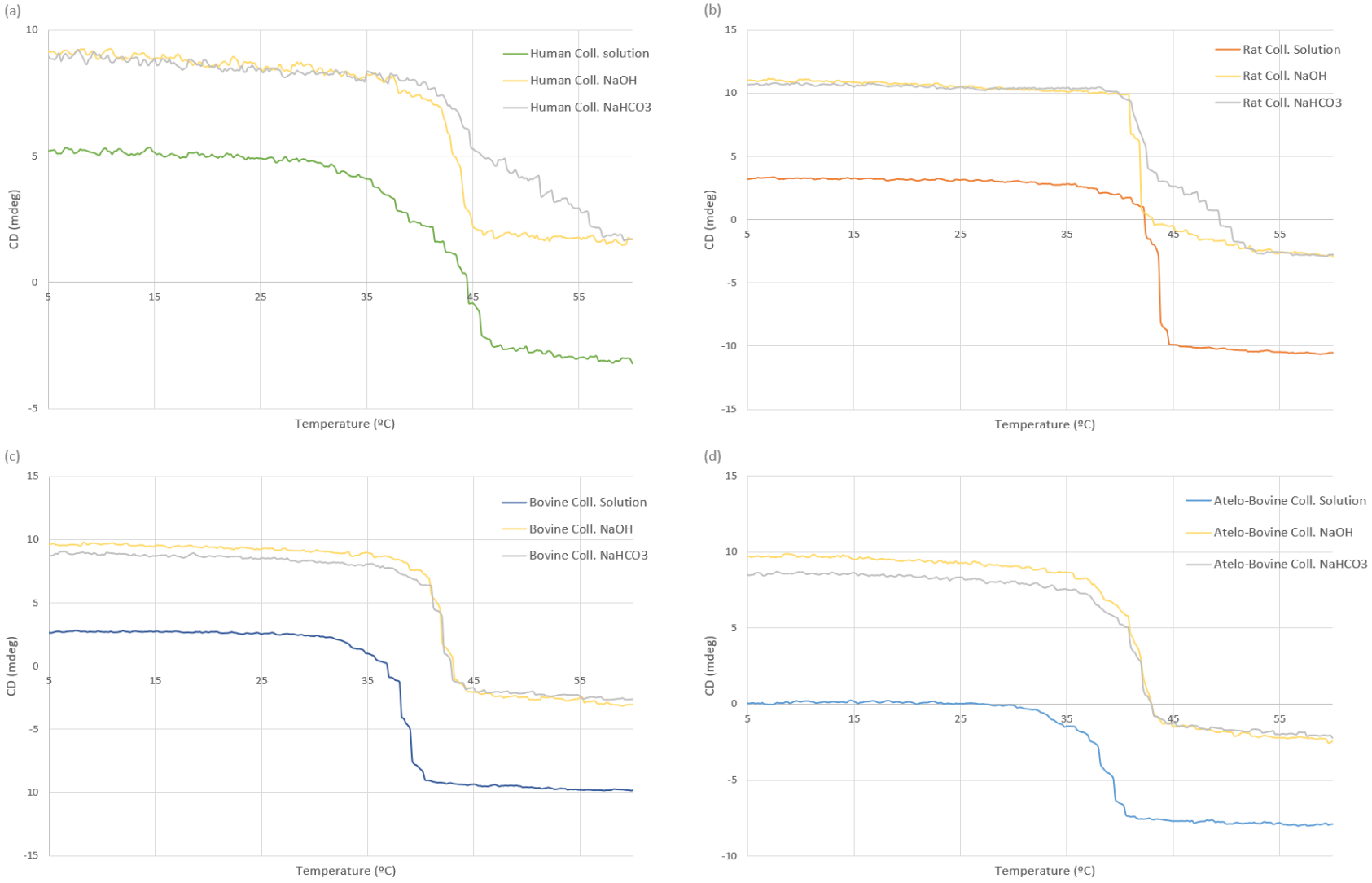

Figure 6. 4. Comparison of the thermal degradation of the triple helix content in collagen solutions and their corresponding gels neutralised with NaOH and $NaHCO_3$. Collagen solutions were obtained from different sources including (a) human, (b) rat, (c) telo-bovine and (d) atelo-bovine collagen.

6.2.3. Fibrillar Organisation of Dermal Matrix

During the neutralisation of collagen solutions to a physiological pH, collagen monomers recover their original chemical interactions and restore their native fibrillar configuration. The characterisation of the collagen gels by Scanning Electron Microscopy (SEM) revealed remarkable differences in the resulting matrix depending on the collagen origin and the selected neutralisation method (Fig. 6.5).

Human collagen gels produced with NaOH were characterised by the presence of thin fibres situated closer to each other, but without following an apparent pattern. Although the thickness of the fibres in rat and human collagen neutralised with NaOH was similar, their arrangement differed. The neutralisation of rat collagen with NaOH resulted in the conglomeration of the fibres forming spherical bundles, with a diameter comprehended between one and two micrometers. In the case of telo-bovine collagen neutralised with NaOH, the resulting matrix was characterised by thick fibres aligned across the matrix and with diameters five times larger than the ones found in the previous samples. These wide fibres were especially distinguished by the entanglement of thinner fibres around them. These results contradicted the aleatory arrangement and the slightly reduced thickness of the fibres in atelo-bovine collagen prepared with NaOH.

On the other hand, using sodium bicarbonate resulted in the generation of dermal matrices characterised by a higher porosity and smaller fibre diameters than those gels prepared with sodium hydroxide. As a result, human and rat collagen gels prepared with $NaHCO_3$ presented similar fibrillar organisation and fibre thickness. These results contrasted with the broader thickness and more organised arrangement showed by telo-bovine collagen neutralised with $NaHCO_3$. Oppositely, atelo-bovine collagen gels neutralised with $NaHCO_3$ were characterised by a disarranged matrix of thinner and broken fibres.

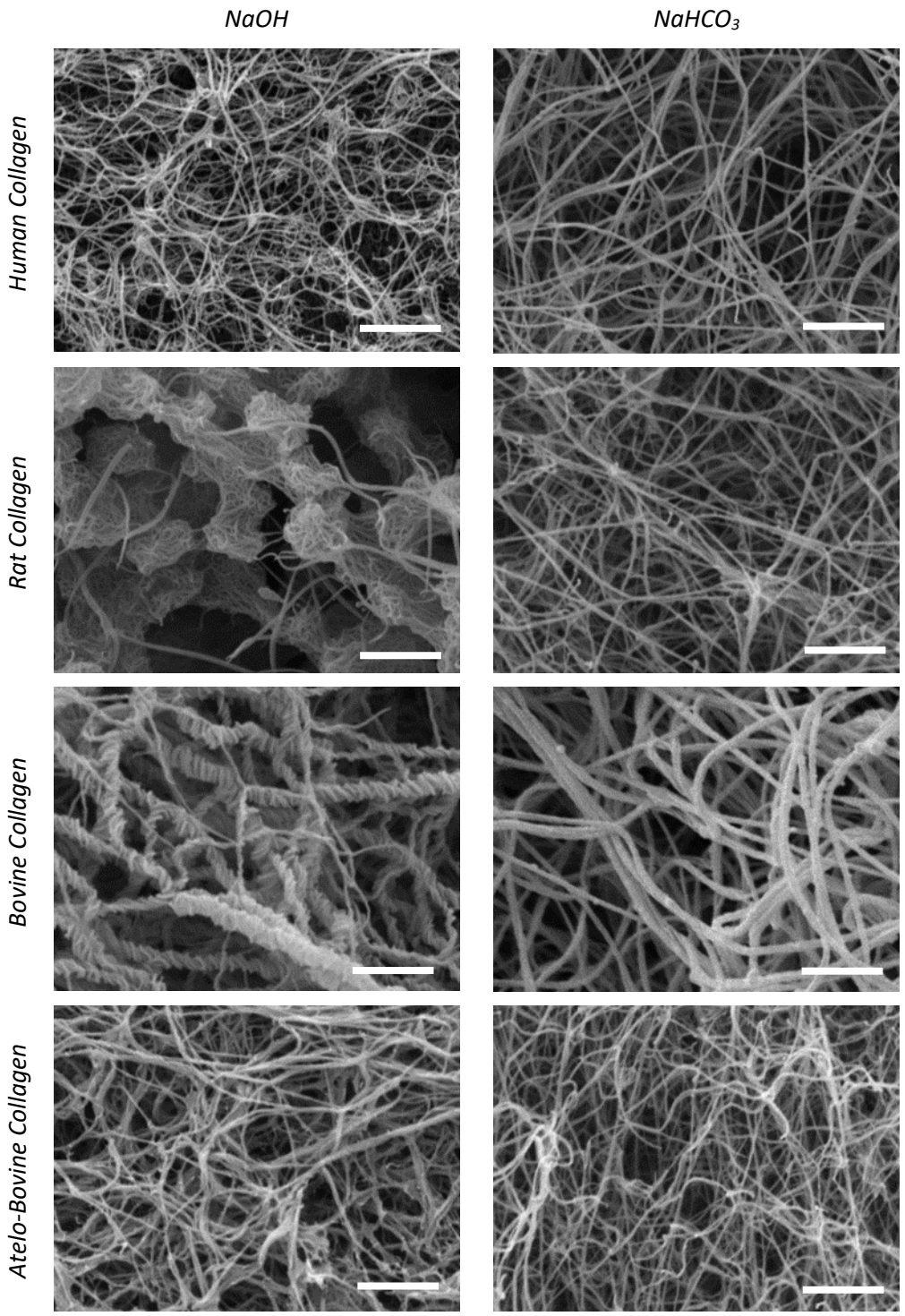

Figure 6. 5. Characterisation by SEM of collagen matrix generated from collagen solutions neutralised with NaOH and $NaHCO_3$. Collagen solutions were obtained from different sources, including human, rat, telo-bovine and atelo-bovine collagen. Scale bars correspond to 2 μm.

The incorporation of RAFT^{TM} absorber system during the generation of rat collagen gels, resulted in a significant modification of the fibrillar organisation (Fig. 6.6). Regardless the neutralisation method used, the RAFT^{TM} absorber system resulted in the generation of matrix with higher fibrillar compaction, reducing the matrix porosity and increasing the fibre alignment in some regions.

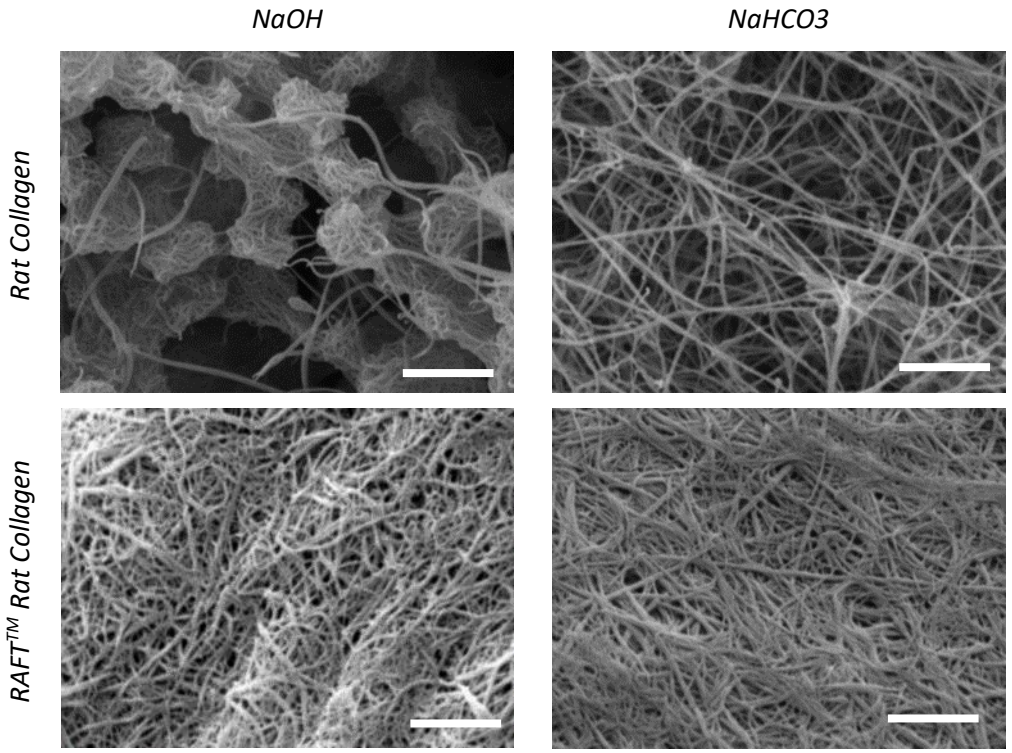

Figure 6. 6. Comparison between the fibrillar organisation and porosity of matrices of rat collagen neutralised with NaOH and $NaHCO_3$ and rat collagen samples prepared with and without applying RAFT^{TM} absorbers. Images obtained by SEM with scale bars representing 2 µm.

The combination of fibrinogen with alginate and collagen to generate fibrin-based gels also demonstrated to vary the properties of the final matrix (Fig. 6.7). The mixture of fibrinogen with thrombin resulted in the generation of a compacted matrix characterised by thin fibres organised aleatory. By incorporating atelo-bovine collagen into the fibrin bioink formulation, it was possible to create less condensed matrix comprised of fibres with different thicknesses. Meanwhile, the mix of alginate and fibrin in the bioink resulted in the formation of gels with high porosity and thin structures. Finally, the combination of fibrin, alginate and collagen originated a more organised matrix with higher porosity and contained more heterogeneous fibrillar networks.

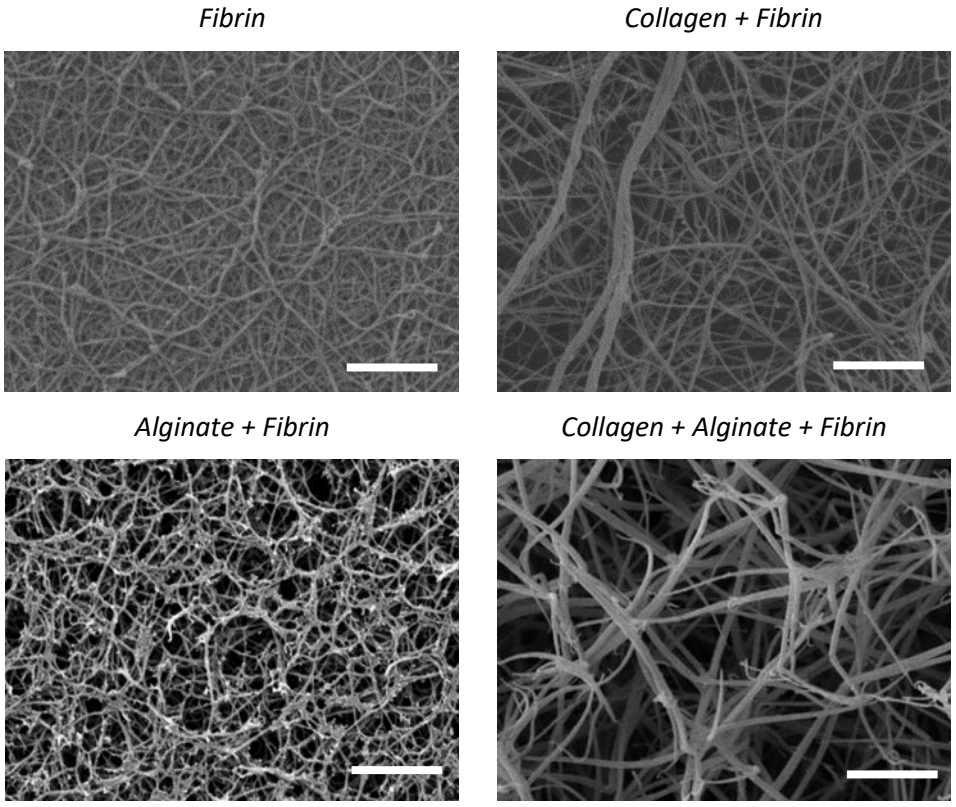

Figure 6. 7. Comparison between the fibrillar characteristics of matrices produced by fibrin, fibrin combined with collagen, fibrin combined with alginate, and fibrin combined with collagen and alginate. Images obtained by SEM with a scale bar corresponding to 2 µm.

6.2.4. Rheological Properties of Dermal Bioinks

As collagen fibres assemble to form the final collagen matrix, the mechanical properties of the sample vary until the complete formation of collagen gels. For that reason, it was possible to evaluate the fibrillogenesis of the samples by measuring the changes in the material stiffness after the mixture of the gel precursor and crosslinker (Fig. 6.8-6.9). Storage modulus (G') was selected as representative value of the material stiffness.

The selection of sodium hydroxide as neutralisation method resulted in an initial stabilisation of the storage modulus values after 4 minutes for all collagen sources, except for human collagen (Fig. 6.8a). From this point, only rat collagen showed stable values, suggesting the completion of their gelation. For the rest of the collagens neutralised with NaOH, the stabilisation of the storage modulus could only be observed after 40 minutes. The extraction method utilised on bovine collagen did not show an apparent effect on their fibrillogenesis

profile. Only the presence of two small deflections after 290 and 1600 seconds in the gelation spectra of telo-bovine differentiated both samples.

Neutralising collagen solutions with sodium bicarbonate resulted in a quicker initial stabilisation of collagen gels after only 3 minutes (Fig. 6.8b). Only human collagen required almost 15 minutes to steady the storage modulus values. The use of sodium bicarbonate in rat collagen gels delayed the completion of their gelation, requiring more than 40 minutes to reach stable values. Telo and atelo-bovine collagen showed a complete gelation after 35 minutes, however, their fibrillogenesis profile differed. On this occasion, the increase in the storage modulus presented by atelo-collagen neutralised with sodium bicarbonate was characterised by a higher slope. The appearance of two deflective peaks in the fibrillogenesis profile of telo-bovine collagen was again visible after 260 and 510 seconds using sodium bicarbonate as neutralisation method.

In comparison to collagen samples, fibrin-based gels presented a faster gelation profile (Fig. 6.9a). All the fibrin-based gels showed an initial stabilisation after only two minutes, followed by an increase in their storage modulus, reaching their complete gelation in less than 20 minutes. The combination of fibrin with either collagen or alginate enabled a slightly faster stabilisation of the storage modulus.

By assessing the storage modulus in the first minutes after the start of the gelation process, it was possible to determine the speed of the crosslinking reaction and the initial characteristics of the generated gels. These values were especially important to determine the bioink printability using the ReJI system. Fibrin-based gels showed a fast-crosslinking reaction regardless their formulation, increasing their storage modulus from 1 Pa to 10 Pa in less than 60 seconds (Fig. 6.9b). Moreover, the obtention of stiffness values closer to 100 Pa in 180 seconds confirmed their ability to generate stable gels quickly. The utilisation of bioinks comprised of fibrin, fibrin combined with alginate, or fibrin combined with alginate and collagen, resulted in similar crosslinking profiles. However, the combination of fibrin with collagen enhanced the crosslinking speed, reaching storage modulus above 10 Pa in less than 10 seconds, and generating gels with values higher than 100 Pa in only 100 seconds.

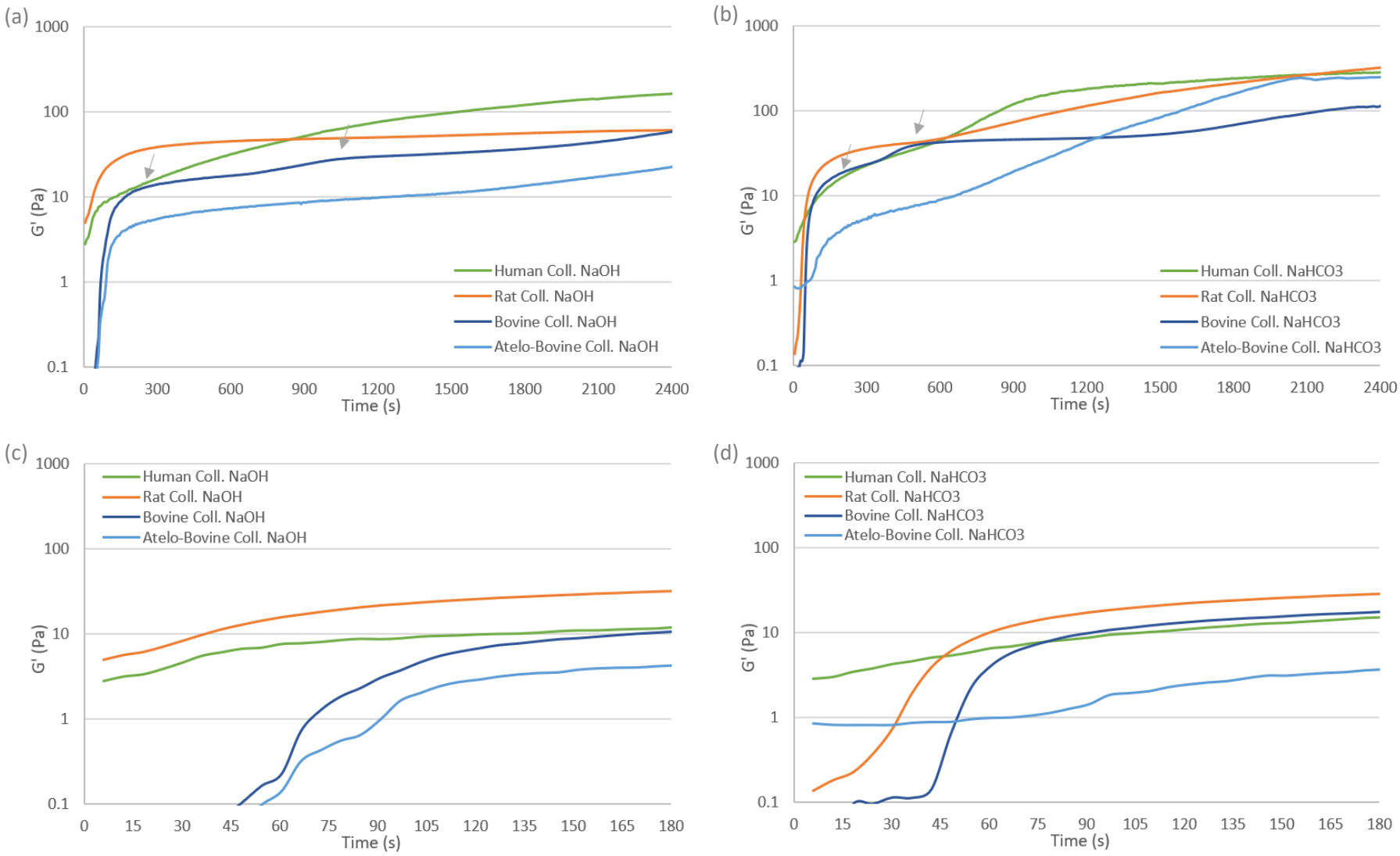

Figure 6. 8. Study of fibrillogenesis profile of collagen gels from different sources, including human, rat, telo- and atelo-bovine, by measuring the variations on the storage modulus (G') over time. The effect of the neutralization method on the properties of the final collagen gels was studied by comparing the use of (a-c) NaOH and (b-d) $NaHCO_3$. The presence of deflective regions during the fibrillar formation of telo-bovine collagen is indicated by grey arrows.

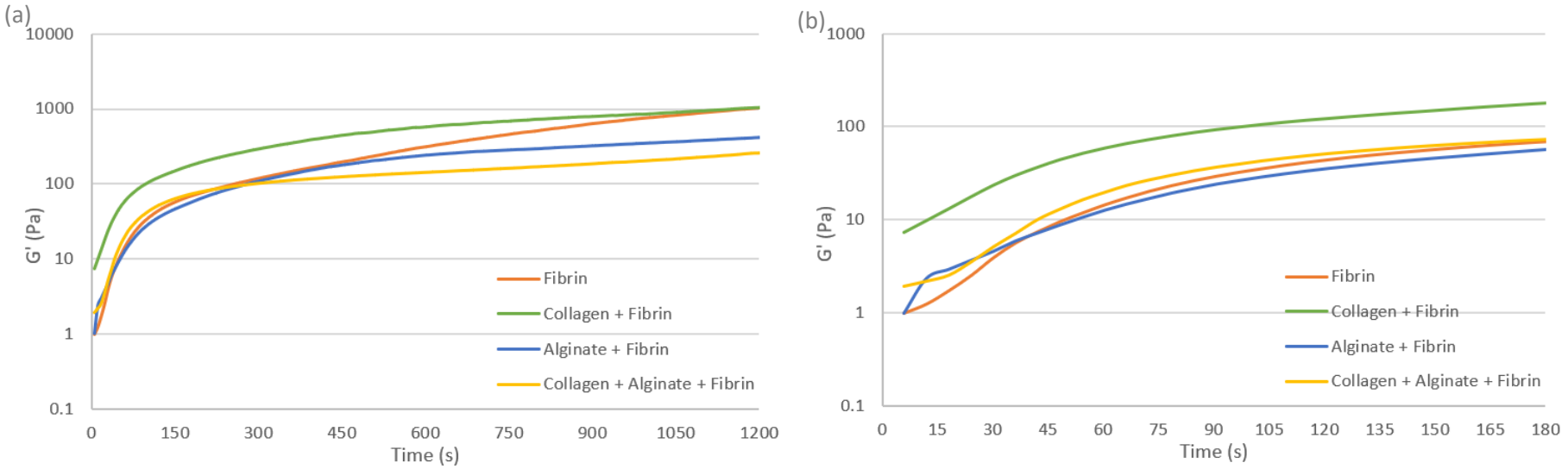

Figure 6. 9. Evaluation of the fibrillogenesis profiles of different fibrin-based gels by studying the variations on the storage modulus (G') over time. The impact of the composition of the fibrin-based gels on their fibrillar formation was studied by comparing fibrin gels, with fibrin combined with collagen and alginate.

In comparison to fibrin formulations, only rat collagen gels reached stiffness values higher than 10 Pa in less than 20 or 60 seconds when using NaOH or $NaHCO_3$ as neutralisation method, respectively (Fig. 6.8 c-d). Additionally, the stabilisation of the storage modulus after reaching these points confirmed their quick generation of gels. Human collagen gels can also reach values above 10 Pa, but they required more than 100 seconds. Similarly, telo-bovine collagen gels showed stiffness higher than 10 Pa after 180 and 90 seconds, when they were neutralised with NaOH and $NaHCO_3$, respectively. However, their initial storage modulus values below 1 Pa underlined the liquid state of bovine collagen samples in the first 45 seconds.

Viscosity measurements were also considered a fundamental criteria for assessing the bioink printability using the ReJI system. The evaluation of gel precursors showed a range of viscosity values from 23.48 to 19.10 mPa·s (Table 6.2). Human and rat collagen presented the highest viscosities among the collagen solutions. Meanwhile, the incorporation of alginate into the fibrin solutions derived in a significant increase in the original values of fibrin bioinks. The analysis of gel crosslinkers demonstrated their lower viscosity values, comprehended between 2.76 and 0.96 mPa·s. The high water content in the crosslinker solutions could explain the proximity of their values to the water viscosity.

Table 6. 2. Viscosity values at 20°C of collagen and fibrin-based bioink precursors and their corresponding crosslinker solutions. Water measurement was incorporated as control solution.

Human Collagen	**Rat Collagen**	**Bovine Collagen**	**Atelo-Bovine Collagen**
21.00 ± 0.23 mPa·s	23.48 ± 0.18 mPa·s	19.13 ± 0.08 mPa·s	19.10 ± 0.10 mPa·s
Fibrin	**Collagen + Fibrin**	**Alginate + Fibrin**	**Collagen + Fibrin + Alginate**
20.38 ± 0.03 mPa·s	19.62 ± 0.40 mPa·s	25.36 ± 0.47 mPa·s	20.13 ± 0.63 mPa·s
NaOH	**$NaHCO_3$**	**Thrombin + $CaCl_2$**	**Water**
0.96 ± 0.05 mPa·s	1.17 ± 0.02 mPa·s	2.76 ± 0.03 mPa·s	0.99 ± 0.04 mPa·s

Before comparing the mechanical properties of the different dermal matrices, the selected dermal gels were incubated for 24 hours to ensure their complete gelation. Then, various measurements were performed on the final gels to determine their final stiffness and their response to external stimulus (Fig. 6.10-6.14).

On the one hand, the measurement of storage modulus uncovered significant differences in the mechanical strength of the studied dermal gels (Fig. 6.10-6.11). All collagen samples neutralised with sodium hydroxide presented different storage modulus depending on their animal sources (Fig. 6.10). Gels prepared with rat collagen neutralised with NaOH represented the stiffest collagen with a value of 111 Pa. This storage modulus was significantly higher than the one found in other collagen samples, which presented values lower than 42 Pa. Telo-bovine collagen neutralised with NaOH represented the second stiffest collagen gel, with significantly higher mechanical strength than atelo-bovine collagen and human collagen.

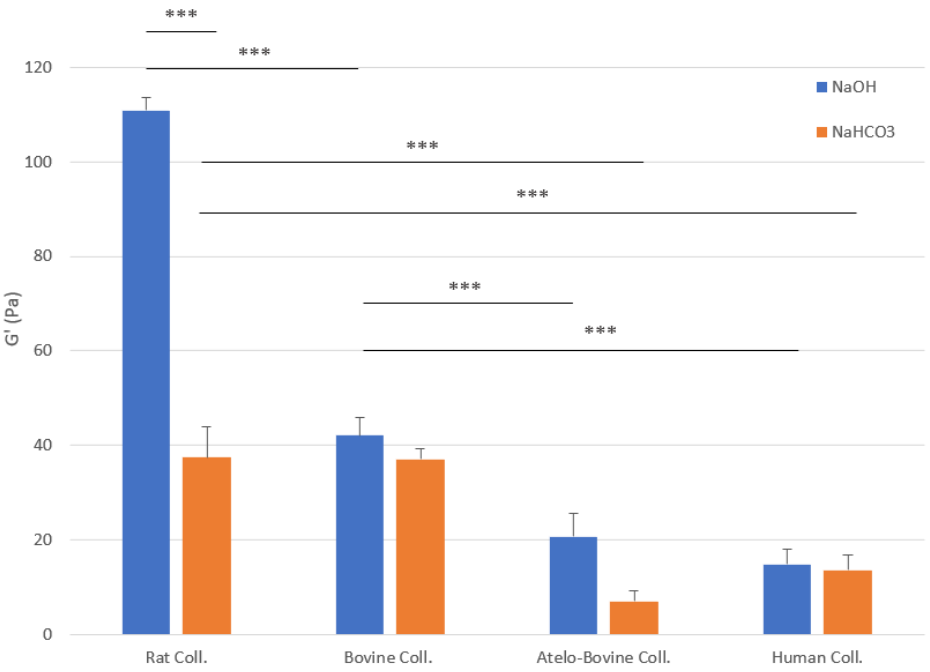

*Figure 6. 10. Evaluation of the storage modulus (G') of collagen gels neutralised with NaOH and $NaHCO_3$ after 24 hours of incubation. The impact of the collagen sources and their extraction method on the stiffness of the final gels was studied by comparing rat, telo-bovine, atelo-bovine and human collagen. Error bars represent the standard deviation (SD), n = 3. Symbols *, ** and *** indicate the significant difference between groups at the level p<0.05, p<0.01 and p<0.001, respectively.*

Collagen gels neutralised with sodium bicarbonate presented a slight reduction in the storage modulus compared to those prepared with sodium hydroxide (Fig. 6.10). Only the values of rat collagen gels were significantly different depending on the neutralisation method. Rat and bovine collagen neutralised with $NaHCO_3$ presented stiffness values closer to 40 Pa, while human and atelo-bovine collagens showed limited mechanical strength.

The formulation of fibrin-based gels also demonstrated a significant impact on their final mechanical strength (Fig. 6.11). Gels containing only fibrin presented a remarkable stiffness with a storage modulus of 106 Pa. By incorporating collagen into the fibrin formulation, it was possible to increase the mechanical strength of the gel significantly. Contrarily, the combination of fibrin with alginate resulted in a reduction by half of the stiffness values observed in fibrin gels. As a result, the gels comprised of alginate and fibrin presented similar values to the bovine collagen gels prepared with NaOH. Finally, the combination of collagen, alginate and fibrin resulted in a similar mechanical strength to fibrin gels. In general, all the fibrin-based formulations, except for fibrin combined with alginate, presented higher stiffness than collagen gels. Only rat collagen neutralised with NaOH showed similar mechanical strength to fibrin and CAF gels.

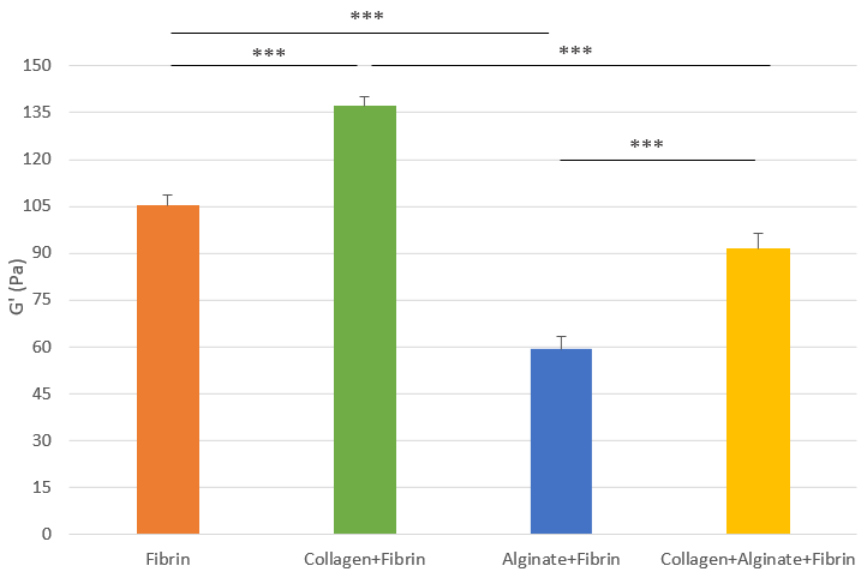

*Figure 6. 11. Study of the storage modulus (G') of fibrin-based gels after 24 hours of incubation. The impact of collagen and alginate on the stiffness of fibrin gels was evaluated comparing the differences on the G' values of fibrin, fibrin combined with collagen, fibrin combined with alginate and fibrin combined with alginate and collagen. Error bars represent the standard deviation (SD), n = 3. Symbols *, ** and *** indicate the significant difference between groups at the level p<0.05, p<0.01 and p<0.001, respectively.*

The storage modulus measured in the previous studies provided a general overview of the mechanical support that dermal matrices could provide to the fibroblasts after their seeding. However, the measurement of the changes in the storage modulus after the application of increased angular frequencies could also provide some information about the capacity of cells to remodel these fibrillar matrices (Fig. 6.12-6.14).

By exposing the collagen gels neutralised with NaOH to a range of angular frequencies, it is possible to observe an increment in the storage modulus values (G') for human, telo and atelo-bovine collagen samples (Fig. 6.12 a,c,d). The increment on the storage modulus values, while the loss modulus values (G'') are maintained, correspond to the rearrangement and alignment of the matrix fibres, and the subsequent rise in the stiffness values. On the other hand, the lack of variations in the storage and loss modulus observed in rat collagens neutralised with NaOH is produced when the matrix remains unalterable (Fig. 6.12b). In the case of collagen gels neutralised with $NaHCO_3$, the storage modulus of all samples showed a progressive increase as the angular frequencies rose (Fig. 6.13). The comparison between collagens from different animal sources underlined the ability of bovine collagen to reach a storage modulus as high as 300 Pa regardless of the neutralisation method employed (Fig. 6.13b-6.14b). These values contrasted with the 150 Pa obtained in the rest of collagen samples when applying the maximum angular frequency.

Fibrin-based gels responded differently to their exposition to angular frequencies (Fig. 6.14). Gels containing only fibrin showed stable stiffness values regardless of the frequency. Only a slight decrease in the storage modulus could be observed after applying frequencies higher than 60 rad/s (Fig. 6.14a). On the other hand, the combination of collagen with fibrin resulted in the rise from 137 Pa to 517 Pa on the storage module as the angular frequency increased (Fig. 6.14b). This response to the frequency contrasted with the one observed in the gels comprised of fibrin mixed with alginate (Fig. 6.14c). The exposition of these gels to angular frequencies resulted in the drop of the storage modulus until reaching values lower than the loss modulus, indicating the gel breaking. Finally, the combination of fibrin, collagen and alginate resulted in the generation of CAF gels with intermediate properties between the previous fibrin-based materials (Fig. 6.14d). These gels initially maintained a stable shear modulus similar to fibrin gels. However, their stiffness increased by four as the frequency reached values above 30 rad·s.

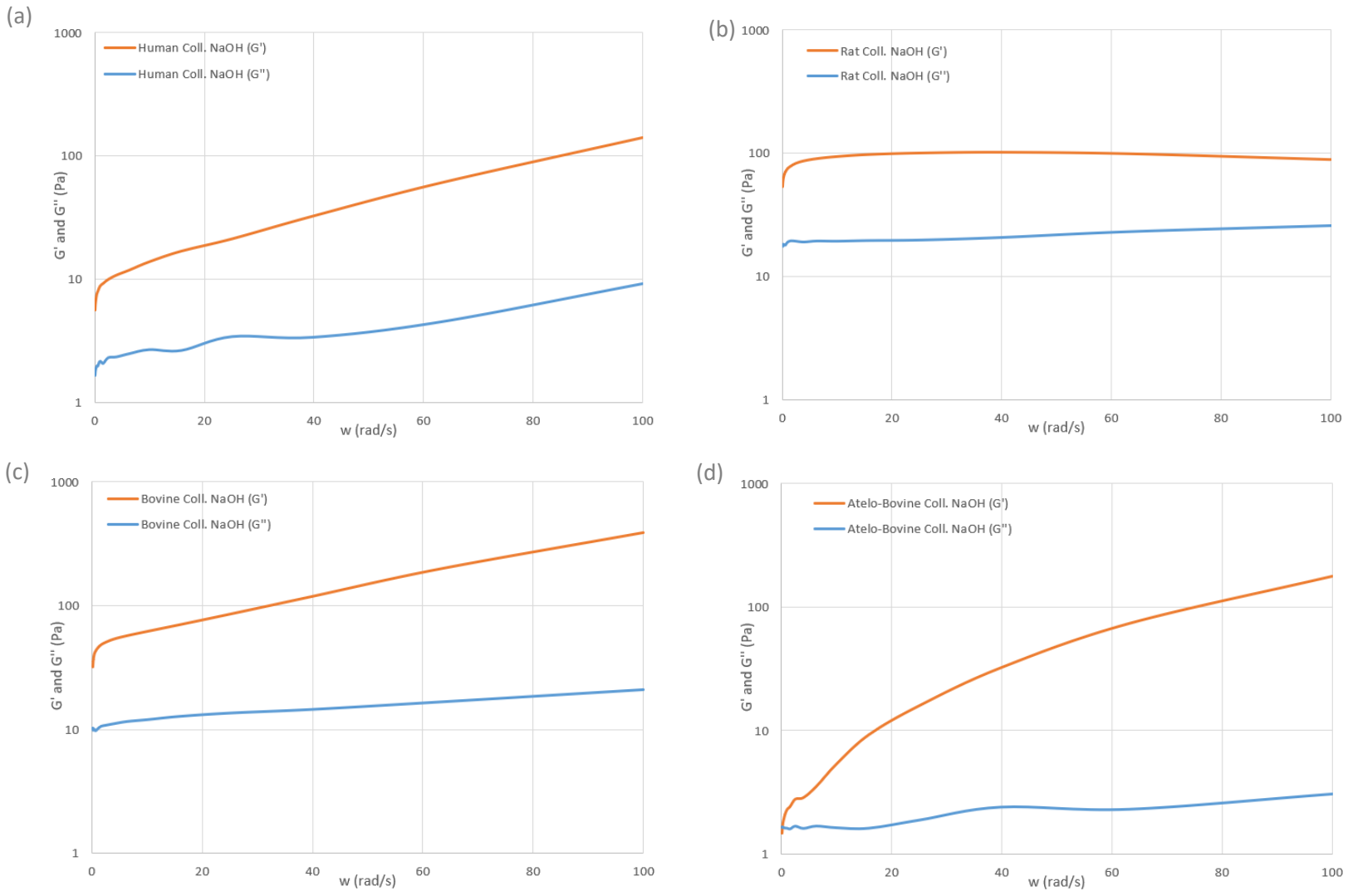

Figure 6. 12. Study of variations on the storage (G') and loss modulus (G'') of collagen gels neutralized with NaOH, incrementing the angular frequencies from 0.1 to 100 rad/s. The effect of the collagen sources on the storage and loss modulus was assessed by comparing collagen from (a) human, (b) rat, (c) telo-bovine and (d) atelo-bovine.

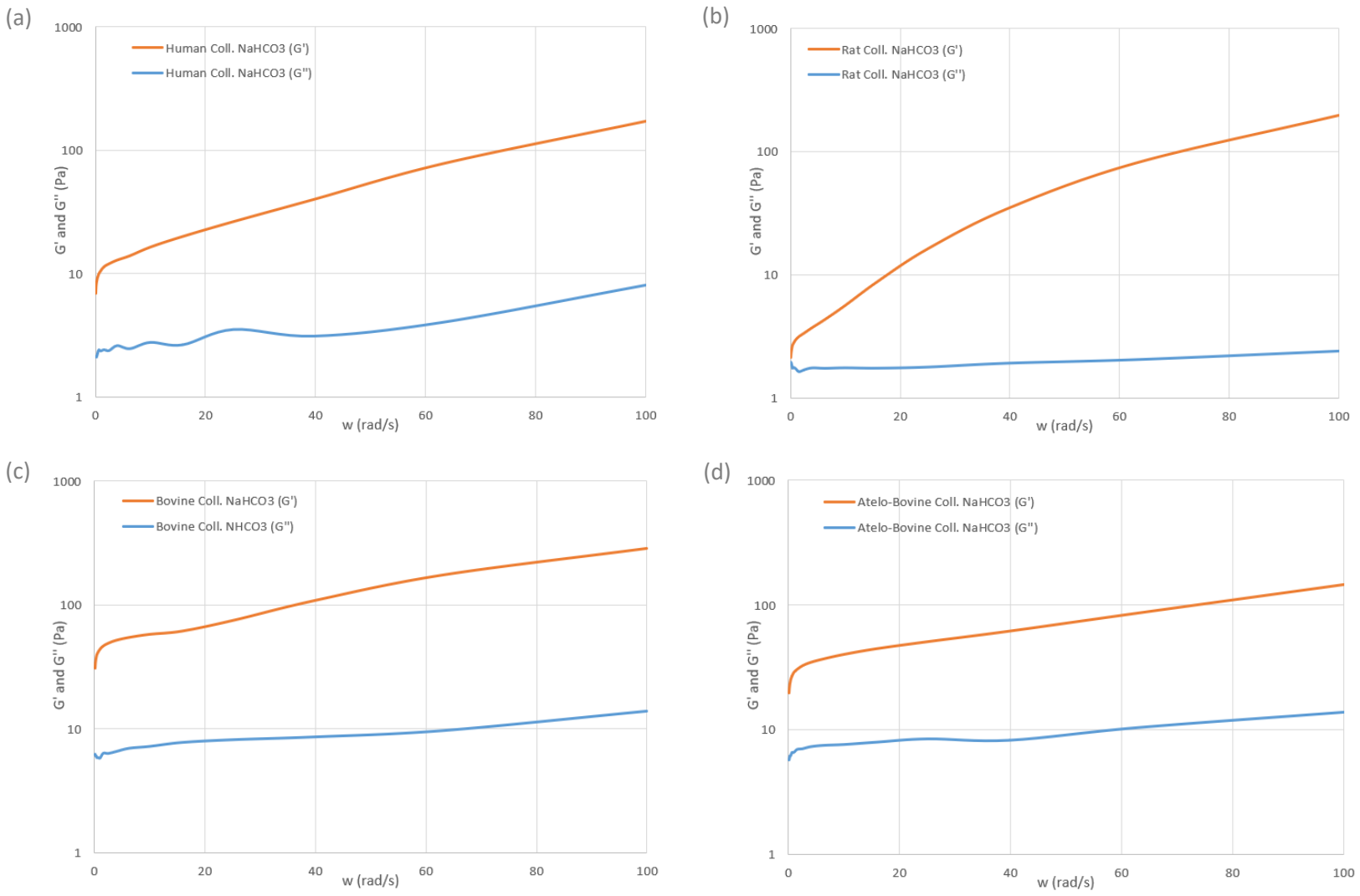

Figure 6. 13. Study of variations on the storage (G') and loss modulus (G'') of collagen gels neutralized with $NaHCO_3$, incrementing the angular frequencies from 0.1 to 100 rad/s. The effect of collagen sources on the storage and loss modulus was assessed by comparing collagen from (a) human, (b) rat, (c) telo-bovine and (d) atelo-bovine.

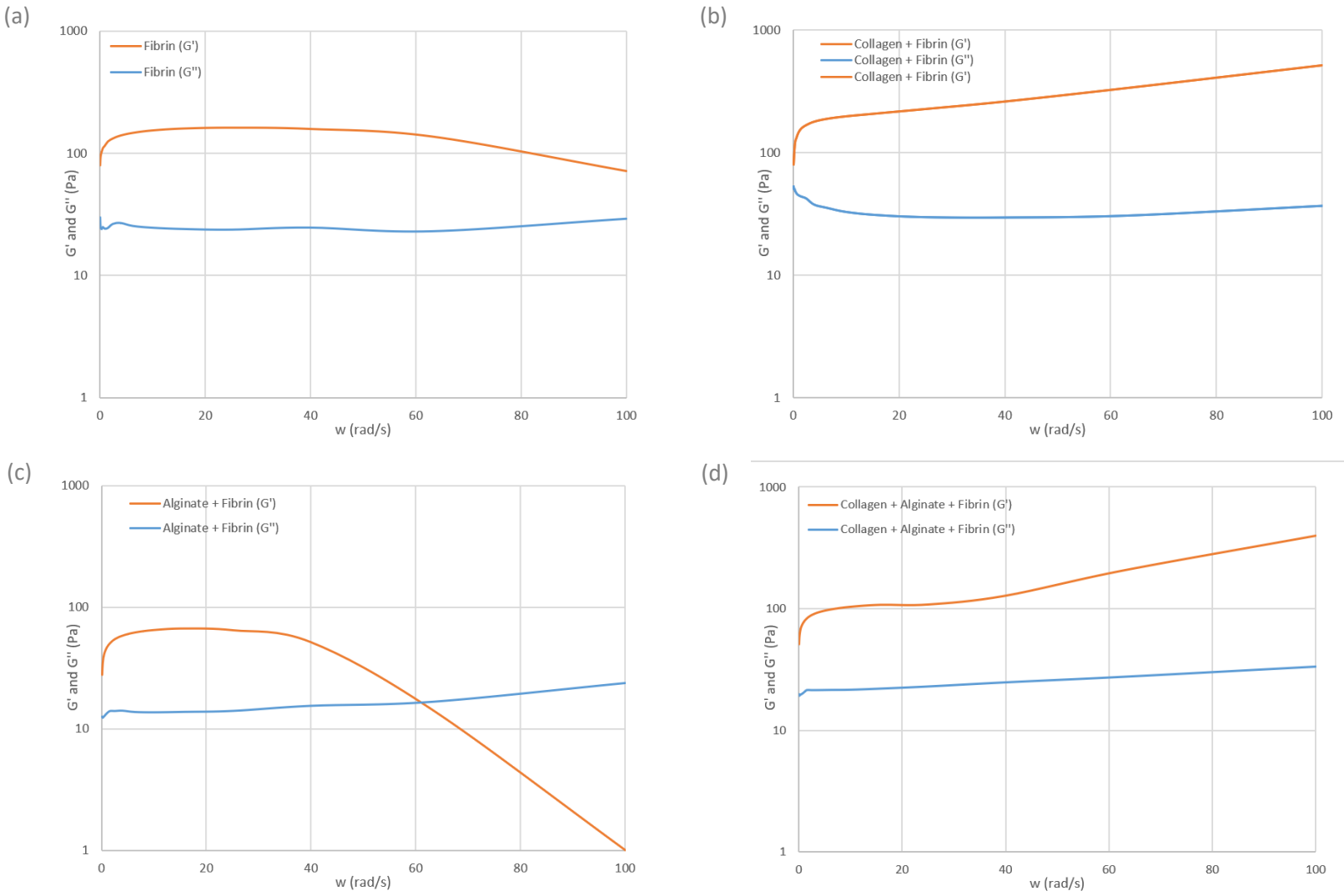

Figure 6. 14. Study of variations on the storage (G') and loss modulus (G'') of fibrin-based gels, incrementing the angular frequencies from 0.1 to 100 rad/s. The influence of collagen and alginate on the fibrin properties was studied by comparing (a) fibrin gels with (b) fibrin combined with collagen, (c) fibrin with alginate and (d) fibrin mixed with alginate and collagen.

6.3. Biological Assays

6.3.1. Fibroblast Morphology and Distribution in Dermal Models

The staining of F-actin filaments expressed by fibroblasts allowed to determine differences in the cell morphology and distribution depending on the matrix composition (Fig. 6.15-6.18).

In collagen gels, the adaptation of fibroblasts to the dermal matrix was particularly influenced by the collagen origin (Fig. 6.15-6.16). For instance, fibroblasts embedded in human and rat collagen required at least 3 days to adapt to the new environment. Meanwhile, fibroblasts encapsulated in telo- and atelo-bovine collagen showed a defined elongated shape after only 1 day. Similarly, the distribution of fibroblasts and their proliferation showed remarkable differences depending on the collagen source. In the case of bovine collagen, a high number of fibroblasts homogenously distributed were found on the initial days, enabling the formation of complex cellular structures at day 7. Contrarily, only a reduced number of fibroblasts situated in isolated groups could be observed in human and rat collagen gels after 7 days. Just in those human collagen gels prepared with $NaHCO_3$, an increase in the number of cells could be observed after 7 days. Fibroblasts in these collagen samples were characterised by their homogeneous distribution and angular morphology.

The selection of neutralisation method also proved to affect the fibroblast behaviour. Generally, gels prepared with $NaHCO_3$ showed a delayed adaptation of fibroblasts to the collagen matrix, which often implied a decrease in the total number of cells at day 7. In the case of bovine collagen, the impact of the neutralisation method was especially higher than in other collagen samples. Fibroblasts encapsulated in bovine collagen neutralised with NaOH presented a closer proximity and a high expression of F-actin filaments after only 3 days. Their interaction and tensional forces were increased as the number of cells rose after 7 days. In contrast, fibroblasts in bovine collagen neutralised with $NaHCO_3$ were distributed in distant locations, presenting a spindle morphology at day 3. As the number of fibroblasts rose, the cell confluency increased and the fibroblast morphology became more elongated. However, no notable increment on the number F-actin filaments could be observed after 7 days. The behaviour of atelo-collagen neutralised with NaOH was similar to the one in telo-bovine collagen, but with a lower number of fibroblasts and a higher expression of F-actin filaments only after 7 days. Whereas, the degradation of atelo-bovine collagen prepared with $NaHCO_3$ after 5 days resulted in the presence of confluent monolayers of fibroblast at day 7.

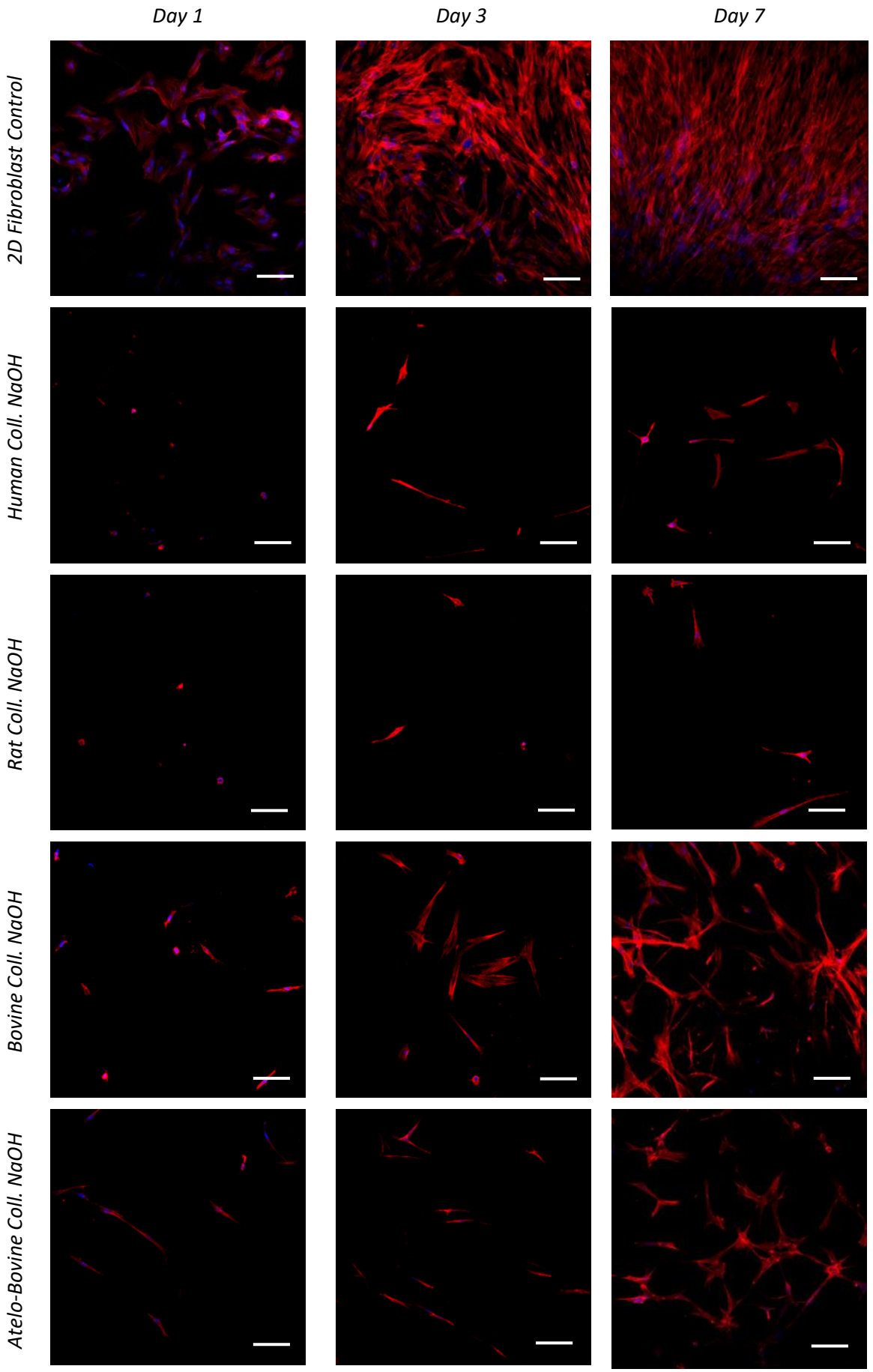

Figure 6. 15. Comparison of fibroblast morphology and distribution in collagen gels after 1, 3 and 7 days. The effect of collagen source and extraction method was studied by comparing human, rat, atelo- and telo-bovine collagen neutralised with NaOH. In these images, red staining represents F-actin filaments and blue staining the cell nuclei. Scale bars correspond to 100 µm.

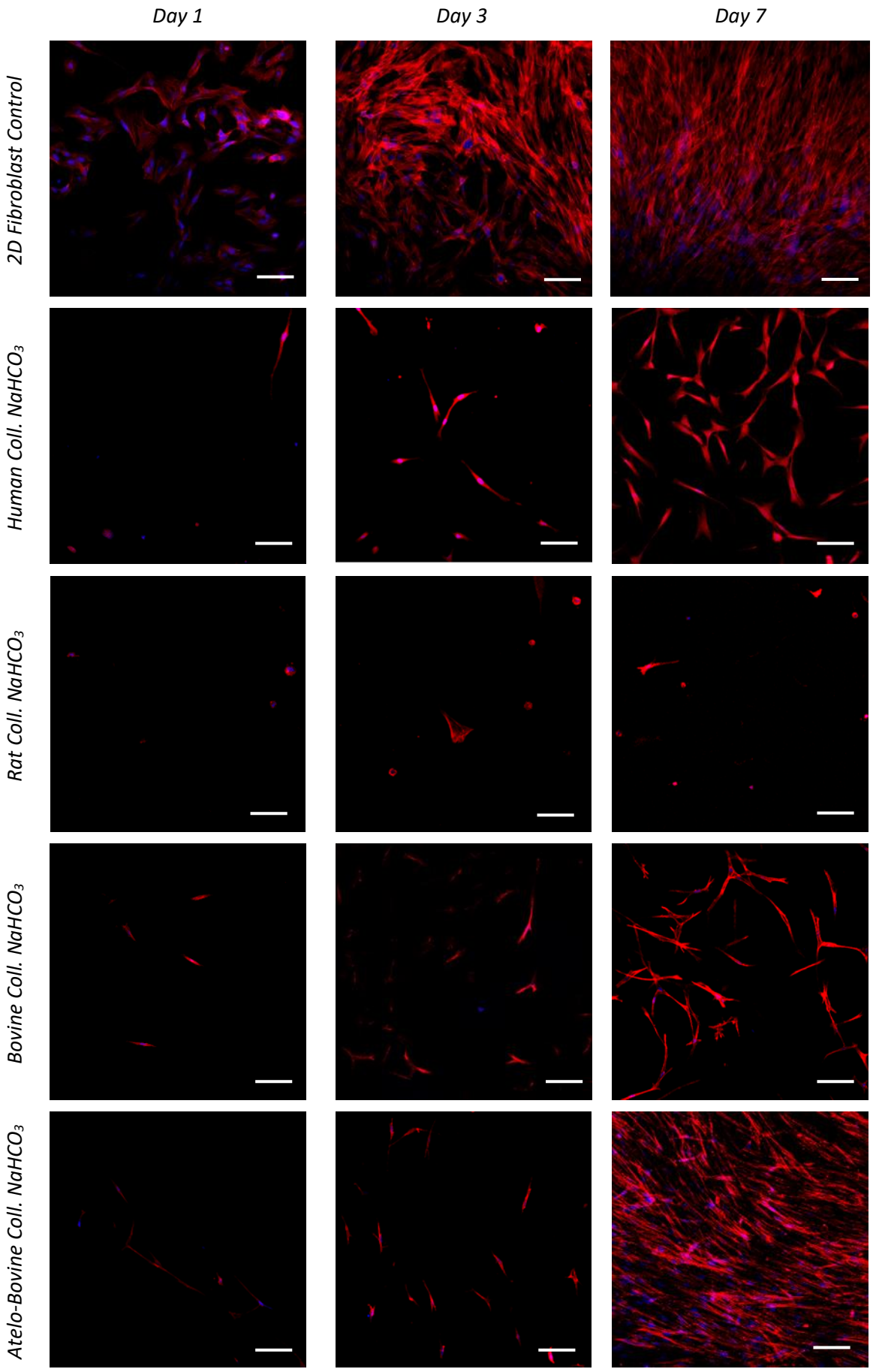

Figure 6. 16. Comparison of fibroblast morphology and distribution in collagen gels after 1, 3 and 7 days. The effect of collagen source and extraction method was studied by comparing human, rat, atelo- and telo-bovine collagen neutralised with $NaHCO_3$. In these images. red staining represents F-actin filaments and blue staining the cell nuclei. Scale bars correspond to 100 µm.

The implementation of RAFT^{TM} absorber systems during the production of rat collagen gels demonstrated to initially condensate the fibroblasts present in the gel, as shown in the images at day 1 (Fig. 6.17). As a result, fibroblasts presented more notable confluency and a higher expression of F-actin filaments at day 7 in the rat collagen gels prepared with RAFT^{TM} system.

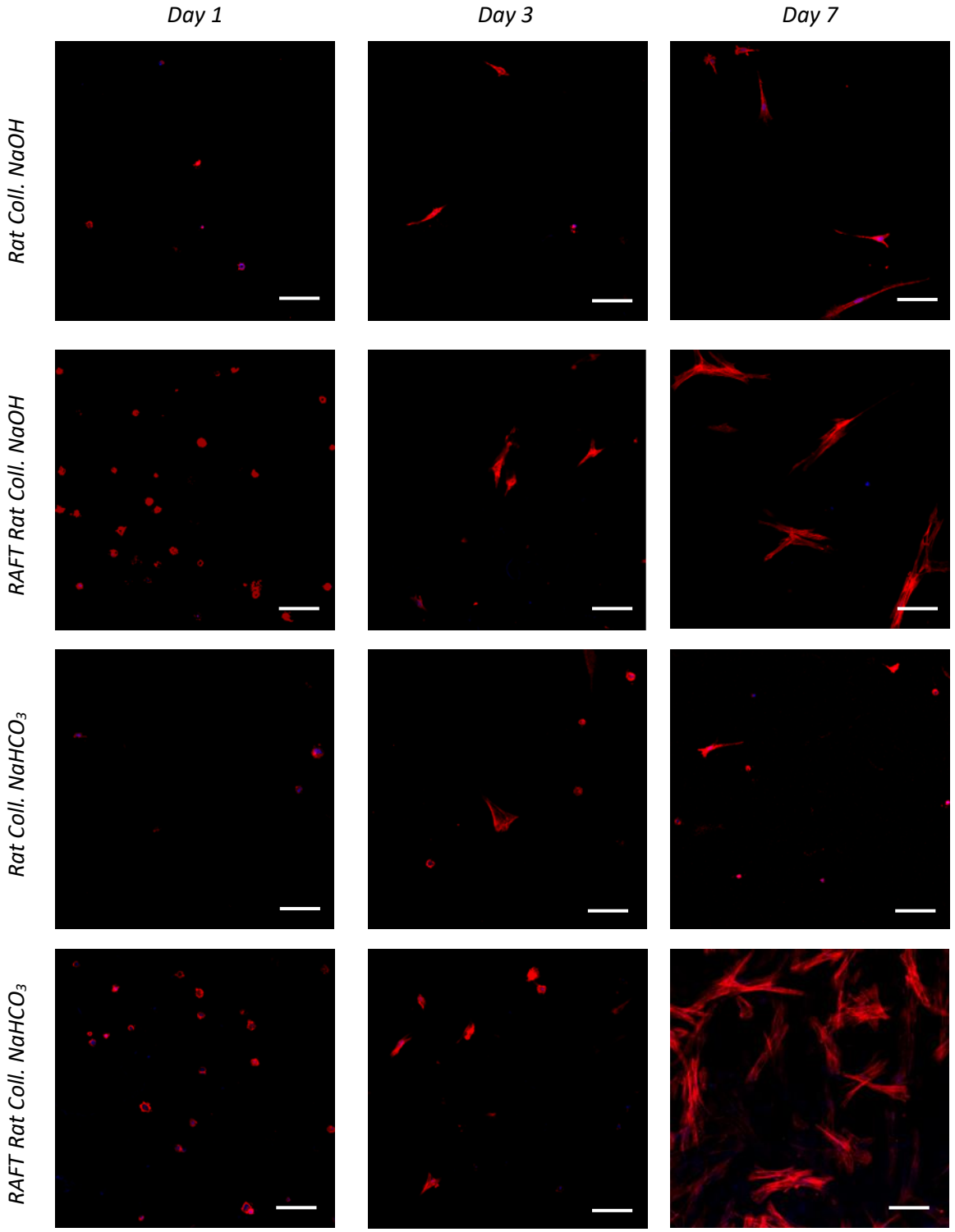

Figure 6. 17. Comparison of fibroblast morphology and distribution after 1, 3 and 7 days in collagen gels prepared with and without implementing the RAFT^{TM} system. In these images, red staining represents F-actin filaments and blue staining the cell nuclei. Scale bars correspond to 100 µm.

In contrast to collagen gels, the presence of fibrin in the dermal models resulted in a faster adherence and adaption of fibroblasts at day 1 (Fig. 6.18). The formulation of the fibrin-based gels showed to influence the fibroblast organisation differently. Fibroblasts encapsulated in gels containing only fibrin or fibrin combined with collagen were homogeneously distributed and presented a polygonal morphology. The increase in the number of fibroblasts at day 7 originated the formation of an organised network of cells, comprised of more elongated and thinner polygonal cells with an enhanced content of F-actin filaments. Those fibroblasts embedded in gels containing a mix of fibrin with collagen showed a lower expression of F-actin filaments and a more elongated morphology. On the other hand, the combination of fibrin with alginate to generate dermal models resulted in the formation of fibroblast aggregates. After 7 days, some of these cell groups increased, but most of the cells were spread through the matrix showing high confluency and presenting diverse morphologies and different expressions of F-actin filaments. Finally, fibroblasts embedded in a gel containing a mix of fibrin, alginate and collagen, resulted in the presence of a higher number of fibroblasts at day 3 than in the previous samples. These cells presented a polygonal morphology and some interactions between each other. The proliferation of fibroblasts in this gel resulted in the formation of fully confluent cell layers and the presence of heterogeneous fibroblasts shapes and different expressions of F-actin filaments.

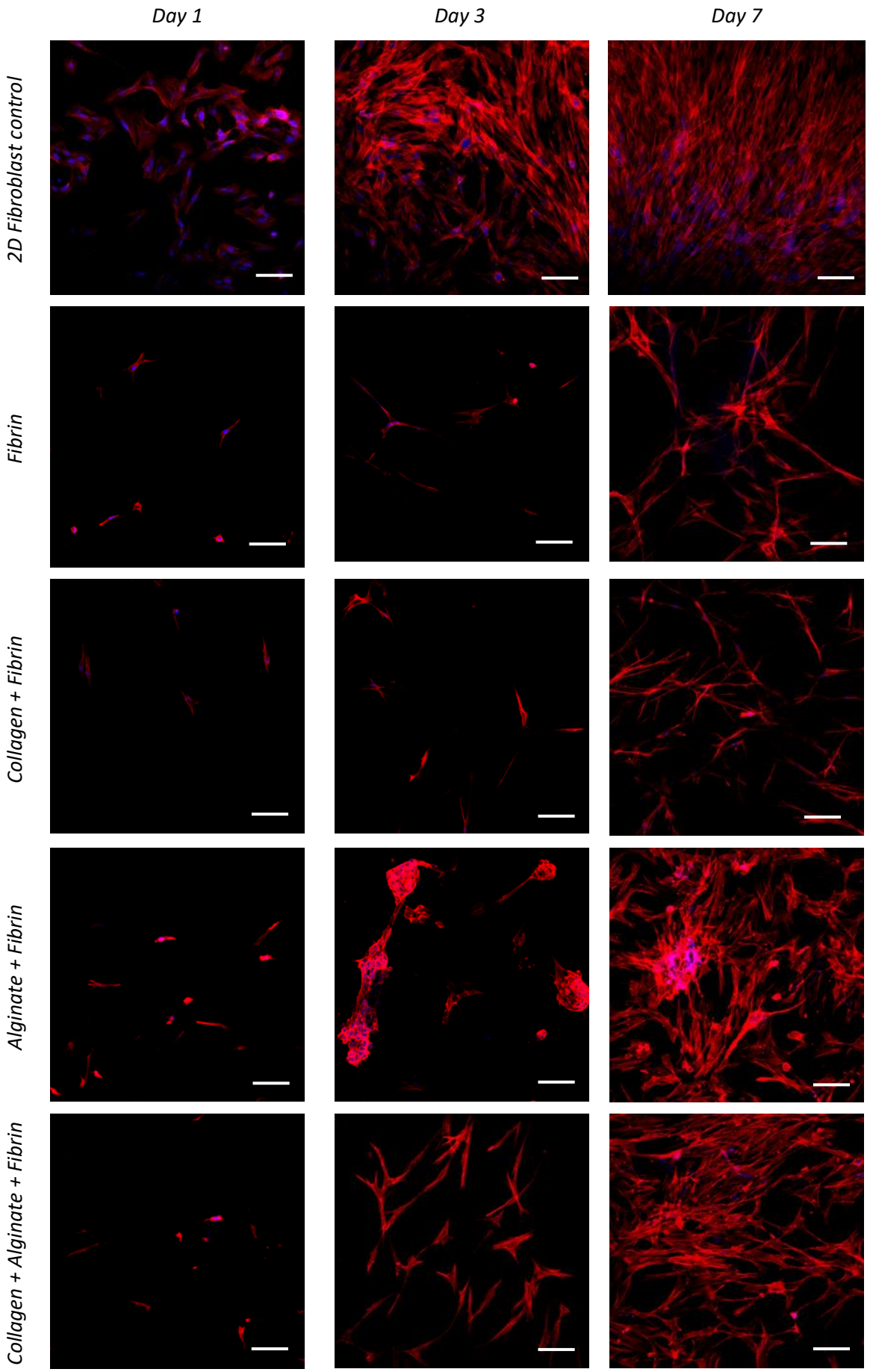

Figure 6. 18. Comparison of fibroblast morphology and distribution in fibrin-based gels after 1, 3 and 7 days. The impact on the fibroblasts of combining fibrin with collagen and alginate was also assessed. In these images, red staining represents F-actin filaments and blue staining the cell nuclei. Scale bars correspond to 100 µm.

6.3.2. Fibroblast Proliferation in Dermal Models

The evaluation of the number of fibroblasts over time demonstrated remarkable differences in the fibroblast proliferation depending on the matrix composition (Fig. 6.19-6.23).

In collagen-based dermal models, human and rat collagen gels showed a significantly lower number of fibroblasts than in the other samples (Fig. 6.19-6.20). Contrarily, telo-bovine collagen exhibited the highest cell proliferation, presenting three to five times higher cell values than human and rat collagen on day 7. Only the degradation of atelo-bovine collagen neutralised with $NaHCO_3$ resulted in fibroblast values above the ones measured in telo-bovine collagen on day 7.

The impact of the collagen neutralisation method on fibroblast proliferation was remarkable different in each sample (Fig. 6.21). In the case of rat collagen gels, fibroblast showed similar cell values regardless of the neutralisation method. On the other hand, human collagen gels presented a higher number of fibroblasts in those gels prepared with $NaHCO_3$. In contrast, bovine collagen showed a more significant rise in the number of fibroblasts with the use of sodium hydroxide as neutralisation method. These differences between telo-bovine collagens were especially notable at day 7, increasing by two the fibroblast values when preparing the gels with NaOH.

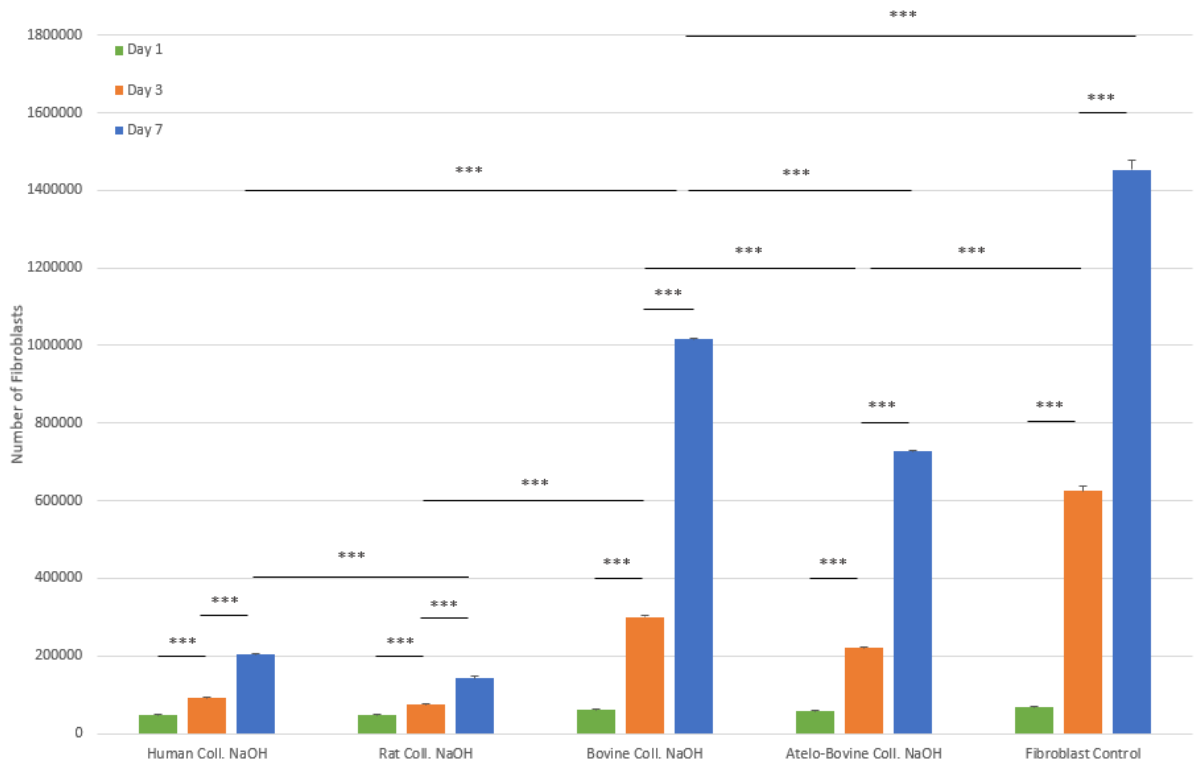

*Figure 6. 19. Study of the number of fibroblasts in collagen gels neutralised with NaOH after 1, 3 and 7 days. The impact of the collagen sources on the fibroblast proliferation was assessed by comparing human, rat, telo- and atelo-bovine collagen with fibroblasts seeded on a tissue culture treated well. Error bars represent the standard deviation (SD), n = 3. Symbols *, ** and *** indicate the significant difference between groups at the level p<0.05, p<0.01 and p<0.001, respectively.*

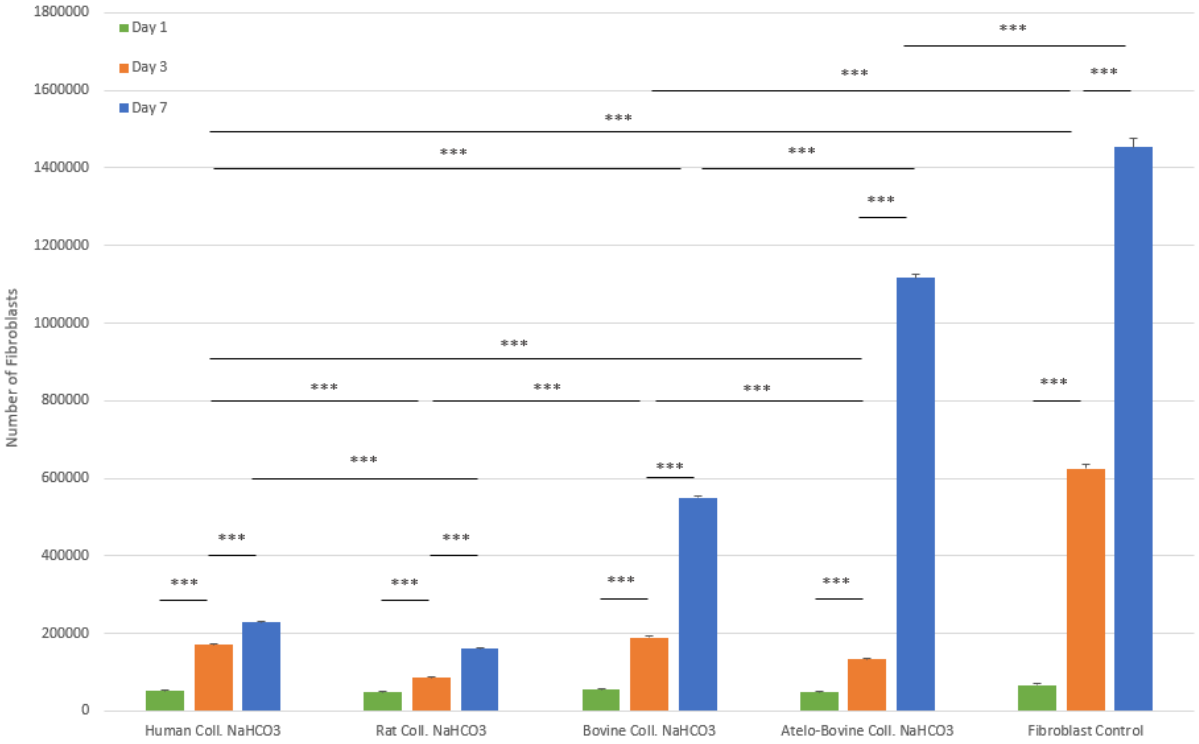

*Figure 6. 20. Comparison of the number of fibroblasts in collagen gels neutralised with $NaHCO_3$ after 1, 3 and 7 days. The impact of the collagen sources on the fibroblast proliferation was assessed by comparing human, rat, telo- and atelo-bovine collagen with fibroblast seeded on a tissue culture treated well. Error bars represent the standard deviation (SD), n = 3. Symbols *, ** and *** indicate the significant difference between groups at the level p<0.05, p<0.01 and p<0.001, respectively.*

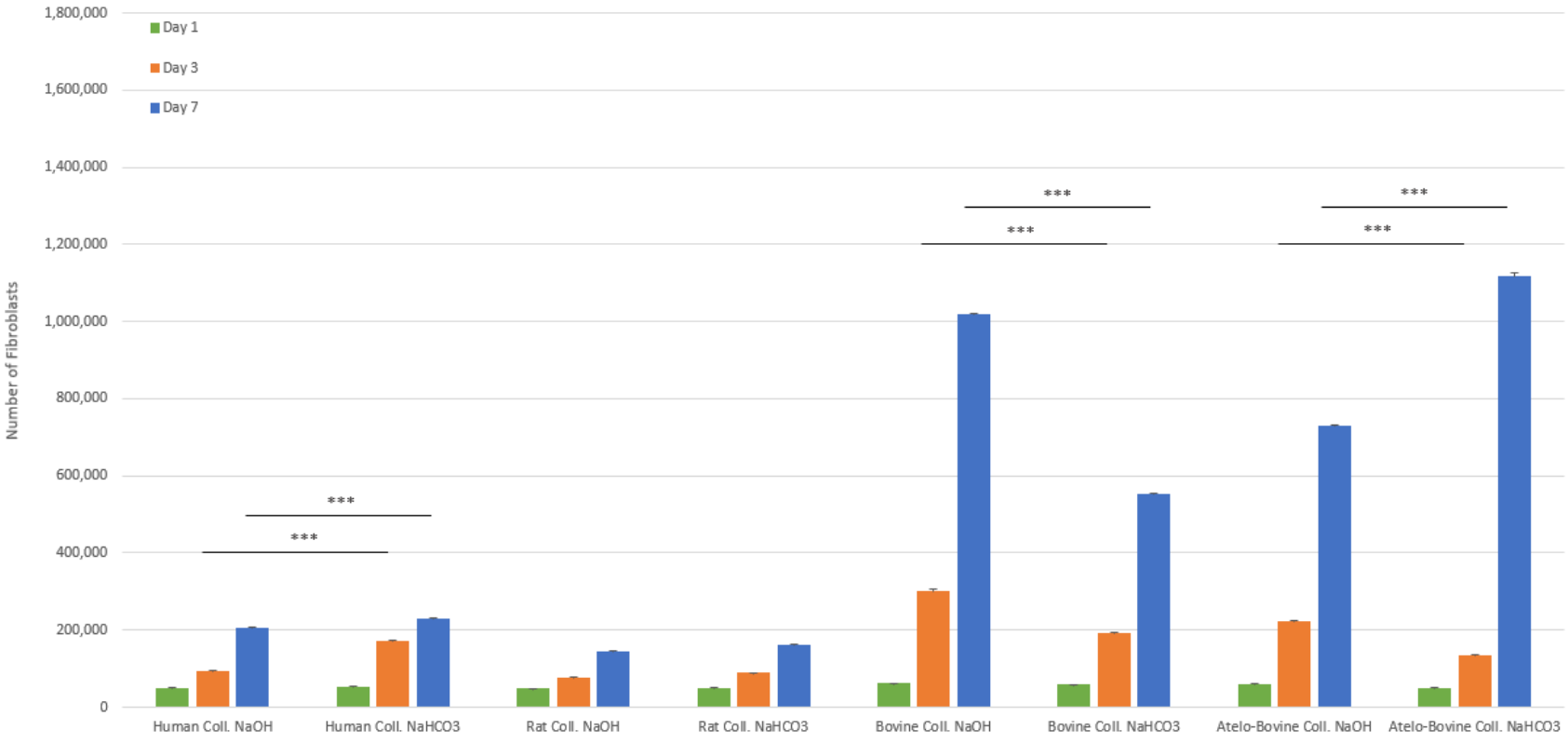

*Figure 6. 21. Study of the impact of using NaOH and $NaHCO_3$ to generate collagen gels on the fibroblast proliferation. The proliferation was determined quantifying the number of fibroblasts at day 1, 3 and 7. Error bars represent the standard deviation (SD), n = 3. Symbols *, ** and *** indicate the significant difference between groups at the level p<0.05, p<0.01 and p<0.001, respectively.*

The incorporation of RAFT^{TM} systems for the production of rat collagen gels also demonstrated to boost the proliferation of fibroblasts (Fig. 6.22). Despite a significant rise in the number of fibroblasts already happened on day 3 in those gels prepared with RAFT^{TM} system, a more remarkable increase occurred on day 7. At this point, rat collagen gels treated with RAFT^{TM} systems showed fibroblast values two and three times higher than non-treated samples.

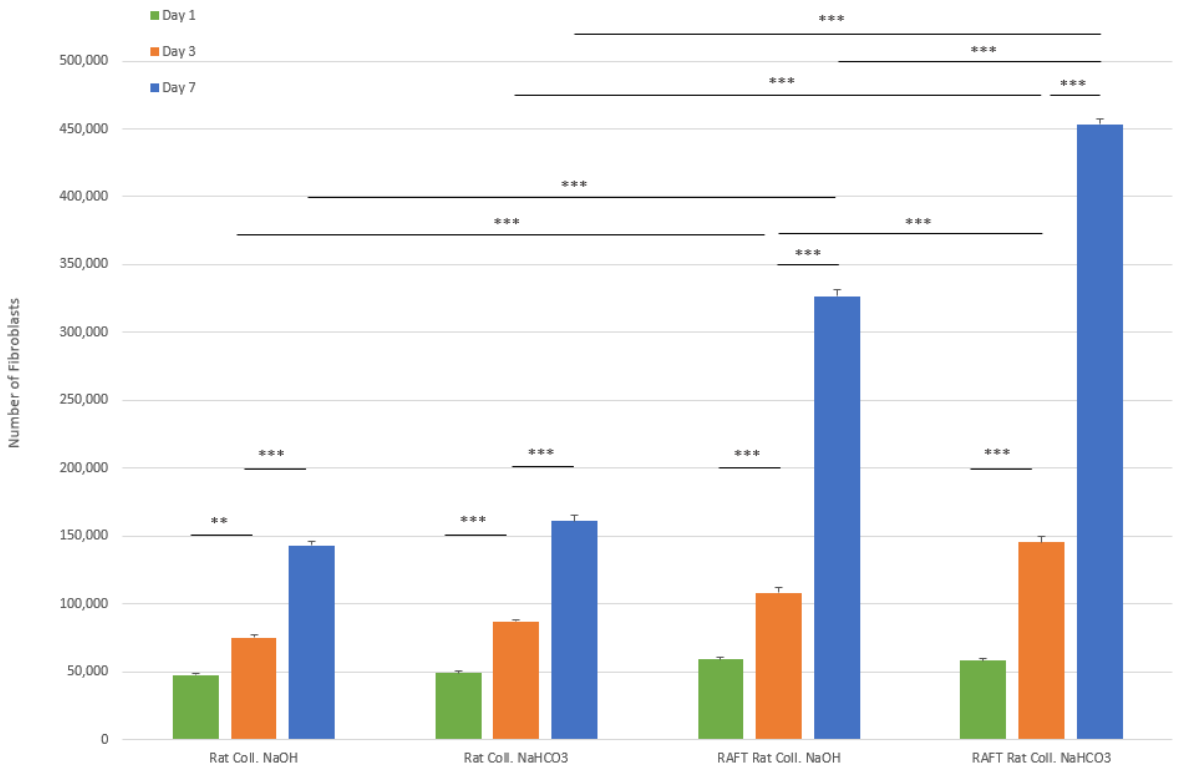

*Figure 6. 22. Comparison of the proliferation of fibroblasts in rat collagen gels prepared with and without applying the RAFT^{TM} system. Error bars represent the standard deviation (SD), n = 3. Symbols *, ** and *** indicate the significant difference between groups at the level p<0.05, p<0.01 and p<0.001, respectively.*

Fibroblast encapsulated in fibrin-based gel showed a notable boost in their proliferation after 3 days, increasing by more than five times their values between day 3 and day 7 (Fig. 6.23). Still, the number of fibroblasts in these gels differed significantly depending on their formulation. By incorporating collagen into fibrin gels, it was possible to observe a slight increment in the fibroblast at day 3 compared to gels containing only fibrin. However, the final number of fibroblasts at day 7 was higher in fibrin gels. Oppositely, the combination of fibrin with alginate resulted in the highest fibroblast values from day 3 compared to the other gels, overcoming the number of fibroblasts found in two-dimensional fibroblast control on day 7. Finally, the combination of collagen, alginate and fibrin resulted in the promotion of a higher proliferation of fibroblasts than in gels containing fibrin or fibrin combined with collagen, but lower fibroblast values than in those gels based on the combination of alginate with fibrin.

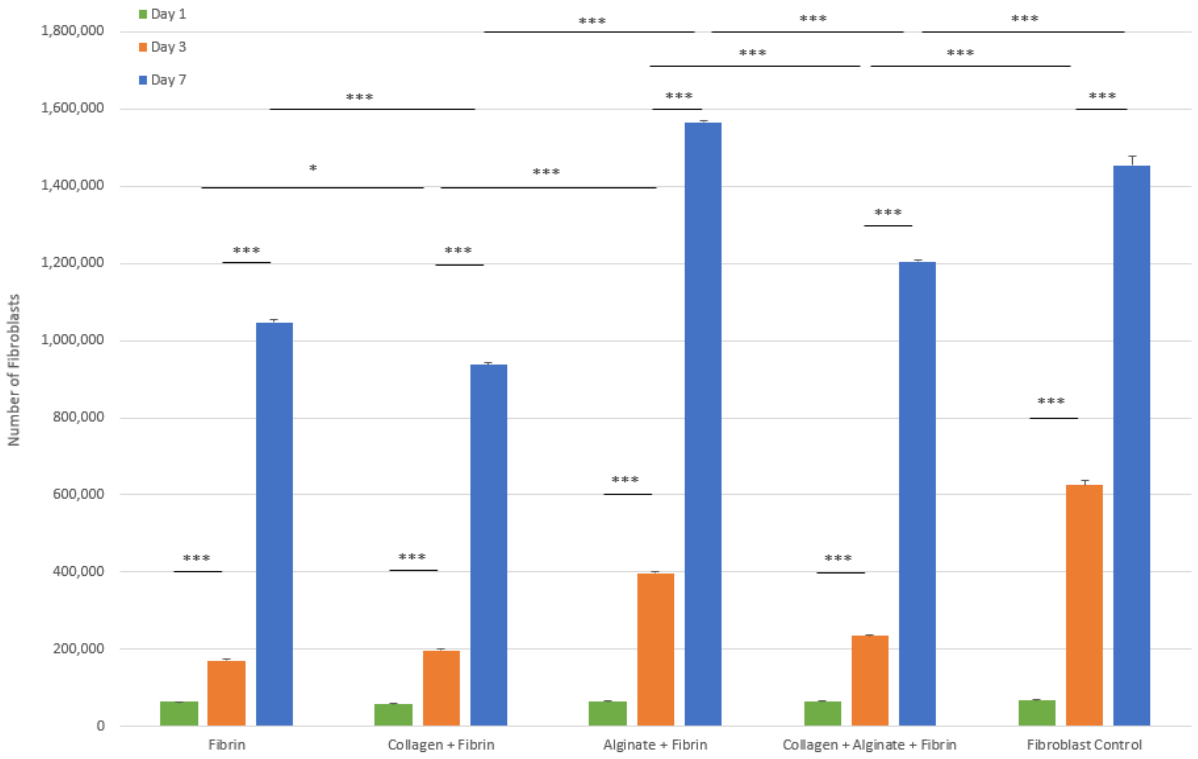

*Figure 6. 23. Comparison of the number of fibroblasts in fibrin-based gels depending on their formulation after 1, 3 and 7 days. Error bars represent the standard deviation (SD), n = 3. Symbols *, ** and *** indicate the significant difference between groups at the level p<0.05, p<0.01 and p<0.001, respectively.*

6.3.3. Production of New Extracellular Matrix Components by Fibroblasts

The immunostaining of collagen type I and collagen type III allowed the identification of variations in the production of these proteins by fibroblasts in the different dermal models. Due to the presence of collagen type I and III in various acellular dermal gels, the fluorescence gain values were normalised to ensure the removal of background signals originated by the bioink components, ensuring the comparability between samples (Fig. 6.24).

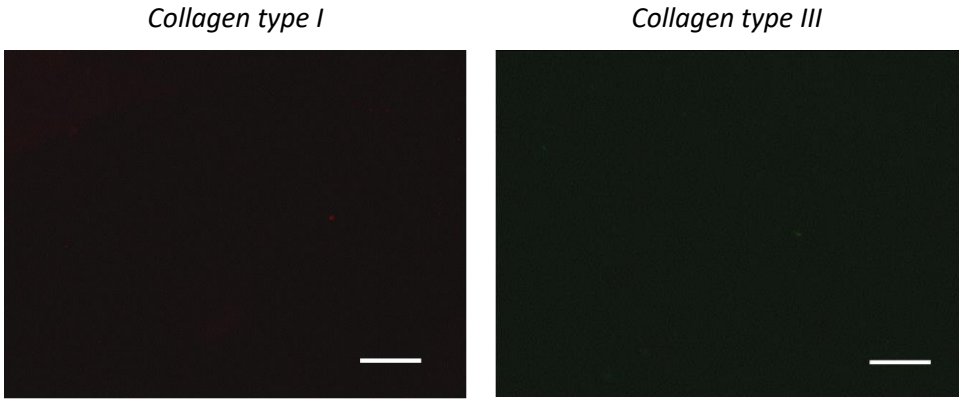

Figure 6. 24. Images of the immunostaining of acellular bovine collagen gels, selected as negative control after normalizing the fluorescence intensity to remove any background signal associated to the acellular biomaterial. Red staining represents collagen type I, and green staining represents collagen type III. Scale bars correspond to 200 µm.

The animal origin of collagen gels employed in the production of dermal models showed a significant influence on the production of new collagen type I proteins by fibroblasts (Fig. 6.25-26). Only human and rat collagen gels neutralised with NaOH showed the presence of new collagen type I on day 3 (Fig. 6.25). In both samples, the amount of collagen type I exhibited a notable increase from day 3 to day 7. Similarly, new collagen type I content was found at day 3 in human and rat collagen gels neutralised with $NaHCO_3$ (Fig. 6.26). However, the amount of collagen type I did not increase after 7 days in these samples. On the other hand, atelo-bovine collagen gels neutralised with $NaHCO_3$ also showed the presence of new collagen type I on day 7. In contrast to collagen type I, the presence of collagen type III was only detected in dermal models prepared with bovine collagen, showing an increase in the collagen type III over time (Fig. 6.27-6.28). In general, telo-bovine collagen gels presented a higher amount of collagen type III than atelo-bovine collagen. In parallel, those gels prepared with sodium hydroxide showed a boost on the production of collagen type III, compared to those prepared with sodium bicarbonate.

The implementation of RAFT^{TM} system on the production of rat collagen gels demonstrated to promote the production of collagen type I and type III by fibroblasts (Fig. 6.25-6.28). In contrast to non-treated rat collagen gels, a significantly increase in collagen type I was observed in the RAFT^{TM} treated samples at day 3 and 7. Additionally, the presence of collagen type III could be observed from day 3 only in those gels prepared with the RAFT^{TM} system.

In the case of fibrin-based gels, the presence of new collagen type I was observed in all samples, but the amount of this protein varied considerably depending on the gel formulation (Fig. 6.29). At day 3, those dermal models prepared with only fibrin showed a higher content of collagen type I than the rest of samples. But on day 7, the quantity of collagen type I was significantly higher in those samples prepared by mixing fibrin with alginate. The production of collagen type III also varied between the fibrin-based models (Fig. 6.30). Those gels combining collagen, alginate and fibrin were the only samples showing the presence of collagen type III at day 3. However, at day 7, the amount of collagen type III was higher in those samples prepared with fibrin and fibrin mixed with collagen. Only in the case of gels prepared combining fibrin with alginate, it was almost not possible to identify any collagen type III content.

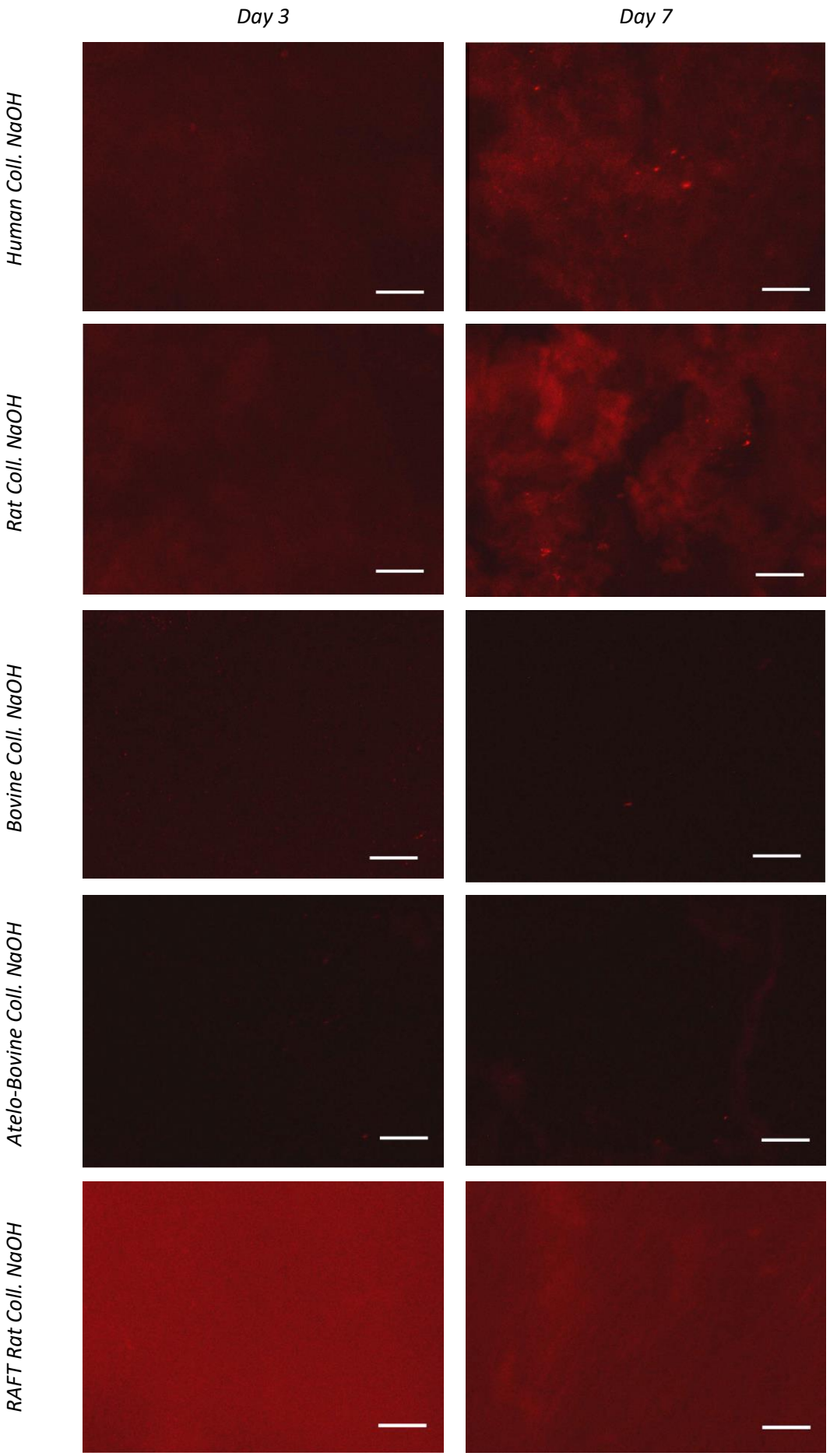

Figure 6. 25. Comparison of the secretion of collagen type I (red) after 3 and 7 days by fibroblasts encapsulated in collagen gels neutralised with NaOH . Scale bars correspond to 200 µm.

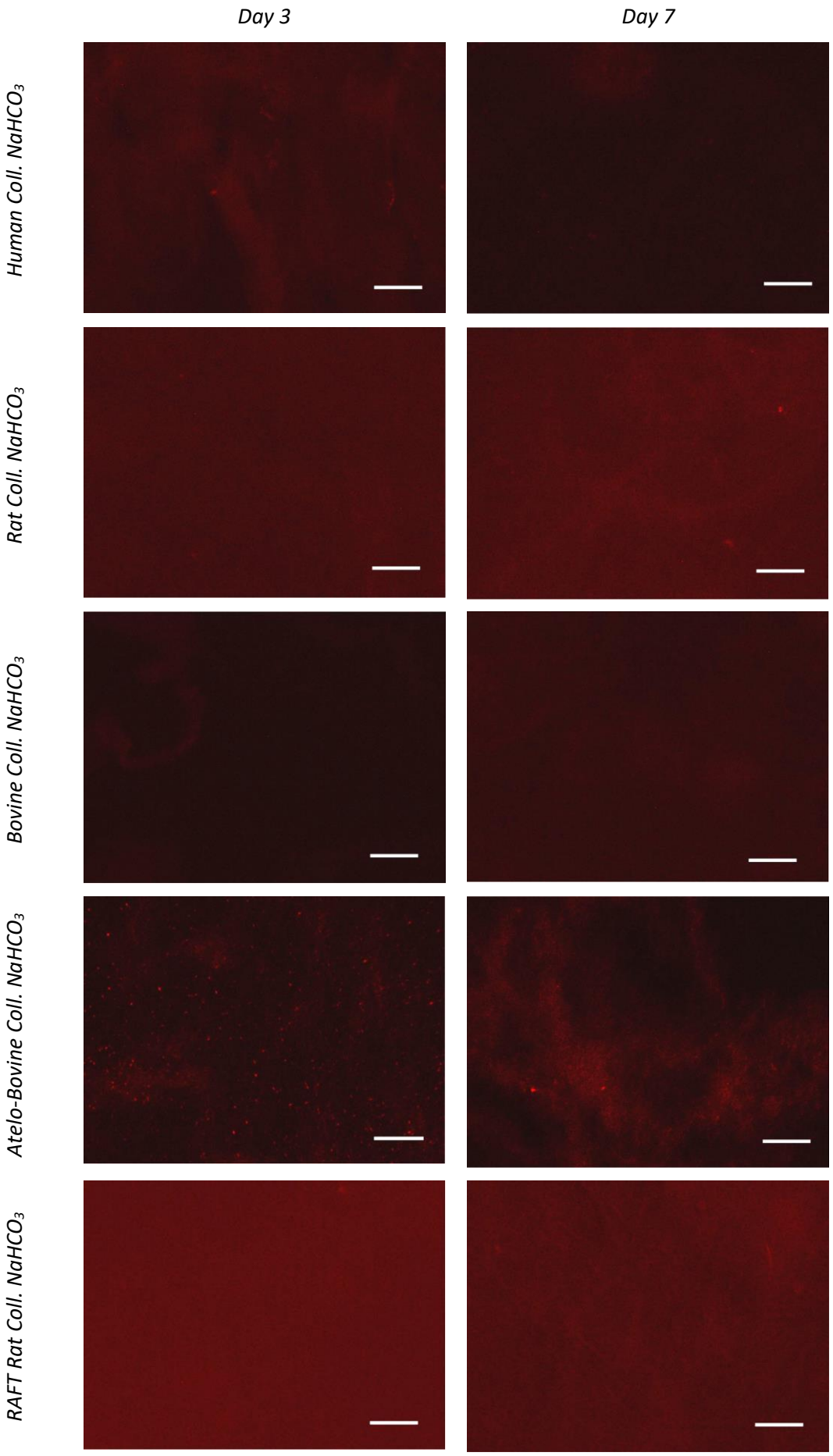

Figure 6. 26. Comparison of the secretion of collagen type I (red) after 3 and 7 days by fibroblasts encapsulated in collagen gels neutralized with $NaHCO_3$. Scale bars correspond to 200 µm.

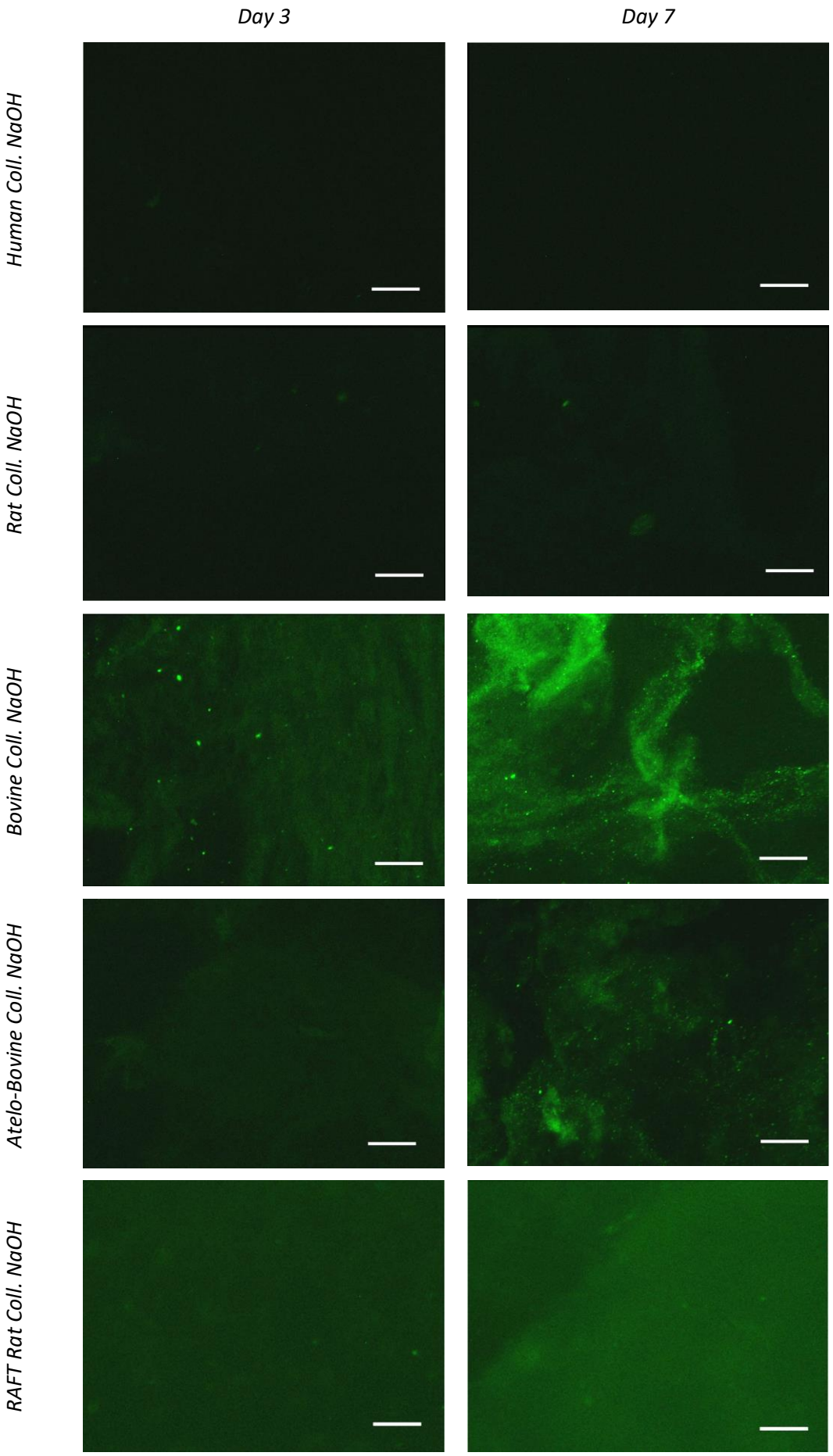

Figure 6. 27. Comparison of the production of collagen type III (green) after 3 and 7 days by fibroblasts encapsulated in collagen gels neutralised with NaOH. Scale bars correspond to 200 µm.

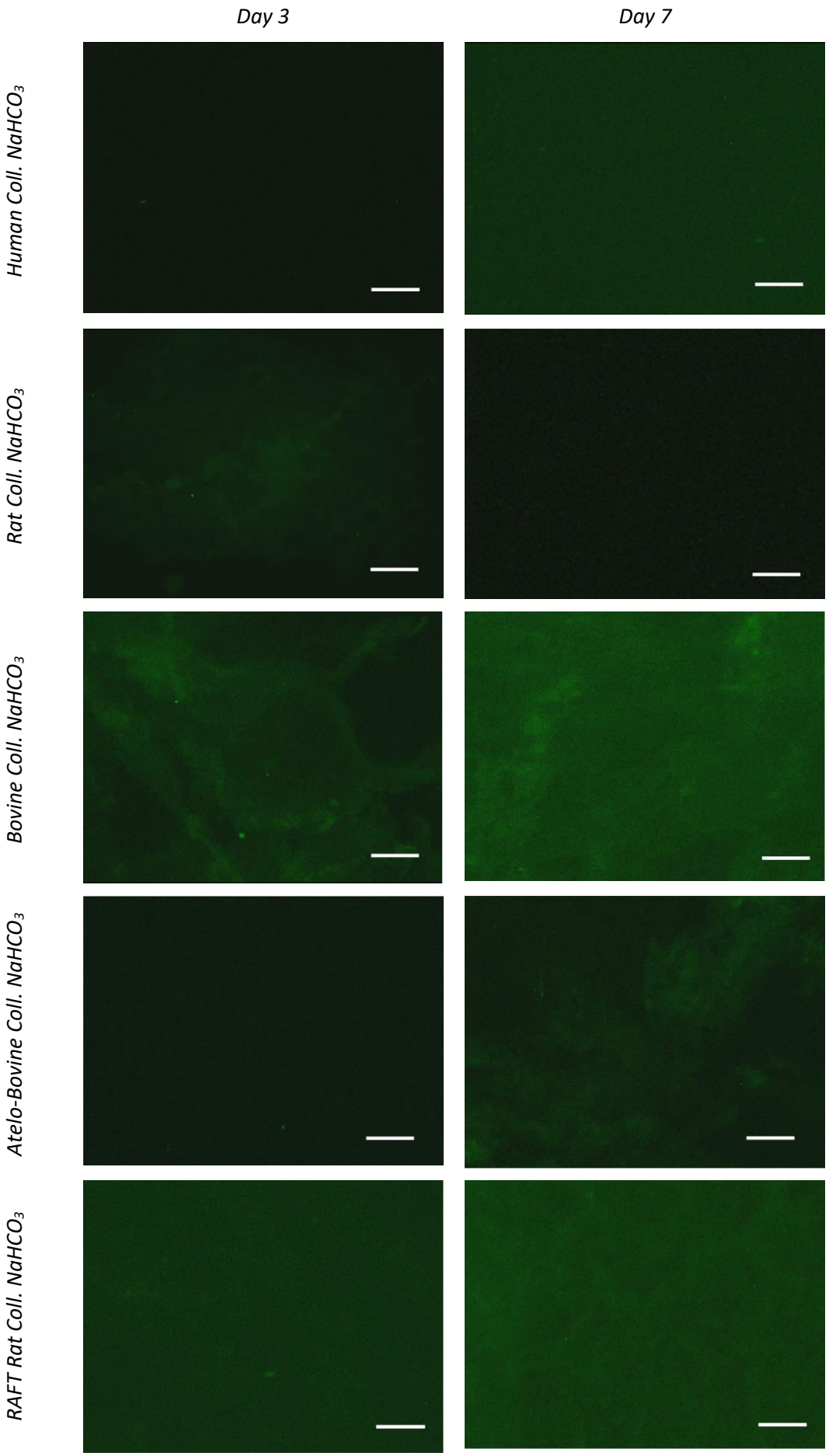

Figure 6. 28. Comparison of the production of collagen type III (green) after 3 and 7 days by fibroblasts encapsulated in collagen gels neutralised with $NaHCO_3$. Scale bars correspond to 200 µm.

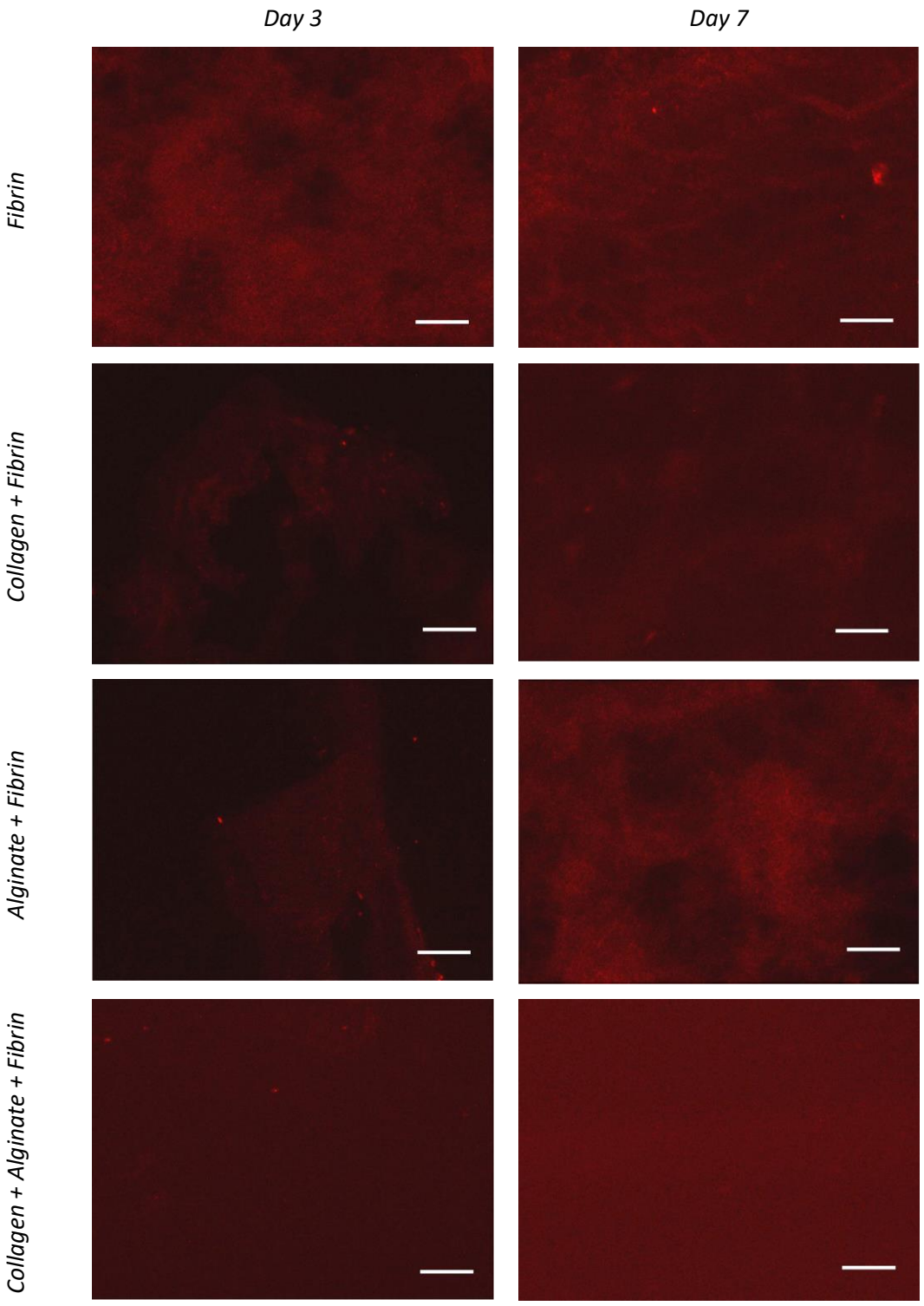

Figure 6. 29. Comparison of the secretion of collagen type I (red) after 3 and 7 days by fibroblasts encapsulated in fibrin-based gels. Scale bars correspond to 200 µm.

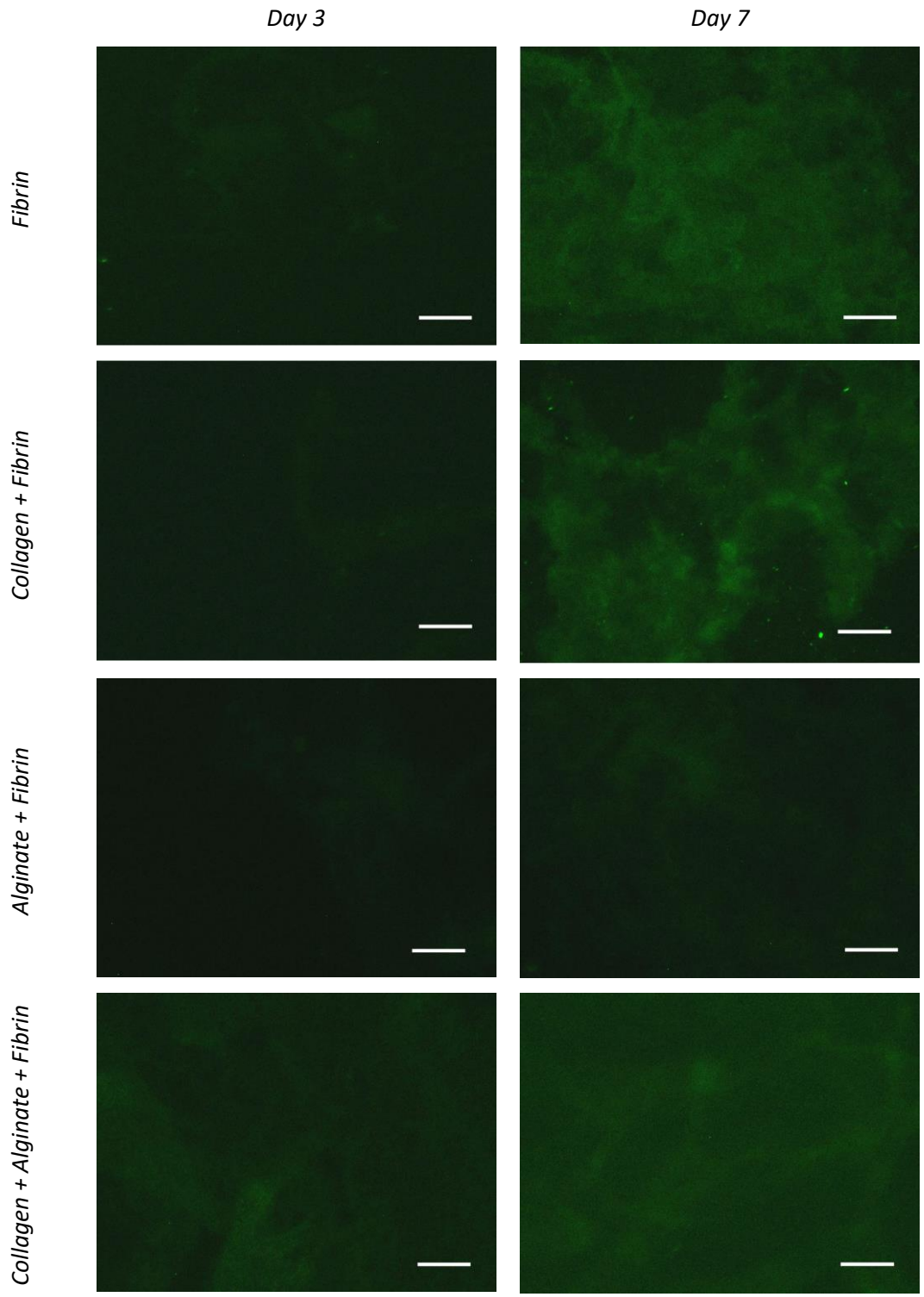

Figure 6. 30. Comparison of the production of collagen type III (green) after 3 and 7 by fibroblasts encapsulated in fibrin-based gels. Scale bars correspond to 200 µm.

6.4. Chapter Discussion

6.4.1. Characterisation of Dermal Bioinks

The chemical analysis of collagen solutions confirmed the presence of the most representative chemical groups in collagen type I in all samples (Belbachir et al., 2009). Still, these studies also revealed chemical differences between collagen solutions depending on their origin. Some of these divergences are exemplified by the presence of additional chemical bonds, or by the differences in the relative intensities between chemical groups such as amides. Variations in the purity of collagen type I in the solutions could explain their chemical differences. The method selected for the extraction of collagen type I influences the precision of its isolation (Bak et al., 2018; Zhang et al., 2022c). For instance, the implementation of enzymatic treatments, such as pepsin, implies the removal of telopeptide regions at both ends of the collagen chain, resulting in a more accurate extraction of collagen type I (Fig. 6.31). Meanwhile, the use of acid solutions as extraction method is based on the dissolution of collagen polymers into monomers by reducing the pH values. Due to the limited specificity of the acid treatments, the possibilities of extracting additional components are higher than by enzymatic processes (Matinong et al., 2022). The impact of the extraction method on the purity of collagen solutions could justify the differences between the FTIR spectras from telo and atelo-bovine collagen solutions (Ju et al., 2020). Atelo-bovine collagen presented fewer additional absorption bands, such as the one found at 945 cm^{-1} , and it showed an enhancement in the intensity of the chemical groups associated with the tertiary amide, with respect to the intensity of the primary amide.

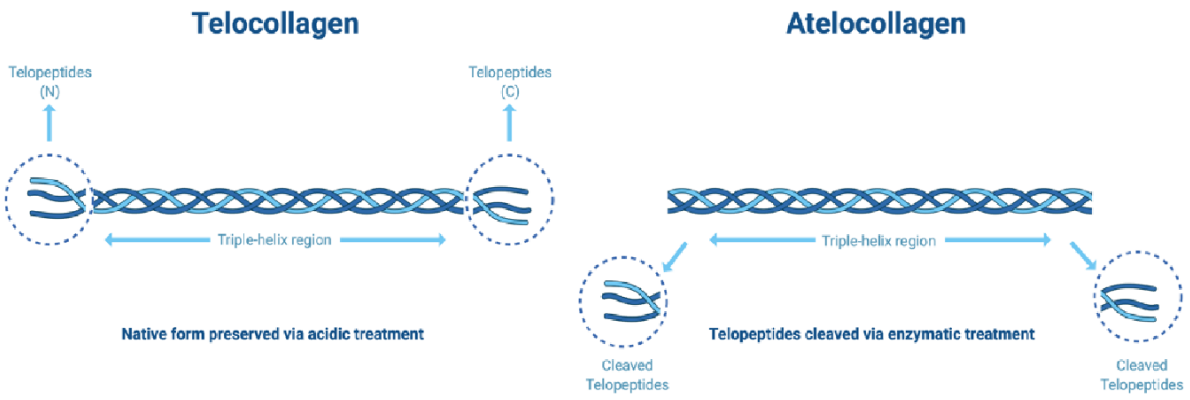

Figure 6. 31. Representation of the differences between the collagen structure in atelo- and telo-collagen. Image obtained from PromedBioscience.

The body area from which collagen type I was isolated could also be a determinant factor in the purity of the extracted collagen samples (Amirrah et al., 2022). In particular, the removal of bovine tendons entails a more complex procedure than the extraction of tendons from rat tails, increasing the chances of obtaining heterogeneous samples (Techatanawat et al., 2011). Furthermore, some studies have claimed the presence of chemical variations in collagen type I fibres depending on the tissue to which they belong (Avery & Bailey, 2008). The variations in the hydroxylation of telopeptide lysines are considered one of the key elements responsible for the mechanical differences between collagen fibres. In tissues such as skin or rat tails, these lysines are barely hydroxylated, contrasting with the high presence of hydroxylines in bone collagen. As a result, the interaction between collagen molecules to form collagen microfibrils depend on the lysine hydroxylation (Yamauchi & Sricholpech, 2012). In the presence of a small number of hydroxylated telopeptide lysines, the reaction between collagen molecules results in the formation of divalent aldimine crosslinks, which are stable under physiological conditions but can be removed by acid treatments. Meanwhile, the high presence of hydroxyled telopeptide lysines can derivate on the formation of divalent keto-amine crosslink, and even the generation of pyridinoline and pyrrole trivalent crosslinks. The strength of these groups can prevent their degradation with acid treatments and interfere with the properties of the final collagen fibres. The FTIR analysis performed in the collagen solutions does not allow quantifying the hydroxylation of lysine groups or determining the presence of residual groups from the interaction between microfibrils. Therefore, further chemical analysis complementing the FTIR analysis with Raman Spectroscopy would be required in the future to conclude the differences between the collagen solutions and their potential impact on the properties of collagen gels (Hashimoto et al., 2019).

Due to the non-destructive character of the acidic treatment employed in the extraction of collagen type I, most of the original chemical interactions between collagen microfibrils could be recovered by exposing the collagen solutions to physiological conditions (Fig. 6.32) (Shayegan et al., 2016). The optimisation of the neutralisation method by combining sodium hydroxide with PBS buffer allowed a higher control on the pH variations, and the generation of collagen gels with more homogeneous characteristics than the ones obtained following conventional protocols.

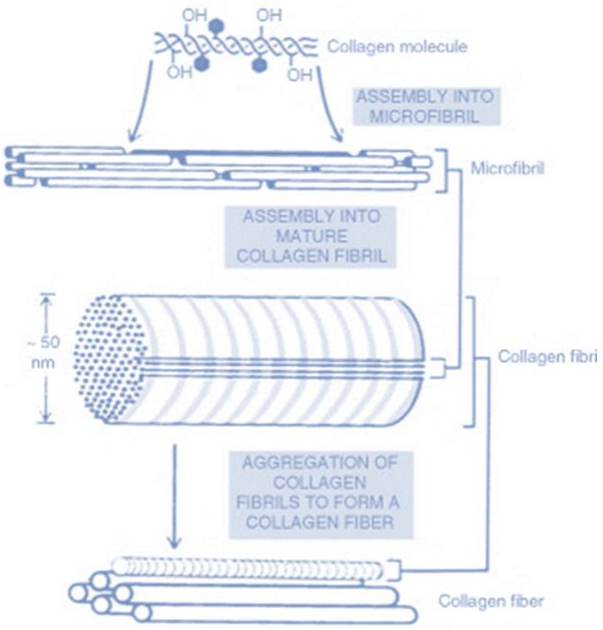

Figure 6. 32. Diagram of the steps involved in the formation of collagen fibres from collagen molecules. Image obtained from Fratzl et al 2008.

Only collagen solutions obtained from calf skin and jellyfish did not form any gel after their neutralisation to pH 7.4. The inability to generate stable gels using calf and jellyfish collagen solutions could be explained by their triple helix spectra (Grant et al., 2009; Venugopal et al., 1994). In the case of calf collagen, the low triple helix content measured by circular dichroism suggested their denaturalisation. The degradation of collagen type I usually originates the formation of gelatin, which presents an aqueous state at 37°C (Alipal et al., 2021). Gelatin is capable of restoring part of its triple-helix structure at lower temperatures, recovering their gel properties (Bigi et al., 2004; Wüstneck et al., 1988). However, the low levels of triple helix content observed regardless of the temperature, and the inability to generate gels at lower temperatures, invalidated this hypothesis. Despite repeating these results using different batches of calf collagen, it was not possible to generate a gel. The thermal or chemical treatment employed during the collagen extraction by the manufacturer could be the reason behind these results. On the other hand, the triple helix in jellyfish collagen presented a significant degradation at temperatures above 24°C, which could be justified by the low body temperature characteristic of jellyfish (Fitt & Costley, 1998). The need of skin cells to be incubated at 37°C for their correct functioning, and the inability to generate stable gels at this temperature prevented the use of jellyfish collagen in the generation of skin models.

The thermal stability of the triple helix showed some significant variation in the other collagens depending on their origin. The differences in the internal temperature of the animals from which the collagen was extracted could be one of the variables that explain these variations according to previous studies (Zhang et al., 2020). Moreover, the formation of collagen gel was an important factor in enhancing the resistance of triple helix to thermal degradation. The recovery of chemical interactions between triple helix structures to generate collagen microfibres, could explain their higher resilience and protection against the increase in the temperature after the formation of collagen gels (Fratzl, 2008; Orgel et al., 2014). The possibility of maintaining the triple helix structure in human, rat and bovine collagen gels at 37°C underlined their suitability for generating dermal matrices.

One of the most significant differences between the selected collagens was their contrasting fibrillar organisation. Collagen matrices are usually defined by their high porosity and disordered arrangement of thin fibres. However, only rat and human collagen gels prepared with $NaHCO_3$ presented similar characteristics to the ones reported in previous studies (Achilli & Mantovani, 2010; Holder et al., 2018). The distinctive assembly of collagen fibres observed in the SEM images could be explained by the chemical differences detected in the collagen solutions. Besides, the presence of additional chemical groups in some samples could justify some differences observed in the collagen matrices depending on the selected neutralisation method.

The impact of the animal source on the matrix properties was especially evident with the use of sodium hydroxide as neutralisation method. The strong basic character of sodium hydroxide could accelerate the fibrillogenesis process and promote reactions between the additional chemical groups, causing more notable variations between samples (Avery & Bailey, 2008). Contrarily, using a weaker base, such as sodium bicarbonate, would result in the slower formation of collagen fibres, and the need for additional time to form the gels, as it was shown on their fibrillogenesis profiles (Antoine et al., 2014). This limited reaction speed could explain the small thickness of the generated fibres, the increased porosity, and overall, the higher resemblance between the collagen matrices regardless their animal origin when using this basic solution. The role of the neutralisation method on the matrix properties was especially representative in rat collagen. Despite the thickness of the fibres was similar, the aleatory distribution in the rat collagen gels neutralised with sodium bicarbonate contrasted with the

collagen bundles formed with the use of sodium hydroxide. The formation of these spherical fibre aggregates could be caused by the fast crosslinking caused by sodium hydroxide.

The influence of additional compounds present in the collagen solutions on the characteristics of the dermal matrix was especially evident after comparing telo and atelo-bovine collagen. The presence of fibres with different thicknesses in telo-bovine collagen gels could correspond to the mixture of collagen type I and type III. Tendons contain a high concentration of both types of collagens, which interact, forming entanglements between their fibres similar to the ones observed in telo-bovine collagen gels neutralised with NaOH (Lapiere et al., 2009; Buckley et al., 2013). The presence of these two types of fibres could explain the two deflective regions observed only in the fibrillogenesis profile of telo-bovine collagen, regardless of their neutralisation method. The characterisation of these collagen gels by Transmission Electron Microscopy (TEM) could be a potential method to confirm the presence of collagen type III. Based on previous studies, the existence of collagen type III modifies the diameter of collagen type I fibres and its characteristic D-banding in the TEM images (Fig. 6.33) (Asgari et al., 2017).

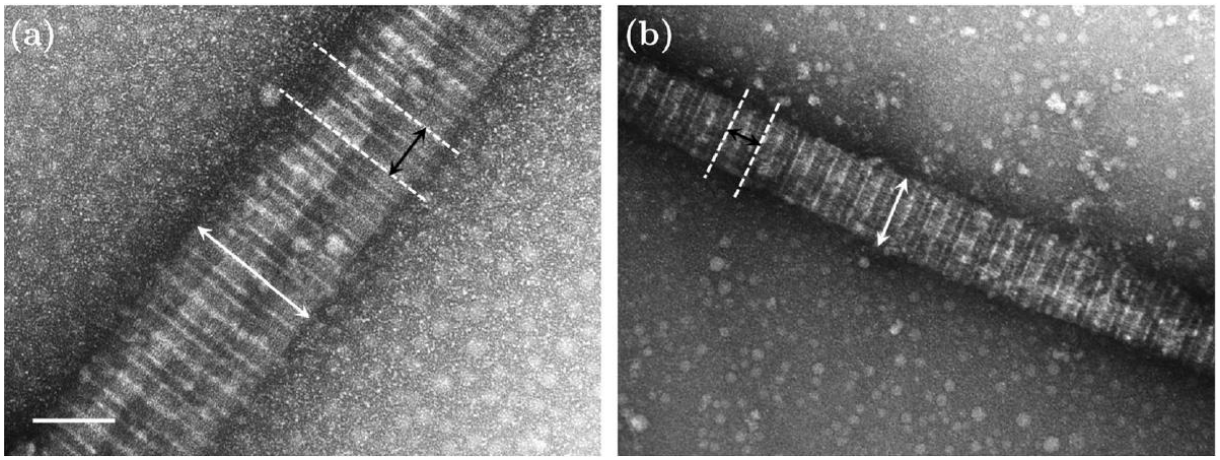

Figure 6. 33. Transmission Electron Microscopic (TEM) images of (a) collagen type I and (b) a combination of collagen type III and collagen type I in a 50:50 volume ratio. Scale bar represents 100 nm. Images obtained from Asgari et al. 2017.

The extraction method also had a significant effect on the matrix formation. Despite the fibrillogenesis profile was similar for telo- and atelo- bovine collagen neutralised with sodium hydroxide, the use of sodium bicarbonate resulted in a delayed formation of atelo-bovine collagens. The absence of telopeptide ends in atelo-collagen and the limited strength of sodium bicarbonate could have implied the creation of weaker interactions between the collagen molecules and the brittle aspect of the resulting collagen matrix.

The implementation of RAFT^{TM} system also demonstrated to be a feasible method to tailor the fibrillar arrangement in collagen gels. This commercial system is based on absorbers capable of removing the excess of water in collagen gels, implying an increase in the collagen concentration, and consequently, the acceleration of the fibre formation (Kayal et al., 2019). As a result, collagen gels prepared using the RAFT^{TM} system presented a more condensed fibrillar organisation and a partial alignment of the fibres. In addition, the pressure applied by the absorbers could also be an important factor in the reorganisation of the fibrillar arrangement.

In contrast to collagen samples, fibrin gels are characterised by the quick formation of gels due to the fast enzymatic reaction between fibrin and thrombin (Shinowara, 1966). As a result, fibrin gels showed a matrix with high fibre content and limited porosity. By combining fibrin with an additional fibrillar protein such as collagen type I, it was possible to increase the spaces between fibres and generate more heterogeneous samples (Wang et al., 2022; Rowe & Stegemann, 2006). Oppositely, the introduction of a polysaccharide such as alginate in the fibrin bioink increased the matrix porosity. In this sample, alginate showed a similar function than natural proteoglycans in the dermis, providing separation between fibres to improve the diffusion of molecules (Soleimanpour et al., 2022). Finally, the integration of these three biocomponents into a single bioink formulation resulted in the combination of their individual properties, generating a matrix characterised by its high porosity and the presence of fibres with different thicknesses.

The variations in the fibre properties and matrix organisation proved to directly impact the mechanical properties of dermal gels. For instance, the thinner fibres and higher porosity in collagen gels neutralised with $NaHCO_3$ resulted in matrix with significantly lower stiffness than those prepared with NaOH (Seo et al., 2020). In the same way, the resemblance of the matrix generated from human collagen gels prepared with NaOH and $NaHCO_3$ implied a similar stiffness in both samples regardless of the selected neutralisation method. Furthermore, the fibrillar organisation also demonstrated to influence the resistance of the matrices to be remodelled by external agents. The disorganised arrangement and high distance between fibres in most collagen samples facilitate their reorganisation, which would explain the increase in the storage modulus after applying high angular frequencies (Stojkov et al., 2021). Conversely, the compacted fibre bundles found in rat collagen neutralised with NaOH could

explain its notable stiffness and the stabilisation of its storage modulus due to the inability to change the matrix configuration. Other factors, such as the presence of thick fibres or the fibrillar alignment, demonstrated to improve the matrix stiffness and the response to external stimulus in telo-bovine collagen gels.

The high matrix density characteristic of fibrin gels could justify their high stiffness and the inability to remodel their organisation compared to most collagen gels (Moreno-Arotzena et al., 2015; Wachendörfer et al., 2022). The combination of collagen and fibrin made possible to enforce the stiffness of the fibrin matrix. However, it is still not clear if this improvement is caused by the entanglement between their fibres or any potential interaction between their fibres (Lai et al., 2012). Additionally, the creation of spaces between fibres could explain the possibility of remodelling this matrix, but the inability to modify the matrix containing only fibrin. In contrast to previous samples, the incorporation of alginate resulted in the reduction of the gel stiffness. The spatial separation between fibrin fibres caused by alginate could justify this decrease, and the possibility of breaking the gel after exposing it to different angular frequencies (Ramli et al., 2022). Finally, the heterogenicity and high porosity of the gels produced with the combination of collagen, alginate and fibrin, could explain their intermediate mechanical strength. Additionally, these matrix characteristics could also justify the ability of these gels to maintain stable storage modulus values, showing only a remodelling and increase of the matrix stiffness at high angular frequencies.

An initial assessment of the printability of the studied dermal formulation was possible by measuring the viscosity of the gel precursors and crosslinkers, and the evaluation of the gel formation. The use of microvalves in the ReJI system requires the selection of bioinks with a viscosity range between 1 and 70 mPa·s to ensure the correct droplet formation and avoid the clogging of the valve nozzle. All the selected gel precursors and crosslinkers presented viscosity values comprehended between this range, confirming their feasibility to be incorporated in microvalve-based bioprinting systems. In the case of collagen gels, it was essential to verify the stability of the collagen solutions at room temperature. The stability of the triple helix spectra in the collagen solutions at temperatures lower than 30°C confirmed the possibility of printing the collagen solutions at room temperature, without any risk of denaturalisation.

On the other hand, ReJI system is based on the fast reaction between the gel precursor and crosslinker, to enable the printing of subsequent layers without the need of waiting times. The

studied bioink formulation containing fibrin combined with alginate and collagen had already been validated in previous studies for its printing using the ReJI process (da Conceicao Ribeiro, 2019). This bioink was characterised by a fast-crosslinking reaction, reaching a stiffness higher than 10 Pa in 60 seconds. The use of only fibrin, or the combination of fibrin with alginate resulted in similar crosslinking profiles. Just the use of fibrin combined with collagen enabled a slight acceleration of the reaction, showing stiffness higher than 10 Pa in 10 seconds. In comparison to the fibrin gels, only rat collagen neutralised with NaOH was capable of reaching stiffness values higher than 10 Pa in 30 seconds, and therefore, it can be considered suitable for its incorporation in the ReJI process. Rat collagen neutralised with $NaHCO_3$ also presented a fast crosslinking reaction getting a storage modulus above 10 Pa in less than 60 seconds. Still, its initial liquid state and slower reaction hinder its suitability for the impingement process. Finally, the incorporation of human collagen into the ReJI process could also be considered. These samples showed stable storage modulus near 10 Pa in the initial minutes, however, it would be necessary to evaluate the stability of the printed layers before concluding the suitability of these collagens.

These performed studies provided an initial screening of the printability of the selected dermal bioinks. However, the analysis of further parameters, such as surface tension or bioink density, will be required to confirm their printability and optimise their printing parameters (Ng et al., 2017).

6.4.2. Fibroblast Behaviour in the Studied Dermal Models

The combination of the results obtained in the study of fibroblast morphology, distribution, proliferation and production of new dermal proteins, provided a general overview of the adaptation and response of fibroblasts to the different dermal matrices.

Although the collagen origin is usually a dismissed variable in the production of dermal matrices, fibroblast behaviour demonstrated to vary significantly depending on the animal source of collagen. In the case of human and rat collagen, fibroblasts showed a slow adaptation to the gels and a limited increase in the number of fibroblasts over time compared to bovine collagen samples. The characteristics of their matrix could explain the reduced mobility and low proliferation of fibroblasts in these samples. For instance, the small diameter of collagen fibres and the limited mechanical strength of these matrices could be responsible for the incapacity of the cells to adapt and expand (D'Urso & Kurniawan, 2020; Bott et al., 2010). In the case of rat collagen neutralised with NaOH, despite presenting a higher mechanical strength, the inability of fibroblasts to modify the matrix could also explain this response by the cells (Rhee, 2009). Based on the limited quality of the dermal matrix, fibroblasts would require to produce their own fibrillar network before initiating their migration and proliferation through the dermal construct. The initial need to secrete new matrix components correlates with the high presence of new collagen type I proteins on the first days shown in the immunostaining images. The behaviour of fibroblasts in these samples, along with their polygonal morphology, could imply the possibility of replicating the reticular dermis using these materials. In order to confirm the reticular character of fibroblasts in these samples, Real-Time Quantitative Reverse Transcription Polymerase Chain Reaction (qPCR) was carried out. The study of the expression of versican, collagen type I and elastin by fibroblasts was performed to determine the reticular character of fibroblasts. In contrast, the expression of decorin, collagen type III and fibronectin were studied to determine the presence of papillary fibroblasts (Sriram et al., 2015; Janson et al., 2012). Although different attempts were performed on the qPCR analysis of these samples, some problems related to the cDNA synthesis hindered the generation of data with enough quality to determine the fibroblast phenotype in the different dermal models. Therefore, repetition of these analyses will be required to conclude the capacity of these bioinks to recreate the specific characteristics of native dermal regions. In the case of dermal models produced with bovine collagen, fibroblasts presented a faster adaptation to the new environment, showing a defined morphology from

the first day. Only atelo-bovine collagen neutralised with $NaHCO_3$ represented the exception, showing higher similarities to the results obtained with human and rat collagen gels. The brittle character of this atelo-bovine collagen sample could justify its fast degradation by fibroblasts after only 5 days (Berg et al., 1980). In contrast, the rest of bovine collagen gels are characterised by thicker fibres and a higher organisation of their matrix, which could justify their enhanced support to the cells (Li et al., 2021). These characteristics could also explain the high proliferation of fibroblasts in these samples and their movement through the matrix to form different cellular configurations. The possibility of fibroblasts to travel through the dermal layer and remodel the fibrillar arrangement would justify the reduced expression of new matrix components in these samples, with just the expression of collagen type III after 7 days (Mathew-Steiner et al., 2021). On the other hand, the variations in the mechanical properties between bovine collagens could be related to the differences in the fibroblast behaviour observed between these samples. In the case of bovine collagen neutralised with NaOH, the high expression of F-actin filaments by fibroblasts observed from day 3 could be explained by the high stiffness of these gels and the response of fibroblasts to the generated tensional forces (Martino et al., 2018; Shinde et al., 2017). As the number of fibroblasts increased, the stiffness of the matrix could also be incremented due to the pull of the fibres by fibroblasts during the matrix remodelling (Jagiełło et al., 2022). This phenomenon would justify the further increase in the expression of F-actin filaments observed at day 7, and the cell configuration adopted by the cells. The formation of similar cell structures in telo-bovine collagen neutralised with $NaHCO_3$, despite the lower expression of F-actin filaments by fibroblasts, could be explained by their reduced stiffness compared to the same gels prepared with NaOH. The higher separation between cells showed in these samples at day 3, could also justify the lower number of fibroblasts at day 7 compared to the bovine collagen samples neutralised with NaOH. In the same way, the reduced stiffness of atelo-bovine collagen, compared to telo-bovine collagen, could explain the slower proliferation rate of fibroblasts in these samples, and the absence of clearly defined F-actin filaments in the cells. Overall, the high proliferation and mobility of fibroblasts, along with the predominant spindle-like morphology of the encapsulated cells suggest the suitability of bovine collagen gels to recreate the papillary dermis (Tan et al., 2022).

The importance of the fibrillar organisation and matrix properties on the cell behaviour was especially underlined by the incorporation of RAFT^{TM} system into the production of rat collagen gels. The capacity of this technology to increase the condensation and alignment of

the fibres implied a modification in the fibroblast behaviour. For instance, the new fibre configuration resulted in an increased proliferation of fibroblasts after 7 days compared to non-treated rat collagen gels. Meanwhile, the enhancement of the mechanical strength of the matrix could explain the increase in the expression of F-actin filaments in these samples. Although it was not possible to prove this enhancement on the matrix stiffness, previous works have reported the capacity of the RAFT^{TM} system to improve the mechanical properties of collagen gels (Kayal et al., 2019). On the other hand, the limited porosity of the resulting collagen matrix showed a restriction on fibroblast mobility. The need to create a new matrix in order to travel through the dermis could explain the high secretion of new extracellular matrix proteins observed by immunostaining.

The selection of fibrin as main dermal component resulted in a faster adaptation of fibroblasts to the matrix compared to collagen samples. This adaptability could be justified by the natural interaction between fibroblasts and fibrin during the wound-healing process (Moretti et al., 2022). Similarly, the high cell proliferation and secretion of new extracellular matrix observed in these samples could be explained by the promotion of natural signal cascades associated with the dermal regeneration (Fuchs et al., 2020; Tracy et al., 2016). By combining fibrin with collagen and alginate, it was possible to modify the distribution and alter the proliferation of fibroblasts. For instance, the integration of collagen into the fibrin bioinks could be responsible of the drop in the tensional forces presented by fibroblasts and their decrease on the expression of F-actin filaments after 7 days. The higher stiffness of this material compared to fibrin gels cannot justify this phenomenon. However, a reduction in the stiffness values due to the remodelling of the matrix by fibroblasts, could be a feasible explanation for this phenomenon. In the case of gels combining fibrin with alginate, a large number of cell aggregates could be observed on day 3. The absence of cellular recognition sites in alginate could illustrate its role on the observed cell encapsulation and the generation of cell groups (Kang et al., 2021). The presence of fibrin, the high proximity between cells and the alginate degradation could explain the significant increment in the number of cells observed and the high increase in the ECM proteins in these samples after 7 days (Vorwald et al., 2020). Finally, the combination of fibrin with collagen and alginate resulted in a high proliferation and mobility of fibroblasts without generating tensional forces between cells. The intermediate stiffness of the matrix and the possibility of modifying its configuration could justify this cell behaviour compared to previous samples.

6.4.3. Tailoring the Dermal Model Properties

The formulation of dermal bioinks has demonstrated to be an essential factor to control the fibroblast behaviour and customise the properties of the dermal models. Therefore, the specific selection and combination of dermal components could help to improve the complexity of skin models and enable the recreation of dermal microenvironments.

The stiffness of the dermal models is one of the variables which can be customised with the selection of dermal bioinks. Choosing specific collagen sources, such as bovine collagen, can help to enhance the mechanical strength of the models. Selection of other parameters, such telo-collagens or the selection of sodium hydroxide as neutralisation methods, has also demonstrated to improve the sample stiffness. In the case of fibrin-based models, their mechanical properties can be modified by introducing collagen to enhance the matrix strength, or alginate to decrease the stiffness values.

Fibroblasts are characterised by their ability to respond to the mechanical changes in their surrounding environment. However, other elements, such as the porosity and fibrillar properties of the dermal matrix or the nature of the dermal biocomponents, have demonstrated in this study to influence fibroblasts. Further research will still be required to conclude the resemblance of the produced dermal models with the composition and properties of the different natural dermal microenvironments. Still, the reproduction of some specific fibroblast behaviours was possible with the selection of specific dermal formulations. For instance, by introducing human or rat collagen as main dermal biocomponents, it was possible to recreate some of the characteristic behaviour of reticular fibroblasts. Meanwhile, the use of bovine collagen promoted the recreation of an environment similar to the one in the papillary dermis. On the other hand, the introduction of fibrin as main biocomponent or the implementation of RAFT^{TM} system on the production of collagen gels could help to generate more complex models, with more significant cell confluency and higher quantity of extracellular matrix components. In these samples, tracking the changes in the stiffness and ECM content will be essential to avoid the generation of fibrotic tissue (Theocharis et al., 2019; Wells, 2013).

Of all the studied dermal bioinks, only the fibrin-based bioinks, along with rat collagen solution combined with sodium hydroxide, had proved their printability with the ReJI process. Still, the selection of the best dermal bioink will depend on the impact of these formulations on the reliability of the final skin models.

CHAPTER 7. SELECTION OF EPIDERMAL BIOINKS

7.1. Introduction

The difficulties controlling the location of keratinocytes during the manual seeding of skin models and the inability to ensure their homogeneous distribution often result in an uneven epidermal formation. Consequently, skin equivalents usually present inconsistent properties between batches, hindering the reliability and reproducibility of the assays performed.

To solve this problem, the encapsulation of keratinocytes in natural-based bioinks is proposed in this chapter as a new approach to control the keratinocyte distribution and accelerate the epidermal stratification. The research described below focuses on evaluating the differences in the keratinocyte behaviour based on the formulation of the epidermal bioinks. Fibrin, collagen type I and alginate were selected as principal biomaterials for encapsulating keratinocytes due to their popularity in treating extensive skin burns (Heher et al., 2018; ter Horst et al., 2018; Thomas, 2013).

The viability and adhesion of keratinocytes after their encapsulation was first assessed to determine the feasibility of the epidermal bioinks. Additionally, the ability of the formulated bioinks to improve the homogeneity of epidermal layers was determined by comparing the distribution of keratinocytes encapsulated to the seeding of keratinocytes suspended in cell media. Finally, the capacity of the selected bioinks to promote the correct epidermal formation was concluded by studying the changes in the expression of keratinocyte markers related to their proliferation and differentiation process.

7.2. Effect of Keratinocyte Encapsulation

7.2.1. Keratinocyte Viability and Distribution

The selected epidermal bioinks have demonstrated to affect the viability of the encapsulated keratinocytes and their distribution in a different manner depending on their formulation. The encapsulation of keratinocytes in bovine collagen and fibrin-based gels resulted in a similar cell viability over time to those keratinocyte monolayers seeded in tissue culture-treated wells (Fig. 7.1-7.2). In the case of cells encapsulated in bovine collagen, a homogeneous cell distribution could be observed through the three-dimensional gel over time (Fig. 7.2). Meanwhile, the use of fibrin-based bioinks also resulted in high cell viability over time (Fig. 7.1). In these samples, keratinocytes started to form cell groups, which was particularly notable after 3 days. Keratinocyte distribution was influenced by the specific composition of the fibrin-based bioinks. Samples with higher fibrin concentrations presented larger agglomerations of keratinocytes without affecting their viability. Meanwhile, the combination of fibrin with collagen and alginate to generate CAF gels resulted in a reduction of keratinocyte groups, which were only visible after 7 days.

In contrast, using alginate as encapsulation agent resulted in a reduced number of cells (Fig. 7.2). On day 1, keratinocytes presented a combination of red and green staining, suggesting the death of most encapsulated cells. The number of cells barely varied over time, although most keratinocytes showed only a green signal associated with the presence of live cells after 3 days. The increment in the calcium chloride concentration, from 0.1% to 1%, to generate the alginate gels, resulted in an increase in the number of cells on day 1. However, problems with the live/dead staining were also observed in these alginate samples. Only after 7 days, a slight increase in the number of live cells could be denoted.

The comparison between control samples containing keratinocytes incubated in normal conditions, and those cultured with a medium containing a higher concentration of calcium chloride, underlined the effect of calcium ions on keratinocyte viability. By increasing the concentration of calcium chloride to 1% in the cell medium, the number of live keratinocytes significantly dropped after 1 day. The number of dead cells increased over time, reducing the keratinocyte survival after 7 days.

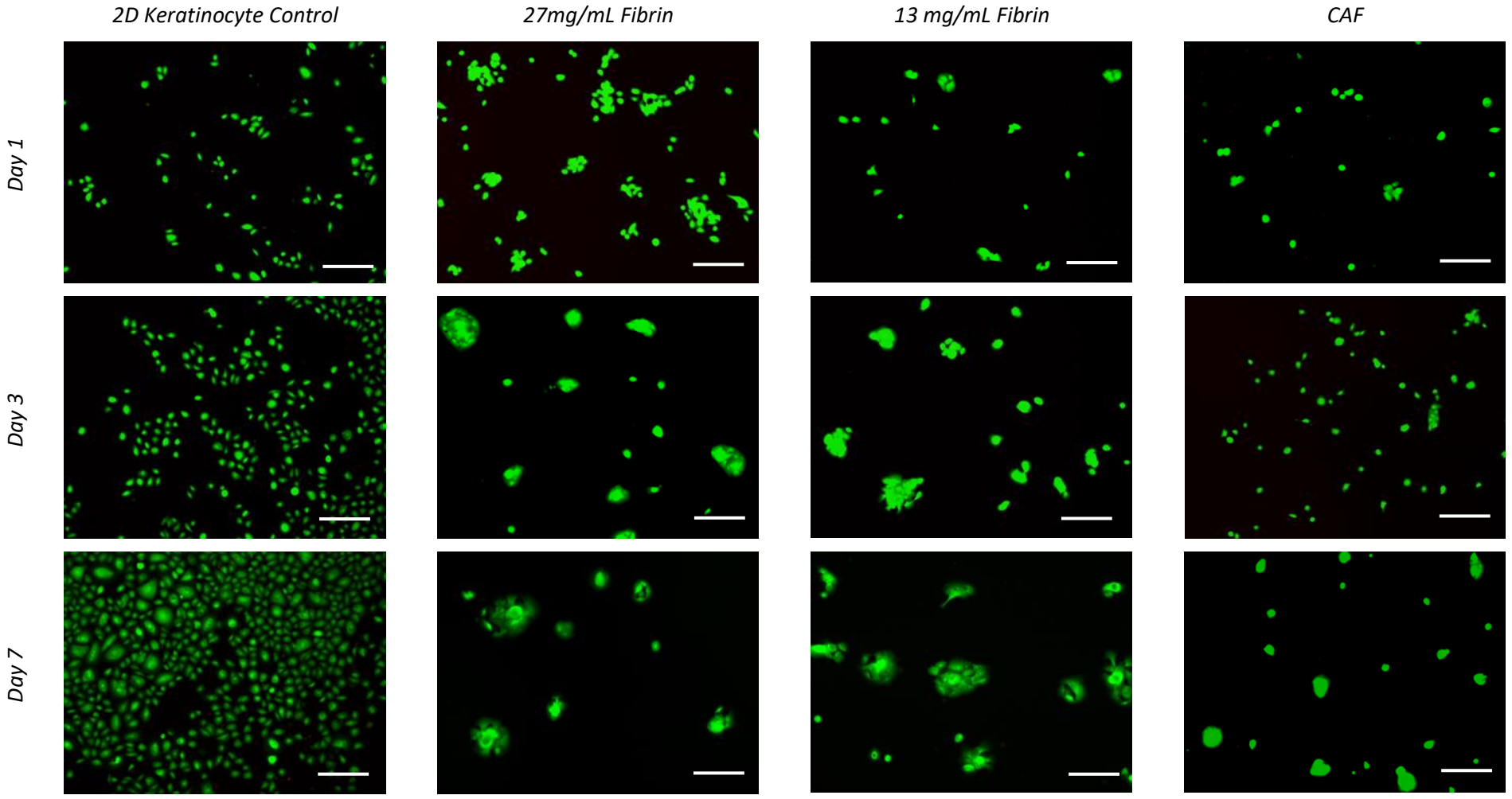

Figure 7. 1. Evaluation of the viability and distribution after 1, 3 and 7 days of keratinocytes encapsulated in fibrin-based gels in comparison to keratinocyte monolayers seeded on tissue culture-treated wells. Dead cells are represented in red and living cells in green. The scale bars correspond to 200 µm.

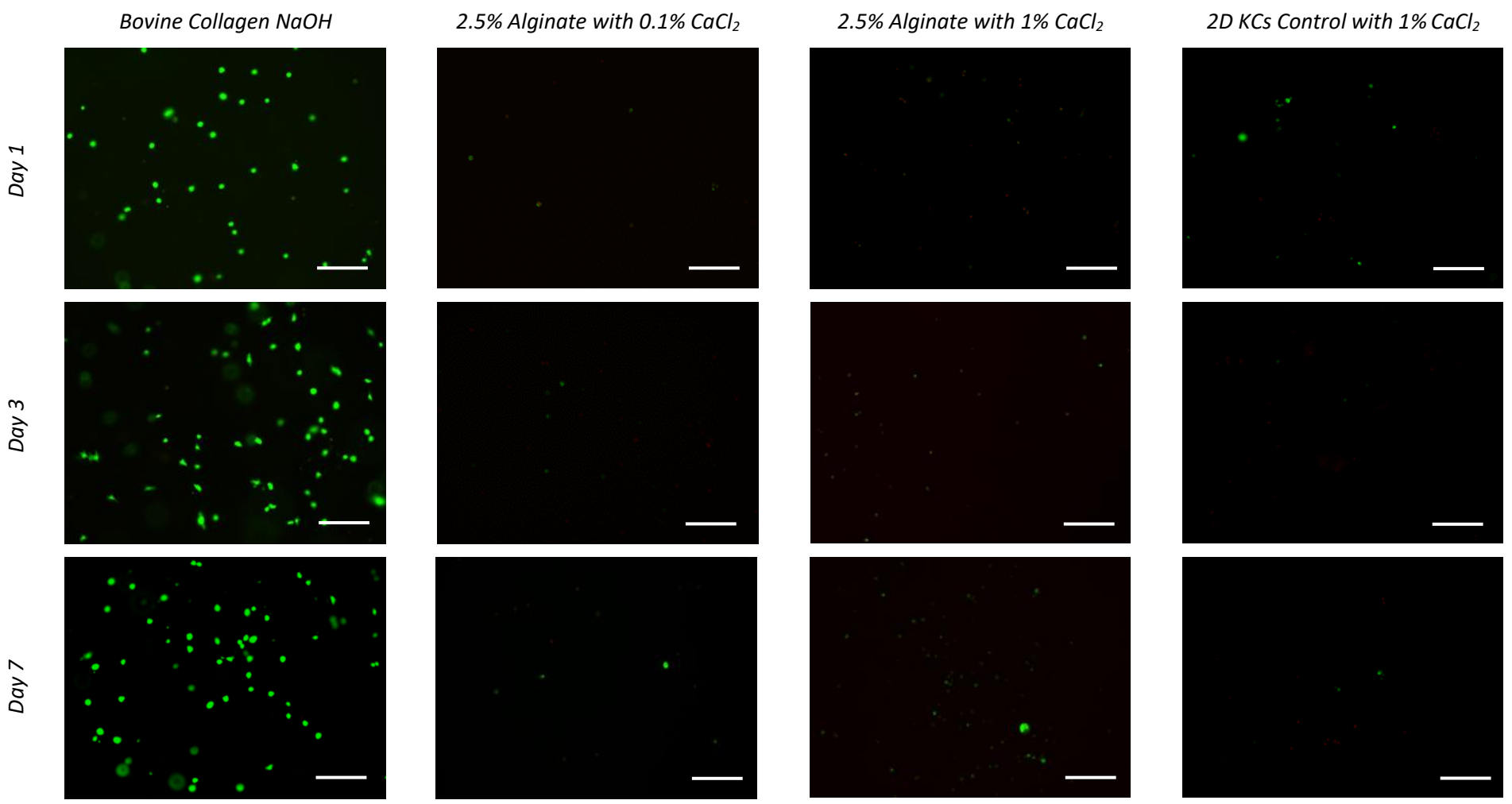

Figure 7. 2. Evaluation of the viability and distribution after 1, 3 and 7 days of keratinocytes encapsulated in collagen gels and alginate gels prepared with 0.1% and 1% CaCl2, respectively, in comparison to keratinocyte monolayers (KCs) incubated in medium containing 1% $CaCl_2$. Dead cells are represented in red and living cells in green. The scale bars correspond to 200 µm.

7.2.2. Keratinocyte Proliferation and Differentiation

Epidermal bioinks showed a different effect on keratinocyte proliferation and differentiation depending on their formulation. The expression of cytokeratin 14, involucrin and filaggrin by the encapsulated cells was assessed to determine the progressive changes in the proliferation, and the early and late differentiative state of keratinocytes, respectively. The expression of cytokeratin 14 could be observed from the first day on the control sample, and it was maintained over time, showing a signal reduction after 7 days (Fig. 7.3). At this point, involucrin started to be expressed by keratinocytes (Fig. 7.7). This differentiation marker could also be observed in contracted groups of keratinocytes at day 14, after incubating for 7 days in a cell medium containing a higher concentration of $CaCl_2$. Keratinocytes encapsulated in bovine collagen presented an initial high cytokeratin 14 expression, which was maintained over time as the number of keratinocytes increased (Fig. 7.4). On this occasion, none of the studied differentiation markers could be observed in the samples (Fig. 7.6-7.8).

The effect of fibrin-based bioinks on the formation of keratinocytes agglomeration was confirmed by cytokeratin 14 staining (Fig. 7.3). These cell groups maintained a high proliferative state on the first days and increased their size as the number of keratinocytes increased. The characteristics of keratinocyte agglomeration differed between samples depending on the fibrin concentration and the presence of other biocomponents. In the case of gels with higher fibrin concentrations, keratinocyte accumulation was observed from day 1, resulting in larger keratinocyte associations over time in comparison to the rest of fibrin-based samples. After 7 days, the filaggrin expression could be observed in the nucleus of the cell agglomerations formed in the fibrin gels (Fig. 7.5). The presence of filaggrin was directly related to the size of the keratinocyte groups, being higher in the gels with higher fibrin concentrations. These results contrasted with the absence of filaggrin at day 7 in the collagen and control samples (Fig. 7.5-7.6). An initial expression of involucrin could be seen at day 7 in the encapsulated keratinocytes in fibrin-based gels regardless their position (Fig. 7.7). Involucrin signal increased after 14 days, especially on those samples containing larger keratinocyte groups.

Keratinocytes encapsulated in alginate gels showed the expression of cytokeratin-14 from the first day, confirming the presence of proliferative cells (Fig. 7.4). The number of keratinocytes expressing this marker was significantly increased at day 7 in alginate gels crosslinked with 0.1% $CaCl_2$, but it was maintained in the gels prepared with higher calcium chloride

concentration. The expression of differentiative markers also differed between these samples. Keratinocytes embedded in alginate gels prepared with lower calcium chloride concentration did not express filaggrin or involucrin over time (Fig. 7.6-7.8). In contrast, alginate gels crosslinked with 1% $CaCl_2$, triggered a reduced expression of involucrin and a notable filaggrin signal in some encapsulated keratinocytes from day 7. Filaggrin markers were also observed at day 7 in keratinocyte control cultured with cell media with higher calcium chloride concentrations (Fig. 7.6). Compared to the keratinocyte cultured under normal conditions, the number of proliferative cells dramatically dropped when calcium levels increased (Fig. 7.3-7.4). Only a reduced number of keratinocytes maintained their proliferative state over time, resulting in small, isolated groups of cells after 7 days. In contrast to the cells encapsulated in alginate with 1% $CaCl_2$, these keratinocytes did not show the presence of involucrin, but they exhibited an early expression of filaggrin from day 3 (Fig. 7.6-7.8).

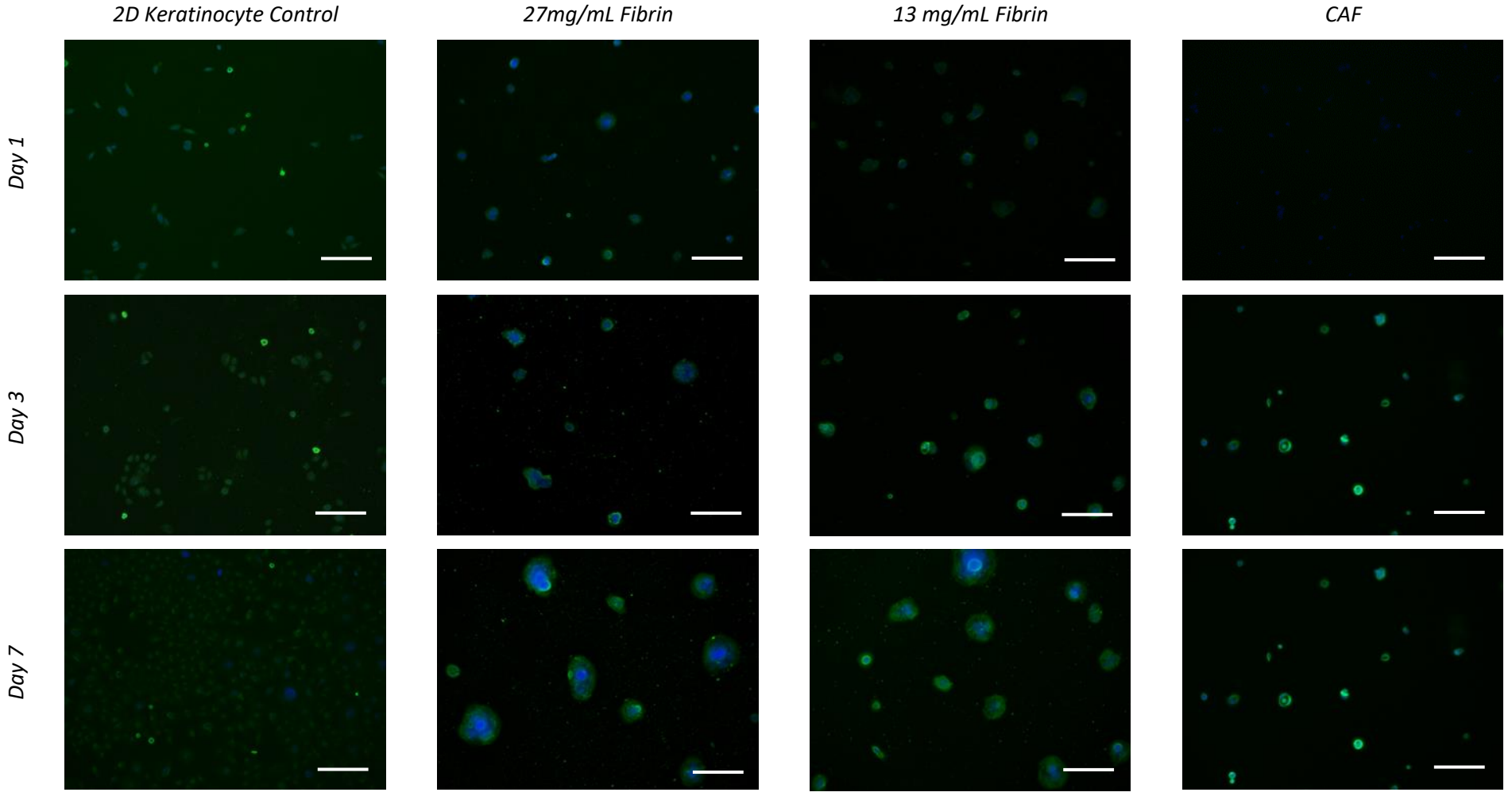

Figure 7. 3. Expression of cytokeratin 14 by keratinocytes encapsulated in fibrin-based gels in comparison to keratinocyte monolayers seeded on tissue culture-treated wells. The immunostaining was performed after incubating the cells for 1, 3 and 7 days, with cytokeratin 14 represented in green and cell nucleus is represented in blue. The scale bars correspond to 200 µm.

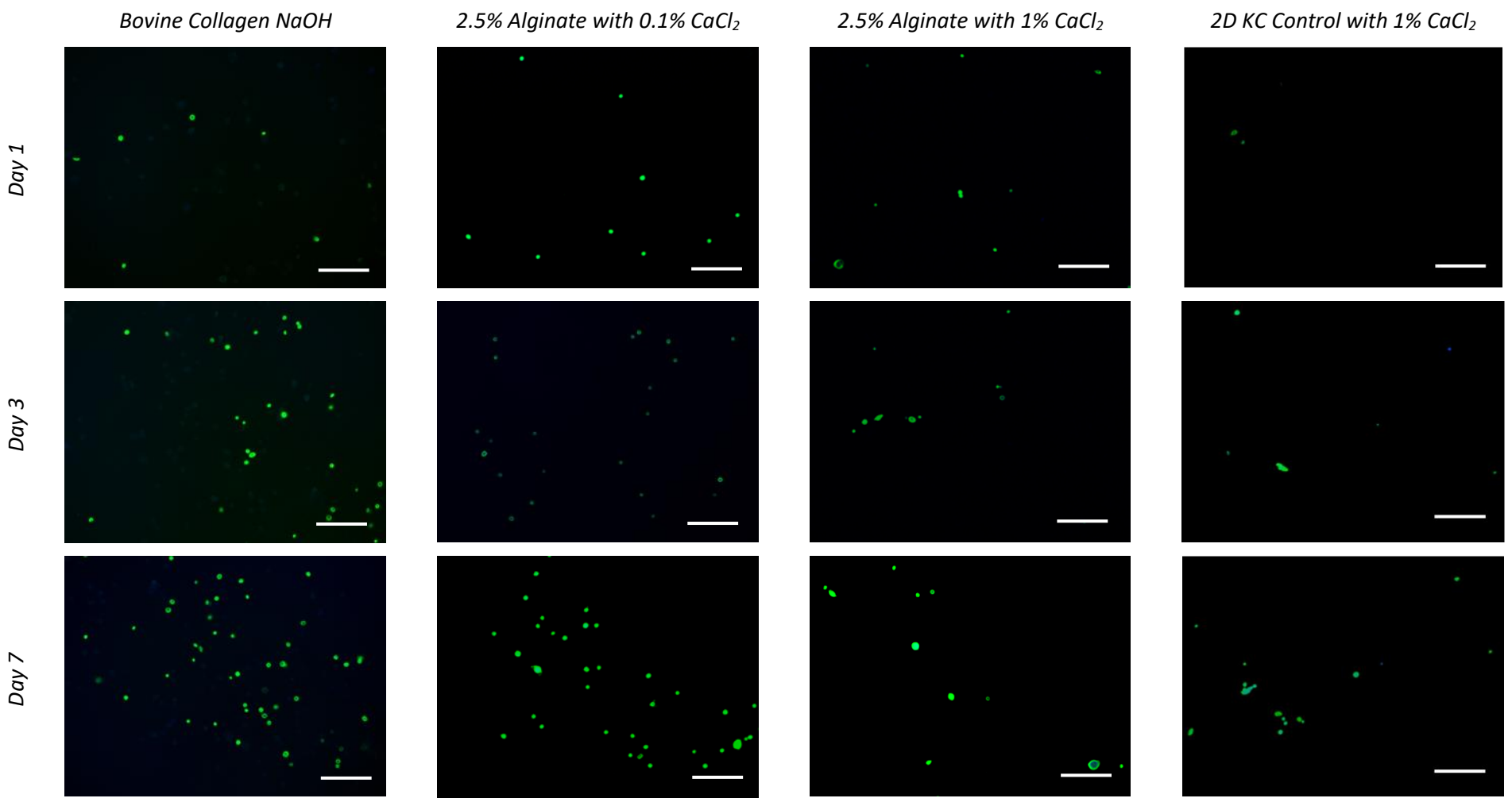

Figure 7. 4. Expression of cytokeratin 14 by keratinocytes encapsulated in collagen gels, alginate gels prepared with 0.1% and 1% CaCl2, respectively, in comparison to keratinocyte monolayers (KC) incubated in medium containing 1% $CaCl_2$. The immunostaining was performed after incubating the cells for 1, 3 and 7 days, with cytokeratin 14 represented in green and cell nucleus in blue. The scale bars correspond to 200 µm.

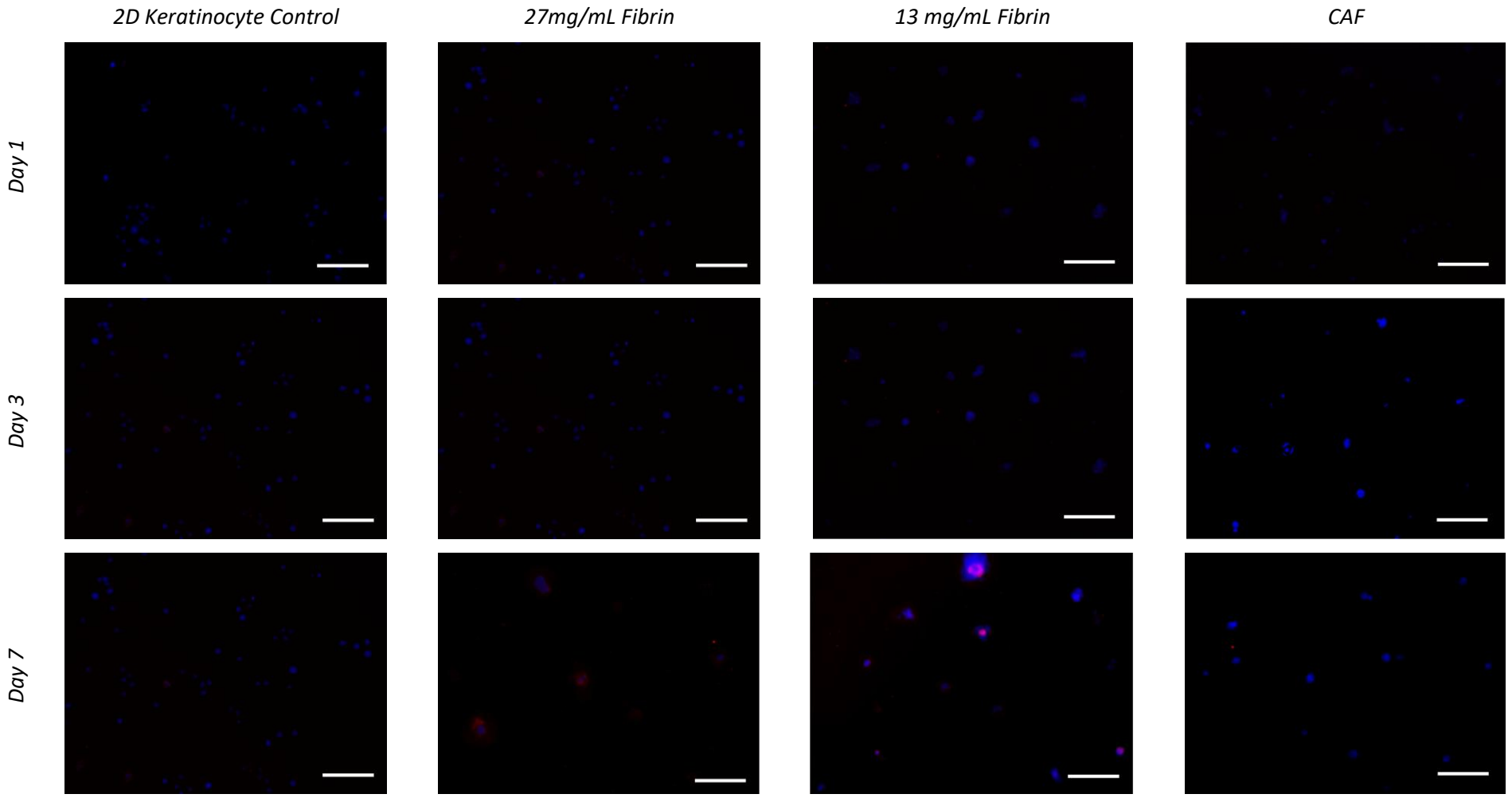

Figure 7. 5. Expression of filaggrin by keratinocytes encapsulated in fibrin-based gels in comparison to keratinocyte monolayers seeded in tissue culture-treated wells. The immunostaining was performed after incubating the cells for 1, 3 and 7 days, with filaggrin represented in red and cell nucleus in blue. The scale bars correspond to 200 µm.

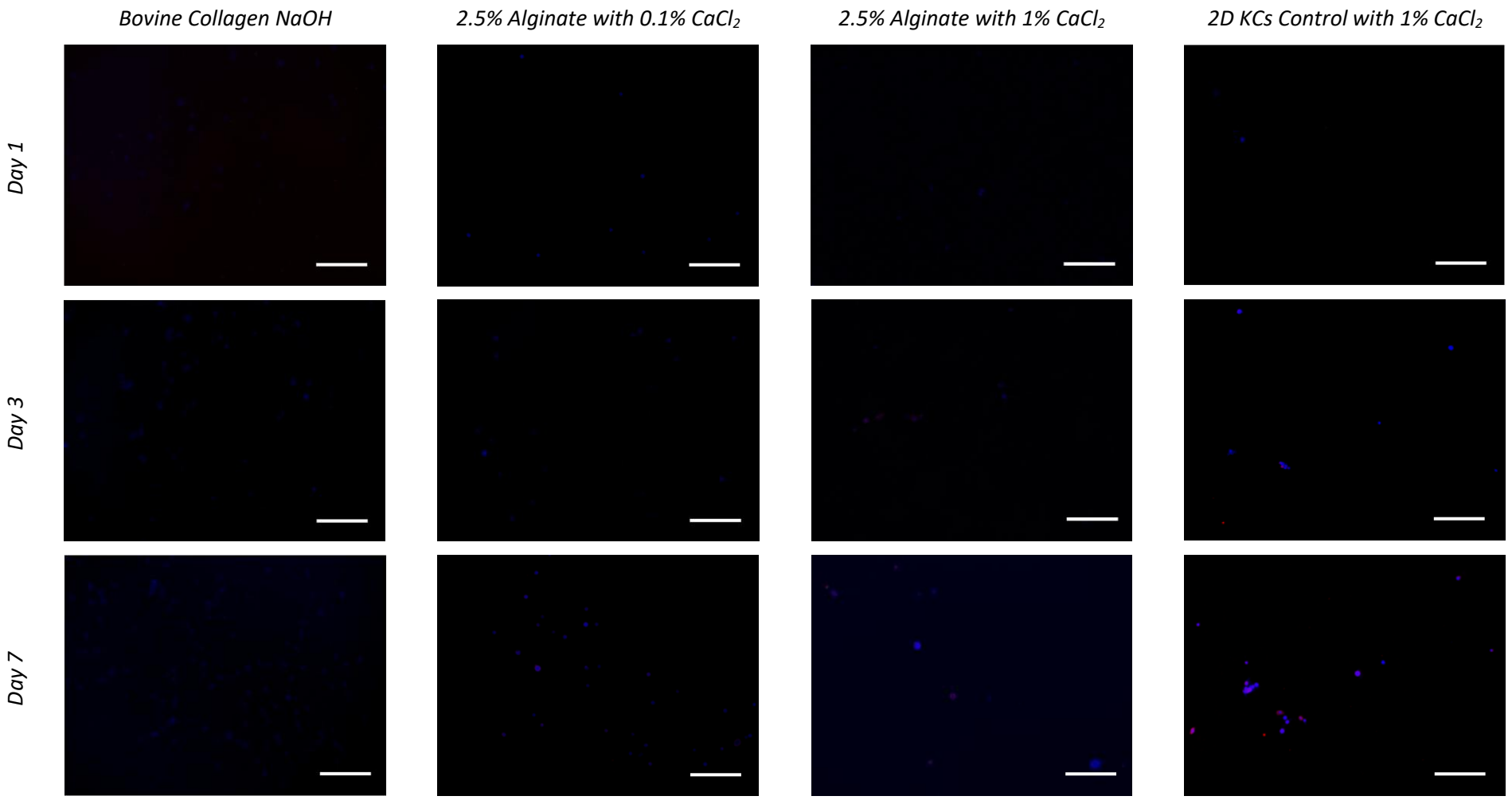

Figure 7. 6. Expression of filaggrin by keratinocytes encapsulated in collagen gels and alginate gels prepared with 0.1% and 1% $CaCl_2$, respectively, in comparison to keratinocyte monolayers (KC) incubated in medium containing 1% $CaCl_2$. The immunostaining was performed after incubating the cells for 1, 3 and 7 days, with filaggrin represented in red and cell nucleus in blue. The scale bars correspond to 200 µm.

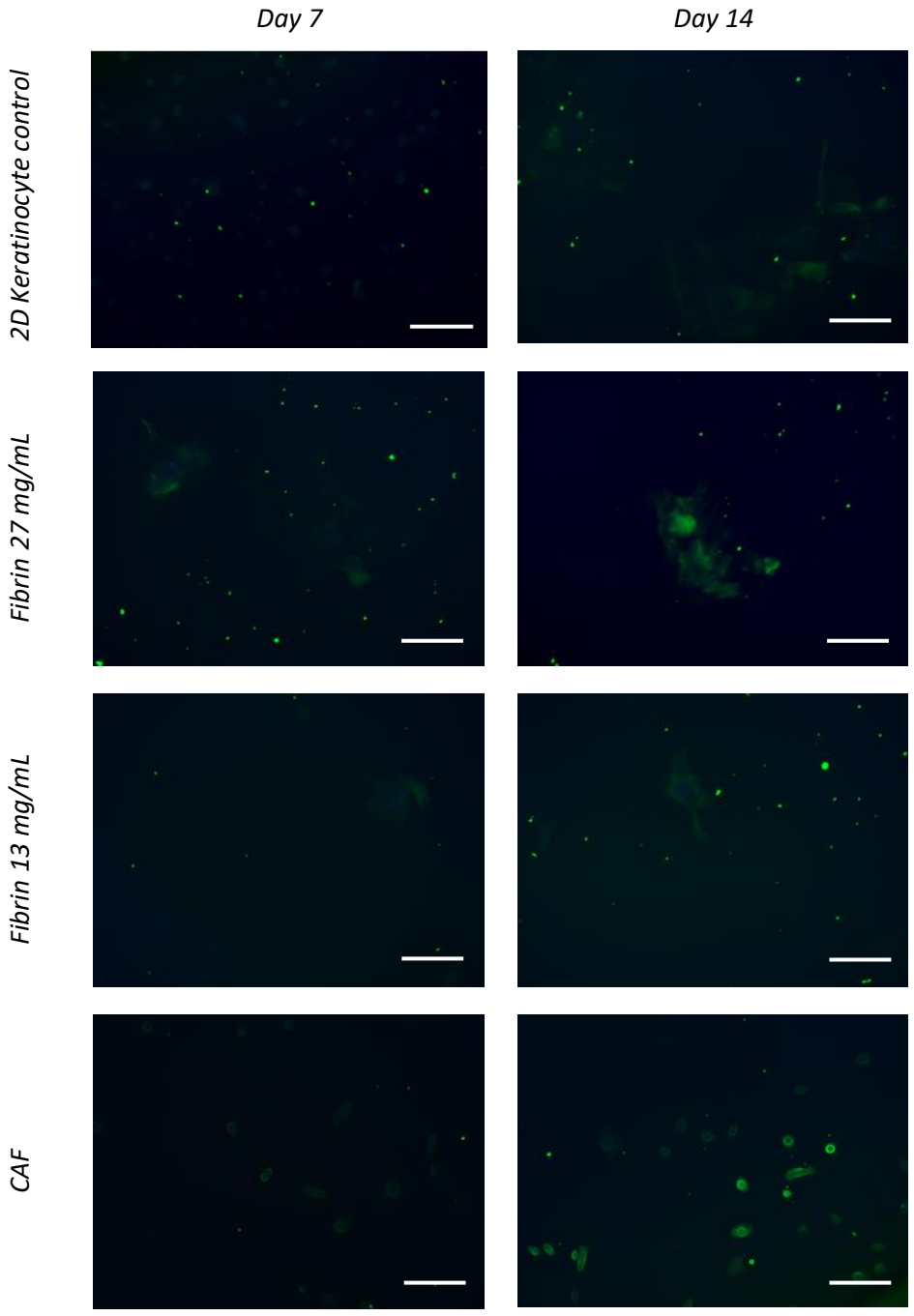

Figure 7. 7. Expression of involucrin by keratinocytes encapsulated in fibrin-based gels in comparison to keratinocyte monolayers seeded on tissue culture-treated wells. The immunostaining was performed after incubating the cells for 7 and 14 days, with involucrin represented in green and cell nucleus in blue. Scale bars correspond to 200 µm.

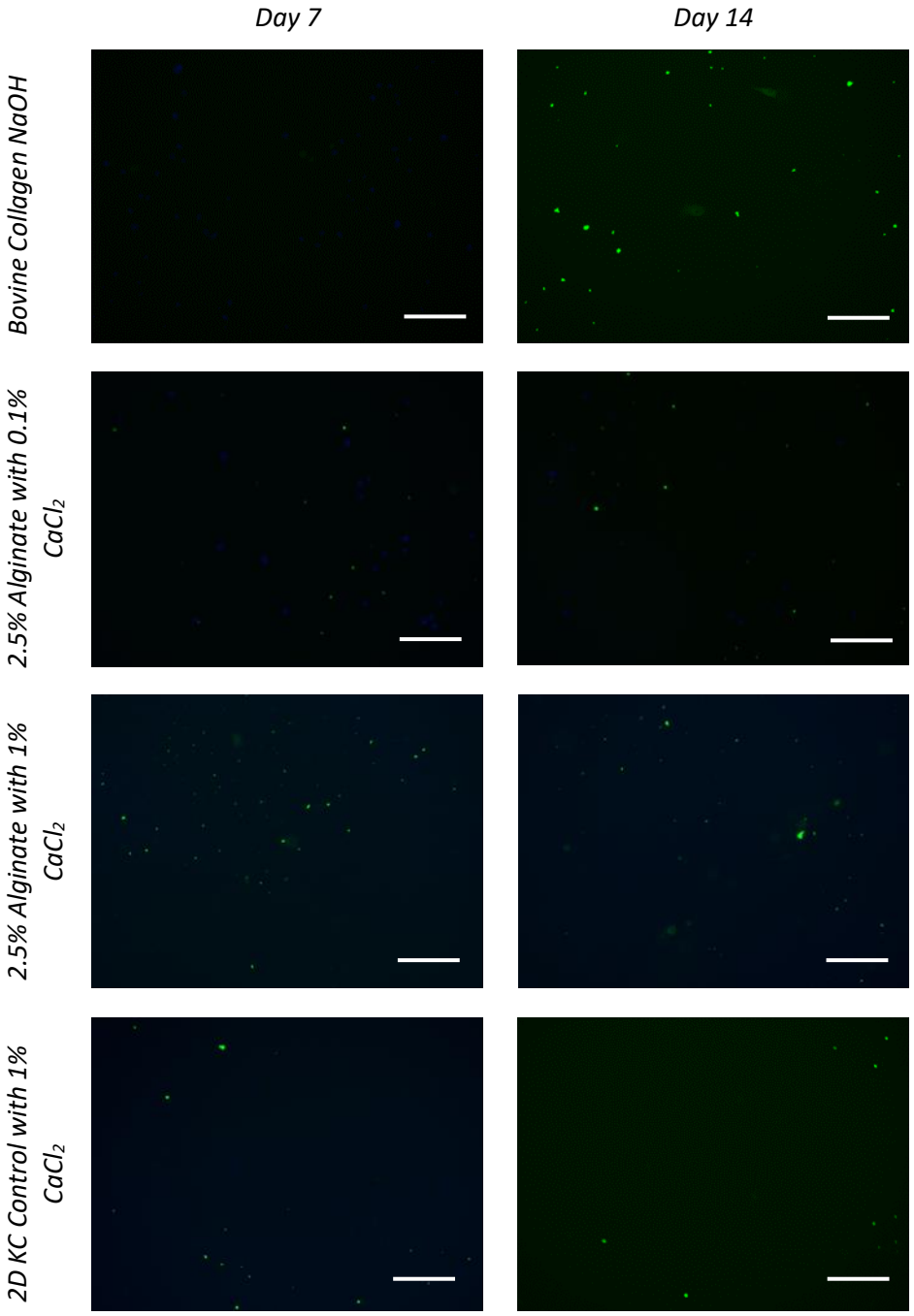

Figure 7. 8. Expression of involucrin by keratinocytes encapsulated in collagen gels, alginate gels prepared with 0.1% and 1% $CaCl_2$, respectively, in comparison to keratinocyte monolayers (KC) incubated in medium containing 1% $CaCl_2$. The immunostaining was performed after 7 and 14 days, with involucrin represented in green and cell nucleus in blue. Scale bars correspond to 200 µm.

7.3. Chapter Discussion

7.3.1. Effect of Epidermal Bioinks on Keratinocyte Viability and Distribution

The natural interaction of collagen type I with the keratinocytes in the epidermal basal layer could explain the good adaptation of keratinocytes to the collagen environment and their maintained viability over time (Pfisterer et al., 2021). Additionally, the homogenous distribution presented by keratinocytes through the collagen gels with the absence of cell sedimentation, suggests a quick adhesion and strong interaction of keratinocytes to the collagen samples. Using fibrin-based gels as encapsulating agents also resulted in high keratinocyte viability. The biocompatibility and adhesion in these samples could be explained by the direct natural contact between fibrin and keratinocytes when skin integrity is damaged (Heino, 2002). In contrast to the other samples, keratinocytes embedded in fibrin gels form cell aggregations from the first days. This cellular organization could be explained by the natural interaction between the fibrin matrix and keratinocytes during the wound-healing process. The presence of crosslinking points, observed in the SEM images of fibrin gels in section 6.2.3, could explain the agglomeration of keratinocytes in these areas. This phenomenon could represent a natural strategy to enhance keratinocyte proliferation by cell-contact signalling and accelerate skin reepithelization (Koivisto et al., 2014). By decreasing the fibrin concentration, the number of crosslinking points is reduced, and the size of the keratinocyte groups is decreased. Similarly, the combination of fibrin with collagen and alginate also results in the reduction of keratinocyte aggregations. The correlation between the characteristics of the fibrin matrix and the formation of keratinocyte aggregates suggests the possibility of controlling the keratinocyte distribution by modifying the formulation of fibrin gels.

In contrast to previous epidermal bioinks, the number of cells present in alginate gels was significantly lower. Only a slight increase in the keratinocyte number could be observed when a higher calcium chloride concentration was used to generate the alginate gels. This increment implies a faster crosslinking reaction, which could have affected the keratinocyte distribution. Despite the restricted quantity of live keratinocytes observed in the alginate samples, the low number of dead cells encapsulated in alginate complicates the explanation of the keratinocyte fate. The effect of calcium ions released from the alginate gels could be responsible for reducing keratinocyte viability and proliferation. By increasing the calcium chloride

concentration in the keratinocyte control, it could be seen a decrease in the keratinocyte number, which can be explained by the low adhesion of keratinocytes under the presence of calcium ions. In native skin, calcium gradients are the main factor in the regulation of keratinocyte differentiation. The extracellular calcium levels progressively increase from the stratum basale to the stratum granulosum, initiating the keratinocyte differentiation via a calcium receptor, ultimately triggering cell death (Bikle et al., 2014). Despite the feasibility of this hypothesis to explain the limited number of keratinocytes on the initial days, the slight increase in the cell viability over time and the absence of dead cells cannot be justified. Alternatively, the low porosity of alginate gels could be responsible for the limited penetration of the staining solution, and the subsequent restriction on the cellular labelling (Beghin et al., 2022; Ng et al., 2005). Due to the inability to conclude the state of encapsulated keratinocytes in alginate, it will be necessary to evaluate their expression of proliferative markers, such as cytokeratin 14, and differentiative markers, such as involucrin or filaggrin, before concluding the effect of alginate over the encapsulated keratinocytes.

7.3.2. Effect of Epidermal Bioinks on Keratinocyte Behaviour

Keratinocytes encapsulated in collagen presented a gradual increment in the number of cells over time. The high expression of cytokeratin 14 and the absence of differentiation markers in the first seven days resemble the behaviour of keratinocytes in direct contact with collagen type I in the basal epidermal layer. Previous studies have suggested a decrease in the mobility of keratinocytes seeded on collagen type I, compared to keratinocytes on tissue-cultured treated plastics, due to the limited stiffness of collagen type I (Guo et al., 1990; Kenny et al., 2018). Still, no notable differences in the mobility and distribution of keratinocytes were observed between the two-dimensional keratinocyte control and the cells encapsulated in collagen in figures 7.3 and 7.4. The performed studies in this chapter only provide an initial overview of the distribution and behaviour of embedded keratinocytes. Therefore, further studies will be required to conclude the significant differences between the samples. To compare the mobility and proliferation of encapsulated cells quantitatively, it will be necessary to consider the three-dimensional character of the samples in contrast to the two-dimensional keratinocyte controls, and the differences on the degradation rate of the epidermal bioinks. Preliminary studies showed a notable reduction on the volume of those epidermal models containing fibrin and collagen, compared to the ones containing alginate. However, further studies will be necessary to assess the role of keratinocytes on the degradation of these bioink components, and the long-term effect of the presence of these biomaterials on the keratinocyte functions. The generation of three-dimensional images for each sample can be considered as an option to delve into the precise location of encapsulated cells over time. Nonetheless, due to the small size of keratinocytes, the time required to obtain images with enough resolution was too elevated and hindered their incorporation in this study. In future work, the extraction of keratinocytes from the gels could be an alternative to quantify and compare their proliferation rate and expression of specific markers. An alternative to the previously described dsDNA quantification will be necessary to assess the keratinocyte proliferative rate, discerning the proliferative keratinocytes from those in their differentiative stages. For instance, the assessment of growth markers, such as Ki-67 and proliferating cell nuclear antigen (PCNA) by immunohistochemistry, have demonstrated to be a reliable method to quantify the keratinocyte proliferation in previous publications (Onuma et al., 2001).

The expression of cytokeratin-14 by keratinocytes embedded in fibrin-based gels confirmed the maintenance of their proliferative state from the first day, and their distribution in agglomerates as suggested by the previous live/dead staining. The proximity between the keratinocytes in these cell groups triggers the boost in their proliferation after 3 days resulting in significantly large cell agglomerates after 7 days. Despite this improvement, the high keratinocyte confluency in these located areas also promotes the appearance of differentiated keratinocytes in the nucleus of the cell aggregates. The exposition of the cells to higher calcium concentrations after 7 days results in a similar contraction and expression of involucrin in the cells embedded in fibrin gels and the keratinocyte control (Deyrieux & Wilson, 2007). The small size of these contracted cell groups hinders the evaluation of the real impact of the encapsulating agents on the epidermal stratification. In future studies, an increment in the keratinocyte densities will be required to evaluate the quality of the generated epidermal layers and their stability over time. As it was observed previously, the reduction in the fibrin concentration and the introduction of other biomaterials like collagen or alginate to the gels influence the keratinocyte distribution, reducing their accumulation, and consequently delaying their differentiation. The ability of fibrin-based gels to control the keratinocyte growth and location could be a potential advantage in the improvement of epidermal consistency, and it could help to accelerate the epidermal formation. By increasing the number of keratinocytes encapsulated in fibrin gels, it could be possible to create a uniform basal layer formed by adhered keratinocytes groups, which could trigger a controlled differentiation of keratinocytes.

Fibrin gels have already demonstrated their capacity to accelerate the epidermal regeneration in clinical applications (Heher et al., 2018). The advantages of fibrin on the wound healing have resulted in their incorporation as active ingredients in different commercial products (Clark, 2005). The spray or spreading of fibrin on the wound site promotes the quick sealing of the tissue, reducing the bleeding and potential infections (Currie et al., 2003). Additionally, the resulting fibrin matrix serves as provisional support for cell migration (Clark et al., 1982). Similar to the natural wound healing process, commercial products containing fibrin have demonstrated to enhance keratinocyte proliferation, migration and differentiation during skin reepithelization (Currie et al., 2001; ter Horst et al., 2018). Fibrin has also shown to promote their migration and improve keratinocyte growth *in vitro* (Geer et al., 2004; Krasna et al., 2005). The expression of specific growth factors, such as TGF-b1 and PDGF-BB, have been associated with the rise in keratinocyte proliferation in fibrin surfaces. The secretion of active forms of

these growth factors was especially higher in fibrin gels, compared to the values obtained by keratinocytes seeded in conventionally used tissue culture-treated plastic surfaces (Acevedo et al., 2010). Additionally, a decrease in keratinocyte differentiation after the keratinocyte encapsulation on fibrin in previous works (Alexaline et al., 2019), contrasting with the obtained results in this project.

Despite the number of studies investigating the influence of fibrin on keratinocyte behaviour, only the work performed by Gugerell *et al*. has demonstrated the impact of fibrin formulation on keratinocyte distribution (Gugerell et al., 2012). In their study, thrombin concentration was proved to decrease cell adhesion and proliferation, leading to keratinocyte apoptosis when thrombin reached concentrations higher than 820 IU/mL. Consequently, keratinocytes presented higher agglomeration at 4 IU/mL thrombin concentration, and the cell groups were reduced as the thrombin concentration rose to 505 IU/mL (Fig. 7.9). These images concur with the results obtained in this chapter. The crosslinking of fibrinogen with a thrombin concentration of 50 IU/mL in this chapter resulted in a similar keratinocyte adhesion and agglomeration after 24 hours to the one expected, considering the results from Gugerell *et al*. study.

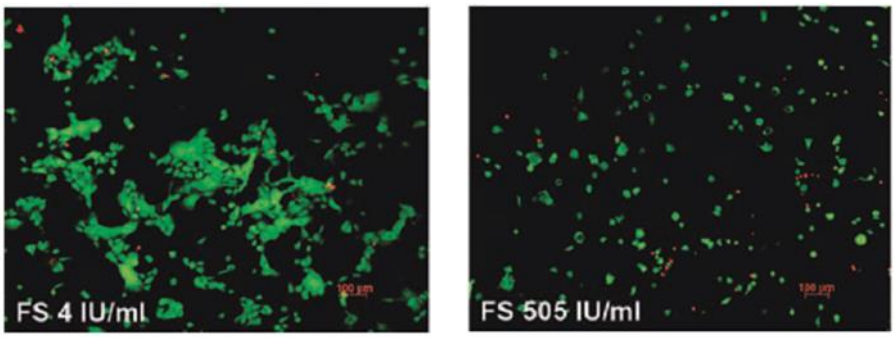

Figure 7. 9. Distribution after 24 hours of keratinocytes seeded on fibrin clots prepared with 4 IU/mL and 505 IU/mL of thrombin. Scale bars represent 100 µm. Image obtained from Gugerell et al. 2012.

The substrate stiffness has also evidenced to influence the keratinocyte behaviour in previous publications. Keratinocyte migration and proliferation have demonstrated to improve in stiffer surfaces, and by contrast, their differentiation rate has been proven to increase in softer materials (Wang et al., 2012). This behaviour could be explained by the similar process occurring in the wound site, when the keratinocyte proliferative state is triggered during the surge of tensional forces in the natural wound site (Kuehlmann et al., 2020; Barnes et al., 2018). The comparison between the stiffness of the selected fibrin and collagen-based epidermal

bioinks obtained in section 6.2.4 could help to elucidate the influence of the bioink mechanical properties on the keratinocyte behaviour. The increment by two in the stiffness values of 27 mg/mL fibrin gels compared to collagen gels could explain the higher number of keratinocytes in fibrin samples after 7 days. However, when comparing the proliferation of 13 mg/mL fibrin gels with collagen gels, the stiffness of these fibrin gels is lower than the collagen gels, despite showing a higher cell number after 7 days. Therefore, these results highlight the relevance of the biomaterial nature on the impact on keratinocyte behaviour.

The incorporation of keratinocytes into alginate hydrogels resulted in a reduction in the number of proliferative cells in comparison to fibrin and collagen-based gels. The increase in the number of cells expressing cytokeratin 14 over time verifies the ability of keratinocytes to proliferate. These results contradict the reduced number of live cells observed in the viability studies. The biocompatibility of alginate due to its natural origin has been widely explored in previous studies (Lee & Mooney, 2012). However, the absence of cell-binding groups for mammalian cells in this material could help to explain the obtained results (Neves et al., 2020). Keratinocytes require the presence of binding sites to adhere to the alginate surfaces. The inability of keratinocytes to attach to alginate could have resulted in their maintenance in a transitional state, reducing the effectivity of the live/dead staining solution. As keratinocytes were released from the gels, they could have recovered their natural morphology and their proliferative character. This process could explain the increment of the cytokeratin 14 over time in alginate samples. Nonetheless, the degradation of non-treated alginate gels is proved to be slow and unpredictable based on previous studies, hindering the estimation of the degradation rate and the controlled release of keratinocytes using alginate gels (Boontheekul et al., 2005). Only two previous investigations have explored the impact of encapsulating keratinocytes in alginate. In these studies, keratinocytes maintained a rounded morphology over time, suggesting the absence of cellular adhesion (Sai'Aan et al., 2016; Leong et al., 2017). Despite the lack of cell attachment to the alginate gels, the number of encapsulated cells increased over time, and the presence of released cells outside the gels could be observed after 8 days (Fig. 7.10). These results support the previous hypothesis about the behaviour of keratinocytes encapsulated in alginate gels.

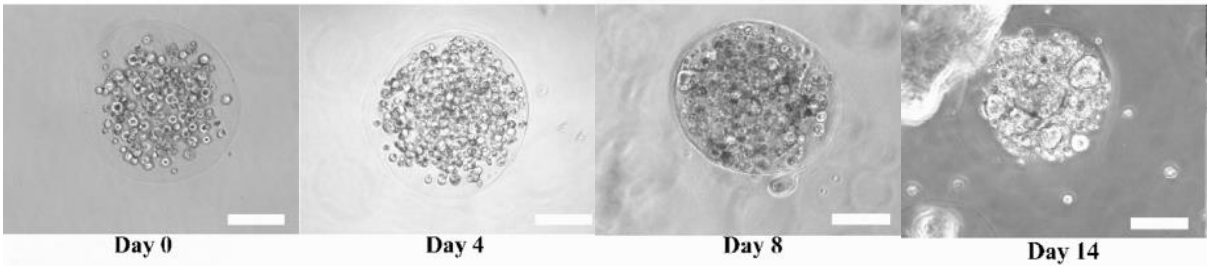

Figure 7. 10. Distribution of keratinocytes encapsulated in alginate gels after 0, 4, 8 and 14 days. Scale bar represents 100 µm. Image obtained from Leong et al. 2017.

The rise from 0.1% to 1% in the calcium chloride concentration used to prepare alginate gels has also shown to influence the keratinocyte behaviour. The use of alginate gels prepared with 1% $CaCl_2$ results in a lower expression of cytokeratin-14 and the expression of filaggrin after 7 days, like in the case of keratinocytes incubated with medium containing 1% $CaCl_2$. The ability of keratinocytes encapsulated in alginate to differentiate could also be observed on day 14 in the study performed by Leong *et al.* (Fig. 7.10). In previous works, the use of alginate as support material has demonstrated to decrease the proliferation of keratinocytes, inhibiting their migration and inducing their differentiation (Doyle et al., 1996; Stenvik et al., 2012). According to these studies, most of these cell behaviours are mediated by the calcium ion release in exchange for sodium ions in the cell media.

Alginate has been extensively used to encapsulate keratinocytes during the healing of chronic wounds (ter Horst et al., 2018; Thomas, 2013; Hampton, 2004). Nonetheless, the obtained results contradict the suitability of alginate as graft components and cannot explain the mechanism of action behind their healing properties. The specific environment present in the wound site could be responsible for the benefits of alginate for wound healing. The composition of the wound environment and the surrounding cells could help to accelerate the degradation of alginate and the release of encapsulated keratinocytes (Aderibigbe & Buyana, 2018). Additionally, the control liberation of calcium ions from the alginate gels could also help to improve the uniformity of the keratinocyte differentiation and the overall quality of the new epidermal layer. To determine the real effect of alginate bioinks on the keratinocyte behaviour, it will be essential to incorporate them into the manufacturing of skin models. This step will help to understand the degradation of alginate and the capacity of released keratinocytes to produce a correct epidermal stratification.

7.3.3. Implications of Keratinocyte Encapsulation

This study has demonstrated the advantages of keratinocyte encapsulation on the control over the keratinocyte distribution and the importance of bioink formulation on the control over the keratinocyte behaviour. The selection of biocomponents present in native skin, such as collagen and fibrin as encapsulating agents, has proved to promote a uniform keratinocytes distribution and ensure a high proliferative rate. Moreover, the encapsulation of keratinocytes in fibrin-based gels has demonstrated to originate a consistent number of keratinocyte aggregates. The close interaction between cells in the generated groups entails an improvement in their proliferative rate and a higher control over their differentiation. The properties of these keratinocyte associations can be customized by modifying the fibrin concentration or the integration of alginate and collagen. The incorporation of additional natural components, such as collagen type IV or heparin, could be explored in future works to modulate the adherence, migration and growth of encapsulated keratinocytes (Wang et al., 2019b; Harvima et al., 2004).

Despite the advantages of keratinocyte encapsulation demonstrated in this chapter, it will be necessary to incorporate the developed epidermal bioinks in the manufacturing of skin models to determine their real implications over the complete epidermal formation. The correct interaction of keratinocytes with the dermal components will be fundamental to ensure the skin integrity. Additionally, it will be essential to assess the capacity of encapsulated keratinocytes to properly differentiate after their exposition to air-liquid interface. The interaction of the keratinocytes to the air interface is essential to promote pro-filaggrin synthesis and the correct formation of the epidermal granular layer, which is restricted under immersed conditions (Fatimah et al., 2013; Bernstam et al., 1986). The permeability of the gels to the calcium gradients and the study of the degradation of epidermal bioinks will be a critical factor at this stage.

CHAPTER 8. DEVELOPMENT OF SKIN MODELS

8.1. Introduction

The reproduction of a reliable epidermal structure is one of the most fundamental criteria for the validation of *in vitro* skin models. The quality of the final epidermal layer is influenced by different factors, including the initial keratinocyte distribution or the interaction between keratinocytes and fibroblasts. For that reason, this chapter explores the impact of introducing the diverse dermal and epidermal bioinks studied in previous chapters, along with the ReJI process, on the manufacturing of skin models. The quality of the epidermal stratification in the resulting skin models was selected as the first criteria to determine the suitability of each dermal and epidermal bioink for the production of skin models. Initially, the protocols followed for manufacturing skin models were optimised by evaluating the effect of seeding different keratinocyte densities on the quality of skin models. The progressive proliferation, differentiation and distribution of keratinocytes in the skin models were assessed to determine the best culture conditions. Besides, the presence of keratinocyte markers associated with the different epidermal sublayers was evaluated to ensure the correct epidermal stratification and, ultimately, the formation of a cornified layer.

8.2. Optimisation of Keratinocyte Densities on Skin Models

8.2.1. Haematoxylin and Eosin Staining of Skin Models

The skin equivalents were optimised by initially assessing the best cell density to generate a correct epidermal stratification. As a proof of concept, skin models were produced by manually seeding 100,000; 250,000 and 500,000 keratinocytes on top of a dermal layer comprised by fibroblasts encapsulated in telo-bovine collagen neutralized with NaOH. The staining of the skin sections with haematoxylin and eosin confirmed the presence of a homogeneous keratinocyte monolayer on top of the dermis after culturing the models for 7 days under immersed conditions (Fig. 8.1). As the number of keratinocytes was augmented from 100,000 to 500,000 keratinocytes per model, the confluency of keratinocytes increased.

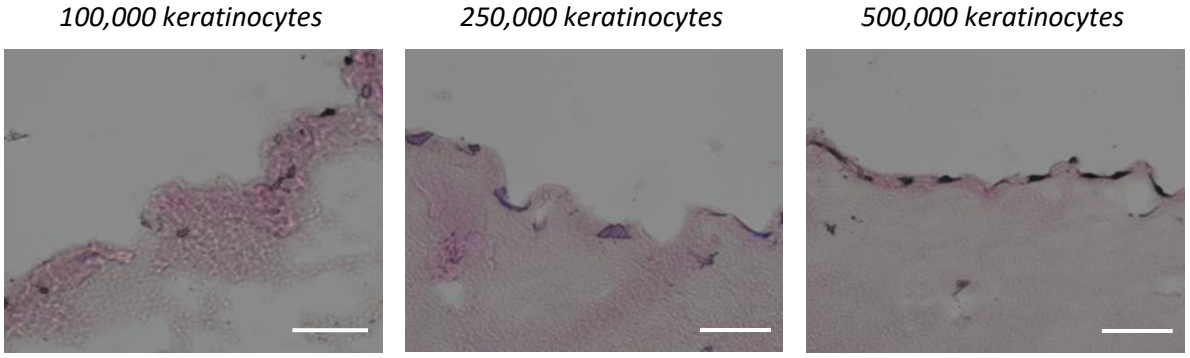

Figure 8. 1. Hematoxylin and eosin staining of skin models produced with 100,000; 250,000 and 500,000 keratinocytes per model, respectively, seeded on top of a dermal layer comprised by fibroblasts encapsulated in telo-bovine collagen neutralized with NaOH. Images were taken after incubating 7 days the skin models under immersed conditions Scale bars correspond to 100 µm.

The further evaluation of these skin equivalents after exposing them to 7 and 14 days of air-liquid interface (ALI) revealed a significant difference in the epidermal thickness depending on the selected keratinocyte density (Fig. 8.2). Skin models generated after seeding 100,000 keratinocytes presented an epidermal layer with two differentiated keratinocyte morphologies, especially after exposing them to 14 days of air-liquid interface. By increasing the keratinocyte density, the thickness of the differentiated epidermal layers was enlarged. Only in those models produced with 500,000 keratinocytes, an outer epidermal layer with an aspect resembling the cornified epidermal layers could be observed after exposing them for 14 days to the air-liquid interface.

Despite the presence of cells with rounded morphology in the bottom stratum similar to the basal keratinocytes and more compacted keratinocytes on the upper layers, the shape and

distribution of keratinocytes in these models did not resemble the ones observed in the different epidermal sub-layers from native human skin (Fig. 8.2). The generated epidermal layers showed some inconsistencies through the skin models, with the absence or detachment of the epidermis in some regions.

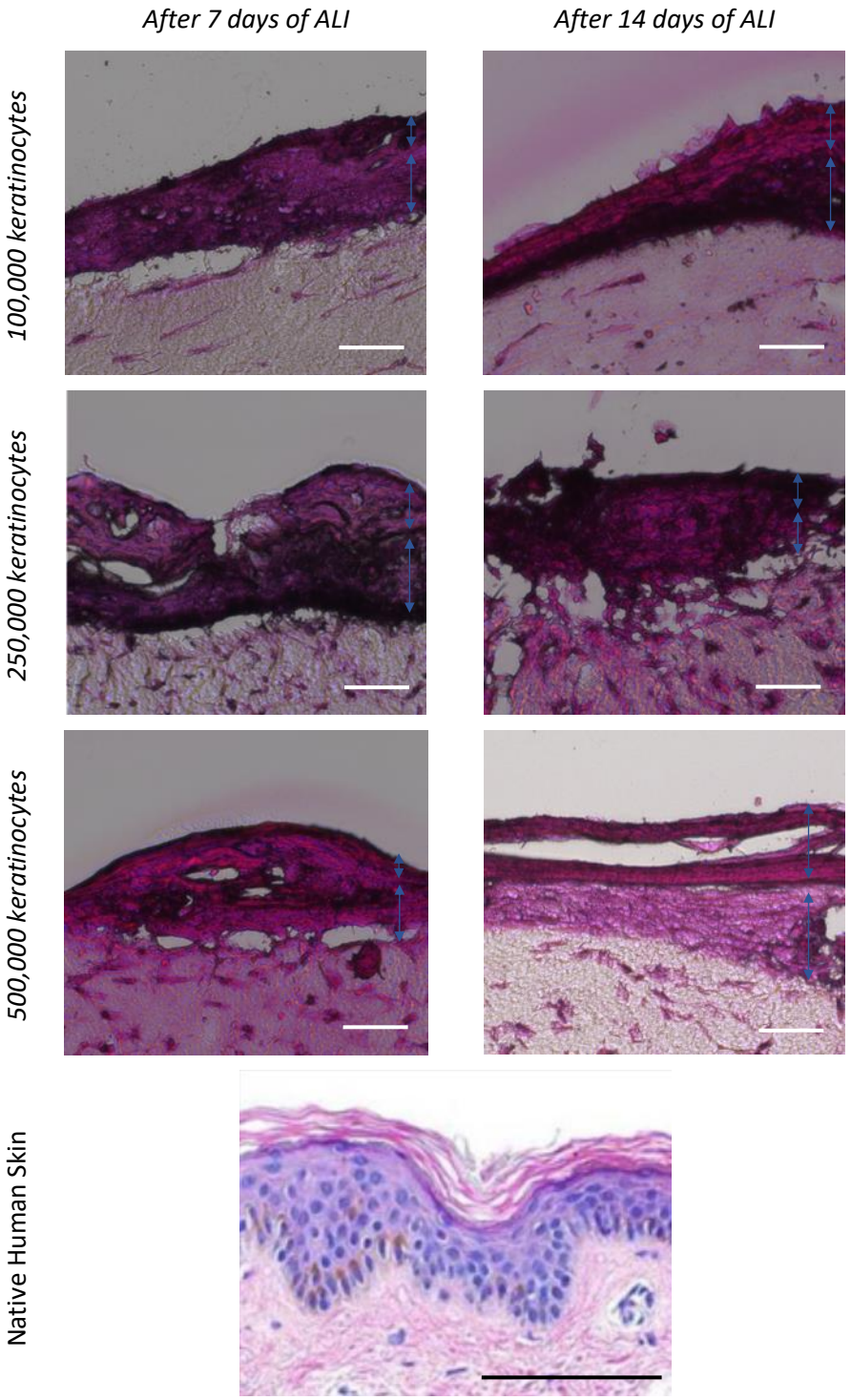

Figure 8. 2. Hematoxylin and eosin staining of skin models produced with 100,000; 250,000 and 500,000 keratinocytes per model seeded on top of a dermal layer comprised by fibroblasts encapsulated in telo-bovine collagen neutralized with NaOH. Images were taken after incubating 7 days the skin models under immersed conditions, and subsequently exposing the models for 7 and 14 days to the air-liquid interface, respectively. Blue arrows mark the different regions observed in the epidermis. Hematoxylin and eosin staining of human skin from a 25-year-old Caucasian donor, obtained from Roger et al. 2019, was selected as the control image. Scale bars correspond to 100 µm.

8.2.2. Immunohistochemistry of Skin Models

The immunostaining of the models confirmed the presence of differentiated epidermal stratums in all skin equivalents regardless of the selected keratinocyte densities. An innermost layer of proliferative keratinocytes expressing cytokeratin 14 could be observed in all samples after 7 and 14 days of exposing them to ALI (Fig. 8.3-8.4). The thickness of this basal layer showed a slight variation between the model, with an enhanced thickness in the models prepared with a higher number of keratinocytes. The involucrin expression could be observed in the areas above the layer containing proliferative keratinocytes, confirming the presence of the *stratum granulosum* in the epidermis. This differentiative maker showed a varying signal depending on the keratinocyte densities, with a higher presence in those models containing lower cell densities (Fig. 8.3-8.4). The complete differentiation of keratinocytes could be confirmed by the expression of filaggrin in all models regardless the initial keratinocyte density. Filaggrin marker could be observed in the outermost epidermal layers, suggesting the presence of the *stratum corneum* (Fig. 8.3-8.4). However, the thickness and arrangement of the stained epidermal layers differed from those found in the native human skin. In some areas, the unforeseen expression of cytokeratin-14 could be observed in some keratinocytes present on top of areas stained by filaggrin.

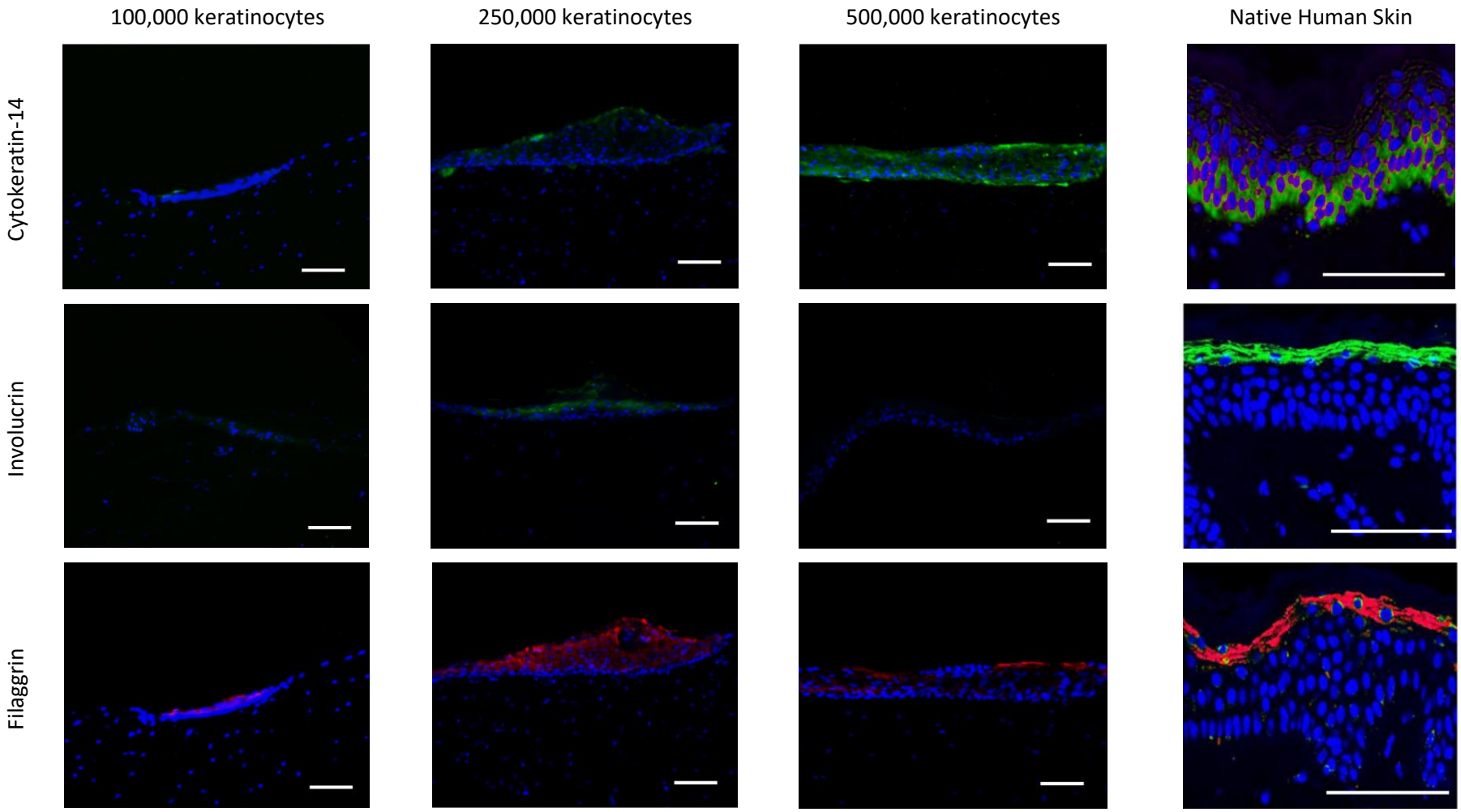

Figure 8. 3. Immunofluorescence staining of models produced with 100,000; 250,000 and 500,000 keratinocytes per model seeded on top of a dermal layer comprised by fibroblasts encapsulated in telo-bovine collagen neutralized with NaOH. Cytokeratin-14 present in the stratum basale and involucrin characteristics of the stratum granulosum are represented in green, whereas filaggrin characteristic of the stratum corneum is represented in red and cell nucleus stained with DAPI is shown in blue. Images were taken after incubating 7 days the skin models under immersed conditions, and subsequently exposing the models for 7 days to the air-liquid interface. Immunostained human skin sections from a 25-year-old Caucasian donor, obtained from Roger et al. 2019, were selected as control images. Scale bars correspond to 100 µm.

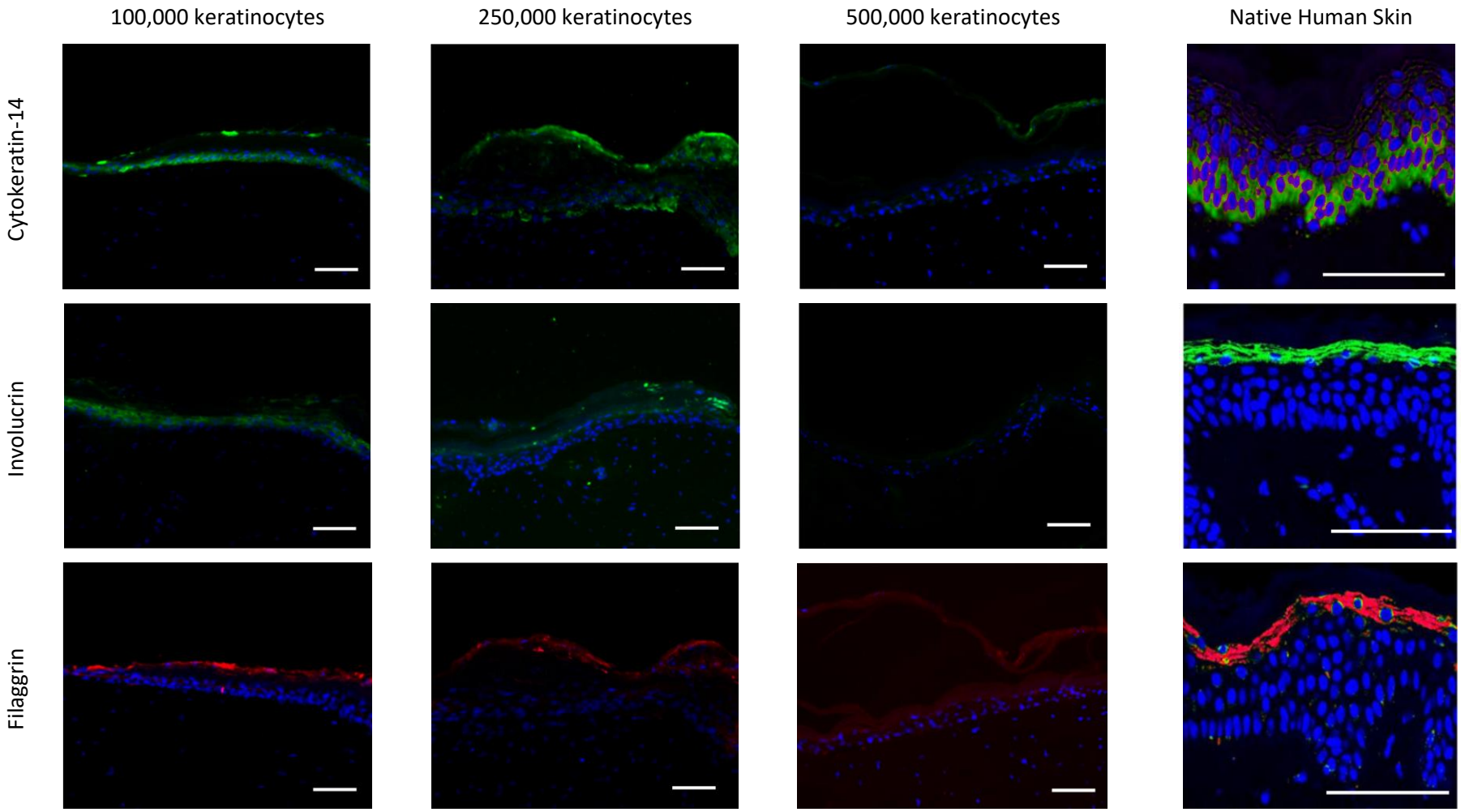

Figure 8. 4. Immunofluorescence staining of models produced with 100,000; 250,000 and 500,000 keratinocytes per model seeded on top of a dermal layer comprised by fibroblasts encapsulated in telo-bovine collagen neutralized with NaOH. Cytokeratin-14 present in the stratum basale and involucrin characteristics of the stratum granulosum are represented in green, whereas filaggrin characteristic of the stratum corneum is represented in red and cell nucleus stained with DAPI is shown in blue. Images were taken after incubating 7 days the skin models under immersed conditions, and subsequently exposing the models for 14 days to the air-liquid interface. Immunostained human skin sections from a 25-year-old Caucasian donor, obtained from Roger et al. 2019, were selected as control images. Scale bars correspond to 100 µm.

8.3. Effect of Dermal Bioinks on Skin Models

8.3.1. Haematoxylin and Eosin Staining of Skin Models

The impact of the dermal composition on the epidermal stratification was studied by first assessing the use of collagen from different animal sources. However, regardless the selected dermal bioinks, an uneven keratinocyte arrangement was obtained in all samples (Fig. 8.5). Haematoxylin and eosin staining of skin cryosections showed the presence of thick epidermal layers after exposing the models for only 7 days to the air-liquid interface (ALI).

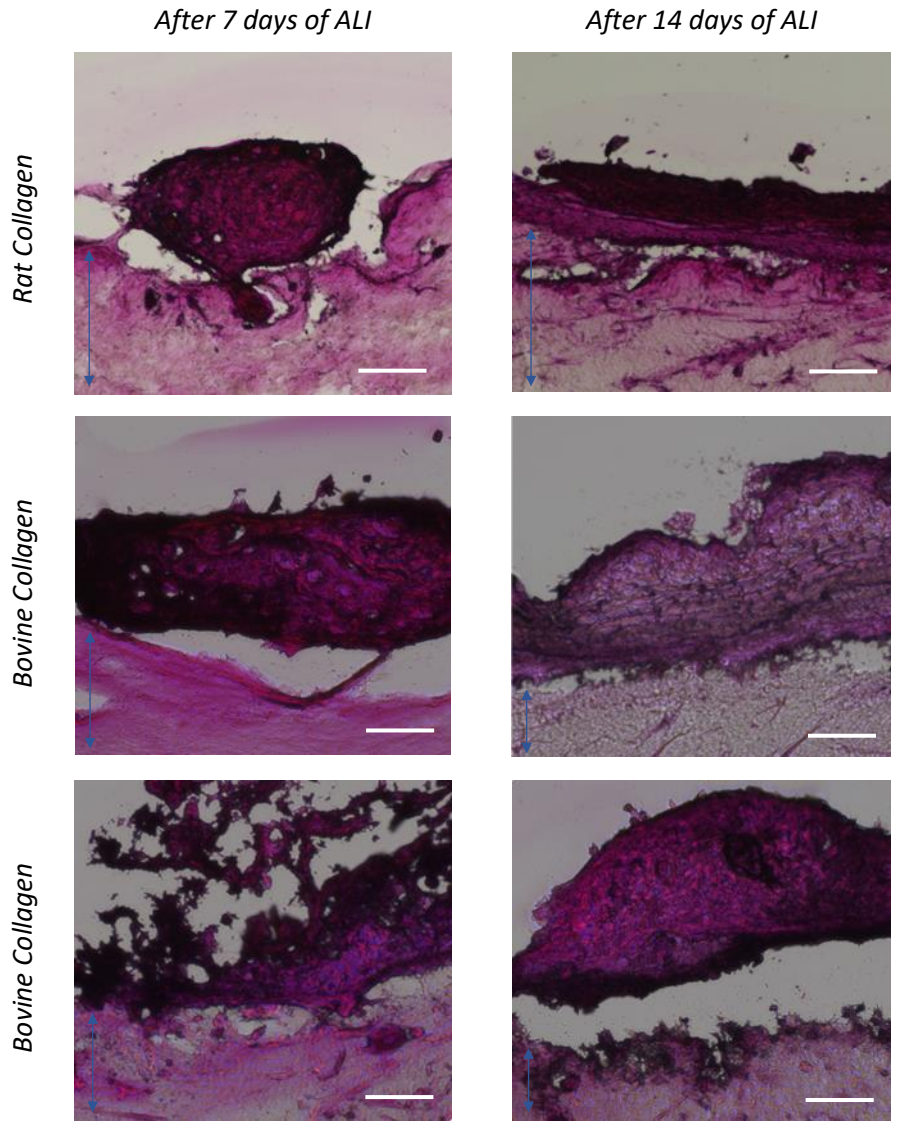

Figure 8. 5. Hematoxylin and eosin staining after the cryosections of skin models produced with rat, bovine and atelo-bovine collagen type I neutralised with NaOH as dermal matrix. Images were taken after incubating 7 days the skin models under immersed conditions, and subsequently exposing the models for 7 and 14 days to the air-liquid interface, respectively. Blue arrows mark the dermal layer. Scale bars correspond to 100 µm.

In most areas, these keratinocyte layers presented a low attachment to the dermis. The presence of two differentiated stratums could be denoted after 14 days of ALI in some epidermal regions (Fig. 8.5). Still, it was not possible to find a defined arrangement of keratinocytes. Only in the case of skin models produced with rat collagen type I, a slight improvement in the organisation and consistency on the epidermal layers was observed after 14 days of ALI.

To discard the effect of the sectioning process on the quality of the epidermal layers and their adhesion to the dermis, skin models were embedded in paraffin before proceeding to their sectioning (Fig. 8.6). Despite the lower impact of these preservation process on the skin structure and the production of thinner sections, epidermal layers also showed a significant detachment and inconsistent structural organisation through the skin models.

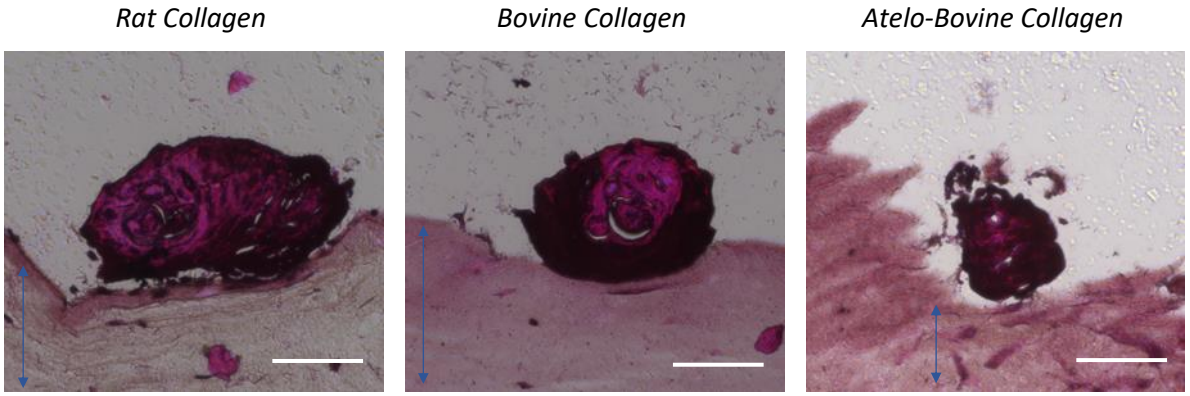

Figure 8. 6. Hematoxylin and eosin staining from the sections of paraffin-embedded skin models produced with rat, bovine and atelo-bovine collagen type I neutralised with NaOH as dermal matrix. Images were taken after incubating 7 days the skin models under immersed conditions, and subsequently exposing the models for 14 days to the air-liquid interface, respectively. Blue arrows mark the dermal region. Scale bars correspond to 100 µm.

8.3.2. Immunohistochemistry of Skin Models

The comparison between the skin models after 7 days of ALI underlined the variation in the epidermal formation depending on the selected collagen type I as dermal layer (Fig. 8.7). The use of rat collagen type I resulted in more uniform epidermal layers, with well-defined proliferative and differentiated keratinocyte layers. This epidermal consistency differed from the results obtained with telo-bovine collagen. As it was mentioned before, these models present epidermal layers with limited reproducibility. The use of atelo-bovine collagen showed a lower adhesion of keratinocytes and the formation of keratinocyte groups with non-defined organisation.

The further exposition of these models to the air-liquid interface for seven additional days implied the formation of thick filaggrin layers, suggesting an excessive cornification of the epidermis in all samples (Fig. 8.8). As a result, the epidermal homogeneity was reduced in the skin equivalents regardless the dermal bioink. In the case of the models produced with atelo-bovine collagen, the adhesion between the epidermal and dermal layer was still limited. In all samples, the maintenance of the proliferative character of keratinocytes was confirmed by the presence of cytokeratin-14 in all samples. However, the expression of involucrin in these models was reduced compared to the models after 7 days of ALI. The unpredicted presence of proliferative keratinocytes expressing cytokeratin-14 on the outermost epidermal layers was observed in all models, but especially in the skin models prepared with telo-bovine collagen. These results suggest the disorganized structure and uneven differentiation of the obtained epidermis.

The images of the skin models shown in this section correspond to some of the most representative results obtained using different dermal bioinks. In most samples, the lack of adhesion between the epidermal layer and the dermis did not allow to conclude the impact of the dermal components on the skin properties. Similarly, the implications of incorporating the ReJI system on the production of skin models could not be evaluated.

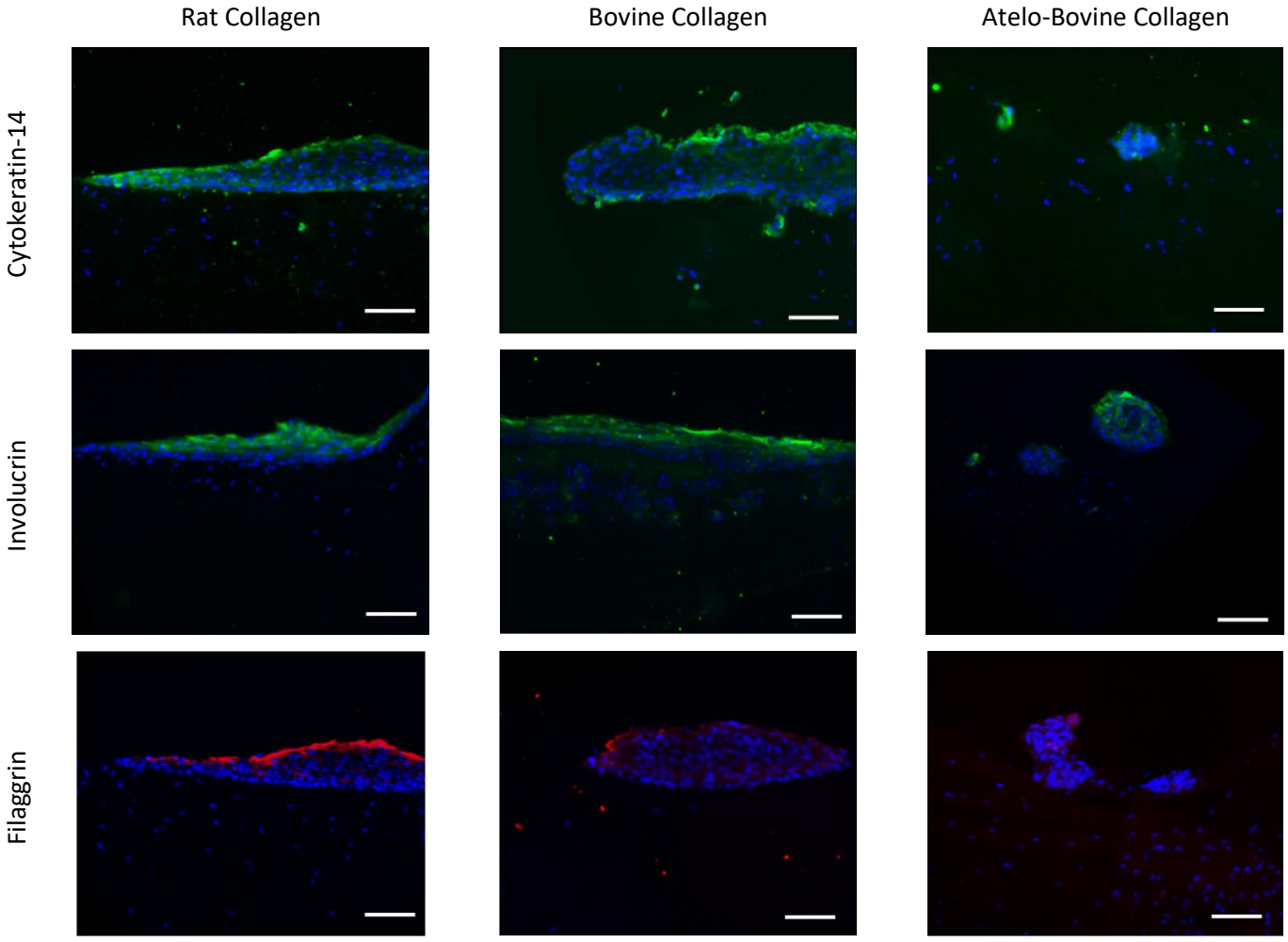

Figure 8. 7. Immunofluorescence staining of models produced with rat, bovine and atelo-bovine collagen type I neutralised with NaOH as dermal matrix. Cytokeratin-14 present in the stratum basale and involucrin characteristics of the stratum granulosum are represented in green, whereas filaggrin characteristic of the stratum corneum is represented in red and cell nucleus stained with DAPI is represented in blue. Images were taken after incubating 7 days the skin models under immersed conditions, and subsequently exposing the models for 7 days to the air-liquid interface. Scale bars correspond to 100 µm.

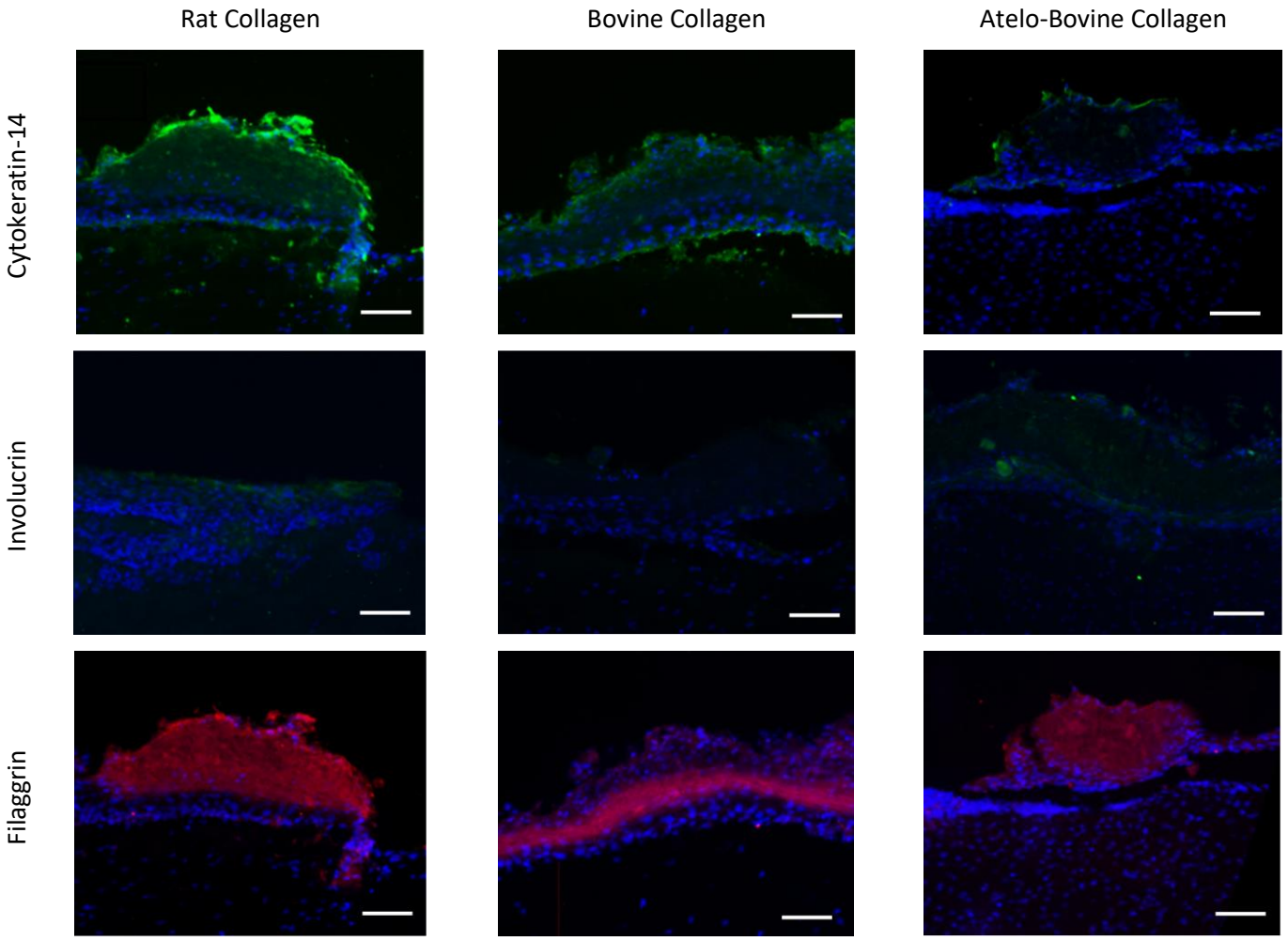

Figure 8. 8. Immunofluorescence staining of models produced with rat, bovine and atelo-bovine collagen type I neutralised with NaOH as dermal matrix. Cytokeratin-14 present in the stratum basale and involucrin characteristics of the stratum granulosum are represented in green, whereas filaggrin characteristic of the stratum corneum is represented in red and cell nucleus stained with DAPI is represented in blue. Images were taken after incubating 7 days the skin models under immersed conditions, and subsequently exposing the models for 14 days to air-liquid interface. Scale bars correspond to 100 µm.

8.4. Effect of Epidermal Bioinks on Skin Models

8.4.1. Haematoxylin and Eosin Staining of Skin Models

The encapsulation of keratinocytes improved the homogeneity of the keratinocyte distribution across the skin models based on the haematoxylin and eosin staining (Fig. 8.9). The use of collagen and fibrin-based epidermal bioinks resulted in the creation of thin compacted epidermal layers, with a more uniform and consistent distribution across the skin model than in previous models. Using alginate as encapsulating agent showed the formation of isolated keratinocyte groups. The size of these keratinocyte aggregates was correlated to the concentration of calcium used to generate the alginate gels. In the case of alginate containing a lower calcium chloride concentration, the keratinocyte formed larger cell spheres.

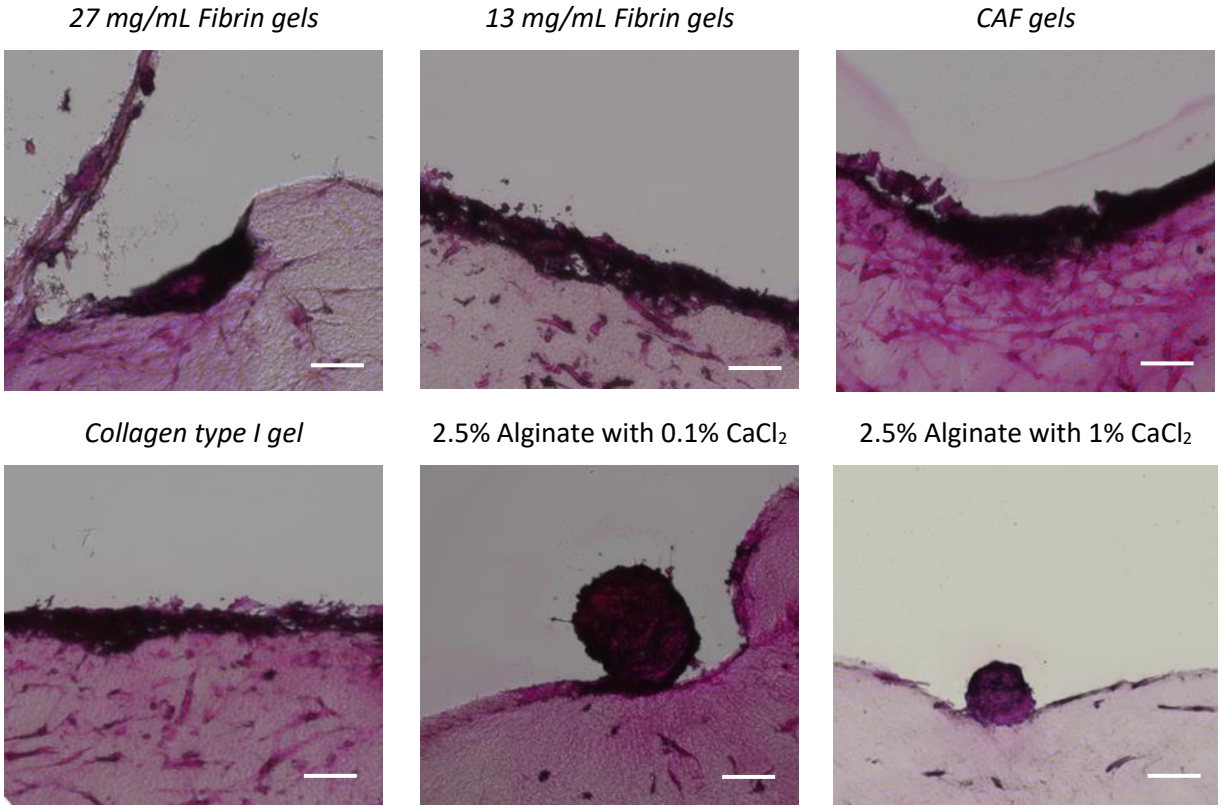

Figure 8. 9. Hematoxylin and eosin staining of skin models produced with keratinocytes encapsulated in fibrin, CAF, collagen and alginate gels and seeded on top of dermal layers comprised by fibroblasts encapsulated in telo-bovine collagen neutralized with NaOH. Images were taken after incubating 7 days the skin models under immersed conditions, and subsequently exposing the models for 14 days to the air-liquid interface, respectively. Scale bars correspond to 100 µm.

8.4.2. Immunohistochemistry of Skin Models

The control over the keratinocyte distribution with the introduction of epidermal bioinks was confirmed by immunohistochemistry. In the case of keratinocytes encapsulated in fibrin-based gels, the homogeneity of the epidermal layers was improved with the selection of fibrin as unique bioink component (Fig. 8.10). The use of a higher fibrin concentration resulted in a reduced epidermal thickness. Still, these models presented a consistent and well-defined epidermal composition, regardless of the fibrin concentration. In the case of keratinocytes encapsulated in CAF gels, a high expression of cytokeratin-14 could be observed across the skin model (Fig. 8.10). However, it was not possible to observe differentiative markers, except in certain areas containing small groups of fully differentiated keratinocytes. The use of collagen as encapsulation method also resulted in the formation of epidermal layers with a clear structure (Fig. 8.11), but a lower uniformity across the skin than the one observed in fibrin gels.

The formation of keratinocyte aggregations after their encapsulation in alginate was also proved by immunostaining (Fig. 8.11). The expression of cytokeratin-14 could be observed in the outermost keratinocytes, followed by the expression of involucrin by the subsequent inner cells. The nucleus of these cell groups was formed by fully differentiated keratinocytes, expressing filaggrin. The increment on the calcium chloride from 0.1% to 1% to generate alginate gels resulted in the rise of the filaggrin expression by the encapsulated keratinocytes and the drop on the number of proliferative keratinocytes.

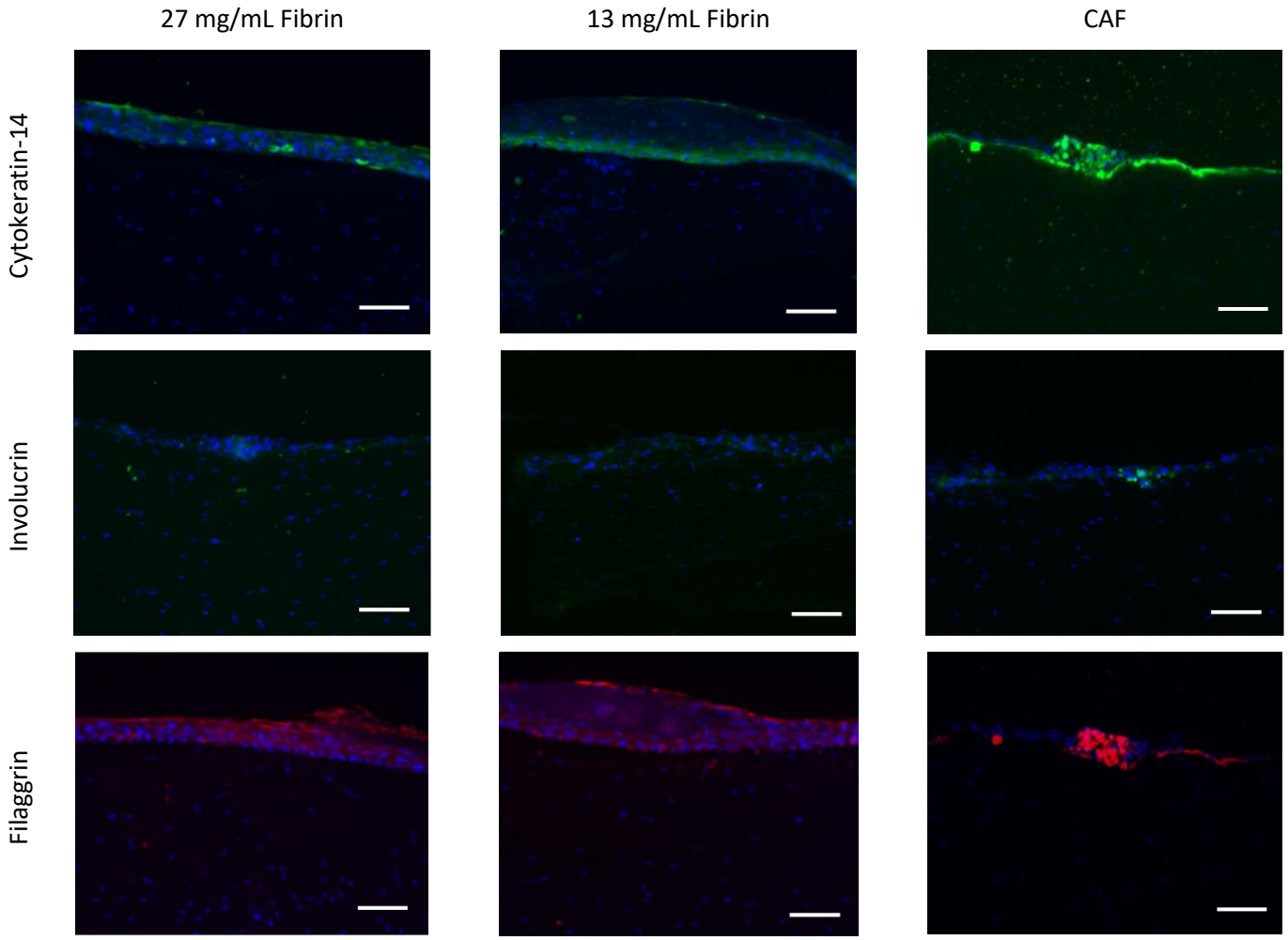

Figure 8. 10. Immunofluorescence staining of models produced from skin models produced with keratinocytes encapsulated in fibrin and CAF gels and seeded on top of dermal layers comprised by fibroblasts encapsulated in telo-bovine collagen neutralized with NaOH. Cytokeratin-14 present in the stratum basale and involucrin characteristics of the stratum granulosum are represented in green, whereas filaggrin characteristic of the stratum corneum is represented in red and cell nucleus stained with DAPI is shown in blue. Images were taken after incubating 7 days the skin models under immersed conditions, and subsequently exposing the models for 14 days to the air-liquid interface, respectively. Scale bars correspond to 100 µm.

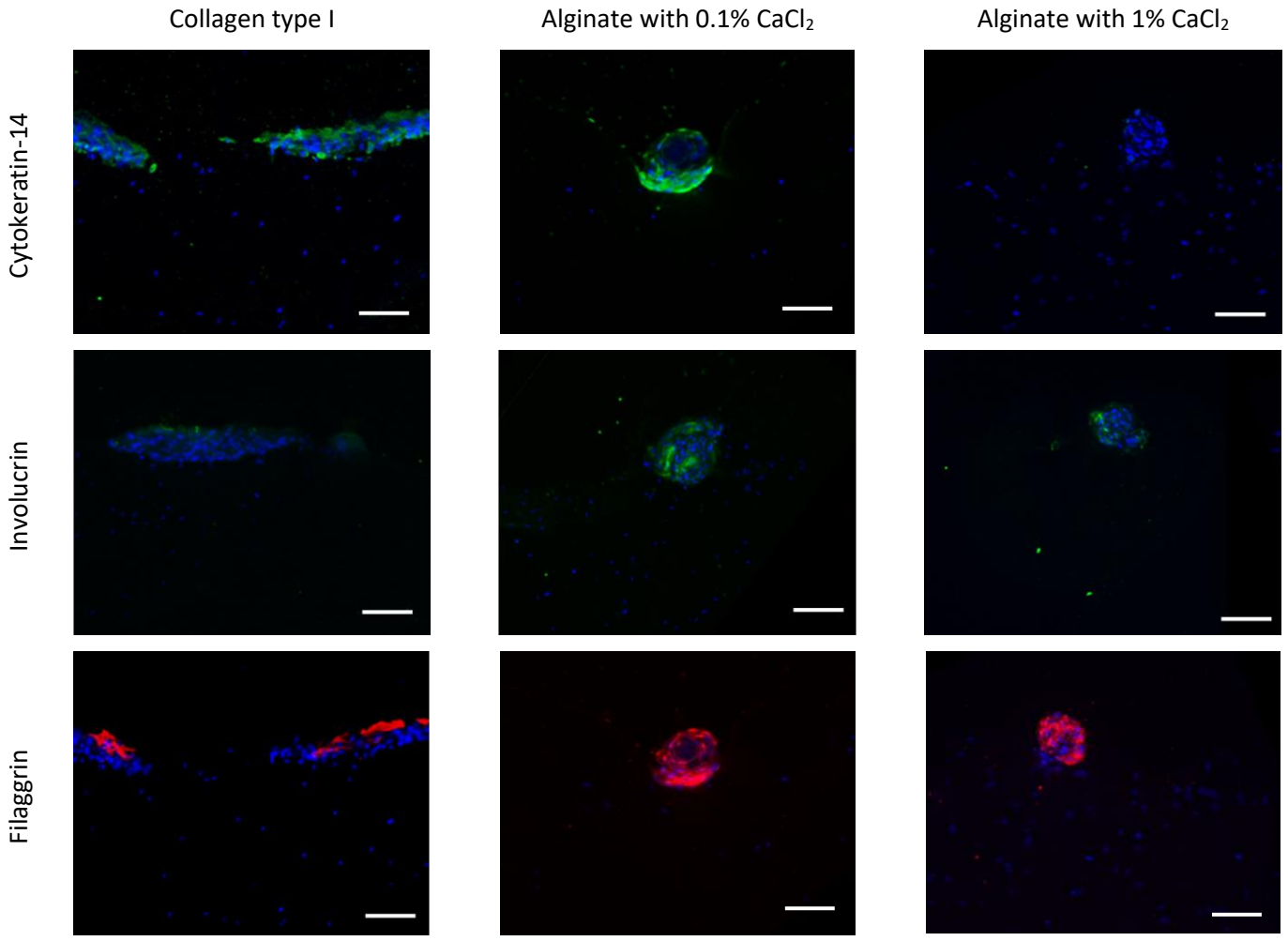

Figure 8. 11. Immunofluorescence staining of models produced from skin models produced with keratinocytes encapsulated in collagen and alginate gels and seeded on top of dermal layers comprised by fibroblasts encapsulated in telo-bovine collagen neutralized with NaOH. Cytokeratin-14 present in the stratum basale and involucrin characteristics of the stratum granulosum are represented in green, whereas filaggrin characteristic of the stratum corneum is represented in red and cell nucleus stained with DAPI is shown in blue. Images were taken after incubating 7 days the skin models under immersed conditions, and subsequently exposing the models for 14 days to the air-liquid interface, respectively. Scale bars correspond to 100 µm.

8.5. Chapter Discussion

8.5.1. Production of Skin Models

Keratinocyte behaviour is directly influenced by their proximity and interaction with other cells, as it was observed in previous chapters. Therefore, selecting the best keratinocyte density for creating a reliable epidermal structure was considered the first step required for optimising the skin equivalents. The seeding of 100,000; 250,000 and 500,000 keratinocytes per model resulted in the formation of homogeneous keratinocyte monolayers after 7 days, regardless of the selected cell density, with a keratinocyte confluency proportional to the number of seeded cells.

After exposing the skin models to the air-liquid interface (ALI) for 7 days, the epidermal thickness showed a significant difference based on the selected keratinocyte density. Skin models prepared using 100,000 keratinocytes presented a thin epidermis. In contrast, the seeding of 500,000 keratinocytes resulted in the formation of a thicker epidermal layer with a more defined epidermal sub-layer. The need for additional time in the models seeded with 100,000 keratinocytes to generate fully confluent basal layers could explain the delay in the formation of subsequent epidermal stratums. The presence of proliferative and differentiative markers in all samples suggests an initial correct epidermal formation, regardless of the selected cell density and despite the initial differences in maturation speed.

The apparent defined epidermal stratification observed by immunohistochemistry after 7 days of ALI was disturbed as shown in the images after 14 days of ALI. At this point, skin models presented a thicker epidermis, with a high number of terminally differentiated keratinocytes expressing filaggrin. The incorrect stratification of the epidermal layer could be confirmed by examining the sections stained with haematoxylin and eosin. The absence of a clear organisation observed in the keratinocytes at the basal stratum could have promoted the uneven cell differentiation and the dysregulation of the epidermal organisation compared to other reconstructed human epidermal models (Fig. 8.12). Lack of organisation in the basal layer could be explained by their manual seeding process. The restricted epidermal homogeneity across the skin equivalent highlights the importance of incorporating bioprinting techniques to enhance the control over their components and ensure the correct formation and reproducibility of skin models.

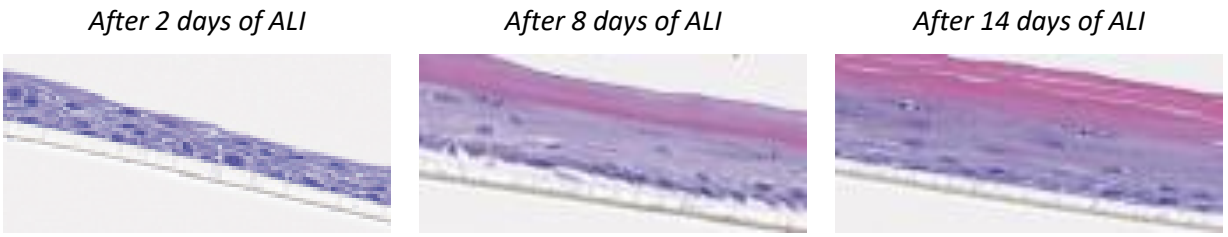

Figure 8. 12. Progression on the keratinocyte morphology and distribution after the exposition to 2, 8 and 14 days of air-liquid (ALI) interface in manually seeded reconstructed human epidermal models. Images obtained from Mathes et al. 2014.

Skin models prepared seeding 500,000 keratinocytes per model presented a slightly clearer epidermal organisation and the presence of outermost layers that resembled the cornified layers after 14 days of ALI. The improved cell organisation and epidermal layout in these skin models could be caused by their faster epidermal stratification. The early confluency and differentiation of keratinocytes in these samples could be responsible for an improved regulation over the balance between keratinocyte proliferation and differentiation based on previous studies (Poumay & Pittelkow, 1995). This hypothesis could explain the lower expression of involucrin associated with the upper *spinosum and granulosum stratum*, despite the high presence of a terminal differentiation marker like filaggrin in these models (Steven et al., 1990; Banks-Schlegel & Green, 1981).

The wide range of keratinocyte densities utilised for the production of skin models in previous studies endorses the low correlation between the number of seeded keratinocytes and the incorrect epidermal formation observed in these samples (Carlson et al., 2008; Black et al., 2005). However, other factors, such as excessive calcium concentration or media formulation, are also associated to the dysregulation of keratinocyte functionality (Bikle et al., 2012). The calcium levels in the cell medias utilised for this study were selected following the concentrations used in published protocols for producing skin equivalents *in vitro* (Roger et al., 2019; Poumay et al., 2004). Still, the incorrect diffusion of cell medium through the skin model during the air-liquid interface could have caused their irregular keratinocyte differentiation. Additionally, the unexpected appearance of isolated keratinocytes expressing cytokeratin-14 in the outermost layers of the epidermis suggests the effect of humidity levels on the epidermal formation. Keratinocytes need to be exposed to the air interface and dry conditions for their complete differentiation (Rosdy & Clauss, 1990; Carlson et al., 2008). The exposition of external keratinocytes to environments with high humidity could have resulted in the formation of external proliferative cell layers. Moreover, variations in water levels could have also altered the desquamation of the skin models, modifying the epidermal thickness and

layout (Bouwstra et al., 2008; Watkinson et al., 2001). Despite the previous hypothesis, the unforeseen cytokeratin-14 signals observed in these models could be explained by the generation of fluorescent artefact originated by the interface between the skin edge and the glass slide.

The significant stiffness of bovine collagen compared to other collagen type I gel, quantified in Chapter 6, could also be an influencing factor on the obtained epidermal properties. Previous studies have demonstrated the upregulation of genes associated with keratinocyte proliferation after their seeding in stiff materials (Nasrollahi et al., 2017). As consequence of an abnormal increase in the number of cells in the basal layer, the differentiation of keratinocytes could also be enhanced and ultimately lead to hypertrophic scarring (Ghaffari et al., 2009). To discard the effect of dermal components on the epidermal properties, diverse collagen type I gels with different mechanical properties were introduced as dermal biomaterials. But the haematoxylin and eosin staining of the resulting skin models revealed the low homogeneity and disorganised epidermal stratification regardless of the selected dermal composition.

Despite the lack of a correct epidermal stratification in the skin models, some significant differences could be appreciated in the immunostaining images depending on the selected collagen source. In contrast to the maintained three-dimensional structure in the rest of skin models over time, the use of atelo-bovine collagen produced the partial degradation of the skin construct after ten days, restricting their applications for the manufacturing of skin equivalents. In addition, the weak mechanical properties of atelo-bovine collagen could be responsible for the lower adhesion of keratinocytes to the dermis observed in these samples. On the other hand, the use of rat collagen type I demonstrated an improved epidermal structure compared to skin equivalents generated with bovine collagen. The lower stiffness and the higher similarity of fibroblasts in rat collagen type I to the behaviour presented by papillary fibroblasts could be explained by the observed enhancement of the epidermal stratification in these samples.

The implications of the fibrin-based gels and the ReJI process on the quality of the skin equivalents could not be determined because of the detachment of the epidermis in these models. However, fibrin is often used as the main dermal component in the production of skin models (Fig. 8.13), and they have demonstrated to promote keratinocyte proliferation and migration (Geer et al., 2004; Alexaline et al., 2019; Montero et al., 2021a).

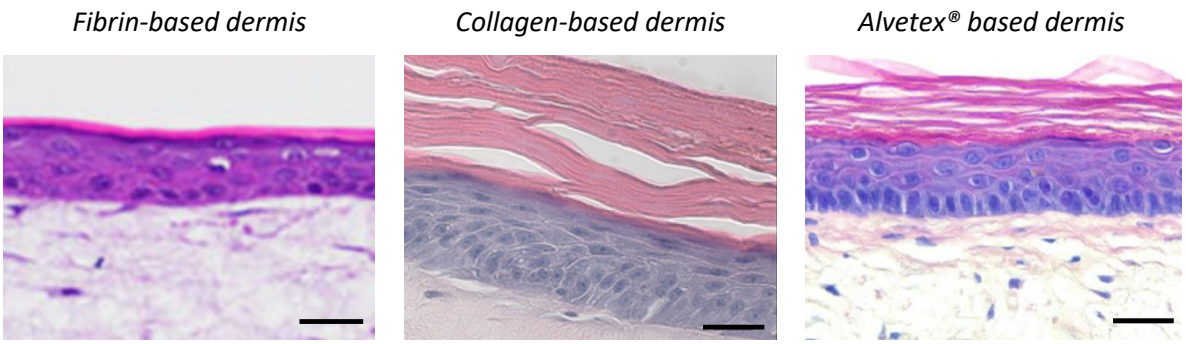

Figure 8. 13. Histological analysis of the epidermal organization in previously published skin models fabricated using fibrin and collagen and Alvetex® as main dermal biomaterials. Images obtained from Schmidt et al., 2020, Leong et al., 2018 and Roger et al., 2019, respectively. Scale bars correspond to 30 µm.

Because epidermal layers detached from the dermis in some skin areas, the sectioning process was considered as potential responsible for the variations observed in the epidermal consistency. The cryopreservation of skin models for its sectioning could have generated thermal damage if their gradual freezing was not performed correctly (Taylor et al., 2019). However, the reduced uniformity of the epidermal layers observed also in the paraffin-embedded models discarded this hypothesis. On the other hand, the epidermal dissociation could be explained by the incorrect formation of the dermal-epidermal junction (Yang et al., 2016). The absence of essential proteins, such as collagen type VII and XVII, in these layers could be responsible for the fragile anchoring between the dermal and epidermal layers (Aleemardani et al., 2021). Laminin has been incorporated in previous skin models to overcome this problem, enhancing the adhesion of keratinocytes to the dermis and improving the formation of the dermo-epidermal junction in the skin models (Derr et al., 2019; Yi et al., 2001; Tsunenaga et al., 1998).

Cell sources are often one of the main responsible for variations in the skin models. Neonatal human keratinocytes were selected for this study due their high proliferative rate and lower tendency to differentiate in comparison to adult keratinocytes (Mateu et al., 2016). Neonatal cells have already been used to produce skin equivalents, and they should not be responsible for the incorrect epidermal cornification (Gangatirkar et al., 2007). However, the genetics of

the donor can influence the cell behaviour and ultimately on the skin properties. Certain conditions that entail an incorrect epidermal formation such as psoriasis, parakeratosis or atopic dermatitis, are linked to genetical mutations (Lowes et al., 2007; Yang et al., 2020; de Stefano & Christiano, 2014; Armengot-Carbo et al., 2015). The lack of expression of certain proteins can weak the dermo-epidermal junction or alter the keratinocyte differentiation causing hyperkeratosis (Fig. 8.14).

Figure 8. 14. Examples of skin conditions affecting the epidermal stratification and the thickness of the cornified layer. Images obtained from the website DermNet New Zealand Trust.

Most studies often incorporate a pool of keratinocytes from different donors to avoid these problems. This approach can restrict the homogeneity between samples but increases the possibility of generating acceptable epidermal layers.

In future work, modifications on the cell source, media content and incubation conditions will be required to ensure the correct epidermal formation and the generation of a fully functional skin model. The correct integrity of the different epidermal stratum and the proper adhesion between the dermal and epidermal layers will be essential to evaluate the impact of the different bioinks and the ReJI process on the skin properties. The quantification by qPCR of the expression of additional epidermal markers and structural proteins present in the dermo-epidermal junction, such as cytokeratin-10, loricrin, collagen IV, collagen VII, collagen XVII or laminin-5, could help to understand better the maturation of the skin model in the future (Nyström & Bruckner-Tuderman, 2019).

8.5.2. Impact of Epidermal Bioinks on Skin Models

Encapsulation of keratinocytes showed a distinct impact on the epidermal formation depending on the nature of the encapsulating agents. The incorporation of keratinocytes to fibrin gels resulted in an improved stratification and uniformity in the epidermal layers compared to the seeding of keratinocytes by conventional methods. The assistance of fibrin in the skin re-epithelisation during the natural wound healing process could explain the observed improvement in the epidermal organisation (Clark et al., 1982; Fenner & Clark, 2016). The thickness of the generated epidermis also varied depending on the fibrin concentration. The reduction in the epidermal height observed at the highest fibrin concentrations could be explained by the fast initial proliferation of keratinocytes and their early localised differentiation observed in Chapter 7. The quick formation of the epidermal layers could have helped to balance the rate of proliferative and differentiative keratinocytes and to create more compacted epidermal layers, similar to what was described in the previous section with the skin models produced with 500,000 keratinocytes.

The introduction of additional components like collagen and alginate to the fibrin gels also promoted the formation of a homogeneous layer of proliferative keratinocytes. However, the expression of involucrin and filaggrin in these samples could only be observed in some areas containing keratinocytes groups. The retention of keratinocytes in these regions could be explained by their encapsulation in the alginate nucleus or by the specific release of calcium ions in these areas. However, it was not possible to find any previous work to support this hypothesis. The encapsulation of keratinocytes in collagen gels could not justify the aggregation of differentiated keratinocytes observed after their encapsulation in CAF gels. The use of collagen type I resulted in an improved homogeneity of the epidermal layer and their correct stratification. The natural interaction between collagen type I and keratinocyte could have been responsible for the enhancement of the epidermal formation compared to the skin models produced in the previous section (Pontiggia et al., 2022). Still, these samples presented some epidermal patches, which could be explained by the natural contraction of collagen gels by keratinocytes after their exposition to the differentiative medium and the air-liquid interface (Souren et al., 1989; Isaac et al., 2011).

The selection of alginate as encapsulating agent resulted in the formation of keratinocyte aggregates. These cell groups presented a different size depending on the calcium chloride selected for the generation of alginate gels. In those gels with lower calcium content, the size of the cell aggregates was larger, and the phenotype of the encapsulated keratinocyte varied through the generated spheres. Proliferative keratinocytes could be found in the outermost layers, followed by the differentiated keratinocytes expressing involucrin in inner layers, and the final presence of filaggrin markers in the nucleus of the keratinocyte aggregates. These findings support some of the hypotheses suggested in Chapter 7. The degradation of alginate gels could clarify the presence of keratinocytes only in the surface layers. Meanwhile, the increment in the calcium levels, the reduction of oxygen diffusion and the high cell confluency in the innermost regions could explain the acceleration of the degradation process in these regions. The limited proliferation of keratinocytes under high calcium levels could also justify the small size of cell aggregates when using alginates crosslinked with higher calcium chloride concentration. Additionally, the presence of high quantities of calcium anions could be responsible for the acceleration of the keratinocyte differentiation, and also explain the high expression of filaggrin in these samples. These results suggest the possibility of generating a cornified stratum by increasing the number of keratinocytes encapsulated in alginate gels and with the optimisation of the calcium concentration. The rapid formation of fully differentiated keratinocyte layers could explain the benefits of embedding keratinocytes in alginate gels for clinical applications. Keratinocyte encapsulation would not accelerate the renewal of skin models. Still, it could promote the generation of a protective layer to reduce any potential infections on the wound site and avoid interruptions in the re-epithelisation process (Aderibigbe & Buyana, 2018).

Despite the promising results obtained with the encapsulation of keratinocytes, further research should be performed on the degradation of the bioink components and their long-term effect on the keratinocytes. Similarly, the study of additional biomarkers associated with the epidermal components and dermo-epidermal junction would help to conclude the reliability of the skin models produced with the encapsulation of keratinocytes in fibrin.

CHAPTER 9. GENERAL DISCUSSION

9.1. Summary

This thesis has explored different strategies for the improvement of skin equivalents, from the implementation of Reactive Jet Impingement (ReJI) system as bioprinting process to the capacity of diverse dermal and epidermal bioinks to recreate specific skin microenvironments. The most relevant results from this research are summarised below.

9.1.1. Reactive Jet Impingement as Bioprinting Process

Optimisation of Reactive Jet Impingement system enabled the high throughput production of biological models maintaining a high resolution. The impingement process promotes the fast gelation of jetted bioink droplets, resulting in the printing of subsequent layers without the need of waiting times compared to other drop-on-demand printing techniques. This quick generation of stable constructs facilitated the printing in parallel of skin models with a volume of 1.5 cm^3 in less than 180 seconds.

On the other hand, ReJI process demonstrated a high control over cell deposition compared to manual cell seeding. The capacity to regulate the cellular location and biomaterial composition at the microscale level helped to improve the sample reproducibility and enhance the control over cell behaviour. In particular, the resulting homogeneous keratinocyte distribution boosted their proliferation rate and promoted a uniform keratinocyte differentiation.

Despite the quick reaction of the jetted droplets in mid-air, the impingement process did not significantly affect the viability and functionality of fibroblasts and keratinocytes regardless the cell density. By comparing the bioprinting of dermal models containing 5,000,000 and 500,000 fibroblasts per mL, it was possible to conclude the importance of cell densities on the dermal formation. The printing of the highest fibroblast density resulted in the faster adaptation of fibroblast to the printed matrix and quicker maturation of the dermal matrix, with the early remodelling and secretion of new extracellular matrix components by fibroblasts.

9.1.2. Selection of Dermal Bioinks

Optimisation of the dermal bioink formulation demonstrated to be a determinant factor in the recreation of specific fibroblast behaviour and dermal characteristics. The particular origin of collagen type I proved to be one of the first parameters to influence the physicochemical properties of the dermal matrix. In contrast to the rest of samples, collagen solutions obtained from calf and jellyfish presented a significantly low triple helix content at 37°C. This factor hindered the generation of stable gels with these collagens, preventing their utilisation of these materials for the production of skin models. On the other hand, human, rat and bovine collagen solutions allowed the generation of stable gels with a distinctive fibrillar arrangement. The choice of collagen neutralisation method was also an influencing factor on the properties of the collagen matrix. For instance, using a weaker base solution, like sodium bicarbonate, resulted in the formation a more disorganised matrix containing thin collagen fibres. In contrast, the strong character of sodium hydroxide resulted in the fast crosslinking of collagens and the generation of distinctive fibrillar configurations depending on the collagen source. The incorporation of RAFT^{TM} system in the production of collagen gels also modified the collagen matrix. By reducing the water content on the collagen gels, this system promoted a higher organisation and density of the collagen fibres. The different matrix characteristics between the collagen gels resulted in samples with significantly different mechanical properties. In the case of bovine collagen samples, the enhanced organisation and the presence of thicker fibres resulted in a higher stiffness than most collagen gels. Whereas, the particular aggregation of the collagen fibres into rounded bundles, observed in rat collagen neutralised with NaOH, originated a matrix with high mechanical strength but with high resistance to its remodelling. In contrast to collagen gels, the enzymatic crosslinking between fibrinogen and thrombin resulted in the fast generation of stable fibrin gels with high stiffness values. The properties of the fibrin samples could be customised with the incorporation of additional natural components. By introducing alginate into the fibrin gels, it was possible to reduce the stiffness of the fibrin gels and increase the porosity of the gels. Whereas the incorporation of collagen type I resulted in more heterogeneous matrices with improved mechanical strength.

The nature of the selected biomaterials, along with their matrix characteristics, showed a direct influence on the fibroblast behaviour. For instance, fibroblasts encapsulated in bovine collagen showed significantly faster adaptation and high proliferation than human and rat collagen samples. The different fibrillar and mechanical properties presented by telo- and

atelo- bovine collagens also influenced the fibroblast distribution and expression of F-actin filaments. Only in the case of atelo-bovine collagen neutralised with $NaHCO_3$, the brittle character of its matrix resulted in its complete degradation by fibroblasts after 5 days. In the case of human and rat collagen gels, their reduced mechanical strength was associated with the limited proliferation and higher production of collagen type I by fibroblasts. By increasing the fibrillar density in the rat collagen matrix using the RAFT^{TM} system, it was possible to boost the production of new extracellular matrix and increase the expression of F-actin filaments in the fibroblasts. The selection of fibrin as dermal component resulted in a faster fibroblast proliferation and production of new extracellular matrix compared to collagen gels. The incorporation of collagen into the fibrin bioinks resulted in similar fibroblast behaviours to the ones observed in fibrin gels. In contrast, the combination of fibrin with alginate resulted in the formation of fibroblast aggregates, boosting the proliferation of fibroblasts to levels significantly higher than in the rest of the samples. By mixing fibrin, collagen and alginate, it was possible to maintain a cell proliferation rate similar to fibrin gels, and a balanced production of collagen type I and III, while reducing the tensional forces between fibroblasts observed in fibrin gels.

The differences in the matrix formation also impacted the printability of dermal bioinks. Only the four fibrin-based bioinks, along with rat collagen neutralised with NaOH, demonstrated to crosslink fast enough to be considered for their utilisation with the ReJI system.

9.1.3. Selection of Epidermal Bioinks

The encapsulation of keratinocytes in natural-based biomaterials allowed an enhanced control over keratinocyte distribution. On one hand, the selection of collagen type I as encapsulating agent ensured the correct adhesion of keratinocytes and the promotion of their uniform proliferation through the collagen gel. On the other hand, the use of fibrin-based biomaterials resulted in an improved control over the location of keratinocytes with the formation of cell aggregates. The homogeneous distribution and high confluency of keratinocytes in the generated cell groups boosted their proliferation and the early differentiation of those cells found in the nucleus of the keratinocyte groups. The size of the created cell aggregates varied with the change in fibrin concentration and the incorporation of alginate and collagen to the epidermal bioinks.

The keratinocyte behaviour observed in these samples contrasted with the reduced viability of keratinocytes in alginate gels. The lack of cell binding groups in the alginate gels was considered the main responsible for the limited proliferation of keratinocytes until day 7. Additionally, the increase in the calcium ion concentration in the alginate gels was considered the main factor in the early differentiation of keratinocytes observed in these gels compared to other samples.

9.1.4. Development of Skin Models

Different strategies were performed to improve the functionality of skin equivalents, including the optimisation of keratinocyte densities, the incorporation of different dermal bioinks and the optimisation of sectioning process.

Despite the correct formation of the epidermal layers in the early stages of the skin models prepared with rat collagen type I as dermal biocomponent and seeding 500,000 keratinocytes per model, the haematoxylin and eosin staining of skin sections revealed a final disorganised and inconsistent epidermal stratification in all samples. Diverse factors such as manual seeding, the incorrect dermo-epidermal formation, the impact of the keratinocyte donor or uneven cultured conditions, including the variations on the humidity or inconsistent diffusion of cell media, were considered as potentially responsible for the incorrect epidermal formation. The inability to produce a standard skin model with the correct structural composition prevented the continuation of this study. Consequently, optimisation of the skin manufacturing process will be essential in future studies before assessing the impact of dermal bioinks and the ReJI process on the reliability and complexity of the final skin models.

On the other hand, the use of epidermal bioinks during the manufacturing of skin equivalents confirmed the advantages of encapsulating keratinocytes to control their distribution and behaviour. The use of collagen as encapsulating agent resulted in an improved epidermal stratification compared to the seeding of keratinocyte suspensions. However, the embedding of keratinocytes in collagen type I still resulted in the lack of consistency of the epidermal layer in some regions. By contrast, fibrin gels allowed the creation of homogeneous epidermal layers through the skin model, which presented different thickness depending on the fibrin concentration. Combination of fibrin with collagen and alginate resulted in the generation of a continuous layer of proliferative keratinocytes, with the presence of isolated keratinocyte aggregates containing differentiated keratinocytes. These cell groups could also be observed using only alginate as encapsulating agent. In these samples, only the cells found in the external layers of the keratinocyte groups presented a proliferative state, while those cells found in the nucleus of the generated keratinocyte sphere were found in a differentiative form. The increase in the calcium chloride concentration during the crosslinking of alginate gels resulted in the formation of smaller keratinocyte aggregates with fully differentiated keratinocytes.

9.2. Novelty

The benefits of incorporating the Reactive Jet Impingement process in the manufacturing of some *in vitro* models, such *as* bone or cartilage micro-tissues, have already been demonstrated in previous studies (Kotlarz et al., 2022; da Conceicao Ribeiro et al., 2018). However, this work has explored for the first time the possibility of adapting this technology to the manufacturing of skin equivalents. The implementation of ReJI system as bioprinting process has confirmed its capacity to improve the control over the location of skin cells and the maturation process compared to traditional tissue engineering techniques. Besides, this research has also demonstrated the advantages of ReJI in terms of printing resolution, speed and scalability of the process in comparison to other technologies already utilised for skin bioprinting.

Although the main steps required to produce *in vitro* skin models are standardised, diverse variables like cell densities, seeding times or dermal biomaterials considerably change between studies (Sriram et al., 2015). For that reason, this project has also focused on assessing for the first time the impact of some of these elements on the properties of the final skin equivalents. Selection of fibroblast density demonstrated to affect the dermal formation directly. By increasing the number of seeded fibroblasts, it was possible to reduce the time required for the dermal maturation. On the other hand, the comparison between collagen and fibrin-based gels proved the importance of biomaterial selection on the final properties of the different skin layers. The evaluation of different commercial collagen solutions evidenced the differences in their physicochemical properties depending on their animal source and extraction method. Besides, the formulation of the base solutions for the crosslinking of collagen gels also demonstrated to influence the collagen homogeneity and affect the characteristics of the dermal matrix. By incorporating additional biomaterials such as alginate or fibrin, it was possible to find a correlation between the individual properties of each material and their influence on the final printability and characteristics of the formulated bioinks. As a result, the link between the physicochemical and mechanical properties of the dermal bioinks and their impact on the fibroblast behaviour could be established. These findings open the door to the recreation of more complex dermal microenvironments, which are often dismissed in the production of skin models.

Finally, this work suggested the formulation of epidermal bioinks based on natural biomaterials as a new strategy to overcome the lack of homogeneity of the epidermis in the skin models. Keratinocyte encapsulation is an extended practice in clinical applications for treating severe skin wounds to improve the integration of grafts and accelerate the healing process. However, the consequences of encapsulating keratinocytes during the manufacturing of in vitro skin equivalents have barely been explored. The experimental results confirmed the possibility of controlling the distribution of keratinocytes and promoting their proliferation and differentiation using natural-based epidermal bioinks.

9.3. Implications of this Research

9.3.1. Overcoming Limitations from Conventional Bioprinting Techniques

Implementation of bioprinting processes into the manufacturing of skin equivalents has already demonstrated to improve the complexity of skin models (Min et al., 2018; Derr et al., 2019; J. Liu et al., 2022b). However, none of these articles has proved the suitability of these technologies for manufacturing skin models at the industrial level. The specific limitations of each bioprinting technique represent the main constraints for the large-scale production of validated skin equivalents.

The complexity of the printing process and the necessity of specialised personnel are one of the main drawbacks to the adaptation and scalability of some bioprinting techniques, such as laser-assisted bioprinting (Liu et al., 2018; Bishop et al., 2017). In this research, the ReJI system has demonstrated to be a technique based on simple principles, which only requires the optimisation of basic parameters related to the selected bioinks, such as the printing pressure needed to operate the system. Furthermore, the simple interface provided by the Jetlab® 4 software and the easy setting up of the printing designs highlights the user-friendly character of this printing system.

On the other hand, the ability of ReJI process to incorporate commonly used biomaterials, such as commercial solutions containing extracellular matrix components, facilitates the adaptation of this technology to the replication of established biological processes (Chopin-Doroteo et al., 2021). This fact counteracts the need to adapt the bioink formulation for extrusion-based bioprinting, by incorporating additional components to increase the bioink viscosity, or in the case of laser-assisted bioprinting, with the introduction of photosensitive materials. Furthermore, utilisation of low viscous biomaterials as bioinks during the printing with ReJI reduces the cell exposition to shear stress and any potential cell damage in comparison to extrusion-based bioprinting process (Ouyang et al., 2016; Hölzl et al., 2016). Different strategies have been explored to decrease the shear stresses generated on the extrusion-based printing processes. For example, the combination of melting electrowriting with extrusion-based bioprinting in a single step, the incorporation of crosslinker baths or the use of multiple bioinks combined in a single nozzle allow the use of less complex bioinks with lower viscosity (Puertas-Bartolomé et al., 2020; de Ruijter et al., 2019; Lee et al., 2021; Visser

et al., 2018). Still, the printing speed and resolution of extrusion-based processes are still restricted in comparison to the ReJI system.

Despite the automatisation of all bioprinting processes, the time required to generate skin equivalents is still one of the main limitations for their implementation as testing platforms at industrial scale. The printing speed of droplet-based technologies, such as inkjet or microvalve-based bioprinting, is especially restricted by the need for additional crosslinking steps to ensure the stability of the printed patterns (Gudapati et al., 2016). For that reason, recent studies have explored the incorporation of peripheral devices that enable the curing of the printed droplets before their deposition on the substrate (Sakurada et al., 2020; Teo et al., 2020). These systems are based on inkjet printing, which allows the generation of complex structures with high precision. Still, these techniques are restricted by the employment of bioinks with significantly low viscosities and a limited range of cell densities to avoid nozzle clogging (Lee et al., 2012). These characteristics differ from the ability of ReJI to print physiological relevant cell densities without affecting their viability or causing any valve blockage, thanks to the use of valves with larger nozzle diameters and the possibility of applying continuous pneumatic pressure.

Overall, ReJI process has demonstrated to be a suitable printing process to overcome some of the limitations found in the production of skin equivalents using conventional bioprinting systems. This technology provides a higher control over the structural composition of the printed models than other droplet-on-demand techniques. The capacity of ReJI process to print subsequent layers containing different biocomponents without waiting times enables the high throughput production of complex biological structures, maintaining a high printing accuracy. As a result, ReJI system has demonstrated to produce skin models in parallel in a few minutes, facilitating the automatisation of the process and its industrial scalability. Moreover, the development of this printing system in-house enables the optimisation of each printer component for the manufacturing of skin models and the adaptation of the printing process for its industrial implementation.

9.3.2. Improved Complexity and Scalability of Skin Equivalents

The recreation of the protective character of native human skin acquires particular importance in those skin models allocated for assessing the safety and efficiency of commercial products (Planz et al., 2016; Bouwstra et al., 2021). Unfortunately, in this thesis, it has not been possible to produce fully functional skin models which could be validated for their use as testing platforms. However, the results obtained from the development of dermal and epidermal bioinks and the implementation of ReJI as bioprinting process could help to enhance the complexity and scalability of current skin equivalents.

The reproduction of skin structural composition is an essential factor to ensure the correct anatomy and physiology of skin equivalents. Variations in the matrix organisation and fibroblast behaviour through the dermis have demonstrated to be crucial for the stability and homeostasis of native human skin (Cole et al., 2018; Karsdal et al., 2017). These diverse dermal microenvironments are usually dismissed during the manufacturing of skin models, and their influence on the quality of the skin models is generally neglected. Nonetheless, this project has proved the possibility of customising the characteristics of the dermal layer with the selection of specific natural biomaterials.

Although the animal origin of collagen type I solutions is often selected without any specific criteria, this research has proved the importance of collagen sources in the recreation of distinct dermal microenvironments. Parameters such as extraction method, selected body area or neutralisation solution significantly influenced the fibre formation, matrix organisation and the final mechanical properties of the collagen gels. Besides, these different characteristics demonstrated to have a direct impact on the fibroblast proliferation, distribution and production of new collagen type I and III. Although it was not possible to determine the resemblance of the generated dermal models to the native dermal regions, fibroblasts presented some behaviours associated with reticular and papillary fibroblasts. Therefore, by combining some of the studied dermal bioinks, it could be possible to improve the complexity and resemblance of the dermal layer in the skin models. The search for replicating the native variations on the collagen architecture across the dermis has only been reported in a recent publication (Ng et al., 2018b). By printing macromolecule-based bioinks containing polyvinylpyrrolidone (PVP) and collagen, this study demonstrated the possibility of altering the collagen fibrillogenesis, enabling the control over the collagen porosity and fibroblast morphology along the dermis.

Fibrin gels are often utilised as a replacement for collagen due to their improved stability and facility to handle. However, in this work, collagen gelation was optimised with the incorporation of buffer solutions to the conventional neutralisation methods to ensure a higher control over the gel formation and collagen contraction. This approach implied an enhancement of the homogeneity of collagen gels and, consequently, an improved reproducibility of skin models. Despite this optimisation, the incorporation of fibrin as dermal matrix accelerated the dermal maturation compared to collagen gels. The natural presence of fibrin in wound sites could be responsible for the recreation of biological signal cascades and fibroblast responses like the ones occurring during the wound healing process, along with the generation of tensional forces accountable for boosting the fibroblast mobility and proliferation (D'Urso & Kurniawan, 2020; Tracy et al., 2016). Additionally, the incorporation of additional components such as collagen and alginate to the fibrin bioinks evidenced the possibility to customise dermal models modifying their mechanical properties and, subsequently, the fibroblast behaviour. Only few articles have explored the combination of fibrin with other biomaterials for the production of dermal layers in the skin equivalents (Pourchet et al., 2017; Derr et al., 2019; Kober et al., 2015). Still, none of them have reported the possibility of tailoring the dermal properties and skin complexity.

The ability to adapt the mechanical properties of the dermal regions based on the selected bioink formulation could also help to improve the epidermal properties. The behaviour of keratinocytes has been reported to vary depending on the stiffness of their substrate. Stiff environments upregulate keratinocyte genes associated to their proliferation, whereas substrates with reduced mechanical properties promote their differentiation (Nasrollahi et al., 2017; Dupont et al., 2011; Rognoni & Walko, 2019). Despite the influence observed on the keratinocytes, the Young Modulus obtained from the collagen gels, ranging from 0.02 to 0.7 kPa, contrast with the values from native human skin, which varies between 0.1 to 10 kPa (Achterberg et al., 2014). The limited stiffness of dermal gels could have prevented a more significant impact on the keratinocyte behaviour. Still, the remodelling of the dermal matrix by fibroblasts over time should also be included, as it could imply a modification of the mechanical values obtained from the acellular dermal gels, resulting in the variation of the keratinocyte functionality (Jagiełło et al., 2022; Ozcelikkale et al., 2017).

On the other hand, the evaluation of molecule diffusion or the assessment of skin care treatments could also benefit from the improvement in the dermal complexity presented in this work. For instance, the recreation of specific skin conditions, skin ageing or photodamage could be optimised by selecting the specific dermal and epidermal bioinks capable of mimicking the specific characteristics of their structural composition (Hausmann et al., 2020; Liu et al., 2022c; Fligiel et al., 2003). Moreover, the incorporation of Reactive Jet Impingement system in the production of these skin models could help to enhance the complexity of the model with the control deposition of material gradients. Besides, the ability of ReJI to print high cell densities without affecting their viability could enable the generation of organoids in specific regions of the skin model, facilitating the recreation of some skin appendages such as hair follicles (Lei et al., 2017; Lee et al., 2022).

One of the most significant limitations of current skin equivalents is the incapacity to adapt their manufacturing process at industrial scale. The implementation of the ReJI process in the production of skin models could help to overcome the restrictions experienced by traditional tissue engineering methods and conventional bioprinting techniques. This research has demonstrated the capacity of ReJI system to automate the generation of skin equivalents producing a large number of models in parallel in a reduced time. Moreover, the accessibility of this technology and the possibility to incorporate biomaterials conventionally used for the generation of skin models facilitate its integration into the industry. On the other hand, the reproducibility of skin models could also be benefited by the implementation of ReJI system in the manufacturing of skin equivalents. The control deposition of cell and biomaterial components and the potential to generate crosslinking points ensures the production of skin constructs with high shape fidelity. Other strategies explored in this research, such as keratinocyte encapsulation, can help to overcome the uneven epidermal formation and the batch-to-batch variations observed in current skin equivalents. By selecting the appropriate epidermal bioink, it could be possible to control the keratinocyte distribution and epidermal stratification.

Despite the initial reduction in the manufacturing time thanks to the ReJI bioprinting process, the time required to mature the skin models would still be one of the main obstacles to the industrial production of skin substitutes. But diverse strategies explored in this project could help to accelerate skin formation. On one hand, bioprinting of high fibroblast densities has demonstrated to decrease the time required for fibroblasts to remodel the dermis and reach a homeostasis state. The quick adaptation of fibroblasts to the CAF gels could enable the seeding of keratinocytes on top of the dermis after only one day, eluding the traditional period of three to seven days required in conventional protocols. On the other hand, the selection of dermal and epidermal bioinks could also boost the maturation of each skin layer. By selecting dermal bioinks capable of promoting the proliferation of fibroblasts and the renewal of the extracellular matrix components, such as fibrin-based biomaterials or telo-bovine collagen, it could be possible to speed up the formation of dermal layers. Meanwhile, the encapsulation of keratinocytes in fibrin-based gels could stimulate the fast proliferation and homogeneity of keratinocytes, accelerating their differentiation and epidermal stratification. The ability of the developed epidermal bioinks to promote different keratinocyte stages could also help to reduce the time required for the epidermal stratification. In a recent publication, the printing of multiple layers of keratinocyte encapsulated in gelatin accelerated the epidermal formation in comparison to the seeding of keratinocyte monolayers (Barros et al., 2021). Therefore, printing of subsequent layers of different epidermal bioinks capable of promoting keratinocyte proliferation and their control differentiation could support the maturation of the different epidermal stratums at the same time, improving the control over the epidermal formation and decreasing the time required for the complete skin model maturation.

Although this project has focused on the optimisation of skin equivalents for product testing, most of the obtained results could also be applied for the improvement of skin substitutes suitable for wound treatment. In the case of clinical application, parameters such as biomaterial integration or the quick promotion of skin regeneration acquire a high importance in the selection of the best graft composition (Savoji et al., 2018; Kaur et al., 2019). Due to the animal origin of the studied biomaterials, only atelo-bovine collagen could be utilised for wound treatment without the high risk of immune rejection (Correia et al., 2020; Dixit et al., 2017). However, the screening of the best materials for wound treatment could benefit from

the lessons learnt in this project about the implications of the physicochemical properties of collagen and fibrin-based gels on the promotion of specific fibroblast functionalities.

Based on the obtained results, atelo-bovine collagen type I could be considered a suitable material for wound treatments due to its quick degradability and its ability to promote fast fibroblast proliferation and early production of new extracellular matrix components. Besides, the incorporation of RAFT^{TM} system into the production of collagen gels could also help to improve current skin substitutes. This system has proved to generate stable thin dermal layers containing fully confluent fibroblasts after only few days, which could help to support the wound site and promote its re-epithelisation. ReJI system could also be implemented in wound healing treatment. By incorporating the printing head containing the ReJI system into a clinical printer, it could be possible to enhance the printing precision and increase the number of skin cells deposited directly on the wound site for the skin regeneration.

9.3.3. Optimisation of In Vitro Tissue Models

The high presence of fibroblasts and collagen type I in other tissues apart from skin, such as tendons, smooth muscles, cornea or cardiac tissue, enables to incorporate some of the discoveries on biomaterial development for the optimisation of other *in vitro* models (Amirrah et al., 2022). Despite the biological differences between these tissues, fibroblasts always provide structural support generating new extracellular matrix components and adapting their behaviour to the mechanical properties of the tissue (Plikus et al., 2021). The composition and characteristics of the extracellular matrix are some of the elements that vary more between tissues (Scott, 2003; Frantz et al., 2010). Variations in the stiffness or viscoelasticity of the matrices have demonstrated to affect the correct function of some of these tissues (Querejeta et al., 2004; Burlew & Weber, 2000). For that reason, tailoring the properties of collagen type I or fibrin matrices, by following the conclusions from previous chapters, could help to enhance the reliability and complexity of these tissue models.

Furthermore, collagen type I also represents an abundant component in hard tissues such as bone (Wiesmann et al., 2004). Although the stiffness of the studied collagen gels significantly differs from the strength of native human bones, other parameters such as fibre orientation, diameter or porosity are essential elements for tailoring the cellular behaviour in these tissues (Tzaphlidou, 2008). By modifying the characteristics of the collagen matrix and combining them with other biomaterials, such as hydroxyapatite, it could be possible to recreate different bone conditions (Garnero, 2015; de Wildt et al., 2019). Finally, the implementation of RAFT^{TM} system on the generation of collagen gels could also help to improve the thickness and the alignment of collagen gel, mimicking the collagen arrangement in native human bones (Georgiadis et al., 2016).

CHAPTER 10. CONCLUSIONS AND FUTURE WORK

10.1. Conclusions

The research presented in this thesis has examined different strategies to improve the complexity and scalability of *in vitro* skin models.

Reactive Jet Impingement process has proved a high control on the deposition of cells and biomaterials compared to manual seeding techniques. The capacity of ReJI system to control the cell location allows the production of three-dimensional structures with homogeneous cell distribution, promoting the cellular proliferation rate and their uniform differentiation. Moreover, the impingement process overcomes some of the technical problems experienced by other printing techniques. This system enables the printing of motifs with high-resolution and the deposition of physiologically relevant cell densities without significantly affecting their viability. The increment in the number of printed fibroblasts has shown a reduction in the time required for dermal matrix maturation, which could help to decrease the habitual time required for producing skin models. In contrast to other bioprinting techniques, ReJI process has demonstrated to generate a remarkable number of complex structures in parallel within a short time. Therefore, although the printing of full-thickness models has not been proven yet, ReJI system can be considered a suitable technique for the industrial scalability of skin bioprinting.

On the other hand, the specific formulation of dermal bioinks has demonstrated to be an important factor in the recreation of dermal structural properties. The selection of collagen type I from different animal sources has shown to affect the physicochemical and mechanical properties of the collagen matrix. As a result, the selection of collagen type and their neutralization method have proved to directly influence fibroblast proliferation and the renewal of the extracellular matrix components. Similarly, the implementation of RAFT^{TM} system on the production of collagen gels has proved to modify their fibrillar organisation, promoting the formation of more complex dermal models. On the other hand, the combination of fibrinogen with other natural biomaterials, such as collagen type I and alginate, has also demonstrated to change the matrix configuration and mechanical properties of fibrin gels. Variables like matrix stiffness, printability or cellular proliferation can be customised by modifying the bioink formulation. Consequently, the selection of dermal biocomponents can

help to enhance the complexity of skin models, promoting certain fibroblast behaviours and replicating specific dermal characteristics.

Finally, the encapsulation of keratinocytes has demonstrated to improve the homogeneity and reproducibility of epidermal layers. The utilisation of natural skin materials like collagen type I has proved to induce keratinocyte adhesion and proliferation. This effect on the cell behaviour can be enhanced with the incorporation of biomaterials present in natural wound healing processes like fibrinogen. By encapsulating the keratinocytes in fibrin gels, it is possible to promote keratinocyte assembly, increasing their proliferation rate, and promoting their homogenous differentiation. In contrast, the use of alginate as encapsulation agent results in the formation of cell aggregates and the acceleration of keratinocyte differentiation. Similar to the dermal bioink formulation, the combination of fibrin with collagen and alginate allows the customisation of keratinocyte behaviour and distribution. Based on these results, the formulation of epidermal bioinks can be a suitable strategy to customise the keratinocyte behaviour and ensure an enhanced control over the epidermal formation.

Reactive Jet Impingement process along with the formulation of dermal and epidermal bioinks, have demonstrated a high control over the structural composition of skin equivalents, promoting the creation of homogeneous models with enhanced characteristics. By combining these elements, it could be possible to produce skin models on demand adapted to the industrial requirements.

10.2. Recommendations for Future Work

10.2.1. Improvement of Skin Models

Due to the incapacity of producing functional skin models, it was not possible to conclude the final implications of the studied bioinks and the ReJI printing process on the properties of the final skin equivalent. Therefore, the next steps in this project would require the manufacturing of reliable skin models which can be used as benchmark.

The support and training from a research group specialised in the production of skin equivalents could be a quick method to overcome the problems experienced in this project. Once the manufacturing of a standard skin model is optimised and established, it could be possible to assess the impact of the variables studied in this project on the skin model.

The new manufacturing protocol will need to be adapted to incorporate the studied dermal bioinks and determine their influence on the recreation of specific dermal regions and the correct epidermal formation. Biomolecular techniques, like qPCR, could help to understand the effect of the generated dermal architecture on the fibroblast phenotypes and verify the presence of additional dermal biocomponents (Janson et al., 2012; Noizet et al., 2016). Considering the diverse mechanical properties and fibroblast behaviours in each studied dermal model, the combination of different bioinks could be tested to potentially recreate the reticular and papillary dermal layers, enhancing the complexity of the model. After confirming the structural composition of skin models, the assessment of the mechanical properties of the whole skin construct could be performed to determine their resemblance to native skin, and ultimately select the best dermal bioink (Joodaki & Panzer, 2018).

Epidermal bioinks could also be introduced during the production of skin models to further investigate their influence on the epidermal formation. The assessment of cellular signalling cascades could provide a better overview of the biological changes experienced by keratinocytes during their encapsulation. Additionally, this data, along with a deeper study on the degradation process of epidermal bioinks, would help to optimize the biomaterial formulation to mimic specific epidermal microenvironments. One of the strategies proposed in this thesis to reduce the time required for skin maturation was the printing of subsequent layers of different epidermal bioinks. The main goal of this approach was to fabricate a skin construct which already contained the four epidermal stratums from the beginning. This strategy could allow the maturation of the different layers in parallel, enhancing the control

over the epidermal stratification, and reducing the time required to obtain the final skin model. In order to ensure the cohesion of the generated epidermis, it would be essential to evaluate the integration between the different printed epidermal sub-layers and the adherence between keratinocytes. Another strategy which could help to accelerate the epidermal stratification is the incorporation of encapsulated components in each epidermal sub-layer. The controlled release of epidermal growth factors or differentiation elements encapsulated in microparticles could help to accelerate certain keratinocyte behaviours during epidermal maturation (Sahle et al., 2017; Pakulska et al., 2016). This approach was recently tested by Suzuki *et al*. with the encapsulation of chlorogenic acid in PLGA nanoparticles to enhance the expression of collagen type XVII by keratinocytes (Suzuki et al., 2020). Regardless of the strategy selected, it is essential that the attempts to decrease the maturation time do not affect the epidermal stratification and the formation of the protective barrier.

Finally, adapting the established skin manufacturing protocol to the ReJI process will be essential to benchmark the printed and manually seeded models. The comparison between both methods could determine the advantages and limitations of ReJI on the manufacturing of reproducible and reliable skin equivalents in a time and cost-effective manner. Once the skin bioprinting process is optimised, the best dermal and epidermal bioinks could be incorporated into the ReJI process to determine the best approach to replicate the structural complexity of native human skin. Additionally, the printing of different fibroblast densities on the production of the skin models could be tested to conclude its impact on the skin quality and the possibility of reducing the overall maturation time.

10.2.2. Industrial Scalability of Bioprinted Skin Models

The produced skin equivalents will need to be validated before their use for product testing. The evaluation of their structural composition and epidermal barrier functionality will be the first assays required for the model validation (Mathes et al., 2014). These studies can determine the deficiency of any skin biocomponent, such as hyaluronic acid or laminin, which can be incorporated during the production of skin substitutes to enhance their complexity (Montero et al., 2021b; Tsunenaga et al., 1998; Smithmyer et al., 2014). Similarly, this data can provide information about any remaining bioink ingredient in the model, which could later interfere with the diffusion of products through the skin model. Penetration and diffusion assays could also help to benchmark the characteristics of the produced models with other established skin equivalents and redirect future research to improve the obtained results (Schulz et al., 2017; Jepps et al., 2013; Abd et al., 2016).

After the model validation, the standardisation of the production process will be necessary for its application at industrial levels. This procedure should be performed under good manufacturing practice, following the appropriate regulatory standard guidelines (Hourd et al., 2015). The creation of standard operating procedures and quality control monitoring will be essential to maintain consistency across batches and ensure the efficiency of the process. Standardisation of cell culture and bioink formulation could become the most complicated step due to the variability associated with the cell donors and material sources. Incorporating stem cells or recombinant biomaterials could help in the future to reduce these problems. Additionally, ReJI system should also be standardised and adapted to the industrial facilities to ensure its accessibility. The implementation of bioreactors could help to improve the automatisation of the skin maturation process. These systems allow the precise control and monitoring of cultured conditions such as pH, oxygen or nutrient supply and waste removal, reducing the need for professional operators to perform these tasks (Rimal et al., 2021; Wendt et al., 2008).

One of the main obstacles during the commercialisation of skin models is their limited shelf-life (Carlson et al., 2008; Mathes & Ruffner, 2014). There is an urgent need to develop an approach which allows the transport and preservation of skin models until their arrival to the customer. Microfluidic systems could help to ensure the long-term maintenance of the model properties and cell survival. These portable platforms allow the control over the flow rates in the skin equivalent, reproducing the air-liquid interface and the physiological transport of

nutrients and oxygen (Ingber, 2022). Different studies have already demonstrated the advantages of using this technology to reproduce the skin structure (Wagner et al., 2013; Sriram et al., 2015). Apart from their advantages on the tissue maintenance, the high control over the liquid flow in these platforms enables a more precise study of the molecules released by the skin during the evaluation of treatment effectiveness (Wufuer et al., 2016; Schimek et al., 2018; Abaci et al., 2015). Moreover, the possibility of integrating vascular channels can also help to overcome the limitations of current models to accurately quantify the vascular drug absorption (Mori et al., 2017). Besides the control of the culturing conditions, these systems allow the incorporation of mechanical movements. Based on previous studies, the reproduction of shear forces like the ones in native skin can improve the epidermal formation and barrier function in the skin models (Tokuyama et al., 2015; Yano et al., 2004).

Finally, the incorporation of biosensors could help to accelerate the detection of changes in the skin models, especially during product testing. Most biochemical changes occur gradually at low concentrations during long periods, hindering the evaluation of their fluctuations by conventional methods. Smart materials capable of sensing variations in the pH, temperature or biomolecular concentrations could be integrated within the skin layers or into the microfluidic system to ensure real-time monitoring (Someya & Amagai, 2019; Zhu et al., 2021). Different biosensors have already demonstrated their lack of interference with cellular functions, and the possibility of producing them using 3D printing technologies (Ferrari et al., 2020; Muñoz & Pumera, 2020). However, there are few publications related to their application in tissue models.

10.2.3. Development of Skin Equivalents with Higher Complexity

Skin is a complex organ, comprised of an extensive number of biological factors that influence its homeostasis. This project has focused on replicating some of the most fundamental elements. However, the incorporation of additional components could help to enhance their complexity and provide a better overview of the skin response to external agents.

To screen the efficiency of topical treatments and their biological effects, it would be essential to generate a broad representation of the most habitual skin types (Sarama et al., 2022; Moniz et al., 2020). The use of cells from donors of different age or ethnic groups have already demonstrated to affect the properties of the final skin models. For instance, the use of epidermal cells with Caucasian and African origins has demonstrated to generate different keratinocyte behaviour and epidermal properties (Girardeau-Hubert et al., 2019).

On the other hand, the incorporation of additional cell types like melanocytes, endothelial cells or Langerhans cells could also increase the reliability of the models and allow the assessment of photodamage, immune reactions and product uptake by the blood system, among other studies (Salameh et al., 2021; Thélu et al., 2020; Bernerd & Asselineau, 2008). Besides, the recreation of hair follicles could also improve the current knowledge about drug uptake through the appendageal pathway, which represents an essential entry for ions and large polar molecules which hardly diffuse through the *stratum corneum* (Blickenstaff et al., 2014; Blank & Scheuplein, 1969). Regardless of the number of elements included in the skin equivalent, the models cannot be expected to recreate all the complexity found in the *in vivo* skin. Consequently, they will need to be adapted based on their final application.

One of the main challenges in the production of skin models is the demand for large numbers of different cell types. The use of induced pluripotent stem cells (iPSCs) could be a future solution for securing enough cells for tissue engineering applications. iPSCs allow the obtention of stem cells after reprograming normal cells, offering an unlimited supply of cells (Singh et al., 2015). iPSCs can be differentiated towards various cell types, including fibroblast, keratinocytes, melanocytes and endothelial cells, reducing the dependency on cells from donors (Ohyama & Okano, 2014; Abaci et al., 2016). Additionally, these cells maintain disease-specific genetic changes, which could help to replicate *in vitro* some skin conditions (Khurana et al., 2021; Rowe & Daley, 2019). By incorporating patient-derived cells, it could be possible to analyse the causes of each disease in more detail and their response to specific treatments. Nonetheless, the isolation, expansion and maturation of iPSCs are still complex, and further

research is necessary to make this process time and cost-effective (Doss & Sachinidis, 2019). Another method to reproduce skin conditions and create customised models could be the incorporation of CRISPR/Cas-9. This system has proved to replicate some specific conditions such as albinism by introducing specific mutations into the cells (Seruggia et al., 2020).

Finally, the incorporation of microbiota into the skin models could also become an important future project. Bacteria present in the human skin is one of the first elements in contact with pharmaceutical treatments and cosmetic products, interacting with them and, on some occasions, altering their formulation (Boxberger et al., 2021; Byrd et al., 2018). By printing an outermost layer containing skin microbiota, it could be possible to improve the study of product absorption and the treatment of skin infections (Rademacher et al., 2018).

REFERENCES

Abaci, H. E., Coffman, A., Doucet, Y., Chen, J., Jacków, J., Wang, E., Zongyou, G., Shin, J. U., Jahoda, C. A., Christiano, A. M. (2018). 'Tissue engineering of human hair follicles using a biomimetic developmental approach', *Nature communications*, 9(1), 5301.

Abaci, H.E., Gledhill, K., Guo, Z., Christiano, A.M. & Shuler, M.L. (2015) 'Pumpless microfluidic platform for drug testing on human skin equivalents', *Lab on a chip*, 15(3), p. 882.

Abaci, H.E., Guo, Z., Coffman, A., Gillette, B., Lee, W.H., Sia, S.K. & Christiano, A.M. (2016) 'Human skin constructs with spatially-controlled vasculature using primary and iPSC-derived endothelial cells', *Advanced healthcare materials*, 5(14), p. 1800.

Abd, E., Yousef, S.A., Pastore, M.N., Telaprolu, K., Mohammed, Y.H., Namjoshi, S., Grice, J.E. & Roberts, M.S. (2016) 'Skin models for the testing of transdermal drugs', *Clinical Pharmacology: Advances and Applications*, 8pp. 163-176.

Acevedo, C.A., Somoza, R.A., Weinstein-Oppenheimer, C., Brown, D.I. & Young, M.E. (2010) 'Growth factor production from fibrin-encapsulated human keratinocytes', *Biotechnology Letters*, 32(7), pp. 1011–1017.

Achilli, M. & Mantovani, D. (2010) 'Tailoring Mechanical Properties of Collagen-Based Scaffolds for Vascular Tissue Engineering: The Effects of pH, Temperature and Ionic Strength on Gelation', *Polymers 2010, Vol. 2, Pages 664-680*, 2(4), pp. 664–680.

Achterberg, V.F., Buscemi, L., Diekmann, H., Smith-Clerc, J., Schwengler, H., Meister, J.J., Wenck, H., Gallinat, S. & Hinz, B. (2014) 'The nano-scale mechanical properties of the extracellular matrix regulate dermal fibroblast function', *Journal of Investigative Dermatology*, 134(7), pp. 1862–1872.

Ackermann, K., Lombardi Borgia, S., Korting, H.C., Mewes, K.R. & Schäfer-Korting, M. (2010) 'The Phenion® Full-Thickness Skin Model for Percutaneous Absorption Testing', *Skin Pharmacology and Physiology*, 23(2), pp. 105–112.

Aderibigbe, B.A. & Buyana, B. (2018) 'Alginate in Wound Dressings', *Pharmaceutics*, 10(2).

Adhikari, Jaideep, Roy, Avinava, Das, Anindya, Ghosh, Manojit, Thomas, Sabu, Sinha, Arijit, Kim, Jinku, Saha, Prosenjit, Adhikari, J, Das, A, Sinha, A, Roy, A, Ghosh, M, Thomas, S, Kim, J & Saha, P (2021) 'Effects of Processing Parameters of 3D Bioprinting on the Cellular Activity of Bioinks', *Macromolecular Bioscience*, 21(1), p. 2000179.

Agonia, A.S., Palmeira-de-Oliveira, A., Cardoso, C., Augusto, C., Pellevoisin, C., Videau, C., Dinis-Oliveira, R.J. & Palmeira-de-Oliveira, R. (2022) 'Reconstructed Human Epidermis: An Alternative Approach for In Vitro Bioequivalence Testing of Topical Products', *Pharmaceutics*, 14(8), p. 1554.

Alam, H., Sehgal, L., Kundu, S.T., Dalal, S.N. & Vaidya, M.M. (2011) 'Novel function of keratins 5 and 14 in proliferation and differentiation of stratified epithelial cells', *Molecular Biology of the Cell*, 22(21), p. 4068.

Albanna, M., Binder, K.W., Murphy, S. v., Kim, J., Qasem, S.A., Zhao, W., Tan, J., El-Amin, I.B., Dice, D.D., Marco, J., Green, J., Xu, T., Skardal, A., Holmes, J.H., Jackson, J.D., Atala, A. & Yoo, J.J. (2019) 'In Situ Bioprinting of Autologous Skin Cells Accelerates Wound Healing of Extensive Excisional Full-Thickness Wounds', *Scientific Reports 2019 9:1*, 9(1), pp. 1–15.

Aleemardani, M., Trikić, M.Z., Green, N.H. & Claeyssens, F. (2021) 'The Importance of Mimicking Dermal-Epidermal Junction for Skin Tissue Engineering: A Review', *Bioengineering*, 8(11).

Alépée, N., Grandidier, M.H. & Cotovio, J. (2019) 'Usefulness of the EpiSkin™ reconstructed human epidermis model within Integrated Approaches on Testing and Assessment (IATA) for skin corrosion and irritation', *Toxicology in Vitro*, 54pp. 147–167.

Alépée, N., Hélène, M. & Cotovio, J. (2017) 'Assessment of the Human Epidermis SkinEthic™ RHE Model for In Vitro Skin Corrosion Testing of Chemicals', *Alternatives for Dermal Toxicity Testing*, pp. 143–157.

Alépée, N., Tornier, C., Robert, C., Amsellem, C., Roux, M.H., Doucet, O., Pachot, J., Méloni, M. & de Brugerolle de Fraissinette, A. (2010) 'A catch-up validation study on reconstructed human epidermis (SkinEthic™ RHE) for full replacement of the Draize skin irritation test', *Toxicology in Vitro*, 24(1), pp. 257–266.

Alexaline, M.M., Magne, B., Zuleta Rodríguez, A., Nivet, M., Bacqueville, D., Lataillade, J.J. & Trouillas, M. (2019) 'Influence of fibrin matrices and their released factors on epidermal substitute phenotype and engraftment', *Journal of Tissue Engineering and Regenerative Medicine*, 13(8), pp. 1362–1374.

Ali, N., Hosseini, M., Vainio, S., Taïeb, A., Cario-André, M. & Rezvani, H.R. (2015) 'Skin equivalents: skin from reconstructions as models to study skin development and diseases', *British Journal of Dermatology*, 173(2), pp. 391–403.

Alipal, J., Mohd Pu'ad, N.A.S., Lee, T.C., Nayan, N.H.M., Sahari, N., Basri, H., Idris, M.I. & Abdullah, H.Z. (2021) 'A review of gelatin: Properties, sources, process, applications, and commercialisation', *Materials Today: Proceedings*, 42pp. 240–250.

Almeida, A., Sarmento, B. & Rodrigues, F. (2017) 'Insights on in vitro models for safety and toxicity assessment of cosmetic ingredients', *International Journal of Pharmaceutics*, 519(1–2), pp. 178–185.

Alonso, C., Carrer, V., Espinosa, S., Zanuy, M., Córdoba, M., Vidal, B., Domínguez, M., Godessart, N., Coderch, L. & Pont, M. (2019) 'Prediction of the skin permeability of topical drugs using in silico and in vitro models', *European Journal of Pharmaceutical Sciences*, 136p. 104945.

Amiri, N., Golin, A.P., Jalili, R.B. & Ghahary, A. (2022) 'Roles of cutaneous cell-cell communication in wound healing outcome: An emphasis on keratinocyte-fibroblast crosstalk', *Experimental Dermatology*, 31(4), pp. 475–484.

Amirrah, I.N., Lokanathan, Y., Zulkiflee, I., Wee, M.F.M.R., Motta, A. & Fauzi, M.B. (2022) 'A Comprehensive Review on Collagen Type I Development of Biomaterials for Tissue Engineering: From Biosynthesis to Bioscaffold', *Biomedicines*, 10(9).

Anderson, E.D., Sastalla, I., Earland, N.J., Mahnaz, M., Moore, I.N., Otaizo-Carrasquero, F., Myers, T.G., Myles, C.A., Datta, S.K. & Myles, I.A. (2018) 'Prolonging culture of primary human keratinocytes isolated from suction blisters with the Rho kinase inhibitor Y-27632', *PLoS ONE*, 13(9), pp. 1–16.

Antoine, E.E., Vlachos, P.P. & Rylander, M.N. (2014) 'Review of Collagen I Hydrogels for Bioengineered Tissue Microenvironments: Characterization of Mechanics, Structure, and Transport', *Tissue Engineering. Part B, Reviews*, 20(6), p. 683.

Armengot-Carbo, M., Hernández-Martín & Torrelo, A. (2015) 'The Role of Filaggrin in the Skin Barrier and Disease Development', *Actas Dermo-Sifiliográficas (English Edition)*, 106(2), pp. 86–95.

Asgari, M., Latifi, N., Heris, H.K., Vali, H. & Mongeau, L. (2017) 'In vitro fibrillogenesis of tropocollagen type III in collagen type I affects its relative fibrillar topology and mechanics', *Scientific reports*, 7(1).

Auxenfans, C., Lequeux, C., Perrusel, E., Mojallal, A., Kinikoglu, B. & Damour, O. (2012) 'Adipose-derived stem cells (ASCs) as a source of endothelial cells in the reconstruction of endothelialized skin equivalents', *Journal of Tissue Engineering and Regenerative Medicine*, 6(7), pp. 512–518.

Avci, P., Sadasivam, M., Gupta, A., de Melo, W.C., Huang, Y.Y., Yin, R., Chandran, R., Kumar, R., Otufowora, A., Nyame, T. & Hamblin, M.R. (2013) 'Animal models of skin disease for drug discovery', *Expert opinion on drug discovery*, 8(3), pp. 331–355.

Avery, N.C. & Bailey, A.J. (2008) 'Restraining cross-links responsible for the mechanical properties of collagen fibers: Natural and artificial', *Collagen: Structure and Mechanics*, pp. 81–110.

Avior, Y., Sagi, I. & Benvenisty, N. (2016) 'Pluripotent stem cells in disease modelling and drug discovery', *Nature Reviews Molecular Cell Biology 2016 17:3*, 17(3), pp. 170–182.

Azzarone, B. & Macieira-Coelho, A. (1982) 'Heterogeneity of the kinetics of proliferation within human skin fibroblastic cell populations', *Journal of Cell Science*, 57(1), pp. 177–187.

Bak, S.Y., Lee, S.W., Choi, C.H. & Kim, H.W. (2018) 'Assessment of the Influence of Acetic Acid Residue on Type I Collagen during Isolation and Characterization', *Materials*, 11(12).

Baltazar, T., Merola, J., Catarino, C., Xie, C.B., Kirkiles-Smith, N.C., Lee, V., Hotta, S., Dai, G., Xu, X., Ferreira, F.C., Saltzman, W.M., Pober, J.S. & Karande, P. (2020) 'Three Dimensional Bioprinting of a Vascularized and Perfusable Skin Graft Using Human Keratinocytes, Fibroblasts, Pericytes, and Endothelial Cells', *Tissue Engineering. Part A*, 26(5–6), p. 227.

Banks-Schlegel, S. & Green, H. (1981) 'Involucrin synthesis and tissue assembly by keratinocytes in natural and cultured human epithelia', *The Journal of Cell Biology*, 90(3), p. 732.

Barnes, L.A., Marshall, C.D., Leavitt, T., Hu, M.S., Moore, A.L., Gonzalez, J.G., Longaker, M.T. & Gurtner, G.C. (2018) 'Mechanical Forces in Cutaneous Wound Healing: Emerging Therapies to Minimize Scar Formation', *Advances in Wound Care*, 7(2), p. 47.

Barros, N.R., Kim, H.J., Gouidie, M.J., Lee, K.J., Bandaru, P., Banton, E.A., Sarikhani, E., Sun, W., Zhang, S., Cho, H.J., Hartel, M.C., Ostrovidov, S., Ahadian, S., Hussain, S.M., Ashammakhi, N., Dokmeci, M.R., Herculano, R.D., Lee, J. & Khademhosseini, A. (2021) 'Biofabrication of endothelial cell, dermal fibroblast, and multilayered keratinocyte layers for skin tissue engineering', *Biofabrication*, 13(3), p. 035030.

Beghin, A., Grenci, G., Sahni, G., Guo, S., Rajendiran, H., Delaire, T., Mohamad Raffi, S.B., Blanc, D., de Mets, R., Ong, H.T., Galindo, X., Monet, A., Acharya, V., Racine, V., Levet, F., Galland, R., Sibarita, J.B. & Viasnoff, V. (2022) 'Automated high-speed 3D imaging of organoid cultures with multi-scale phenotypic quantification', *Nature Methods 2022 19:7*, 19(7), pp. 881–892.

Belbachir, K., Noreen, R., Gouspillou, G. & Petibois, C. (2009) 'Collagen types analysis and differentiation by FTIR spectroscopy', *Analytical and Bioanalytical Chemistry*, 395(3), pp. 829–837.

Bellas, E., Seiberg, M., Garlick, J. & Kaplan, D.L. (2012) 'In vitro 3D full thickness skin equivalent tissue model using silk and collagen biomaterials', *Macromolecular bioscience*, 12(12), p. 1627.

Benning, M.J. & Dalgarno, K.W. (2019) *WO2019008373- Printing Apparatus and Method*.

Berg, R.A., Schwartz, M.L. & Crystal, R.G. (1980) 'Regulation of the production of secretory proteins: Intracellular degradation of newly synthesized "defective" collagen', *Proceedings of the National Academy of Sciences of the United States of America*, 77(8), p. 4746.

Bernard, F.X., Barrault, C., Deguercy, A., de Wever, B. & Rosdy, M. (2000) 'Development of a highly sensitive in vitro phototoxicity assay using the SkinEthic™ reconstructed human epidermis', *Cell Biology and Toxicology*, 16(6), pp. 391–400.

Bernerd, F. & Asselineau, D. (2008) 'An organotypic model of skin to study photodamage and photoprotection in vitro', *Journal of the American Academy of Dermatology*, 58(5 SUPPL. 2), pp. S155–S159.

Bernstam, L.I., Vaughan, F.L. & Bernstein, I.A. (1986) 'Keratinocytes grown at the air-liquid interface', *In Vitro Cellular and Developmental Biology - Animal*, 22(12), pp. 695–705.

Bessou, S., Cario-Andre, M., Gontier, E., Maresca, V., Picardo, M. & Taieb, A. (1999) 'The reconstructed epidermis with melanocytes: a new tool to study pigmentation and photoprotection', *Cellular Molecular Biology*, 45(7), pp. 931–942.

Bigi, A., Panzavolta, S. & Rubini, K. (2004) 'Relationship between triple-helix content and mechanical properties of gelatin films', *Biomaterials*, 25(25), pp. 5675–5680.

Bikle, D.D., Xie, Z. & Tu, C.L. (2012) 'Calcium regulation of keratinocyte differentiation', *Expert review of endocrinology & metabolism*, 7(4), p. 461.

Bishop, E.S., Mostafa, S., Pakvasa, M., Luu, H.H., Lee, M.J., Wolf, J.M., Ameer, G.A., He, T.C. & Reid, R.R. (2017) '3-D bioprinting technologies in tissue engineering and regenerative medicine: Current and future trends', *Genes & Diseases*, 4(4), pp. 185–195.

Black, A.F., Bouez, C., Perrier, E., Schlotmann, K., Chapuis, F. & Damour, O. (2005) 'Optimization and Characterization of an Engineered Human Skin Equivalent', *https://home.liebertpub.com/ten*, 11(5–6), pp. 723–733.

Blank, I.H. & Scheuplein, Robert.J. (1969) 'Transport into and within the skin', *British Journal of Dermatology*, 81pp. 4–10.

Blickenstaff, N.R., Coman, G., Blattner, C.M., Andersen, R. & Maibach, H.I. (2014) 'Biology of percutaneous penetration', *Reviews on Environmental Health*, 29(3), pp. 145–155.

Boehnke, K., Mirancea, N., Pavesio, A., Fusenig, N.E., Boukamp, P. & Stark, H.J. (2007) 'Effects of fibroblasts and microenvironment on epidermal regeneration and tissue function in long-term skin equivalents', *European Journal of Cell Biology*, 86(11–12), pp. 731–746.

Boelsma, Susan Gibbs, Maria Ponec, E. (1998) 'Expression of skin-derived antileukoproteinase (SKALP) in reconstructed human epidermis and its value as a marker for skin irritation', *Acta Dermato-Venereologica*, 78(2), pp. 107–113.

Boontheekul, T., Kong, H.J. & Mooney, D.J. (2005) 'Controlling alginate gel degradation utilizing partial oxidation and bimodal molecular weight distribution', *Biomaterials*, 26(15), pp. 2455–2465.

Borowiec, A.S., Delcourt, P., Dewailly, E. & Bidaux, G. (2013) 'Optimal Differentiation of In Vitro Keratinocytes Requires Multifactorial External Control', *PLOS ONE*, 8(10), p. e77507.

Bott, K., Upton, Z., Schrobback, K., Ehrbar, M., Hubbell, J.A., Lutolf, M.P. & Rizzi, S.C. (2010) 'The effect of matrix characteristics on fibroblast proliferation in 3D gels', *Biomaterials*, 31(32), pp. 8454–8464.

Bouwstra, J.A., Groenink, H.W.W., Kempenaar, J.A., Romeijn, S.G. & Ponec, M. (2008) 'Water Distribution and Natural Moisturizer Factor Content in Human Skin Equivalents Are Regulated by Environmental Relative Humidity', *Journal of Investigative Dermatology*, 128(2), pp. 378–388.

Bouwstra, J.A., Helder, R.W.J. & el Ghalbzouri, A. (2021) 'Human skin equivalents: Impaired barrier function in relation to the lipid and protein properties of the stratum corneum', *Advanced Drug Delivery Reviews*, 175p. 113802.

Bouwstra, J.A. & Ponec, M. (2006) 'The skin barrier in healthy and diseased state', *Biochimica et Biophysica Acta (BBA) - Biomembranes*, 1758(12), pp. 2080–2095.

Boxberger, M., Cenizo, V., Cassir, N. & la Scola, B. (2021) 'Challenges in exploring and manipulating the human skin microbiome', *Microbiome 2021 9:1*, 9(1), pp. 1–14.

Brenner, M. & Hearing, V.J. (2008) 'The Protective Role of Melanin Against UV Damage in Human Skin', *Photochemistry and photobiology*, 84(3), p. 539.

Brohem, C.A., da Silva Cardeal, L.B., Tiago, M., Soengas, M.S., de Moraes Barros, S.B. & Maria-Engler, S.S. (2011) 'Artificial Skin in Perspective: Concepts and Applications', *Pigment cell & melanoma research*, 24(1), p. 35.

Brown, T.M. & Krishnamurthy, K. (2022) 'Histology, Dermis', *StatPearls*,

Brunel, L.G., Hull, S.M. & Heilshorn, S.C. (2022) 'Engineered assistive materials for 3D bioprinting: support baths and sacrificial inks', *Biofabrication*, 14(3), p. 032001.

Buckley, M.R., Evans, E.B., Matuszewski, P.E., Chen, Y.L., Satchel, L.N., Elliott, D.M., Soslowsky, L.J. & Dodge, G.R. (2013) 'Distributions of Types I, II and III Collagen by Region in the Human Supraspinatus Tendon', *Connective tissue research*, 54(6), p. 374.

Burlew, B.S. & Weber, K.T. (2000) 'Connective Tissue and The Heart: Functional Significance and Regulatory Mechanisms', *Cardiology Clinics*, 18(3), pp. 435–442.

Byrd, A.L., Belkaid, Y. & Segre, J.A. (2018) 'The human skin microbiome', *Nature Reviews Microbiology 2018 16:3*, 16(3), pp. 143–155.

Caddeo, S., Boffito, M. & Sartori, S. (2017) 'Tissue engineering approaches in the design of healthy and pathological in vitro tissue models', *Frontiers in Bioengineering and Biotechnology*, 5(AUG), p. 40.

Caley, M.P., Martins, V.L.C. & O'Toole, E.A. (2015) 'Metalloproteinases and Wound Healing', *Advances in Wound Care*, 4(4), p. 225.

Caliari, S.R. & Burdick, J.A. (2016) 'A Practical Guide to Hydrogels for Cell Culture', *Nature methods*, 13(5), p. 405.

Candi, E., Schmidt, R. & Melino, G. (2005) 'The cornified envelope: a model of cell death in the skin', *Nature Reviews Molecular Cell Biology 2005 6:4*, 6(4), pp. 328–340.

Capallere, C., Plaza, C., Meyrignac, C., Arcioni, M., Brulas, M., Busuttil, V., Garcia, I., Bauza, É. & Botto, J.M. (2018) 'Property characterization of reconstructed human epidermis equivalents, and performance as a skin irritation model', *Toxicology in Vitro*, 53pp. 45–56.

Carlson, M.W., Alt-Holland, A., Egles, C. & Garlick, J.A. (2008) 'Three-Dimensional Tissue Models of Normal and Diseased Skin', *Current protocols in cell biology,* 41.

Chang, R., Nam, J. & Sun, W. (2008) 'Effects of Dispensing Pressure and Nozzle Diameter on Cell Survival from Solid Freeform Fabrication–Based Direct Cell Writing', *https://home.liebertpub.com/tea*, 14(1), pp. 41–48.

Chapman, S., McDermott, D.H., Shen, K., Jang, M.K. & McBride, A.A. (2014) 'The effect of Rho kinase inhibition on long-term keratinocyte proliferation is rapid and conditional', *Stem Cell Research and Therapy*, 5(2).

Chen, H., Zhang, Y., Zhou, D., Ma, X., Yang, S. & Xu, T. (2022) 'Mechanical engineering of hair follicle regeneration by in situ bioprinting', *Biomaterials Advances*, 142p. 213127.

Chiba, H., Osanai, M., Murata, M., Kojima, T. & Sawada, N. (2008) 'Transmembrane proteins of tight junctions', *Biochimica et Biophysica Acta (BBA) - Biomembranes*, 1778(3), pp. 588–600.

Chopin-Doroteo, M., Mandujano-Tinoco, E.A. & Krötzsch, E. (2021) 'Tailoring of the rheological properties of bioinks to improve bioprinting and bioassembly for tissue replacement', *Biochimica et Biophysica Acta (BBA) - General Subjects*, 1865(2), p. 129782.

Clayton, K., Vallejo, A.F., Davies, J., Sirvent, S. & Polak, M.E. (2017) 'Langerhans cells-programmed by the epidermis', *Frontiers in Immunology*, 8(NOV), p. 1676.

Clark, R.A.F. (2005) 'Fibrin sealant in wound repair: a systematic survey of the literature', *Expert Opinion on Investigational Drugs*, 9(10), pp. 2371–2392.

Clark, R.A.F., Lanigan, J.M., DellaPelle, P., Manseau, E., Dvorak, H.F. & Colvin, R.B. (1982) 'Fibronectin and fibrin provide a provisional matrix for epidermal cell migration during wound reepithelialization', *The Journal of investigative dermatology*, 79(5), pp. 264–269.

Cohen, D.L., Malone, E., Lipson, H. & Bonassar, L.J. (2006) 'Direct Freeform Fabrication of Seeded Hydrogels in Arbitrary Geometries', *Tissue Engineering*, 12(5), pp. 1325–1335.

Cole, M.A., Quan, T., Voorhees, J.J. & Fisher, G.J. (2018) 'Extracellular matrix regulation of fibroblast function: redefining our perspective on skin aging'. Journal of Cell Communication and Signaling 12 (1) p.pp. 35–43.

Concannon, E., Damkat-Thomas, L., Coghlan, P., Greenwood, J.E., Concannon, E., Damkat-Thomas, L., Coghlan, P. & Greenwood, J.E. (2022) 'Role of Skin Substitutes in Burn Wound Reconstruction', *Wound Healing - Recent Advances and Future Opportunities.*

da Conceicao Ribeiro, R. (2019) *Development of Bio-inks for Bioprinting Applications*. [Online]. Newcastle University.

da Conceicao Ribeiro, R., Pal, D., Ferreira, A.M., Gentile, P., Benning, M. & Dalgarno, K. (2018) 'Reactive jet impingement bioprinting of high cell density gels for bone microtissue fabrication', *Biofabrication*, 11(1), p. 015014.

Contard, P., Bartel, R.L., Jacobs, L., Perlish, J.S., MacDonald, E.D., Handler, L., Cone, D. & Fleischmajer, R. (1993) 'Culturing Keratinocytes and Fibroblasts in a Three-Dimensional Mesh Results in Epidermal Differentiation and Formation of a Basal Lamina-Anchoring Zone', *Journal of Investigative Dermatology*, 100(1), pp. 35–39.

Cooke, M.E. & Rosenzweig, D.H. (2021) 'The rheology of direct and suspended extrusion bioprinting', *APL Bioengineering*, 5(1), p. 011502.

Correa, S., Grosskopf, A.K., Lopez Hernandez, H., Chan, D., Yu, A.C., Stapleton, L.M. & Appel, E.A. (2021) 'Translational Applications of Hydrogels', *Chemical Reviews*, 121(18), pp. 11385–11457.

Correia, C.R., Nadine, S. & Mano, J.F. (2020) 'Cell Encapsulation Systems Toward Modular Tissue Regeneration: From Immunoisolation to Multifunctional Devices', *Advanced Functional Materials*, 30(26), p. 1908061.

Cubo, N., Garcia, M., del Cañizo, J.F., Velasco, D. & Jorcano, J.L. (2016) '3D bioprinting of functional human skin: production and in vivo analysis', *Biofabrication*, 9(1), p. 015006.

Currie, L.J., Martin, R., Sharpe, J.R. & James, S.E. (2003) 'A comparison of keratinocyte cell sprays with and without fibrin glue', *Burns*, 29(7), pp. 677–685.

Currie, L.J., Sharpe, J.R. & Martin, R. (2001) 'The use of fibrin glue in skin grafts and tissue-engineered skin replacements: a review.', *Plastic and Reconstructive Surgery*, 108(6), pp. 1713–1726.

Daamen, W.F., Veerkamp, J.H., van Hest, J.C.M. & van Kuppevelt, T.H. (2007) 'Elastin as a biomaterial for tissue engineering', *Biomaterials*, 28(30), pp. 4378–4398.

Daly, A.C., Davidson, M.D. & Burdick, J.A. (2021) '3D bioprinting of high cell-density heterogeneous tissue models through spheroid fusion within self-healing hydrogels', *Nature Communications 2021 12:1*, 12(1), pp. 1–13.

Danilenko, D.M., Phillips, G.D.L. & Diaz, D. (2016) 'In Vitro Skin Models and Their Predictability in Defining Normal and Disease Biology, Pharmacology, and Toxicity', *Toxicologic Pathology*, 44(4), pp. 555–563.

Decante, G., Costa, J.B., Silva-Correia, J., Collins, M.N., Reis, R.L. & Oliveira, J.M. (2021) 'Engineering bioinks for 3D bioprinting', *Biofabrication*, 13(3), p. 032001.

Dellambra**,** E., Odorisio, T., D'Arcangelo, D., Failla, C.M. & Facchiano, A. (2019) 'Non-animal models in dermatological research', *ALTEX*, 36(2), pp. 177–202.

Deo, P.N. & Deshmukh, R. (2018) 'Pathophysiology of keratinization', *Journal of Oral and Maxillofacial Pathology : JOMFP*, 22(1), p. 86.

Derakhshanfar, S., Mbeleck, R., Xu, K., Zhang, X., Zhong, W. & Xing, M. (2018) '3D bioprinting for biomedical devices and tissue engineering: A review of recent trends and advances', *Bioactive Materials*, 3(2), pp. 144–156.

Derby, B. (2010) 'Inkjet Printing of Functional and Structural Materials: Fluid Property Requirements, Feature Stability, and Resolution', *https://doi.org/10.1146/annurev-matsci-070909-104502*, 40pp. 395–414.

DermNet New Zealand Trust. (2022) *DermNet | Dermatology Resource*. [Online] [online]. Available from: https://dermnetnz.org/ (Accessed 19 November 2022).

Derr, K., Zou, J., Luo, K., Song, M.J., Sittampalam, G.S., Zhou, C., Michael, S., Ferrer, M. & Derr, P. (2019) 'Fully Three-Dimensional Bioprinted Skin Equivalent Constructs with Validated Morphology and Barrier Function', *Tissue Engineering. Part C, Methods*, 25(6), p. 334.

Desanlis, A., Albouy, M., Rousselle, P., Thépot, A., Santos, M. dos, Auxenfans, C. & Marquette, C. (2021) 'Validation of an implantable bioink using mechanical extraction of human skin cells: First steps to a 3D bioprinting treatment of deep second degree burn', *Journal of Tissue Engineering and Regenerative Medicine*, 15(1), pp. 37–48.

Deshmukh, G.R., Kumar, K.H., Reddy, P.V.S. & Rao, B.S. (2012) 'In vitro skin corrosion: Human skin model test – A validation study', *Toxicology in Vitro*, 26(6), pp. 1072–1074.

Deyrieux, A.F. & Wilson, V.G. (2007) 'In vitro culture conditions to study keratinocyte differentiation using the HaCaT cell line', *Cytotechnology*, 54(2), p. 77.

Dixit, S., Baganizi, D.R., Sahu, R., Dosunmu, E., Chaudhari, A., Vig, K., Pillai, S.R., Singh, S.R. & Dennis, V.A. (2017) 'Immunological challenges associated with artificial skin grafts: available solutions and stem cells in future design of synthetic skin', *Journal of Biological Engineering 2017 11:1*, 11(1), pp. 1–23.

Doolin, M.T., Smith, I.M. & Stroka, K.M. (2021) 'Fibroblast to myofibroblast transition is enhanced by increased cell density', *Molecular biology of the cell*, 32(22).

Dos Santos, J. F., Freitas-Marchi, B. L., Reigado, G. R., de Assis, S. R., Maria Engler, S. S., Chambergo Alcalde, F. S., & Nunes, V. A. (2023). 'Mesenchymal stem cells express epidermal markers in an in vitro reconstructed human skin model'. *Frontiers in Cell and Developmental Biology*, 10, 1012637.

Doss, M.X. & Sachinidis, A. (2019) 'Current Challenges of iPSC-Based Disease Modeling and Therapeutic Implications', *Cells*, 8(5).

Dou, C., Perez, V., Qu, J., Tsin, A., Xu, B. & Li, J. (2021) 'A State-of-the-Art Review of Laser-Assisted Bioprinting and its Future Research Trends', *ChemBioEng Reviews*, 8(5), pp. 517–534.

Dovedytis, M., Liu, Z.J. & Bartlett, S. (2020) 'Hyaluronic acid and its biomedical applications: A review', *Engineered Regeneration*, 1pp. 102–113.

Doyle, J.W., Roth, T.P., Smith, R.M., Li, Y.Q. & Dunn, R.M. (1996) 'Effects of calcium alginate on cellular wound healing processes modeled in vitro', *Journal of Biomedical Materials Research*, 32(4), pp. 561–568.

Dragoo, J.L., Shapiro, S.A., Bradsell, H. & Frank, R.M. (2021) 'The essential roles of human adipose tissue: Metabolic, thermoregulatory, cellular, and paracrine effects', *Journal of Cartilage & Joint Preservation*, 1(3), p. 100023.

Drozdoff, V. & Pledger, W.J. (1993) 'Commitment to differentiation and expression of early differentiation markers in murine keratinocytes in vitro are regulated independently of extracellular calcium concentrations', *The Journal of Cell Biology*, 123(4), p. 909.

D'Souza, T., Langer, J. & Willstaedt, T. (2017) 'RAFT ™ 3D Cell Culture System Provides a Versatile Platform for Co-Culture and Barrier Models', *Lonza - BioScience Solutions.*

Duarte Campos, D.F., Rohde, M., Ross, M., Anvari, P., Blaeser, A., Vogt, M., Panfil, C., Yam, G.H.F., Mehta, J.S., Fischer, H., Walter, P. & Fuest, M. (2019) 'Corneal bioprinting utilizing collagen-based bioinks and primary human keratocytes', *Journal of Biomedical Materials Research Part A*, 107(9), pp. 1945–1953.

Dudman, J.P.R., Ferreira, A.M., Gentile, P., Wang, X., Ribeiro, R.D.C., Benning, M. & Dalgarno, K.W. (2020) 'Reliable inkjet printing of chondrocytes and MSCs using reservoir agitation', *Biofabrication*, 12(4), p. 045024.

Dupont, S., Morsut, L., Aragona, M., Enzo, E., Giulitti, S., Cordenonsi, M., Zanconato, F., le Digabel, J., Forcato, M., Bicciato, S., Elvassore, N. & Piccolo, S. (2011) 'Role of YAP/TAZ in mechanotransduction', *Nature 2011 474:7350*, 474(7350), pp. 179–183.

Dura, G., Peters, D.T., Waller, H., Yemm, A.I., Perkins, N.D., Ferreira, A.M., Crespo-Cuadrado, M., Lakey, J.H. & Fulton, D.A. (2020) 'A Thermally Reformable Protein Polymer', *Chem*, 6(11), pp. 3132–3151.

D'Urso, M. & Kurniawan, N.A. (2020) 'Mechanical and Physical Regulation of Fibroblast–Myofibroblast Transition: From Cellular Mechanoresponse to Tissue Pathology', *Frontiers in Bioengineering and Biotechnology*, 8p. 1459.

Edqvist, P.H.D., Fagerberg, L., Hallström, B.M., Danielsson, A., Edlund, K., Uhlén, M. & Pontén, F. (2015) 'Expression of Human Skin-Specific Genes Defined by Transcriptomics and Antibody-Based Profiling', *Journal of Histochemistry and Cytochemistry*, 63(2), p. 129.

El-Ghalbzouri, A., Gibbs, S., Lamme, E., van Blitterswijk, C.A. & Ponec, M. (2002) 'Effect of fibroblasts on epidermal regeneration', *British Journal of Dermatology*, 147(2), pp. 230–243.

Elkaseer, A., Schneider, S., Deng, Y. & Scholz, S.G. (2022) 'Effect of Process Parameters on the Performance of Drop-On-Demand 3D Inkjet Printing: Geometrical-Based Modeling and Experimental Validation', *Polymers*, 14(13).

Emmermacher, J., Spura, D., Cziommer, J., Kilian, D., Wollborn, T., Fritsching, U., Steingroewer, J., Walther, T., Gelinsky, M. & Lode, A. (2020) 'Engineering considerations on extrusion-based bioprinting: interactions of material behavior, mechanical forces and cells in the printing needle', *Biofabrication*, 12(2), p. 025022.

European Commission (2019) *Ban on animal testing*. [Online] [online]. Available from: https://single-market-economy.ec.europa.eu/sectors/cosmetics/ban-animal-testing_en (Accessed 26 May 2022).

Fatimah, S.S., Chua, K., Tan, G.C., Azmi, T.I., Tan, A.E. & Rahman, H.A. (2013) 'Organotypic culture of human amnion cells in air-liquid interface as a potential substitute for skin regeneration', *Cytotherapy*, 15(8), pp. 1030–1041.

Fay, C.D. (2020) 'Computer-Aided Design and Manufacturing (CAD/CAM) for Bioprinting', *Methods in Molecular Biology*, 2140pp. 27–41.

Fenner, J. & Clark, R.A.F. (2016) ‘Chapter 1 - Anatomy, Physiology, Histology, and Immunohistochemistry of Human Skin’, in Mohammad Z Albanna & James H Holmes IV (eds.) *Skin Tissue Engineering and Regenerative Medicine*. [Online]. Boston: Academic Press. pp. 1–17.

Fentem, J.H. & Botham, P.A. (2019) ‘ECVAM’s Activities in Validating Alternative Tests for Skin Corrosion and Irritation’, *https://doi.org/10.1177/026119290203002S09*, 30(SUPPL. 2), pp. 61–67.

Ferrari, E., Palma, C., Vesentini, S., Occhetta, P. & Rasponi, M. (2020) ‘Integrating Biosensors in Organs-on-Chip Devices: A Perspective on Current Strategies to Monitor Microphysiological Systems’, *Biosensors*, 10(9).

Filaire, E., Nachat-Kappes, R., Laporte, C., Harmand, M.F., Simon, M. & Poinsot, C. (2022) ‘Alternative in vitro models used in the main safety tests of cosmetic products and new challenges’, *International Journal of Cosmetic Science*, 44(6), pp. 604–613.

Fitt, W.K. & Costley, K. (1998) ‘The role of temperature in survival of the polyp stage of the tropical rhizostome jellyfish Cassiopea xamachana’, *Journal of Experimental Marine Biology and Ecology*, 222(1–2), pp. 79–91.

Fitzgerald, K.A., Malhotra, M., Curtin, C.M., O’Brien, F.J. & O’Driscoll, C.M. (2015) ‘Life in 3D is never flat: 3D models to optimise drug delivery’, *Journal of Controlled Release*, 215pp. 39–54.

Flamand, N., Marrot, L., Belaidi, J.P., Bourouf, L., Dourille, E., Feltes, M. & Meunier, J.R. (2006) ‘Development of genotoxicity test procedures with Episkin, a reconstructed human skin model: towards new tools for in vitro risk assessment of dermally applied compounds?’, *Mutation research*, 606(1–2), pp. 39–51.

Flaten, G.E., Palac, Z., Engesland, A., Filipović-Grčić, J., Vanić, Ž. & Škalko-Basnet, N. (2015) ‘In vitro skin models as a tool in optimization of drug formulation’, *European Journal of Pharmaceutical Sciences*, 75pp. 10–24.

Fleischmajer, R., Schechter, A., Bruns, M., Perlish, J.S., MacDonald, E.D., Pan, T.C., Timpl, R. & Chu, M.L. (1995) ‘Skin Fibroblasts Are the Only Source of Nidogen During Early Basal Lamina Formation In Vitro’, *Journal of Investigative Dermatology*, 105(4), pp. 597–601.

Fligiel, S.E.G., Varani, J., Datta, S.C., Kang, S., Fisher, G.J. & Voorhees, J.J. (2003) 'Collagen degradation in aged/photodamaged skin in vivo and after exposure to matrix metalloproteinase-1 in vitro', *Journal of Investigative Dermatology*, 120(5), pp. 842–848.

Frantz, C., Stewart, K.M. & Weaver, V.M. (2010) 'The extracellular matrix at a glance', *Journal of Cell Science*, 123(24), pp. 4195–4200.

Fratzl, P. (2008) 'Collagen: Structure and mechanics, an introduction', in *Collagen: Structure and Mechanics*. [Online]. Springer US. pp. 1–13.

Freedberg, I.M., Tomic-Canic, M., Komine, M. & Blumenberg, M. (2001) 'Keratins and the Keratinocyte Activation Cycle', *Journal of Investigative Dermatology*, 116(5), pp. 633–640.

Fromm, J.E. (1984) 'Numerical Calculations of the Fluid Dynamics of Drop-on-Demand Jets.', *IBM Journal of Research and Development*, 28(3), pp. 322–333.

Fuchs, P.Ö., Calitz, C., Pavlović, N., Binet, F., Solbak, S.M.Ø., Danielson, U.H., Kreuger, J., Heindryckx, F. & Gerwins, P. (2020) 'Fibrin fragment E potentiates TGF-β-induced myofibroblast activation and recruitment', *Cellular Signalling*, 72p. 109661.

Galli, S.J. & Tsai, M. (2010) 'Mast cells in allergy and infection: Versatile effector and regulatory cells in innate and acquired immunity', *European journal of immunology*, 40(7), p. 1843.

Gangatirkar, P., Paquet-Fifield, S., Li, A., Rossi, R. & Kaur, P. (2007) 'Establishment of 3D organotypic cultures using human neonatal epidermal cells', *Nature Protocols 2007 2:1*, 2(1), pp. 178–186.

Garnero, P. (2015) 'The Role of Collagen Organization on the Properties of Bone', *Calcified Tissue International*, 97(3), pp. 229–240.

Geer, D.J., Swartz, D.D. & Andreadis, S.T. (2004) 'Fibrin Promotes Migration in a Three-Dimensional in Vitro Model of Wound Regeneration', *https://home.liebertpub.com/ten*, 8(5), pp. 787–798.

van Gele, M., Geusens, B., Brochez, L., Speeckaert, R. & Lambert, J. (2011) 'Three-dimensional skin models as tools for transdermal drug delivery: challenges and limitations', *Expert Opinion on Drug Delivery*, 8(6), pp. 705–720.

Georgiadis, M., Müller, R. & Schneider, P. (2016) 'Techniques to assess bone ultrastructure organization: orientation and arrangement of mineralized collagen fibrils', *Journal of The Royal Society Interface*, 13(119), .

Ghaffari, A., Kilani, R.T. & Ghahary, A. (2009) 'Keratinocyte-Conditioned Media Regulate Collagen Expression in Dermal Fibroblasts', *Journal of Investigative Dermatology*, 129(2), pp. 340–347.

GhavamiNejad, A., Ashammakhi, N., Wu, X.Y. & Khademhosseini, A. (2020) 'Crosslinking Strategies for Three-Dimensional Bioprinting of Polymeric Hydrogels', *Small (Weinheim an der Bergstrasse, Germany)*, 16(35), p. e2002931.

Ghetti, M., Topouzi, H., Theocharidis, G., Papa, V., Williams, G., Bondioli, E., Cenacchi, G., Connelly, J.T. & Higgins, C.A. (2018) 'Subpopulations of dermal skin fibroblasts secrete distinct extracellular matrix: implications for using skin substitutes in the clinic', *The British Journal of Dermatology*, 179(2), p. 381.

Girardeau-Hubert, S., Deneuville, C., Pageon, H., Abed, K., Tacheau, C., Cavusoglu, N., Donovan, M., Bernard, D. & Asselineau, D. (2019) 'Reconstructed Skin Models Revealed Unexpected Differences in Epidermal African and Caucasian Skin', *Scientific Reports 2019 9:1*, 9(1), pp. 1–12.

Govaere, O., Komuta, M., Berkers, J., Spee, B., Janssen, C., de Luca, F., Katoonizadeh, A., Wouters, J., van Kempen, L.C., Durnez, A., Verslype, C., de Kock, J., Rogiers, V., van Grunsven, L.A., Topal, B., Pirenne, J., Vankelecom, H., Nevens, F., van den Oord, J., et al. (2014) 'Original article: Keratin 19: a key role player in the invasion of human hepatocellular carcinomas', *Gut*, 63(4), p. 674.

Grant, C.A., Brockwell, D.J., Radford, S.E. & Thomson, N.H. (2009) 'Tuning the Elastic Modulus of Hydrated Collagen Fibrils', *Biophysical Journal*, 97(11), p. 2985.

Grebenyuk, S. & Ranga, A. (2019) 'Engineering Organoid Vascularization', *Frontiers in Bioengineering and Biotechnology*, 7(MAR), p. 39.

Greenwood, J.E. (2016) 'Chapter 10 - Hybrid Biomaterials for Skin Tissue Engineering', in Mohammad Z Albanna & James H Holmes IV (eds.) *Skin Tissue Engineering and Regenerative Medicine*. [Online]. Boston: Academic Press. pp. 185–210.

Grinnell, F. (2000) 'Fibroblast-collagen-matrix contraction: growth-factor signalling and mechanical loading', *Trends in Cell Biology*, 10(9), pp. 362–365.

Grinnell, F. & Petroll, W.M. (2010) 'Cell Motility and Mechanics in Three-Dimensional Collagen Matrices', *Annual Review of Cell and Developmental Biology,* 26pp. 335–361.

Groeber, F., Holeiter, M., Hampel, M., Hinderer, S. & Schenke-Layland, K. (2011) 'Skin tissue engineering--in vivo and in vitro applications', *Advanced drug delivery reviews*, 63(4–5), pp. 352–366.

Gruene, M., Pflaum, M., Deiwick, A., Koch, L., Schlie, S., Unger, C., Wilhelmi, M., Haverich, A., & Chichkov, B. N. (2011). 'Adipogenic differentiation of laser-printed 3D tissue grafts consisting of human adipose-derived stem cells', *Biofabrication*, 3(1), 015005.

Gudapati, H., Dey, M. & Ozbolat, I. (2016) 'A comprehensive review on droplet-based bioprinting: Past, present and future', *Biomaterials*, 102pp. 20–42.

Gugerell, A., Schossleitner, K., Wolbank, S., Nürnberger, S., Redl, H., Gulle, H., Goppelt, A., Bittner, M. & Pasteiner, W. (2012) 'High thrombin concentrations in fibrin sealants induce apoptosis in human keratinocytes', *Journal of Biomedical Materials Research Part A*, 100A(5), pp. 1239–1247.

Guillemot, F., Souquet, A., Catros, S. & Guillotin, B. (2010) 'Laser-assisted cell printing: principle, physical parameters versus cell fate and perspectives in tissue engineering', *Nanomedicine*, 5(3), pp. 507–515.

Guillotin, B., Souquet, A., Catros, S., Duocastella, M., Pippenger, B., Bellance, S., Bareille, R., Rémy, M., Bordenave, L., Amédée j, J. & Guillemot, F. (2010) 'Laser assisted bioprinting of engineered tissue with high cell density and microscale organization', *Biomaterials*, 31(28), pp. 7250–7256.

Gungor-Ozkerim, P.S., Inci, I., Zhang, Y.S., Khademhosseini, A. & Dokmeci, M.R. (2018) 'Bioinks for 3D bioprinting: an overview', *Biomaterials science*, 6(5), p. 915.

Guo, M., Toda, K.I. & Grinnell, F. (1990) 'Activation of human keratinocyte migration on type I collagen and fibronectin', *Journal of Cell Science*, 96(2), pp. 197–205.

Guth, K., Schäfer-Korting, M., Fabian, E., Landsiedel, R. & van Ravenzwaay, B. (2015) 'Suitability of skin integrity tests for dermal absorption studies in vitro', *Toxicology in Vitro*, 29(1), pp. 113–123.

Hakimi, N., Cheng, R., Leng, L., Sotoudehfar, M., Ba, P.Q., Bakhtyar, N., Amini-Nik, S., Jeschke, M.G. & Günther, A. (2018) 'Handheld Skin Printer: In-Situ Formation of Planar Biomaterials and Tissues', *Lab on a chip*, 18(10), p. 1440.

Hampton, S. (2004) 'The role of alginate dressings in wound healing', *The Diabetic Foot*, 7(4), pp. 162–167.

Harvima, I.T., Lappalainen, K., Hirvonen, M.R., Mättö, M., Kivinen, P.K., Hyttinen, M., Pelkonen, J. & Naukkarinen, A. (2004) 'Heparin modulates the growth and adherence and augments the growth-inhibitory action of TNF-α on cultured human keratinocytes', *Journal of Cellular Biochemistry*, 92(2), pp. 372–386.

Hashimoto, K., Badarla, V.R., Kawai, A. & Ideguchi, T. (2019) 'Complementary vibrational spectroscopy', *Nature Communications 2019 10:1*, 10(1), pp. 1–6.

Hausmann, C., Vogt, A., Kerscher, M., Ghoreschi, K., Schäfer-Korting, M. & Zoschke, C. (2020) 'Optimizing skin pharmacotherapy for older patients: the future is at hand but are we ready for it?', *Drug Discovery Today*, 25(5), pp. 851–861.

Hausmann, C., Zoschke, C., Wolff, C., Darvin, M.E., Sochorová, M., Kováčik, A., Wanjiku, B., Schumacher, F., Tigges, J., Kleuser, B., Lademann, J., Fritsche, E., Vávrová, K., Ma, N. & Schäfer-Korting, M. (2019) 'Fibroblast origin shapes tissue homeostasis, epidermal differentiation, and drug uptake', *Scientific Reports 2019 9:1*, 9(1), pp. 1–10.

Haydont, V., Neiveyans, V., Perez, P., Busson, É., Lataillade, J.J., Asselineau, D. & Fortunel, N.O. (2020) 'Fibroblasts from the Human Skin Dermo-Hypodermal Junction are Distinct from Dermal Papillary and Reticular Fibroblasts and from Mesenchymal Stem Cells and Exhibit a Specific Molecular Profile Related to Extracellular Matrix Organization and Modeling', *Cells*, 9(2), p. 368.

Hegde, A., Ananthan, A.S., Kashyap, C. & Ghosh, S. (2021) 'Wound Healing by Keratinocytes: A Cytoskeletal Perspective', *Journal of the Indian Institute of Science*, 101(1), pp. 73–80.

Heher, P., Mühleder, S., Mittermayr, R., Redl, H. & Slezak, P. (2018) 'Fibrin-based delivery strategies for acute and chronic wound healing', *Advanced Drug Delivery Reviews*, 129pp. 134–147.

Heino, J. (2002) 'Keratinocyte Interactions with Fibronectin During Wound Healing', *Cell Invasion*, pp. 52–74.

Helary, C., Foucault-Bertaud, A., Godeau, G., Coulomb, B. & Giraud Guille, M.M. (2005) 'Fibroblast populated dense collagen matrices: cell migration, cell density and metalloproteinases expression', *Biomaterials*, 26(13), pp. 1533–1543.

Hersel, U., Dahmen, C. & Kessler, H. (2003) 'RGD modified polymers: biomaterials for stimulated cell adhesion and beyond', *Biomaterials*, 24(24), pp. 4385–4415.

Highley, C.B., Rodell, C.B. & Burdick, J.A. (2015) 'Direct 3D Printing of Shear-Thinning Hydrogels into Self-Healing Hydrogels', *Advanced Materials*, 27(34), pp. 5075–5079.

Hill, D.S., Robinson, N.D.P., Caley, M.P., Chen, M., O'Toole, E.A., Armstrong, J.L., Przyborski, S. & Lovat, P.E. (2015) 'A novel fully-humanised 3D skin equivalent to model early melanoma invasion', *Molecular cancer therapeutics*, 14(11), p. 2665.

Holder, A.J., Badiei, N., Hawkins, K., Wright, C., Williams, P.R. & Curtis, D.J. (2018) 'Control of collagen gel mechanical properties through manipulation of gelation conditions near the sol-gel transition', *Soft Matter*, 14(4), pp. 574–580.

Holmes, A.M., Creton, S. & Chapman, K. (2010) 'Working in partnership to advance the 3Rs in toxicity testing', *Toxicology*, 267(1–3), pp. 14–19.

Hölzl, K., Lin, S., Tytgat, L., van Vlierberghe, S., Gu, L. & Ovsianikov, A. (2016) 'Bioink properties before, during and after 3D bioprinting', *Biofabrication*, 8(3), p. 032002.

ter Horst, B., Chouhan, G., Moiemen, N.S. & Grover, L.M. (2018) 'Advances in keratinocyte delivery in burn wound care', *Advanced Drug Delivery Reviews*, 123p. 18.

ter Horst, B., Moiemen, N.S. & Grover, L.M. (2019) 'Natural polymers: biomaterials for skin scaffolds', *Biomaterials for Skin Repair and Regeneration*, pp. 151–192.

Horváth, L., Umehara, Y., Jud, C., Blank, F., Petri-Fink, A., & Rothen-Rutishauser, B. (2015). 'Engineering an in vitro air-blood barrier by 3D bioprinting', *Scientific reports*, 5, 7974.

Hosseini, M., Koehler, K.R. & Shafiee, A. (2022) 'Biofabrication of Human Skin with Its Appendages', *Advanced Healthcare Materials*, 11(22), p. 2201626.

Hourd, P., Medcalf, N., Segal, J. & Williams, D.J. (2015) 'A 3D bioprinting exemplar of the consequences of the regulatory requirements on customized processes', *Regenerative Medicine*, 10(7), pp. 863–883.

Ignatov, B., Zhuravleva, E., Zheng, W., Sortebech, D., Ehrströ, M., Kjellman, P., Eidsmo, L., Lejeune, F., Albouy, M., Forestier, S., Thépot, A., Gendronneau, G., Santos, D., Smith, M.L., Mcbain, A.J. & O'neill, C.A. (2022) 'Tissue-engineered human skin age spot model with individualized hyperpigmentation lesion through high-resolution patterned 3D bioprinting and its use for the evaluation of cosmetic ingredients', *Journal of Investigative Dermatology*, 142(12), p. S271.

Ingber, D.E. (2022) 'Human organs-on-chips for disease modelling, drug development and personalized medicine', *Nature Reviews Genetics 2022 23:8*, 23(8), pp. 467–491.

Isaac, C., Paggiaro, A., Aldunate, J., Herson, M., Altran, S., Mathor, M. & Ferreira, M. (2011) 'Role of keratinocytes in wound contraction: an impact assessment using a model of collagen matrix populated with fibroblasts', *Revista Brasileira de Cirurgia Plástica*, 26(3), pp. 402–406.

van Itallie, C.M. & Anderson, J.M. (2014) 'Architecture of tight junctions and principles of molecular composition', *Seminars in cell & developmental biology*, 0p. 157.

Itoh, M., Umegaki-Arao, N., Guo, Z., Liu, L., Higgins, C.A. & Christiano, A.M. (2013) 'Generation of 3D Skin Equivalents Fully Reconstituted from Human Induced Pluripotent Stem Cells (iPSCs)', *PLOS ONE*, 8(10), p. e77673.

Jacques-Jamin, C., Duplan, H., Rothe, H., Vaillant, O., Eilstein, J., Grégoire, S., Cubberley, R., Lange, D., Ellison, C., Klaric, M., Hewitt, N. & Schepky, A. (2017) 'Comparison of the Skin Penetration of 3 Metabolically Stable Chemicals Using Fresh and Frozen Human Skin', *Skin Pharmacology and Physiology*, 30(5), pp. 234–245.

Jagiełło, A., Castillo, U. & Botvinick, E. (2022) 'Cell mediated remodeling of stiffness matched collagen and fibrin scaffolds', *Scientific Reports 2022 12:1*, 12(1), pp. 1–15.

Janson, D., Saintigny, G., Mahé, C. & Ghalbzouri, A. el (2013) 'Papillary fibroblasts differentiate into reticular fibroblasts after prolonged in vitro culture', *Experimental Dermatology*, 22(1), pp. 48–53.

Janson, D., Saintigny, G., van Adrichem, A., Mahé, C. & el Ghalbzouri, A. (2012) 'Different Gene Expression Patterns in Human Papillary and Reticular Fibroblasts', *Journal of Investigative Dermatology*, 132(11), pp. 2565–2572.

Jepps, O.G., Dancik, Y., Anissimov, Y.G. & Roberts, M.S. (2013) 'Modeling the human skin barrier — Towards a better understanding of dermal absorption', *Advanced Drug Delivery Reviews*, 65(2), pp. 152–168.

Jin, R., Cui, Y., Chen, H., Zhang, Z., Weng, T., Xia, S., Yu, M., Zhang, W., Shao, J., Yang, M., Han, C. & Wang, X. (2021) 'Three-dimensional bioprinting of a full-thickness functional skin model using acellular dermal matrix and gelatin methacrylamide bioink', *Acta Biomaterialia*, 131pp. 248–261.

Joodaki, H. & Panzer, M.B. (2018) 'Skin mechanical properties and modeling: A review', *https://doi.org/10.1177/0954411918759801*, 232(4), pp. 323–343.

Joyce, K., Fabra, G.T., Bozkurt, Y. & Pandit, A. (2021) 'Bioactive potential of natural biomaterials: identification, retention and assessment of biological properties', *Signal Transduction and Targeted Therapy 2021 6:1*, 6(1), pp. 1–28.

Ju, H., Liu, X., Zhang, G., Liu, D. & Yang, Y. (2020) 'Comparison of the Structural Characteristics of Native Collagen Fibrils Derived from Bovine Tendons Using Two Different Methods: Modified Acid-Solubilized and Pepsin-Aided Extraction', *Materials 2020, Vol. 13, Page 358*, 13(2), p. 358.

Kalinin, A., Marekov, L.N. & Steinert, P.M. (2001) 'Assembly of the epidermal cornified cell envelope', *Journal of Cell Science*, 114(17), pp. 3069–3070.

Kandárová, H., Hayden, P., Klausner, M., Kubilus, J., Kearney, P. & Sheasgreen, J. (2009) 'In Vitro Skin Irritation Testing: Improving the Sensitivity of the EpiDerm Skin Irritation Test Protocol', *Alternatives to Laboratory Animals*, 37(6), pp. 671–689.

Kandárová, H. & Liebsch, M. (2017) 'The EpiDerm™ Skin Corrosion Test (EpiDerm™ SCT)', *Alternatives for Dermal Toxicity Testing*, pp. 127–142.

Kandárová, H., Liebsch, M., Spielmann, H., Genschow, E., Schmidt, E., Traue, D., Guest, R., Whittingham, A., Warren, N., Gamer, A.O., Remmele, M., Kaufmann, T., Wittmer, E., de Wever, B. & Rosdy, M. (2006) 'Assessment of the human epidermis model SkinEthic RHE for in vitro skin corrosion testing of chemicals according to new OECD TG 431', *Toxicology in Vitro*, 20(5), pp. 547–559.

Kang, S.M., Lee, J.H., Huh, Y.S. & Takayama, S. (2021) 'Alginate Microencapsulation for Three-dimensional in vitro Cell Culture', *ACS biomaterials science & engineering*, 7(7), p. 2864.

Kanitakis, J. (2002) 'Anatomy, histology and immunohistochemistry of normal human skin.', *European Journal of Dermatology : EJD*, 12(4), pp. 390–9.

Kanta, J. (2015) 'Collagen matrix as a tool in studying fibroblastic cell behavior', *Cell Adhesion & Migration*, 9(4), p. 308.

Karsdal, M.A., Nielsen, S.H., Leeming, D.J., Langholm, L.L., Nielsen, M.J., Manon-Jensen, T., Siebuhr, A., Gudmann, N.S., Rønnow, S., Sand, J.M., Daniels, S.J., Mortensen, J.H. & Schuppan, D. (2017) 'The good and the bad collagens of fibrosis – Their role in signaling and organ function', *Advanced Drug Delivery Reviews*, 121pp. 43–56.

Katsumi, A., Orr, A.W., Tzima, E. & Schwartz, M.A. (2004) 'Integrins in Mechanotransduction', *Journal of Biological Chemistry*, 279(13), pp. 12001–12004.

Kaur, A., Midha, S., Giri, S. & Mohanty, S. (2019) 'Functional Skin Grafts: Where Biomaterials Meet Stem Cells', *Stem Cells International*, 2019.

Kayal, C., Shipley, R.J. & Phillips, J.B. (2019) 'Physical and mechanical properties of RAFT-stabilised collagen gels for tissue engineering applications', *Journal of the Mechanical Behavior of Biomedical Materials*, 99pp. 216–224.

Ke, D., Niu, C. & Yang, X. (2022) 'Evolution of 3D bioprinting-from the perspectives of bioprinting companies', *Bioprinting*, 25p. e00193.

Kelangi, S.S., Theocharidis, G., Veves, A., Austen, W.G., Sheridan, R., Goverman, J. & Bei, M. (2021) 'On skin substitutes for wound healing: Current products, limitations, and future perspectives', *Technology*, 08(01n02), pp. 8–14.

Kenny, F.N., Drymoussi, Z., Delaine-Smith, R., Kao, A.P., Laly, A.C., Knight, M.M., Philpott, M.P. & Connelly, J.T. (2018) 'Tissue stiffening promotes keratinocyte proliferation through activation of epidermal growth factor signaling', *Journal of Cell Science*, 131(10).

Khurana, P., Kolundzic, N., Flohr, C. & Ilic, D. (2021) 'Human pluripotent stem cells: An alternative for 3D in vitro modelling of skin disease', *Experimental Dermatology*, 30(11), pp. 1572–1587.

Kim, B.S., Gao, G., Kim, J.Y. & Cho, D.W. (2019) '3D Cell Printing of Perfusable Vascularized Human Skin Equivalent Composed of Epidermis, Dermis, and Hypodermis for Better Structural Recapitulation of Native Skin', *Advanced Healthcare Materials*, 8(7), p. 1801019.

Kim, B.S., Lee, J.S., Gao, G. & Cho, D.W. (2017) 'Direct 3D cell-printing of human skin with functional transwell system', *Biofabrication*, 9(2), p. 025034.

Kim, D.S., Cho, H.-J., Choi, H.-R., Kwon, S.-B. & Park, K.-C. (2004) 'Isolation of human epidermal stem cells by adherence and the reconstruction of skin equivalents', *Cellular and Molecular Life Sciences CMLS 2004 61:21*, 61(21), pp. 2774–2781.

Kleinstreuer, N.C., Hoffmann, S., Alépée, N., Allen, D., Ashikaga, T., Casey, W., Clouet, E., Cluzel, M., Desprez, B., Gellatly, N., Göbel, C., Kern, P.S., Klaric, M., Kühnl, J., Martinozzi-Teissier, S., Mewes, K., Miyazawa, M., Strickland, J., van Vliet, E., et al. (2018) 'Non-animal methods to predict skin sensitization: an assessment of defined approaches', *Critical Reviews in Toxicology*, 48(5), pp. 359–374.

Klicks, J., von Molitor, E., Ertongur-Fauth, T., Rudolf, R., Hafner, M. & Rüdiger, R. (2017) 'In vitro skin three-dimensional models and their applications', *Journal of Cellular Biotechnology*, 3(1), pp. 21–39.

Klotz, B.J., Oosterhoff, L.A., Utomo, L., Lim, K.S., Vallmajo-Martin, Q., Clevers, H., Woodfield, T.B.F., Rosenberg, A.J.W.P., Malda, J., Ehrbar, M., Spee, B. & Gawlitta, D. (2019) 'A Versatile Biosynthetic Hydrogel Platform for Engineering of Tissue Analogues', *Advanced Healthcare Materials*, 8(19), p. 1900979.

Kober, J., Gugerell, A., Schmid, M., Kamolz, L.P. & Keck, M. (2015) 'Generation of a Fibrin Based Three-Layered Skin Substitute', *BioMed Research International*, 2015.

Koch, L., Deiwick, A., Schlie, S., Michael, S., Gruene, M., Coger, V., Zychlinski, D., Schambach, A., Reimers, K., Vogt, P.M. & Chichkov, B. (2012) 'Skin tissue generation by laser cell printing', *Biotechnology and Bioengineering*, 109(7), pp. 1855–1863.

Koch, L., Kuhn, S., Sorg, H., Gruene, M., Schlie, S., Gaebel, R., Polchow, B., Reimers, K., Stoelting, S., Ma, N., Vogt, P.M., Steinhoff, G. & Chichkov, B. (2009) 'Laser Printing of Skin Cells and Human Stem Cells', *https://home.liebertpub.com/tec*, 16(5), pp. 847–854.

Koivisto, L., Heino, J., Häkkinen, L. & Larjava, H. (2014) 'Integrins in Wound Healing', *Advances in Wound Care*, 3(12), p. 762.

Korosec, A., Frech, S., Gesslbauer, B., Vierhapper, M., Radtke, C., Petzelbauer, P. & Lichtenberger, B.M. (2019) 'Lineage Identity and Location within the Dermis Determine the Function of Papillary and Reticular Fibroblasts in Human Skin', *Journal of Investigative Dermatology*, 139(2), pp. 342–351.

Kotlarz, M., Ferreira, A.M., Gentile, P. & Dalgarno, K. (2022) 'Bioprinting of Cell-Laden Hydrogels onto Titanium Alloy Surfaces to Produce a Bioactive Interface', *Macromolecular Bioscience*, 22(6), p. 2200071.

Krasna, M., Planinsek, F., Knezevic, M., Arnez, Z.M. & Jeras, M. (2005) 'Evaluation of a fibrin-based skin substitute prepared in a defined keratinocyte medium', *International Journal of Pharmaceutics*, 291(1–2), pp. 31–37.

Krieg, T. & Aumailley, M. (2011) 'The extracellular matrix of the dermis: flexible structures with dynamic functions', *Experimental Dermatology*, 20(8), pp. 689–695.

Kubilus, J., Hayden, P.J., Ayehunie, S., Lamore, S.D.K., Servattalab, C., Bellavance, K.L., Sheasgreen, J.E. & Klausner, M. (2019) 'Full Thickness EpiDerm™: A Dermal–Epidermal Skin Model to Study Epithelial–Mesenchymal Interactions', *Alternatives to Laboratory Animals*, 32pp. 75–82.

Kuehlmann, B., Bonham, C.A., Zucal, I., Prantl, L. & Gurtner, G.C. (2020) 'Mechanotransduction in Wound Healing and Fibrosis', *Journal of Clinical Medicine*, 9(5).

Lai, V.K., Lake, S.P., Frey, C.R., Tranquillo, R.T. & Barocas, V.H. (2012) 'Mechanical Behavior of Collagen-Fibrin Co-Gels Reflects Transition From Series to Parallel Interactions With Increasing Collagen Content', *Journal of Biomechanical Engineering*, 134(1), p. 0110041.

Lapiere, C.M., Nusgens, B. & Pierard, G.E. (2009) 'Interaction Between Collagen Type I and Type III in Conditioning Bundles Organization', *Connective Tissue Research*, 5(1), pp. 21–29.

Lee, A., Sudau, K., Ahn, K.H., Lee, S.J. & Willenbacher, N. (2012) 'Optimization of Experimental Parameters to Suppress Nozzle Clogging in Inkjet Printing', *Industrial and Engineering Chemistry Research*, 51(40), pp. 13195–13204.

Lee, D.Y. & Cho, K.H. (2005) 'The effects of epidermal keratinocytes and dermal fibroblasts on the formation of cutaneous basement membrane in three-dimensional culture systems', *Archives of Dermatological Research*, 296(7), pp. 296–302.

Lee, H., Jang, T.S., Han, G., Kim, H.W. & Jung, H. do (2021) 'Freeform 3D printing of vascularized tissues: Challenges and strategies', *Journal of Tissue Engineering*, 12.

Lee, J.M., Ng, W.L. & Yeong, W.Y. (2019) 'Resolution and shape in bioprinting: Strategizing towards complex tissue and organ printing', *Applied Physics Reviews*, 6(1), p. 011307.

Lee, J., van der Valk, W.H., Serdy, S.A., Deakin, C.C., Kim, J., Le, A.P. & Koehler, K.R. (2022) 'Generation and characterization of hair-bearing skin organoids from human pluripotent stem cells', *Nature Protocols 2022 17:5*, 17(5), pp. 1266–1305.

Lee, K.Y. & Mooney, D.J. (2012) 'Alginate: properties and biomedical applications', *Progress in polymer science*, 37(1), p. 106.

Lee, V., Singh, G., Trasatti, J.P., Bjornsson, C., Xu, X., Tran, T.N., Yoo, S.S., Dai, G. & Karande, P. (2014) 'Design and Fabrication of Human Skin by Three-Dimensional Bioprinting', *Tissue Engineering. Part C, Methods*, 20(6), p. 473.

Lee, V. K., Kim, D. Y., Ngo, H., Lee, Y., Seo, L., Yoo, S. S., Vincent, P. A., & Dai, G. (2014b). 'Creating perfused functional vascular channels using 3D bio-printing technology', *Biomaterials*, 35(28), pp. 8092–8102.

Lee, W., Debasitis, J.C., Lee, V.K., Lee, J.H., Fischer, K., Edminster, K., Park, J.K. & Yoo, S.S. (2009) 'Multi-layered culture of human skin fibroblasts and keratinocytes through three-dimensional freeform fabrication', *Biomaterials*, 30(8), pp. 1587–1595.

Lee, W., Lee, V., Polio, S., Keegan, P., Lee, J.H., Fischer, K., Park, J.K. & Yoo, S.S. (2010) 'On-demand three-dimensional freeform fabrication of multi-layered hydrogel scaffold with fluidic channels', *Biotechnology and Bioengineering*, 105(6), pp. 1178–1186.

Lègues, M., Milet, C., Forraz, N., Berthelemy, N., Pain, S., André-Frei, V., Cadau, S. & Mcguckin, C. (2020) 'The World's First 3D Bioprinted Immune Skin Model Suitable for Screening Drugs and Ingredients for Normal and Inflamed Skin', *IFSCC Conference Article*,

Lei, M., Schumacher, L.J., Lai, Y.C., Juan, W.T., Yeh, C.Y., Wu, P., Jiang, T.X., Baker, R.E., Widelitz, R.B., Yang, L. & Chuong, C.M. (2017) 'Self-organization process in newborn skin organoid formation inspires strategy to restore hair regeneration of adult cells', *Proceedings of the National Academy of Sciences of the United States of America*, 114(34), pp. E7101–E7110.

Leong, C., Bigliardi, P. L., Sriram, G., Au, V. B., Connolly, J., & Bigliardi-Qi, M. (2018). 'Physiological doses of red light induce IL-4 release in cocultures between human keratinocytes and immune cells', *Photochemistry and Photobiology*, 94(1), 150-157.

Leong, W.Y., Soon, C.F., Wong, S.C., Tee, K.S., Cheong, S.C., Gan, S.H. & Youseffi, M. (2017) 'In Vitro Growth of Human Keratinocytes and Oral Cancer Cells into Microtissues: An Aerosol-Based Microencapsulation Technique', *Bioengineering*, 4(2).

Levato, R., Jungst, T., Scheuring, R.G., Blunk, T., Groll, J. & Malda, J. (2020) 'From Shape to Function: The Next Step in Bioprinting', *Advanced Materials*, 32(12), p. 1906423.

Li, W., Chi, N., Rathnayake, R.A.C. & Wang, R. (2021) 'Distinctive roles of fibrillar collagen I and collagen III in mediating fibroblast-matrix interaction: A nanoscopic study', *Biochemical and Biophysical Research Communications*, 560pp. 66–71.

Li, X., Liu, B., Pei, B., Chen, J., Zhou, D., Peng, J., Zhang, X., Jia, W. & Xu, T. (2020) 'Inkjet Bioprinting of Biomaterials', *Chemical Reviews*, 120(19), pp. 10793–10833.

Liu, F., Liu, C., Chen, Q., Ao, Q., Tian, X., Fan, J., Tong, H. & Wang, X. (2018) 'Progress in organ 3D bioprinting', *International Journal of Bioprinting*, 4(1).

Liu, J., Zhou, Z., Zhang, M., Song, F., Feng, C. & Liu, H. (2022b) 'Simple and robust 3D bioprinting of full-thickness human skin tissue', *Bioengineered*, 13(4), p. 10087.

Liu, S., Wang, T., Li, S. & Wang, X. (2022a) 'Application Status of Sacrificial Biomaterials in 3D Bioprinting', *Polymers*, 14(11).

Liu, X., Michael, S., Bharti, K., Ferrer, M. & Song, M.J. (2020) 'A Biofabricated Vascularized Skin Model of Atopic Dermatitis for Preclinical Studies', *Biofabrication*, 12(3), p. 035002.

Liu, Y. & Derby, B. (2019) 'Experimental study of the parameters for stable drop-on-demand inkjet performance', *Physics of Fluids*, 31(3), p. 032004.

Liu, Y., Liu, J., Dai, H., Wang, R., Hsiao, A., Wang, W., Betts, R.J., Marionnet, C., Bernerd, F. & Qiu, J. (2022c) 'Photo-aging evaluation - In vitro biological endpoints combined with collagen density assessment with multi-photon microscopy', *Journal of Dermatological Science*, 105(1), pp. 37–44.

Lowes, M.A., Bowcock, A.M. & Krueger, J.G. (2007) 'Pathogenesis and therapy of psoriasis', *Nature 2007 445:7130*, 445(7130), pp. 866–873.

Lukin, I., Erezuma, I., Maeso, L., Zarate, J., Desimone, M.F., Al-Tel, T.H., Dolatshahi-Pirouz, A. & Orive, G. (2022) 'Progress in Gelatin as Biomaterial for Tissue Engineering', *Pharmaceutics*, 14(6), p. 1177.

Maiullari, F., Costantini, M., Milan, M., Pace, V., Chirivì, M., Maiullari, S., Rainer, A., Baci, D., Marei, H. E., Seliktar, D., Gargioli, C., Bearzi, C., & Rizzi, R. (2018). 'A multi-cellular 3D bioprinting approach for vascularized heart tissue engineering based on HUVECs and iPSC-derived cardiomyocytes', *Scientific reports*, 8(1), 13532.

Mallampati, R., Patlolla, R.R., Agarwal, S., Babu, R.J., Hayden, P., Klausner, M. & Singh, M.S. (2010) 'Evaluation of EpiDerm full thickness-300 (EFT-300) as an in vitro model for skin irritation: Studies on aliphatic hydrocarbons', *Toxicology in vitro : an international journal published in association with BIBRA*, 24(2), p. 669.

Mandrycky, C., Wang, Z., Kim, K. & Kim, D.H. (2016) '3D Bioprinting for Engineering Complex Tissues', *Biotechnology advances*, 34(4), p. 422.

Marinkovich, M.P., Keene, D.R., Rimberg, C.S. & Burgeson, R.E. (1993) 'Cellular origin of the dermal-epidermal basement membrane', *Developmental Dynamics*, 197(4), pp. 255–267.

Marionnet, C., Pierrard, C., Vioux-Chagnoleau, C., Sok, J., Asselineau, D. & Bernerd, F. (2006) 'Interactions between fibroblasts and keratinocytes in morphogenesis of dermal epidermal junction in a model of reconstructed skin', *Journal of Investigative Dermatology*, 126(5), pp. 971–979.

Martínez, E., Engel, E., Planell, J.A. & Samitier, J. (2009) 'Effects of artificial micro- and nano-structured surfaces on cell behaviour', *Annals of Anatomy - Anatomischer Anzeiger*, 191(1), pp. 126–135.

Martino, F., Perestrelo, A.R., Vinarský, V., Pagliari, S. & Forte, G. (2018) 'Cellular mechanotransduction: From tension to function', *Frontiers in Physiology*, 9(JUL), p. 824.

Mateu, R., Živicová, V., Krejí, E.D., Grim, M., Strnad, H., Vlek, A., Kolá, M., Lacina, L., Gál, P., Borský, J., Smetana, K. & Dvoánková, B. (2016) 'Functional differences between neonatal and adult fibroblasts and keratinocytes: Donor age affects epithelial-mesenchymal crosstalk in vitro', *International Journal of Molecular Medicine*, 38(4), pp. 1063–1074.

Mathes, S.H. & Ruffner, H. (2014) 'The use of skin models in drug development', *Advanced Drug Delivery Reviews*, 69–70pp. 81–102.

Mathew-Steiner, S.S., Roy, S. & Sen, C.K. (2021) 'Collagen in Wound Healing', *Bioengineering*, 8(5).

Matinong, A.M.E., Chisti, Y., Pickering, K.L. & Haverkamp, R.G. (2022) 'Collagen Extraction from Animal Skin', *Biology 2022, Vol. 11, Page 905*, 11(6), p. 905.

Matter, K. & Balda, M.S. (1999) 'Occludin and the functions of tight junctions', *International review of cytology*, 186pp. 117–146.

McKee, C. & Chaudhry, G.R. (2017) 'Advances and challenges in stem cell culture', *Colloids and Surfaces B: Biointerfaces*, 159pp. 62–77.

McKinley, G.H. & Renardy, M. (2011) 'Wolfgang von Ohnesorge', *Physics of Fluids*, 23(12), p. 127101.

McKnight, G., Shah, J. & Hargest, R. (2022) 'Physiology of the skin', *Surgery (Oxford)*, 40(1), pp. 8–12.

Mehrotra, S., Moses, J.C., Bandyopadhyay, A. & Mandal, B.B. (2019) '3D Printing/Bioprinting Based Tailoring of in Vitro Tissue Models: Recent Advances and Challenges', *ACS Applied Bio Materials*, 2(4), pp. 1385–1405.

Melchels, F.P.W., Domingos, M.A.N., Klein, T.J., Malda, J., Bartolo, P.J. & Hutmacher, D.W. (2012) 'Additive manufacturing of tissues and organs', *Progress in Polymer Science*, 37(8), pp. 1079–1104.

Melchels, F.P.W., Feijen, J. & Grijpma, D.W. (2010) 'A review on stereolithography and its applications in biomedical engineering', *Biomaterials*, 31(24), pp. 6121–6130.

Michael, S., Sorg, H., Peck, C.T., Koch, L., Deiwick, A., Chichkov, B., Vogt, P.M. & Reimers, K. (2013) 'Tissue Engineered Skin Substitutes Created by Laser-Assisted Bioprinting Form Skin-Like Structures in the Dorsal Skin Fold Chamber in Mice', *PLoS ONE*, 8(3).

Miller, E., Phillippi, J., Fisher, G., Campbell, P., Walker, L. & Weiss, L. (2009) 'Inkjet Printing of Growth Factor Concentration Gradients and Combinatorial Arrays Immobilized on Biologically-Relevant Substrates', *Combinatorial Chemistry & High Throughput Screening*, 12(6), pp. 604–618.

Min, D., Lee, W., Bae, I.H., Lee, T.R., Croce, P. & Yoo, S.S. (2018) 'Bioprinting of biomimetic skin containing melanocytes', *Experimental Dermatology*, 27(5), pp. 453–459.

Mine, S., Fortunel, N.O., Pageon, H. & Asselineau, D. (2008) 'Aging Alters Functionally Human Dermal Papillary Fibroblasts but Not Reticular Fibroblasts: A New View of Skin Morphogenesis and Aging', *PLoS ONE*, 3(12).

Miri, A.K., Mirzaee, I., Hassan, S., Mesbah Oskui, S., Nieto, D., Khademhosseini, A. & Zhang, Y.S. (2019) 'Effective Bioprinting Resolution in Tissue Model Fabrication', *Lab on a chip*, 19(11), p. 2019.

Mirshahi, M., Azzarone, B., Soria, J., Mirshahi, F. & Soria, C. (1991) 'The role of fibroblasts in organization and degradation of a fibrin clot', *The Journal of Laboratory and Clinical Medicine*, 117(4), pp. 274–281.

Moll, I., Roessler, M., Brandner, J.M., Eispert, A.C., Houdek, P. & Moll, R. (2005) 'Human Merkel cells – aspects of cell biology, distribution and functions', *European Journal of Cell Biology*, 84(2–3), pp. 259–271.

Moniz, T., Costa Lima, S.A. & Reis, S. (2020) 'Human skin models: From healthy to disease-mimetic systems; characteristics and applications', *British Journal of Pharmacology*, 177(19), pp. 4314–4329.

Montero, A., Atienza, C., Elvira, C., Jorcano, J.L. & Velasco, D. (2021b) 'Hyaluronic acid-fibrin hydrogels show improved mechanical stability in dermo-epidermal skin substitutes', *Materials Science and Engineering: C*, 128 pp. 112352.

Montero, A., Quílez, C., Valencia, L., Girón, P., Jorcano, J.L. & Velasco, D. (2021a) 'Effect of fibrin concentration on the in vitro production of dermo-epidermal equivalents', *International Journal of Molecular Sciences*, 22(13), pp. 6746.

Moon, S., Hasan, S. K., Song, Y. S., Xu, F., Keles, H. O., Manzur, F., Mikkilineni, S., Hong, J. W., Nagatomi, J., Haeggstrom, E., Khademhosseini, A., & Demirci, U. (2010). 'Layer by layer three-dimensional tissue epitaxy by cell-laden hydrogel droplets', *Tissue engineering. Part C, Methods*, 16(1), pp. 157–166.

Moreno-Arotzena, O., Meier, J.G., Amo, C. del & García-Aznar, J.M. (2015) 'Characterization of Fibrin and Collagen Gels for Engineering Wound Healing Models', *Materials*, 8(4), pp. 1636.

Moretti, L., Stalfort, J., Barker, T.H. & Abebayehu, D. (2022) 'The interplay of fibroblasts, the extracellular matrix, and inflammation in scar formation', *Journal of Biological Chemistry*, 298(2).

Mori, N., Morimoto, Y. & Takeuchi, S. (2017) 'Skin integrated with perfusable vascular channels on a chip', *Biomaterials*, 116pp. 48–56.

Moroni, L., Burdick, J.A., Highley, C., Lee, S.J., Morimoto, Y., Takeuchi, S. & Yoo, J.J. (2018) 'Biofabrication strategies for 3D in vitro models and regenerative medicine', *Nature Reviews Materials 2018 3:5*, 3(5), pp. 21–37.

Mota, C., Camarero-Espinosa, S., Baker, M.B., Wieringa, P. & Moroni, L. (2020) 'Bioprinting: From Tissue and Organ Development to in Vitro Models', *Chemical Reviews*, 120(19), pp. 10547–10607.

Müller, S.J., Fabry, B. & Gekle, S. (2022) 'Predicting cell stress and strain during extrusion bioprinting', *bioRxiv*, p. 2022.09.28.509836.

Muñoz, J. & Pumera, M. (2020) '3D-printed biosensors for electrochemical and optical applications', *TrAC Trends in Analytical Chemistry*, 128p. 115933.

Murphy, S. v. & Atala, A. (2014) '3D bioprinting of tissues and organs', *Nature biotechnology*, 32(8), pp. 773–785.

Murphy, S. v., de Coppi, P. & Atala, A. (2019) 'Opportunities and challenges of translational 3D bioprinting', *Nature Biomedical Engineering 2019 4:4*, 4(4), pp. 370–380.

Myers, S., Navsaria, H. & Ojeh, N. (2014) 'Skin Engineering and Keratinocyte Stem Cell Therapy', *Tissue Engineering: Second Edition*, pp. 497–528.

Nagapudi, K., Brinkman, W.T., Thomas, B.S., Park, J.O., Srinivasarao, M., Wright, E., Conticello, V.P. & Chaikof, E.L. (2005) 'Viscoelastic and mechanical behavior of recombinant protein elastomers', *Biomaterials*, 26(23), pp. 4695–4706.

Nair, K., Gandhi, M., Khalil, S., Yan, K.C., Marcolongo, M., Barbee, K. & Sun, W. (2009) 'Characterization of cell viability during bioprinting processes', *Biotechnology Journal*, 4(8), pp. 1168–1177.

Nakazawa, K., Kalassy, M., Sahuc, F., Collombel, C. & Damour, O. (1998) 'Pigmented human skin equivalent - As a model of the mechanisms of control of cell-cell and cell-matrix interactions', *Medical and Biological Engineering and Computing*, 36(6), pp. 813–820.

Nanmo, A., Yan, L., Asaba, T., Wan, L., Kageyama, T. & Fukuda, J. (2022) 'Bioprinting of hair follicle germs for hair regenerative medicine', *Acta Biomaterialia*,

Nasrollahi, S., Walter, C., Loza, A.J., Schimizzi, G. v., Longmore, G.D. & Pathak, A. (2017) 'Past matrix stiffness primes epithelial cells and regulates their future collective migration through a mechanical memory', *Biomaterials*, 146p. 146.

Netzlaff, F., Lehr, C.M., Wertz, P.W. & Schaefer, U.F. (2005) 'The human epidermis models EpiSkin®, SkinEthic® and EpiDerm®: An evaluation of morphology and their suitability for testing phototoxicity, irritancy, corrosivity, and substance transport', *European Journal of Pharmaceutics and Biopharmaceutics*, 60(2), pp. 167–178.

Neupane, R., Boddu, S.H.S., Renukuntla, J., Babu, R.J. & Tiwari, A.K. (2020) 'Alternatives to Biological Skin in Permeation Studies: Current Trends and Possibilities', *Pharmaceutics*, 12(2).

Neves, L.M.G., Wilgus, T.A. & Bayat, A. (2022) 'In Vitro, Ex Vivo, and in Vivo Approaches for Investigation of Skin Scarring: Human and Animal Models', *Advances in Wound Care*, 12(2), pp. 97–116.

Neves, M.I., Moroni, L. & Barrias, C.C. (2020) 'Modulating Alginate Hydrogels for Improved Biological Performance as Cellular 3D Microenvironments', *Frontiers in Bioengineering and Biotechnology*, 8p. 665.

Ng, K.W., Leong, D.T.W. & Hutmacher, D.W. (2005) 'The Challenge to Measure Cell Proliferation in Two and Three Dimensions', *https://home.liebertpub.com/ten*, 11(1–2), pp. 182–191.

Ng, W.L., Chua, C.K. & Shen, Y.F. (2019) 'Print Me An Organ! Why We Are Not There Yet', *Progress in Polymer Science*, 97.

Ng, W.L., Goh, M.H., Yeong, W.Y. & Naing, M.W. (2018b) 'Applying macromolecular crowding to 3D bioprinting: fabrication of 3D hierarchical porous collagen-based hydrogel constructs', *Biomaterials Science*, 6(3), pp. 562–574.

Ng, W.L., Lee, J.M., Yeong, W.Y. & Win Naing, M. (2017) 'Microvalve-based bioprinting – process, bio-inks and applications', *Bniomaterials Science*, 5(4), pp. 632–647.

Ng, W.L., Qi, J.T.Z., Yeong, W.Y. & Naing, M.W. (2018a) 'Proof-of-concept: 3D bioprinting of pigmented human skin constructs', *Biofabrication*, 10(2).

Ng, W.L., Wang, S., Yeong, W.Y. & Naing, M.W. (2016) 'Skin Bioprinting: Impending Reality or Fantasy?', *Trends in Biotechnology*, 34(9), pp. 689–699.

Ng, W.L. & Yeong, W.Y. (2019) 'The future of skin toxicology testing – Three-dimensional bioprinting meets microfluidics', *International Journal of Bioprinting*, 5(2.1), pp. 44–54.

Nguyen, D. G., Funk, J., Robbins, J. B., Crogan-Grundy, C., Presnell, S. C., Singer, T., & Roth, A. B. (2016). 'Bioprinted 3D Primary Liver Tissues Allow Assessment of Organ-Level Response to Clinical Drug Induced Toxicity In Vitro', *PloS one*, 11(7), e0158674.

Nicholas, M.N., Jeschke, M.G. & Amini-Nik, S. (2016) 'Methodologies in Creating Skin Substitutes', *Cellular and molecular life sciences : CMLS*, 73(18), p. 3453.

Niehues, H., Bouwstra, J.A., el Ghalbzouri, A., Brandner, J.M., Zeeuwen, P.L.J.M. & van den Bogaard, E.H. (2018) '3D skin models for 3R research: The potential of 3D reconstructed skin models to study skin barrier function', *Experimental dermatology*, 27(5), pp. 501–511.

Nikolakis, G., Seltmann, H., Hossini, A. M., Makrantonaki, E., Knolle, J., Zouboulis, C. C. (2015). 'Ex vivo human skin and SZ 95 sebocytes exhibit a homoeostatic interaction in a novel coculture contact model', *Experimental Dermatology*, 24(7), 497-502.

Nikolova, M.P. & Chavali, M.S. (2019) 'Recent advances in biomaterials for 3D scaffolds: A review', *Bioactive Materials*, 4pp. 271–292.

Noizet, M., Lagoutte, E., Gratigny, M., Bouschbacher, M., Lazareth, I., Roest Crollius, H., Darzacq, X. & Dugast-Darzacq, C. (2016) 'Master regulators in primary skin fibroblast fate reprogramming in a human ex vivo model of chronic wounds', *Wound Repair and Regeneration*, 24(2), pp. 247–262.

Nyström, A. & Bruckner-Tuderman, L. (2019) 'Matrix molecules and skin biology', *Seminars in Cell & Developmental Biology*, 89pp. 136–146.

OECD (2022) *Chemical safety and biosafety*. [Online] [online]. Available from: https://www.oecd.org/chemicalsafety/ (Accessed 22 October 2021).

Ohyama, M. & Okano, H. (2014) 'Promise of human induced pluripotent stem cells in skin regeneration and investigation', *The Journal of investigative dermatology*, 134(3), pp. 605–609.

Okubo, N., Qureshi, A.J., Dalgarno, K., Goh, K.L. & Derebail, S. (2019) 'Cost-effective microvalve-assisted bioprinter for tissue engineering', *Bioprinting*, 13p. e00043.

Olejnik, A., Semba, J. A., Kulpa, A., Danczak-Pazdrowska, A., Rybka, J. D., & Gornowicz-Porowska, J. (2021) '3D bioprinting in skin related research: recent achievements and application perspectives', *ACS Synthetic Biology*, 11(1), 26-38.

Ono, S., Egawa, G. & Kabashima, K. (2017) 'Regulation of blood vascular permeability in the skin', *Inflammation and Regeneration*, 37(1), pp. 1–8.

Onuma, H., Mastui, C. & Morohashi, M. (2001) 'Quantitative analysis of the proliferation of epidermal cells using a human skin organ culture system and the effect of DbcAMP using markers of proliferation (BrdU, Ki-67, PCNA)', *Archives of Dermatological Research*, 293(3), pp. 133–138.

OpenStax College (2022) *5.1 Layers of the Skin - Anatomy and Physiology 2e | OpenStax*. [Online]. Available from: https://openstax.org/books/anatomy-and-physiology-2e/pages/5-1-layers-of-the-skin (Accessed 11 September 2022).

Orgel, J.P.R.O., Persikov, A. v. & Antipova, O. (2014) 'Variation in the Helical Structure of Native Collagen', *PLOS ONE*, 9(2), p. e89519.

Ouwehand, K., Spiekstra, S.W., Waaijman, T., Scheper, R.J., de Gruijl, T.D. & Gibbs, S. (2011) 'Technical advance: Langerhans cells derived from a human cell line in a full-thickness skin equivalent undergo allergen-induced maturation and migration', *Journal of leukocyte biology*, 90(5), pp. 1027–1033.

Ouyang, L., Yao, R., Zhao, Y. & Sun, W. (2016) 'Effect of bioink properties on printability and cell viability for 3D bioplotting of embryonic stem cells', *Biofabrication*, 8(3), p. 035020.

Ozbolat, I.T. & Hospodiuk, M. (2016) 'Current advances and future perspectives in extrusion-based bioprinting', *Biomaterials*, 76pp. 321–343.

Ozbolat, I.T. & Yu, Y. (2013) 'Bioprinting toward organ fabrication: Challenges and future trends', *IEEE Transactions on Biomedical Engineering*, 60(3), pp. 691–699.

Ozcelikkale, A., Dutton, J.C., Grinnell, F. & Han, B. (2017) 'Effects of dynamic matrix remodelling on en masse migration of fibroblasts on collagen matrices', *Journal of The Royal Society Interface*, 14(135).

Pakulska, M.M., Donaghue, I.E., Obermeyer, J.M., Tuladhar, A., McLaughlin, C.K., Shendruk, T.N. & Shoichet, M.S. (2016) 'Encapsulation-free controlled release: Electrostatic adsorption eliminates the need for protein encapsulation in PLGA nanoparticles', *Science advances*, 2(5).

Parenteau-Bareil, R., Gauvin, R. & Berthod, F. (2010) 'Collagen-Based Biomaterials for Tissue Engineering Applications', *Materials*, 3(3), p. 1863.

Park, C.H. & Woo, K.M. (2018) 'Fibrin-based biomaterial applications in tissue engineering and regenerative medicine', *Advances in Experimental Medicine and Biology*, 1064pp. 253–261.

Paul, W. & Sharma, C.P. (2015) 'Chapter 3. The anatomy and functions of skin', in *Advances in wound healing materials : science and skin engineering*. [Online].

Pavel, M., Renna, M., Park, S.J., Menzies, F.M., Ricketts, T., Füllgrabe, J., Ashkenazi, A., Frake, R.A., Lombarte, A.C., Bento, C.F., Franze, K. & Rubinsztein, D.C. (2018) 'Contact inhibition controls cell survival and proliferation via YAP/TAZ-autophagy axis', *Nature Communications 2018 9:1*, 9(1), pp. 1–18.

Pazhouhnia, Z., Beheshtizadeh, N., Namini, M.S. & Lotfibakhshaiesh, N. (2022) 'Portable hand-held bioprinters promote in situ tissue regeneration', *Bioengineering & Translational Medicine*, 7(3).

Pellevoisin, C., Videau, C., Briotet, D., Grégoire, C., Tornier, C., Alonso, A., Rigaudeau, A.S., Bouez, C. & Seyler, N. (2018) 'SkinEthic™ RHE for in vitro evaluation of skin irritation of medical device extracts', *Toxicology in Vitro*, 50pp. 418–425.

Pfisterer, K., Shaw, L.E., Symmank, D. & Weninger, W. (2021) 'The Extracellular Matrix in Skin Inflammation and Infection', *Frontiers in Cell and Developmental Biology*, 9p. 1578.

Pittenger, M.F., Discher, D.E., Péault, B.M., Phinney, D.G., Hare, J.M. & Caplan, A.I. (2019) 'Mesenchymal stem cell perspective: cell biology to clinical progress', *npj Regenerative Medicine 2019 4:1*, 4(1), pp. 1–15.

Pittenger, M.F., Mackay, A.M., Beck, S.C., Jaiswal, R.K., Douglas, R., Mosca, J.D., Moorman, M.A., Simonetti, D.W., Craig, S. & Marshak, D.R. (1999) 'Multilineage potential of adult human mesenchymal stem cells', *Science*, 284(5411), pp. 143–147.

Planz, V., Lehr, C.M. & Windbergs, M. (2016) 'In vitro models for evaluating safety and efficacy of novel technologies for skin drug delivery', *Journal of controlled release,* 242pp. 89–104.

Plikus, M. v., Wang, X., Sinha, S., Forte, E., Thompson, S.M., Herzog, E.L., Driskell, R.R., Rosenthal, N., Biernaskie, J. & Horsley, V. (2021) 'Fibroblasts: Origins, definitions, and functions in health and disease', *Cell*, 184(15), pp. 3852–3872.

Ponec, M., Boelsma, E., Gibbs, S. & Mommaas, M. (2002) 'Characterization of Reconstructed Skin Models', *Skin Pharmacology and Physiology*, 15(1), pp. 4–17.

Pontiggia, L., Ahuja, A.K., Yosef, H.K., Rütsche, D., Reichmann, E., Moehrlen, U. & Biedermann, T. (2022) 'Human Basal and Suprabasal Keratinocytes Are Both Able to Generate and Maintain Dermo–Epidermal Skin Substitutes in Long-Term In Vivo Experiments', *Cells*, 11(14).

Poumay, Y., Dupont, F., Marcoux, S., Leclercq-Smekens, M., Hérin, M. & Coquette, A. (2004) 'A simple reconstructed human epidermis: Preparation of the culture model and utilization in in vitro studies', *Archives of Dermatological Research*, 296(5), pp. 203–211.

Poumay, Y. & Pittelkow, M.R. (1995) 'Cell density and culture factors regulate keratinocyte commitment to differentiation and expression of suprabasal K1/K10 keratins', *The Journal of investigative dermatology*, 104(2), pp. 271–276.

Pourchet, L.J., Thepot, A., Albouy, M., Courtial, E.J., Boher, A., Blum, L.J. & Marquette, C.A. (2017) 'Human Skin 3D Bioprinting Using Scaffold-Free Approach', *Advanced Healthcare Materials*, 6(4), p. 1601101.

Proksch, E., Brandner, J.M. & Jensen, J.M. (2008) 'The skin: an indispensable barrier', *Experimental dermatology*, 17(12), pp. 1063–1072.

Promed Bioscience (2022) *Innovative Collagen Biomaterials*. [Online] [online]. Available from: https://www.promedbioscience.com/en/what (Accessed 16 October 2022).

Puertas-Bartolomé, M., Włodarczyk-Biegun, M.K., del Campo, A., Vázquez-Lasa, B. & Román, J.S. (2020) '3D Printing of a Reactive Hydrogel Bio-Ink Using a Static Mixing Tool', *Polymers 2020, Vol. 12, Page 1986*, 12(9), p. 1986.

Querejeta, R., López, B., González, A., Sánchez, E., Larman, M., Martínez Ubago, J.L. & Díez, J. (2004) 'Increased collagen type I synthesis in patients with heart failure of hypertensive origin: relation to myocardial fibrosis', *Circulation*, 110(10), pp. 1263–1268.

Rademacher, F., Simanski, M., Gläser, R. & Harder, J. (2018) 'Skin microbiota and human 3D skin models', *Experimental Dermatology*, 27(5), pp. 489–494.

Ramli, H., Zainal, N.F.A., Hess, M. & Chan, C.H. (2022) 'Basic principle and good practices of rheology for polymers for teachers and beginners', *Chemistry Teacher International*, 4(4), pp. 307–326.

Randolph, R.K. & Simon, M. (1998) 'Dermal Fibroblasts Actively Metabolize Retinoic Acid but not Retinol', *Journal of Investigative Dermatology*, 111(3), pp. 478–484.

Rasmussen, C., Gratz, K., Liebel, F., Southall, M., Garay, M., Bhattacharyya, S., Simon, N., Zanden, M. vander, Winkle, K. van, Pirnstill, J., Pirnstill, S., Comer, A. & Allen-Hoffmann, B.L. (2010) 'The StrataTest® human skin model, a consistent in vitro alternative for toxicological testing', *Toxicology in Vitro*, 24(7), pp. 2021–2029.

Reddy, M.S.B., Ponnamma, D., Choudhary, R. & Sadasivuni, K.K. (2021) 'A Comparative Review of Natural and Synthetic Biopolymer Composite Scaffolds', *Polymers 2021, Vol. 13, Page 1105*, 13(7), p. 1105.

Reisinger, K., Blatz, V., Brinkmann, J., Downs, T.R., Fischer, A., Henkler, F., Hoffmann, S., Krul, C., Liebsch, M., Luch, A., Pirow, R., Reus, A.A., Schulz, M. & Pfuhler, S. (2018) 'Validation of the 3D Skin Comet assay using full thickness skin models: Transferability and reproducibility', *Mutation Research/Genetic Toxicology and Environmental Mutagenesis*, 827pp. 27–41.

Rezaie, F., Momeni-Moghaddam, M. & Naderi-Meshkin, H. (2019) 'Regeneration and Repair of Skin Wounds: Various Strategies for Treatment', 18(3), pp. 247–261.

Rhee, S. (2009) 'Fibroblasts in three dimensional matrices: cell migration and matrix remodeling', *Experimental & Molecular Medicine 2009 41:12*, 41(12), pp. 858–865.

Richter, M., Piwocka, O., Musielak, M., Piotrowski, I., Suchorska, W.M. & Trzeciak, T. (2021) 'From Donor to the Lab: A Fascinating Journey of Primary Cell Lines', *Frontiers in Cell and Developmental Biology*, 9.

Rimal, R., Marquardt, Y., Nevolianis, T., Djeljadini, S., Marquez, A.B., Huth, S., Chigrin, D.N., Wessling, M., Baron, J.M., Möller, M. & Singh, S. (2021) 'Dynamic flow enables long-term maintenance of 3-D vascularized human skin models', *Applied Materials Today*, 25p. 101213.

Rinaldi, A.O., Morita, H., Wawrzyniak, P., Dreher, A., Grant, S., Svedenhag, P. & Akdis, C.A. (2019) 'Direct assessment of skin epithelial barrier by electrical impedance spectroscopy', *Allergy*, 74(10), pp. 1934–1944.

Rocca, M., Fragasso, A., Liu, W., Heinrich, M.A. & Zhang, Y.S. (2018) 'Embedded Multimaterial Extrusion Bioprinting', *SLAS Technology*, 23(2), pp. 154–163.

Roig-Rosello, E. & Rousselle, P. (2020) 'The Human Epidermal Basement Membrane: A Shaped and Cell Instructive Platform That Aging Slowly Alters', *Biomolecules*, 10(12), pp. 1–32.

Roger, M., Fullard, N., Costello, L., Bradbury, S., Markiewicz, E., O'Reilly, S., Darling, N., Ritchie, P., Määttä, A., Karakesisoglou, I., Nelson, G., von Zglinicki, T., Dicolandrea, T., Isfort, R., Bascom, C. & Przyborski, S. (2019) 'Bioengineering the microanatomy of human skin', *Journal of Anatomy*, 234(4), p. 438-455.

Rognoni, E. & Walko, G. (2019) 'The Roles of YAP/TAZ and the Hippo Pathway in Healthy and Diseased Skin', *Cells*, 8(5).

Rosdy, M. & Clauss, L.C. (1990) 'Terminal epidermal differentiation of human keratinocytes grown in chemically defined medium on inert filter substrates at the air-liquid interface', *The Journal of investigative dermatology*, 95(4), pp. 409–414.

Rosenbaum, A.J., Grande, D.A. & Dines, J.S. (2008) 'The use of mesenchymal stem cells in tissue engineering: A global assessment', *Organogenesis*, 4(1), p. 23.

Rowe, R.G. & Daley, G.Q. (2019) 'Induced pluripotent stem cells in disease modelling and drug discovery', *Nature Reviews Genetics 2019 20:7*, 20(7), pp. 377–388.

Rowe, S.L. & Stegemann, J.P. (2006) 'Interpenetrating Collagen-Fibrin Composite Matrices with Varying Protein Contents and Ratios', *Biomacromolecules*, 7(11), p. 2942.

Roy, S., Kulkarni, R., Hewitt, N.J. & Aardema, M.J. (2016) 'The EpiDerm™ 3D human reconstructed skin micronucleus (RSMN) assay: Historical control data and proof of principle studies for mechanistic assay adaptations', *Mutation Research/Genetic Toxicology and Environmental Mutagenesis*, 805pp. 25–37.

de Ruijter, M., Ribeiro, A., Dokter, I., Castilho, M. & Malda, J. (2019) 'Simultaneous Micropatterning of Fibrous Meshes and Bioinks for the Fabrication of Living Tissue Constructs', *Advanced healthcare materials*, 8(7), p. e1800418.

Sahle, F.F., Gerecke, C., Kleuser, B. & Bodmeier, R. (2017) 'Formulation and comparative in vitro evaluation of various dexamethasone-loaded pH-sensitive polymeric nanoparticles intended for dermal applications', *International Journal of Pharmaceutics*, 516(1–2), pp. 21–31.

Sai'Aan, N.H.M., Soon, C.F., Tee, K.S., Ahmad, M.K., Youseffi, M. & Khagani, S.A. (2016) 'Characterisation of encapsulated cells in calcium alginate microcapsules', *IECBES 2016 - IEEE-EMBS Conference on Biomedical Engineering and Sciences*, pp. 611–616.

Sakurada, S., Sole-Gras, M., Christensen, K., Wallace, D.B. & Huang, Y. (2020) 'Liquid-absorbing system-assisted intersecting jets printing of soft structures from reactive biomaterials', *Additive Manufacturing*, 31p. 100934.

Salameh, S., Tissot, N., Cache, K., Lima, J., Suzuki, I., Marinho, P.A., Rielland, M., Soeur, J., Takeuchi, S., Germain, S. & Breton, L. (2021) 'A perfusable vascularized full-thickness skin model for potential topical and systemic applications', *Biofabrication*, 13(3), p. 035042.

Samavedi, S., Poindexter, L.K., van Dyke, M. & Goldstein, A.S. (2014) 'Synthetic Biomaterials for Regenerative Medicine Applications', *Regenerative Medicine Applications in Organ Transplantation*, pp. 81–99.

Sanchez, M.M., Tonmoy, T.I., Park, B.H. & Morgan, J.T. (2022) 'Development of a Vascularized Human Skin Equivalent with Hypodermis for Photoaging Studies', *Biomolecules*, 12(12).

Sandilands, A., Sutherland, C., Irvine, A.D. & McLean, W.H.I. (2009) 'Filaggrin in the frontline: role in skin barrier function and disease', *Journal of Cell Science*, 122(9), p. 1285.

Sarama, R., Matharu, P.K., Abduldaiem, Y., Corrêa, M.P., Gil, C.D. & Greco, K. v. (2022) 'In Vitro Disease Models for Understanding Psoriasis and Atopic Dermatitis', *Frontiers in Bioengineering and Biotechnology*, 10p. 251.

Sarkiri, M., Fox, S.C., Fratila-Apachitei, L.E. & Zadpoor, A.A. (2019) 'Bioengineered Skin Intended for Skin Disease Modeling', *International Journal of Molecular Sciences*, 20(6).

Sasaki, M., Abe, R., Fujita, Y., Ando, S., Inokuma, D. & Shimizu, H. (2008) 'Mesenchymal Stem Cells Are Recruited into Wounded Skin and Contribute to Wound Repair by Transdifferentiation into Multiple Skin Cell Type', *The Journal of Immunology*, 180(4), pp. 2581–2587.

Saunders, R.E. & Derby, B. (2014) 'Inkjet printing biomaterials for tissue engineering: bioprinting', *International Materials Reviews*, 59(8), pp. 430–448.

Saunders, R.E., Gough, J.E. & Derby, B. (2008) 'Delivery of human fibroblast cells by piezoelectric drop-on-demand inkjet printing', *Biomaterials*, 29(2), pp. 193–203.

Savoji, H., Godau, B., Hassani, M.S. & Akbari, M. (2018) 'Skin Tissue Substitutes and Biomaterial Risk Assessment and Testing', *Frontiers in Bioengineering and Biotechnology*, 6p. 86.

Schäfer-Korting, M., Bock, U., Diembeck, W., Düsing, H.J., Gamer, A., Haltner-Ukomadu, E., Hoffmann, C., Kaca, M., Kamp, H., Kersen, S., Kietzmann, M., Korting, H.C., Krächter, H.U., Lehr, C.M., Liebsch, M., Mehling, A., Müller-Goymann, C., Netzlaff, F., Niedorf, F., et al. (2008) 'The Use of Reconstructed Human Epidermis for Skin Absorption Testing: Results of the Validation Study', *Alternatives to Laboratory Animals*, 36(2), pp. 161–187.

Schiele, N.R., Corr, D.T., Huang, Y., Raof, N.A., Xie, Y. & Chrisey, D.B. (2010) 'Laser-based direct-write techniques for cell printing', *Biofabrication*, 2(3), p. 032001.

Schimek, K., Hsu, H.H., Boehme, M., Kornet, J.J., Marx, U., Lauster, R., Pörtner, R. & Lindner, G. (2018) 'Bioengineering of a Full-Thickness Skin Equivalent in a 96-Well Insert Format for Substance Permeation Studies and Organ-On-A-Chip Applications', *Bioengineering*, 5(2).

Schmidt, F.F., Nowakowski, S. & Kluger, P.J. (2020) 'Improvement of a Three-Layered in vitro Skin Model for Topical Application of Irritating Substances', *Frontiers in Bioengineering and Biotechnology*, 8p. 388.

Schmidt, S.K., Schmid, R., Arkudas, A., Kengelbach-Weigand, A. & Bosserhoff, A.K. (2019) 'Tumor Cells Develop Defined Cellular Phenotypes After 3D-Bioprinting in Different Bioinks', *Cells 2019, Vol. 8, Page 1295*, 8(10), p. 1295.

Schonzen, T. & Gerdes, J. (2000) 'The Ki-67 protein: From the known and the unknown', *Journal of Cellular Physiology*, 182(3), pp. 311–322.

Schmook, F.P., Meingassner, J.G. & Billich, A. (2001) 'Comparison of human skin or epidermis models with human and animal skin in in-vitro percutaneous absorption', *International Journal of Pharmaceutics*, 215(1–2), pp. 51–56.

Schoop, V.M., Mirancea, N. & Fusenig, N.E. (1999) 'Epidermal organization and differentiation of HaCat keratinocytes in organotypic coculture with human dermal fibroblasts', *Journal of Investigative Dermatology*, 112(3), pp. 343–353.

Schulz, R., Yamamoto, K., Klossek, A., Flesch, R., Hönzke, S., Rancan, F., Vogt, A., Blume-Peytavi, U., Hedtrich, S., Schäfer-Korting, M., Rühl, E. & Netz, R.R. (2017) 'Data-based modeling of drug penetration relates human skin barrier function to the interplay of diffusivity and free-energy profiles', *Proceedings of the National Academy of Sciences of the United States of America*, 114(14), pp. 3631–3636.

Scott, J.E. (2003) 'Elasticity in extracellular matrix "shape modules" of tendon, cartilage, etc. A sliding proteoglycan-filament model', *The Journal of Physiology*, 553(Pt 2), p. 335.

Semlin, L., Schäfer-Korting, M., Borelli, C. & Korting, H.C. (2011) 'In vitro models for human skin disease', *Drug Discovery Today*, 16(3–4), pp. 132–139.

Seo, B.R., Chen, X., Ling, L., Song, Y.H., Shimpi, A.A., Choi, S., Gonzalez, J., Sapudom, J., Wang, K., Eguiluz, R.C.A., Gourdon, D., Shenoy, V.B. & Fischbach, C. (2020) 'Collagen microarchitecture mechanically controls myofibroblast differentiation', *Proceedings of the National Academy of Sciences of the United States of America*, 117(21), p. 11387.

Seruggia, D., Fernández, A., Cantero, M., Fernández-Miñán, A., Gomez-Skarmeta, J.L., Pelczar, P. & Montoliu, L. (2020) 'Boundary sequences flanking the mouse tyrosinase locus ensure faithful pattern of gene expression', *Scientific Reports 2020 10:1*, 10(1), pp. 1–13.

Setijanti, H.B., Rusmawati, E., Fitria, R., Erlina, T., Adriany, R. & Murtiningsih (2019) 'Development the Technique for the Preparation and Characterization of Reconstructed Human Epidermis (RHE)', *Alternatives to Animal Testing*, pp. 20–32.

Seymour, A.J., Westerfield, A.D., Cornelius, V.C., -, al, Li, Z., Ramos, A., Li, M.-C., Paxton, N., Smolan, W., Böck, T., Melchels, F., Groll, J. & Jungst, T. (2017) 'Proposal to assess printability of bioinks for extrusion-based bioprinting and evaluation of rheological properties governing bioprintability', *Biofabrication*, 9(4), p. 044107.

Shamsul, B., Chowdhury, S., Hamdan, M.Y. & Ruszymah, B.H.I. (2019) 'Effect of cell density on formation of three-dimensional cartilaginous constructs using fibrin & human osteoarthritic chondrocytes', *The Indian Journal of Medical Research*, 149(5), p. 641.

Shayegan, M., Altindal, T., Kiefl, E. & Forde, N.R. (2016) 'Intact Telopeptides Enhance Interactions between Collagens', *Biophysical Journal*, 111(11), p. 2404.

Sheikholeslam, M., Wright, M.E.E., Jeschke, M.G. & Amini-Nik, S. (2018) 'Biomaterials for Skin Substitutes', *Advanced healthcare materials*, 7(5).

Sherratt, M.J. (2009) 'Tissue elasticity and the ageing elastic fibre', *Age*, 31(4), p. 305.

Shinde, A. v., Humeres, C. & Frangogiannis, N.G. (2017) 'The role of α-smooth muscle actin in fibroblast-mediated matrix contraction and remodeling', *Biochimica et Biophysica Acta (BBA) - Molecular Basis of Disease*, 1863(1), pp. 298–309.

Shinowara, G.Y. (1966) 'Human thrombin and fibrinogen the kinetics of their interaction and the preparation of the enzyme', *Biochimica et Biophysica Acta (BBA) - Enzymology and Biological Oxidation*, 113(2), pp. 359–374.

Shiwarski, D.J., Hudson, A.R., Tashman, J.W. & Feinberg, A.W. (2021) 'Emergence of FRESH 3D printing as a platform for advanced tissue biofabrication', *APL Bioengineering*, 5(1), p. 010904.

Silva, R.J. & Tamburic, S. (2022) 'A State-of-the-Art Review on the Alternatives to Animal Testing for the Safety Assessment of Cosmetics', *Cosmetics*, 9(5), p. 90.

Simpson, C.L., Patel, D.M. & Green, K.J. (2011) 'Deconstructing the skin: cytoarchitectural determinants of epidermal morphogenesis', *Nature Reviews Molecular Cell Biology 2011 12:9*, 12(9), pp. 565–580.

Singh, M., Haverinen, H.M., Dhagat, P. & Jabbour, G.E. (2010) 'Inkjet Printing—Process and Its Applications', *Advanced Materials*, 22(6), pp. 673–685.

Singh, V.K., Kalsan, M., Kumar, N., Saini, A. & Chandra, R. (2015) 'Induced pluripotent stem cells: Applications in regenerative medicine, disease modeling, and drug discovery', *Frontiers in Cell and Developmental Biology*, 3(FEB), p. 2.

Sivamani, R.K., Garcia, M.S. & Rivkah Isseroff, R. (2007) 'Wound re-epithelialization: Modulating keratinocyte migration in wound healing', *Frontiers in Bioscience*, 12(8), pp. 2849–2868.

Smiley, A.K., Klingenberg, J.M., Boyce, S.T. & Supp, D.M. (2006) 'Keratin expression in cultured skin substitutes suggests that the hyperproliferative phenotype observed in vitro is normalized after grafting', *Burns*, 32(2), pp. 135–138.

Smithmyer, M.E., Cassel, S.E. & Kloxin, A.M. (2019) 'Bridging 2D and 3D culture: probing impact of extracellular environment on fibroblast activation in layered hydrogels', *AIChE journal. American Institute of Chemical Engineers*, 65(12).

Smithmyer, M.E., Sawicki, L.A. & Kloxin, A.M. (2014) 'Hydrogel scaffolds as in vitro models to study fibroblast activation in wound healing and disease', *Biomaterials Science*, 2(5), pp. 634–650.

Smola, H., Stark, H.J., Thiekötter, G., Mirancea, N., Krieg, T. & Fusenig, N.E. (1998) 'Dynamics of Basement Membrane Formation by Keratinocyte–Fibroblast Interactions in Organotypic Skin Culture', *Experimental Cell Research*, 239(2), pp. 399–410.

Smolle, C., Cambiaso-Daniel, J., Forbes, A.A., Wurzer, P., Hundeshagen, G., Branski, L.K., Huss, F. & Kamolz, L.P. (2017) 'Recent trends in burn epidemiology worldwide: A systematic review', *Burns*, 43(2), pp. 249–257.

Soboleva, A.G., Mezentsev, A., Zolotorenko, A., Bruskin, S. & Pirusian, E. (2014) 'Three-Dimensional Skin Models of Psoriasis', *Cells Tissues Organs*, 199(5–6), pp. 301–310.

Solé-Boldo, L., Raddatz, G., Schütz, S., Mallm, J.P., Rippe, K., Lonsdorf, A.S., Rodríguez-Paredes, M. & Lyko, F. (2020) 'Single-cell transcriptomes of the human skin reveal age-related loss of fibroblast priming', *Communications Biology 2020 3:1*, 3(1), pp. 1–12.

Soleimanpour, M., Mirhaji, S.S., Jafari, S., Derakhshankhah, H., Mamashli, F., Nedaei, H., Karimi, M.R., Motasadizadeh, H., Fatahi, Y., Ghasemi, A., Nezamtaheri, M.S., Khajezade, M., Teimouri, M., Goliaei, B., Delattre, C. & Saboury, A.A. (2022) 'Designing a new alginate-fibrinogen biomaterial composite hydrogel for wound healing', *Scientific Reports 2022 12:1*, 12(1), pp. 1–17.

Someya, T. & Amagai, M. (2019) 'Toward a new generation of smart skins', *Nature Biotechnology 2019 37:4*, 37(4), pp. 382–388.

Sorkio, A., Koch, L., Koivusalo, L., Deiwick, A., Miettinen, S., Chichkov, B., & Skottman, H. (2018). 'Human stem cell based corneal tissue mimicking structures using laser-assisted 3D bioprinting and functional bioinks', *Biomaterials*, 171, pp. 57–71.

Sorrell, J.M., Baber, M.A. & Caplan, A.I. (2004) 'Site-matched papillary and reticular human dermal fibroblasts differ in their release of specific growth factors/cytokines and in their interaction with keratinocytes', *Journal of Cellular Physiology*, 200(1), pp. 134–145.

Sorrell, J.M. & Caplan, A.I. (2009) 'Chapter 4 Fibroblasts—A Diverse Population at the Center of It All', *International Review of Cell and Molecular Biology*, 276(C), pp. 161–214.

Sorrell, J.M. & Caplan, A.I. (2004) 'Fibroblast heterogeneity: more than skin deep', *Journal of Cell Science*, 117(5), pp. 667–675.

Souren, J.E.M., Ponec, M. & van Wijk, R. (1989) 'Contraction of collagen by human fibroblasts and keratinocytes', *In vitro cellular & developmental biology : journal of the Tissue Culture Association*, 25(11), pp. 1039–1045.

Sriram, G., Bigliardi, P.L. & Bigliardi-Qi, M. (2015) 'Fibroblast heterogeneity and its implications for engineering organotypic skin models in vitro', *European Journal of Cell Biology*, 94(11), pp. 483–512.

de Stefano, G.M. & Christiano, A.M. (2014) 'The Genetics of Human Skin Disease', *Cold Spring Harbor Perspectives in Medicine*, 4(10).

Stenvik, J., Sletta, H., Grimstad, O., Pukstad, B., Ryan, L., Aune, R., Strand, W., Tøndervik, A., Helge Torp, S., Skjãk-Bræk, G. & Espevik, T. (2012) 'Alginates induce differentiation and expression of CXCR7 and CXCL12/SDF-1 in human keratinocytes—The role of calcium', *Journal of Biomedical Materials Research Part A*, 100A(10), pp. 2803–2812.

Steven, A.C., Bisher, M.E., Roop, D.R. & Steinert, P.M. (1990) 'Biosynthetic pathways of filaggrin and loricrin—two major proteins expressed by terminally differentiated epidermal keratinocytes', *Journal of Structural Biology*, 104(1–3), pp. 150–162.

Stojkov, G., Niyazov, Z., Picchioni, F. & Bose, R.K. (2021) 'Relationship between Structure and Rheology of Hydrogels for Various Applications', *Gels*, 7(4).

Strudwick, X.L., Lang, D.L., Smith, L.E. & Cowin, A.J. (2015) 'Combination of Low Calcium with Y-27632 Rock Inhibitor Increases the Proliferative Capacity, Expansion Potential and Lifespan of Primary Human Keratinocytes while Retaining Their Capacity to Differentiate into Stratified Epidermis in a 3D Skin Model', *PLoS ONE*, 10(4).

Suhail, S., Sardashti, N., Jaiswal, D., Rudraiah, S., Misra, M. & Kumbar, S.G. (2019) 'Engineered Skin Tissue Equivalents for Product Evaluation and Therapeutic Applications', *Biotechnology journal*, 14(7), p. e1900022.

Sun, J., Ng, J.H., Fuh, Y.H., Wong, Y.S., Loh, H.T. & Xu, Q. (2009) 'Comparison of micro-dispensing performance between micro-valve and piezoelectric printhead', *Microsystem Technologies*, 15(9), pp. 1437–1448.

Sun, W., Starly, B., Daly, A. C., Burdick, J. A., Groll, J., Skeldon, G., Shu, W., Sakai, Y., Shinohara, M., Nishikawa, M., Jang, J., Cho, D.W., Nie, M., Takeuchi, S., Ostrovidov, S., Khademhosseini, A., Kamm, R.D., Mironov, V., Moroni, L., Ozbolat, I. T. (2020) 'The bioprinting roadmap', *Biofabrication*, 12(2), 022002.

Suzuki, T., Sasai, A., Tsujimoto, H., Yasunaga, T., Ogawa, N. & Yamamoto, H. (2020) 'Promoting effect of type 17 collagen production by chlorogenic acid using PLGA nanoparticles in the human epidermal keratinocyte cell', *Journal of Drug Delivery Science and Technology*, 58p. 101624.

Talovic, M., Marcinczyk, M., Ziemkiewicz, N. & Garg, K. (2017) 'Laminin Enriched Scaffolds for Tissue Engineering Applications', *Advances in Tissue Engineering & Regenerative Medicine: Open Access*, 2(3).

Tan, P.C., Zhou, S.B., Ou, M.Y., He, J.Z., Zhang, P.Q., Zhang, X.J., Xie, Y., Gao, Y.M., Zhang, T.Y. & Li, Q.F. (2022) 'Mechanical Stretching Can Modify the Papillary Dermis Pattern and Papillary Fibroblast Characteristics during Skin Regeneration', *Journal of Investigative Dermatology*, 142(9), pp. 2384-2394.

Tanaka, M., Abe, T. & Hara, Y. (2009) 'Roles of focal adhesions and fibronectin-mediated cohesion in proliferation of confluent fibroblasts', *Journal of Cellular Physiology*, 219(1), pp. 194–201.

Taylor, M.J., Weegman, B.P., Baicu, S.C. & Giwa, S.E. (2019) 'New Approaches to Cryopreservation of Cells, Tissues, and Organs', *Transfusion Medicine and Hemotherapy*, 46(3), pp. 197–215.

Techatanawat, S., Surarit, R., Suddhasthira, T. & Khovidhunkit, S.O.P. (2011) 'Type I collagen extracted from rat-tail and bovine Achilles tendon for dental application: A comparative study', *Asian Biomedicine*, 5(6), pp. 787–798.

Teo, M.Y., Kee, S., RaviChandran, N., Stuart, L., Aw, K.C. & Stringer, J. (2020) 'Enabling Free-Standing 3D Hydrogel Microstructures with Microreactive Inkjet Printing', *ACS Applied Materials and Interfaces*, 12(1), pp. 1832–1839.

Thakoersing, V.S., Gooris, G.S., Mulder, A., Rietveld, M., el Ghalbzouri, A. & Bouwstra, J.A. (2011) 'Unraveling Barrier Properties of Three Different In-House Human Skin Equivalents', *Tissue Engineering Part C: Methods*, 18(1), pp. 1–11.

Thakoersing, V.S., van Smeden, J., Mulder, A.A., Vreeken, R.J., el Ghalbzouri, A. & Bouwstra, J.A. (2013) 'Increased Presence of Monounsaturated Fatty Acids in the Stratum Corneum of Human Skin Equivalents', *Journal of Investigative Dermatology*, 133(1), pp. 59–67.

Thélu, A., Catoire, S. & Kerdine-Römer, S. (2020) 'Immune-competent in vitro co-culture models as an approach for skin sensitisation assessment', *Toxicology in Vitro*, 62p. 104691.

Theocharis, A.D., Manou, D. & Karamanos, N.K. (2019) 'The extracellular matrix as a multitasking player in disease', *The FEBS Journal*, 286(15), pp. 2830–2869.

Thomas, S. (2013) 'Alginate dressings in surgery and wound management — part 1', *Journal of Wound Care*, 9(2), pp. 56–60.

Toivola, D.M., Boor, P., Alam, C. & Strnad, P. (2015) 'Keratins in health and disease', *Current Opinion in Cell Biology*, 32pp. 73–81.

Tokuyama, E., Nagai, Y., Takahashi, K., Kimata, Y. & Naruse, K. (2015) 'Mechanical Stretch on Human Skin Equivalents Increases the Epidermal Thickness and Develops the Basement Membrane', *PLOS ONE*, 10(11), p. e0141989.

de la Torre, R.S., Fernández-González, A., Quiñones-Vico, M.I., Montero-Vilchez, T. & Arias-Santiago, S. (2020) 'Bioengineered Skin Intended as In Vitro Model for Pharmacosmetics, Skin Disease Study and Environmental Skin Impact Analysis', *Biomedicines*, 8(11), pp. 1–28.

Tottoli, E.M., Dorati, R., Genta, I., Chiesa, E., Pisani, S. & Conti, B. (2020) 'Skin Wound Healing Process and New Emerging Technologies for Skin Wound Care and Regeneration', *Pharmaceutics*, 12(8), pp. 1–30.

Tracy, L.E., Minasian, R.A. & Caterson, E.J. (2016) 'Extracellular Matrix and Dermal Fibroblast Function in the Healing Wound', *Advances in Wound Care*, 5(3), p. 119.

Tremblay, P.L., Berthod, F., Germain, L. & Auger, F.A. (2005) 'In Vitro Evaluation of the Angiostatic Potential of Drugs Using an Endothelialized Tissue-Engineered Connective Tissue', *Journal of Pharmacology and Experimental Therapeutics*, 315(2), pp. 510–516.

Tsunenaga, M., Adachi, E., Amano, S., Burgeson, R.E. & Nishiyama, T. (1998) 'Laminin 5 can promote assembly of the lamina densa in the skin equivalent model', *Matrix Biology*, 17(8–9), pp. 603–613.

Tunggal, J.A., Helfrich, I., Schmitz, A., Schwarz, H., Günzel, D., Fromm, M., Kemler, R., Krieg, T. & Niessen, C.M. (2005) 'E-cadherin is essential for in vivo epidermal barrier function by regulating tight junctions', *The EMBO Journal*, 24(6), p. 1146.

Tzaphlidou, M. (2008) 'Bone Architecture: Collagen Structure and Calcium/Phosphorus Maps', *Journal of Biological Physics*, 34(1–2), p. 39.

Uitto, J., Olsen, D.R. & Fazio, M.J. (1989) 'Extracellular Matrix of the Skin: 50 Years of Progress', *Journal of Investigative Dermatology*, 92(4), pp. S61–S77.

Varkey, M., Ding, J. & Tredget, E.E. (2014) 'Superficial Dermal Fibroblasts Enhance Basement Membrane and Epidermal Barrier Formation in Tissue-Engineered Skin: Implications for Treatment of Skin Basement Membrane Disorders', *Tissue Engineering. Part A*, 20(3–4), p. 540.

Venugopal, M.G., Brodsky, B., Ramshaw, J.A.M., Braswell, E. & Zhu, D. (1994) 'Electrostatic interactions in collagen-like triple-helical peptides', *Biochemistry*, 33(25), pp. 7948–7956.

Vidal, S.E.L., Tamamoto, K.A., Nguyen, H., Abbott, R.D., Cairns, D.M. & Kaplan, D.L. (2019) '3D biomaterial matrix to support long term, full thickness, immuno-competent human skin equivalents with nervous system components', *Biomaterials*, 198pp. 194–203.

Visser, C.W., Kamperman, T., Karbaat, L.P., Lohse, D. & Karperien, M. (2018) 'In-air microfluidics enables rapid fabrication of emulsions, suspensions, and 3D modular (bio)materials', *Science Advances*, 4(1).

Vohr, H.-W. & Heisler, E. (2005) 'Three-Dimensional Human Skin/Epidermal Models and Organotypic Human and Murine Skin Explant Systems', *Encyclopedic Reference of Immunotoxicology*, pp. 632–637.

Vorwald, C.E., Gonzalez-Fernandez, T., Joshee, S., Sikorski, P. & Leach, J.K. (2020) 'Tunable Fibrin-Alginate Interpenetrating Network Hydrogels to Support Cell Spreading and Network Formation', *Acta biomaterialia*, 108p. 142.

Wachendörfer, M., Buhl, E.M., Messaoud, G. ben, Richtering, W. & Fischer, H. (2022) 'pH and Thrombin Concentration Are Decisive in Synthesizing Stiff, Stable, and Open-Porous Fibrin-Collagen Hydrogel Blends without Chemical Cross-Linker', *Advanced Healthcare Materials*, p. 2203302.

Wagner, I., Materne, E.M., Brincker, S., Süßbier, U., Frädrich, C., Busek, M., Sonntag, F., Sakharov, D.A., Trushkin, E. v., Tonevitsky, A.G., Lauster, R. & Marx, U. (2013) 'A dynamic multi-organ-chip for long-term cultivation and substance testing proven by 3D human liver and skin tissue co-culture', *Lab on a Chip*, 13(18), pp. 3538–3547.

Wang, K., Camman, M., Mosser, G., Haye, B., Trichet, L. & Coradin, T. (2022) 'Synthesis of Fibrin-Type I Collagen Biomaterials via an Acidic Gel', *Molecules,* Vol. 27, Page 2099, 27(7), p. 2099.

Wang, P., Hu, Z., Cao, X., Huang, S., Dong, Y., Cheng, P., Xu, H., Shu, B., Xie, J., Wu, J., Tang, B. & Zhu, J. (2019b) 'Fibronectin precoating wound bed enhances the therapeutic effects of autologous epidermal basal cell suspension for full-thickness wounds by improving epidermal stem cells' utilization', *Stem Cell Research & Therapy*, 10(1).

Wang, T., Zhang, J., Liao, J., Zhang, F. & Zhou, G. (2020) 'Donor genetic backgrounds contribute to the functional heterogeneity of stem cells and clinical outcomes', *STEM CELLS Translational Medicine*, 9(12), pp. 1495–1499.

Wang, Y., Chen, S., Yan, Z. & Pei, M. (2019a) 'A prospect of cell immortalization combined with matrix microenvironmental optimization strategy for tissue engineering and regeneration', *Cell & Bioscience 2019 9:1*, 9(1), pp. 1–21.

Wang, Y., Wang, G., Luo, X., Qiu, J. & Tang, C. (2012) 'Substrate stiffness regulates the proliferation, migration, and differentiation of epidermal cells', *Burns*, 38(3), pp. 414–420.

Watkinson, A., Harding, C., Moore, A. & Coan, P. (2001) 'Water modulation of stratum corneum chymotryptic enzyme activity and desquamation', *Archives of Dermatological Research*, 293(9), pp. 470–476.

Watt, F.M. (1983) 'Involucrin and other markers of keratinocyte terminal differentiation', *The Journal of investigative dermatology*, 81(1 Suppl), pp. S100–S103.

Wei, Z., Liu, X., Ooka, M., Zhang, L., Song, M.J., Huang, R., Kleinstreuer, N.C., Simeonov, A., Xia, M. & Ferrer, M. (2020) 'Two-Dimensional Cellular and Three-Dimensional Bio-Printed Skin Models to Screen Topical-Use Compounds for Irritation Potential', *Frontiers in Bioengineering and Biotechnology*, 8p. 109.

Welss, T., Basketter, D.A. & Schröder, K.R. (2004) 'In vitro skin irritation: facts and future. State of the art review of mechanisms and models', *Toxicology in Vitro*, 18(3), pp. 231–243.

Wells, R.G. (2013) 'Tissue Mechanics and Fibrosis', *Biochimica et biophysica acta*, 1832(7), p. 884.

Wendt, D., Timmins, N., Malda, J., Janssen, F., Ratcliffe, A., Vunjak-Novakovic, G. & Martin, I. (2008) 'Chapter 16 - Bioreactors for tissue engineering', in Clemens van Blitterswijk, Peter Thomsen, Anders Lindahl, Jeffrey Hubbell, David F Williams, Ranieri Cancedda, Joost D de Bruijn, & Jérôme Sohier (eds.) *Tissue Engineering*. [Online]. Burlington: Academic Press. pp. 483–506.

Werkmeister, J.A. & Ramshaw, J.A.M. (2012) 'Recombinant protein scaffolds for tissue engineering', *Biomedical Materials*, 7(1), p. 012002.

Wever, B., Petersohn, D. & Mewes, K. (2013) 'Overview of human three-dimensional skin models used for dermal toxicity assessment', *Alternatives to Animal Testing*, 8(1), pp. 18–22.

Wiesmann, H.P., Meyer, U., Plate, U. & Höhling, H.J. (2004) 'Aspects of Collagen Mineralization in Hard Tissue Formation', *International Review of Cytology*, 242pp. 121–156.

de Wildt, B.W.M., Ansari, S., Sommerdijk, N.A.J.M., Ito, K., Akiva, A. & Hofmann, S. (2019) 'From bone regeneration to three-dimensional in vitro models: tissue engineering of organized bone extracellular matrix', *Current Opinion in Biomedical Engineering*, 10pp. 107–115.

Williams, R., Pawlus, A.D. & Thornton, M.J. (2020) 'Getting under the skin of hair aging: the impact of the hair follicle environment', *Experimental Dermatology*, 29(7), pp. 588–597.

Wnorowski, A., Yang, H. & Wu, J.C. (2019) 'Progress, Obstacles, and Limitations in the Use of Stem Cells in Organ-on-a-Chip Models', *Advanced drug delivery reviews*, 140p. 3.

Wong, R., Geyer, S., Weninger, W., Guimberteau, J.C. & Wong, J.K. (2016) 'The dynamic anatomy and patterning of skin', *Experimental Dermatology*, 25(2), pp. 92–98.

Wouters, O.J., McKee, M. & Luyten, J. (2020) 'Estimated Research and Development Investment Needed to Bring a New Medicine to Market, 2009-2018', *JAMA*, 323(9), p. 844.

Wufuer, M., Lee, G.H., Hur, W., Jeon, B., Kim, B.J., Choi, T.H. & Lee, S.H. (2016) 'Skin-on-a-chip model simulating inflammation, edema and drug-based treatment', *Scientific Reports 2016 6:1*, 6(1), pp. 1–12.

Wüstneck, R., Wetzel, R., Buder, E. & Hermel, H. (1988) 'The modification of the triple helical structure of gelatin in aqueous solution I. The influence of anionic surfactants, pH-value, and temperature', *Colloid & Polymer Science*, 266(11), pp. 1061–1067.

Xu, C., Zhang, M., Huang, Y., Ogale, A., Fu, J. & Markwald, R.R. (2014) 'Study of droplet formation process during drop-on-demand inkjetting of living cell-laden bioink', *Langmuir*, 30(30), pp. 9130–9138.

Xu, T., Zhao, W., Zhu, J.M., Albanna, M.Z., Yoo, J.J. & Atala, A. (2013) 'Complex heterogeneous tissue constructs containing multiple cell types prepared by inkjet printing technology', *Biomaterials*, 34(1), pp. 130–139.

Yamauchi, M. & Sricholpech, M. (2012) 'Lysine post-translational modifications of collagen', *Essays in biochemistry*, 52(1), p. 113.

Yamaguchi, Y., Brenner, M. & Hearing, V.J. (2007) 'The regulation of skin pigmentation', *Journal of Biological Chemistry*, 282(38), pp. 27557–27561.

Yamanaka, S. (2020) 'Pluripotent Stem Cell-Based Cell Therapy—Promise and Challenges', *Cell Stem Cell*, 27(4), pp. 523–531.

Yang, G., Seok, J.K., Kang, H.C., Cho, Y.Y., Lee, H.S. & Lee, J.Y. (2020) 'Skin Barrier Abnormalities and Immune Dysfunction in Atopic Dermatitis', *International journal of molecular sciences*, 21(8).

Yang, S., Sun, Y., Geng, Z., Ma, K., Sun, X. & Fu, X. (2016) 'Abnormalities in the basement membrane structure promote basal keratinocytes in the epidermis of hypertrophic scars to adopt a proliferative phenotype', International Journal of Molecular Medicine, 37(5), pp. 1263–1273.

Yano, S., Komine, M., Fujimoto, M., Okochi, H. & Tamaki, K. (2004) 'Mechanical Stretching In Vitro Regulates Signal Transduction Pathways and Cellular Proliferation in Human Epidermal Keratinocytes', *Journal of Investigative Dermatology*, 122(3), pp. 783–790.

Yi, J.Y., Yoon, Y.H., Park, H.S., Kim, Chun Ho, Kim, Chang Hwan, Kang, H.J., Lee, E.A., Kim, Y.Y., Jin, Y.J., Kim, T.H. & Son, Y.S. (2001) 'Reconstruction of basement membrane in skin equivalent; role of laminin-1', *Archives of Dermatological Research*, 293(7), pp. 356–362.

Yoshida, K., Yokouchi, M., Nagao, K., Ishii, K., Amagai, M. & Kubo, A. (2013) 'Functional tight junction barrier localizes in the second layer of the stratum granulosum of human epidermis', *Journal of Dermatological Science*, 71(2), pp. 89–99.

Yousef, H., Alhajj, M. & Sharma, S. (2022) 'Anatomy, Skin (Integument), Epidermis', *StatPearls*,

Yousef, H., Miao, J.H., Alhajj, M. & Badri, T. (2022) 'Histology, Skin Appendages', *StatPearls*,

Yousefzade, O., Katsarava, R. & Puiggalí, J. (2020) 'Biomimetic Hybrid Systems for Tissue Engineering', *Biomimetics*, 5(4), pp. 1–31.

Zhang, B., Chen, L., Jabbari, E., Nur, S., Oslan, H., Shapawi, R., Azli, R., Mokhtar, M., Norhana, W., Noordin, M. & Huda, N. (2022c) 'Characterization of Acid- and Pepsin-Soluble Collagen Extracted from the Skin of Purple-Spotted Bigeye Snapper', *Gels 2022, Vol. 8, Page 665*, 8(10), p. 665.

Zhang, X., Chen, X., Hong, H., Hu, R., Liu, J. & Liu, C. (2022a) 'Decellularized extracellular matrix scaffolds: Recent trends and emerging strategies in tissue engineering', *Bioactive Materials*, 10pp. 15–31.

Zhang, X., Xu, S., Shen, L. & Li, G. (2020) 'Factors affecting thermal stability of collagen from the aspects of extraction, processing and modification', *Journal of Leather Science and Engineering*, 2(1), pp. 1–29.

Zhang, Z., Feng, Y., Wang, L., Liu, D., Qin, C. & Shi, Y. (2022b) 'A review of preparation methods of porous skin tissue engineering scaffolds', *Materials Today Communications*, 32p. 104109.

Zheng, Z., Eglin, D., Alini, M., Richards, G.R., Qin, L. & Lai, Y. (2021) 'Visible Light-Induced 3D Bioprinting Technologies and Corresponding Bioink Materials for Tissue Engineering: A Review', *Engineering*, 7(7), pp. 966–978.

Zhu, J. & Marchant, R.E. (2011) 'Design properties of hydrogel tissue-engineering scaffolds', *Expert review of medical devices*, 8(5), p. 607.

Zhu, Y., Mandal, K., Hernandez, A.L., Kawakita, S., Huang, W., Bandaru, P., Ahadian, S., Kim, H.J., Jucaud, V., Dokmeci, M.R. & Khademhosseini, A. (2021) 'State of the art in integrated biosensors for organ-on-a-chip applications', *Current Opinion in Biomedical Engineering*, 19p. 100309.

Zou, M.L., Teng, Y.Y., Wu, J.J., Liu, S.Y., Tang, X.Y., Jia, Y., Chen, Z.H., Zhang, K.W., Sun, Z.L., Li, X., Ye, J.X., Xu, R.S. & Yuan, F.L. (2021) 'Fibroblasts: Heterogeneous Cells With Potential in Regenerative Therapy for Scarless Wound Healing', *Frontiers in Cell and Developmental Biology*, 9.

APPENDIX – Conferences, Publications and Awards Arising from this Project

Oral communications at international conferences

2019	EPSRC CDT in Additive Manufacturing Industrial Day (University of Notthingham, UK): *Bioprinting Skin Models as Alternative to Animal Testing in the Cosmetic Industry.* M Crespo-Cuadrado, K Dalgarno, M Birch-Machin, P Hanson, A Ferreira-Duarte, P Mondon, B Chavan.
2020	IFSCC Congress (Yokohama,Japan-online): *Bioprinting Human Skin Equivalents Using Reactive Jet Impingement as Alternative to Animal Testing.* M Crespo-Cuadrado, K Dalgarno, M Birch-Machin, P Hanson, A Ferreira-Duarte, P Mondon, B Chavan.
2021	BioNTERM Conference (online): *Bioprinting Human Skin Equivalents Using Reactive Jet Impingement as Alternative to Animal Testing.* M Crespo-Cuadrado, K Dalgarno, M Birch-Machin, P Hanson, A Ferreira-Duarte, P Mondon, B Chavan.
2021	Three Minute Thesis (3MT) Competition (Newcastle University, UK): *Bioprinting Human Skin as Alternative to Animal Testing.* M Crespo-Cuadrado
2021	VII Symposium Spanish Researchers in the United Kingdom (Oxford,UK-online): *Bioprinting technologies, a new paradigm in regenerative medicine*. M Crespo-Cuadrado
2022	Galenus International Workshop (University of Valencia, Spain): *Bioprinting Skin Models Using Reactive Jet Impingement*. M Crespo-Cuadrado, M Birch-Machin, P Hanson, K Dalgarno, A Ferreira-Duarte, P Mondon, B Chavan.

Poster communications at international conferences

2018	EPSRC CDT Industrial Day (University of Nottingham, UK): *Bioprinting Skin Models for Evaluation of Molecules Toxicity and Active Ingredients for the Cosmetic Industry.* M Crespo-Cuadrado, K Dalgarno, M Birch-Machin, P Hanson, A Ferreira-Duarte, P Mondon, B Chavan.
2019	VII Symposium Spanish Researchers in the United Kingdom (University of Liverpool, UK): *Bioprinting Skin Models for Evaluation of Molecules Toxicity and Active Ingredients for the Cosmetic Industry.* M Crespo-Cuadrado, K Dalgarno, M Birch-Machin, P Hanson, A Ferreira-Duarte, P Mondon, B Chavan.
2021	European Society of Biomaterials (Porto,UK-online): *The impact of collagen type I sources and extraction methods on its physicochemical properties and cell behaviour.* M Crespo-Cuadrado, G Dura, A Ferreira-Duarte, K Dalgarno, P Hanson, M Birch-Machin, P Mondon, B Chavan.

Publications

2020	M Crespo-Cuadrado, K Dalgarno, M Birch-Machin, P Hanson, A Ferreira-Duarte, P Mondon, B Chavan. *Bioprinting skin models using Reactive Jet Impingement.* Conference article EU-TERMIS Chapter 2020.
2020	M Crespo-Cuadrado, K Dalgarno, M Birch-Machin, P Hanson, A Ferreira-Duarte, P Mondon, B Chavan. *Bioprinting Human Skin Equivalents Using Reactive Jet Impingement as Alternative to Animal Testing.* Conference article IFSCC Congress 2020.
2020	Dura, G., Peters, D. T., Waller, H., Yemm, A. I., Perkins, N. D., Ferreira, A. M., Crespo-Cuadrado, M., Lakey, J. H., & Fulton, D. A. (2020). *A Thermally Reformable Protein Polymer*. Chem, 6(11), 3132–3151. https://doi.org/10.1016/J.CHEMPR.2020.09.020
2021	Dura, G., Crespo-Cuadrado, M., Waller, H., Peters, D. T., Ferreira, A. M., Lakey, J. H., & Fulton, D. A. (2021). *Hydrogels of engineered bacterial fimbriae can finely tune 2D human cell culture*. Biomaterials Science, 9(7), 2542–2552. https://doi.org/10.1039/D0BM01966F
2022	Dura, G., Crespo-Cuadrado, M., Waller, H., Peters, D. T., Ferreira-Duarte, A., Lakey, J. H., & Fulton, D. A. (2022). *Exploiting Meltable Protein Hydrogels to Encapsulate and Culture Cells in 3D*. Macromolecular Bioscience, 22(9), 2200134. https://doi.org/10.1002/MABI.202200134